Selective Inhibitors of The Cytochrome P450 Enzyme CYP1B1

Hoon Leong Tan

Submitted in fulfilment of the requirements

for the degree of Doctor of Philosophy

Leicester School of Pharmacy

De Montfort University

March 2006

Sponsers: De Montfort University and Spear Therapeutics Ltd

In memory of my Uncle

Acknowledgements

I would like to thank my first supervisor Gerry Potter for his guidance, enthusiasm and support throughout this project. Thanks to Kenneth Beresford, my second supervisor, who was always there when I needed help. A special thank you to Danny Burke, who gave me a private lecture on all aspects of P450 and the EROD assay. Many thanks to Paul Butler for carrying out cytotoxic testing on the compounds synthesised and his insights into cancer research. I would like to thank Ketan Ruparelia, Nicola Wilsher, Meng Wang, Taeeba Ijaz, Dyan Ankrett, Saba Lodhi, Asma Patel, Somchaiya Surichan and Vasilis Androutsopoulos for exhanging ideas, swapping papers and laughter. Special thanks to Nicola, who helped me setting up the EROD assay and her insights into drug metabolism and pharmacokinetics. My special graditute to Somchaiya for carrying out some initial drug metabolism and pharmacokinetics studies on my compounds. It was my privilege to work with all of you.

I would like to thank Mike Needam and Sonia at Leicester School of Pharmacy for NMR analysis, and John Lamb at the Cancer Biomarkers Group, University of Leicester for his assistance in MS analysis.

I also wish to thank Leena Lakdawala, Mussarath Walji and Nishad Rajabali for synthesising some of the compounds in this research, as part of the final year project of their pharmacy degree.

Lastly, but not least, a big thank you to "CCLP" and my family for your tolerance and support.

This research was supported by De Montfort University and Spear Therapeutics Ltd.

Abstract

The cytochrome P450 CYP1 ezymes, CYP1A1, CYP1A2 and CYP1B1, are members of the cytochrome P450 superfamily which catalyse the oxidative metabolism of a wide range of endogenous and exogenous compounds. CYP1B1 is highly overexpressed in different malignancies but not in the corresponding normal tissues. This significant discovery has provided an opportunity to develop tumour specific intracellular activated anticancer prodrugs, using CYP1B1 as molecular target.

As part of the continuing CYP1B1 activated anticancer prodrugs discovery programme at Leicester School of Pharmacy, this research was set up to delineate the structure-activity relationship of the CYP1 enzymes. This was achieved by studying a range of inhibitors designed and synthesised during this Ph.D. project. The inhibitor's ability to inhibit CYP1 enzymes was quantified using a fluorometric high throughput ethoxyresorufin *O*-deethylase assay.

DMU968 and DMU2157 were identified as inhibitors of CYP1A1. These inhibitors have low intrinsic toxicity and therefore, have potential applications for *in vivo* and cell line based *in vitro* experiments. 9-Acetylphenanthrene was identified as CYP1A2 inhibitor. It was demonstrated that 9-acetylphenahthrene has better potency and selectivity profiles compared with the known CYP1A2 inhibitor furafylline. Fourteen CYP1B1 inhibitors were identified. DMU778 and DMU2103 may have potential applications in cell based assays due to low intrinsic toxicity.

DMU2123 and DMU2127 have been shown to possess tumour specific anticancer properties. These compounds were selectively activated by CYP1A1 and may have the potential as anticancer prodrug since some cancers also highly expressed CYP1A1. It was also found that residual insect P450, present in control microsomes, also bioactivated these compounds. Although the identity of the insect P450 has not been identified, DMU2123 and DMU2127 have a double potential as insect selective pesticides as well as tumour selective anticancer agents. Currently, more detailed studies are being performed on these compounds.

Combining drug metabolism data obtained elsewhere and enzyme inhibition results, pharmacophore models for the CYP1 enzymes were constructed. The pharmacophore models for each CYP1 enzymes have shown distinct structural requirements for selective inhibitors and substrates. These pharmacophore models have contributed towards better prodrug design. Inhibitors synthesised in this research may be used for studying other P450s structure-activity relationships. Selective inhibitors identified in this project also provided valuable molecular probes for drug metabolism and pharmacokinetic studies.

Contents

List of Figures

List of Tables

List of Abbreviations

αNF	α–Naphthaflavone
λ_{em}	Maximum emission wavelength
λ_{ex}	Maximum excitation wavelength
2,4-DNP	2,4-Dinitrophenylhydrazine
3D	Three dimensional
7ER	7-Ethoxyresorufin
2OH-E2	2-Hydroxyestradiol
4OH-E2	4-Hydroxyestradiol
ACA	acacetin
AF	Activation factor
AhR	Aromatic hydrocarbon receptor
AIP	AhR interacting protein
ARA9	AhR-associated protein 9
ARNT	Aromatic hydrocarbon receptor nucleus translocator
bHLH	Basic helix-loop-helix
CO	Carbon monoxide
DMPK	Drug metabolism and pharmacokinetics
DMSO	Dimethylsulfoxide
E2	Estradiol
eq	Equimolar
ER	Endoplasmic reticulum
eSR	Enzyme selectivity ratio
EtOH	Ethanol
EROD	7-Ethoxyresorufin O-deethylase
FAD	Flavin adenine dinucleotide
Fe(V)=O	Fe(V)-oxo complex
FMN	Flavin mononucleotide
G6P	Glucose-6-phosphate
G6PD	Glucose-6-phosphate dehydrogenase
HPLC	High performance liquid chromatography
HSP90	Heat shock protein 90
KH_2PO_4	Potassium dihydrogen orthophosphate
LDA	Lithium diisopropylamide
MeOH	Methanol
mRNA	Messenger ribonucleic acid
$MgCl_2$	Magnesium chloride
MS	Mass spectroscopy
MTT	3-(4,5-Dimethylthiazol-2-yl)-2,5-diphenyl tetrazolium bromide
Na_2HPO_4	Disodium hydrogen orthophosphate
$NADP^+$	β-Nicotinamide adenine dinucleotide phosphate
NADPH	β-Nicotinamide adenine dinucleotide phosphate reduced form
$NADPH+H^+$	NADPH and proton complex
NaOH	Sodium hydroxide
nBuLi	n-Butyl lithium
NFκB	Nuclear factor kappa B

NMR	Nuclear magnetic resonance
PAA	Polycyclic aromatic amines
PAH	Polycyclic aromatic hydrocarbon
PAS	*P*er-ARNT-*S*im
Pi-buffer	Phosphate buffer at pH 7.4
RT-PCR	Reverse transcriptase polymerase chain reaction
SA	Signal-anchor
SAR	Structure-activity relationships
TCDD	3,4,7,8-Tetrachlorodibenzo-*p*-dioxin
THF	Tetrahydrofuran
TLC	Thin layer chromatography
TS	Tumour selective factor
XAP2	Hepatitis B virus X-associated protein 2
UV	Ultra violet

Chapter 1

The Cytochrome P450 CYP1 Family Enzymes and Cancer

1.1 The P450 enzyme superfamily

1.1.1 The discovery of P450

The mammalian cytochrome P450 enzyme complex is a membrane bound oxygenase system that consists of the haem-thiolate P450 and its redox partner NADPH-cytochrome P450 reductase. Initially, it was thought that P450 was a single unique cytochrome but it soon became clear that the P450 exists as multiple forms of enzymes; each with different properties in respect of their substrate selectivity and their ultra-violet (UV) absorption maxima spectra for the P450-carbon monoxide (CO) adducts (Table 1). The multiplicity has led to the enzymes being termed mono-oxygenase[1], to describe their ability to oxidise a large variety of substrates.

Table 1: Some characteristics of mammalian P450-CO adducts UV absorption maxima[2]

CYP	Species	λ_{max}(nm) CO adduct
1A1	rat	447
1A2	rat	447
2A1	rat	451
2C5	rabbit	450
2D9	mouse	449
2E2	rabbit	452
3A6	rabbit	449
4A4	rabbit	450

The discovery of xenobiotics metabolising enzymes in the microsomal subcellular fraction[3] (endoplasmic reticulum vesicles) and the appearance of a vivid orange-red pigment following the complexation of microsomal preparations with CO[4,5] led to the discovery of P450 in the 1950s. However, the catalytic functions of P450 have been observed more than twenty years earlier before Axelrod[3], when Verkade[6] reported the ω-oxidation of fatty acids in dogs and human subjects. Carter[7] and Bergstrom[8] also discovered similar biological oxidation of other α- and β-substituted fatty acids in animals before P450 was named and characterised. The designation of "P450" in early 1960s followed after Omura[9-11] identified the CO binding pigment as a haemprotein which possessed an ultra-violet absorption spectrum with a Soret peak at 450nm.

The P450 mono-oxygenase systems are widespread in nature and are present in all five biological kingdoms[12,13]. It appears that certain primitive species of bacteria do not contain any form of the enzyme, indicating that the ancestral P450 gene may have developed some 3.5 billion years ago[14,15]. In mammals the enzyme system is found predominantly on the endoplasmic reticulum (ER) and in mitochondria. P450 has been found in all tissues examined including lung, small intestine, kidney, colon, the brain and, with greatest abundance, in the liver[16]. As more P450s were identified, the nomenclature of P450s, usually based on how they were identified, was increasingly unmanageable and difficult to follow. Under the leadership of Daniel Nebert[17], a naming system was devised based on amino acid sequence homology of the enzymes. For example, the rat P450 formally known as P450PB1 is now referred to as CYP2B1, while the corresponding gene became *CYP2B1* to indicate family 2, subfamily B and individual enzyme number 1. To date there are over 800 subfamilies of P450 have been discovered[18] and more are added to the list as new P450s are identified and

characterised.

The explosion of P450 research areas and applications was made possible after the successful resolution of microsomal P450 by Coon *et. al.*[19,20] in 1968. The reconstituted system consisting a P450, a NADPH-cytochrome P450 reductase and the lipid component phosphatidylcholine, and was shown to be capable of biotransforming a variety of drug, hydrocarbon and fatty acid substrates[21]. Through the advancement in biochemistry and biotechnology, the use of heterologously expressed P450s for *in vitro* research is now commonplace.

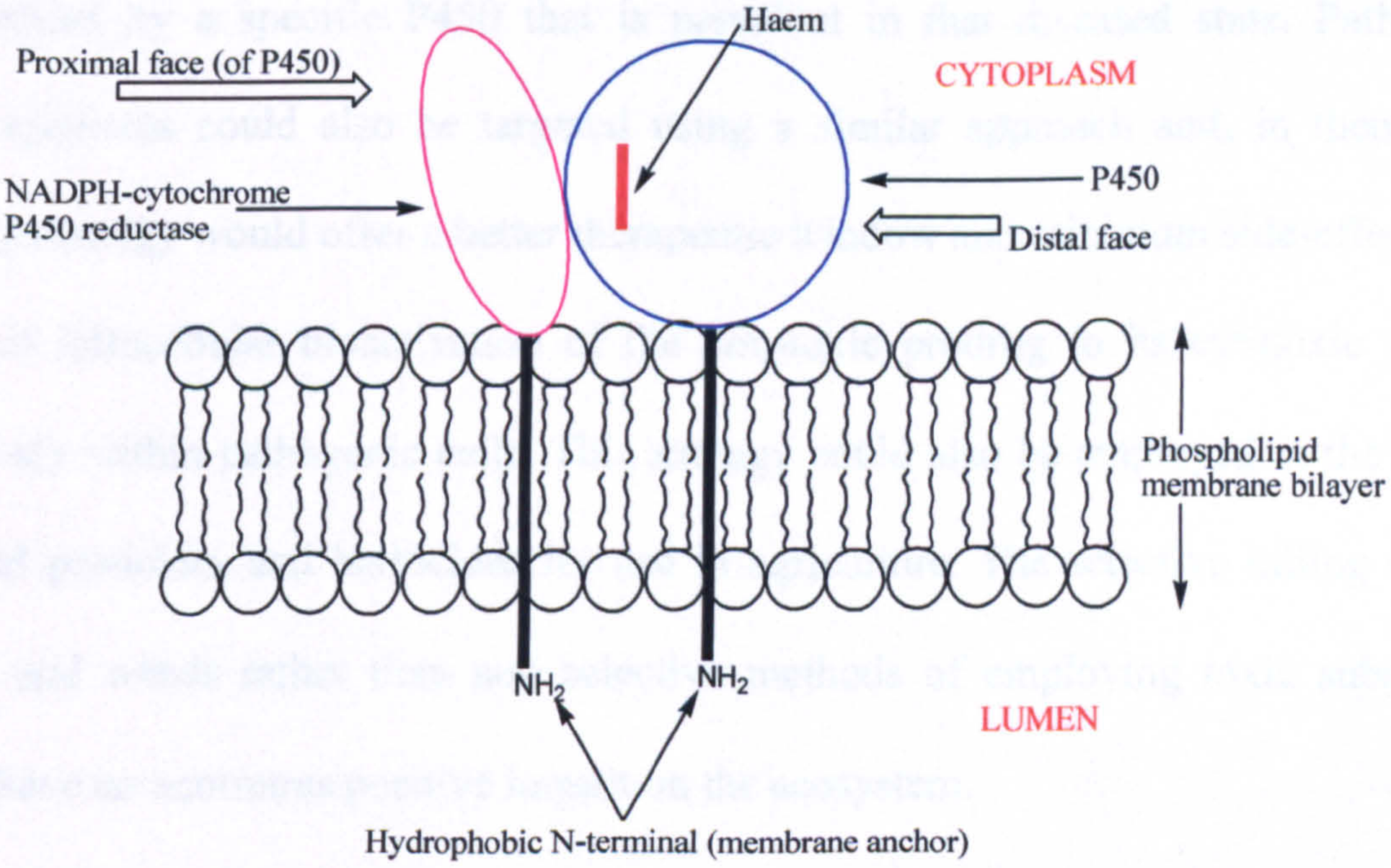

Figure 1: Diagrammatic representation of a typical microsomal P450 mono-oxygenase system

The red bar represents the haem which is embedded within P450 and perpendicular to the plane of the membrane. Broad arrows indicate the proximal and distal faces of P450. The cytoplasmic and luminal faces are indicated in red. The hydrophobic leader sequences of both components are indicated by the bars which protrude into the membrane bilayer to afford anchorage. In some cases, cytochrome b_5 can also act as a source of electrons for P450 (i.e. CYP3A4).

It is no exaggeration to state that the P450 enzymes are the most important biological catalysts known in all life forms. The enzymes catalyse the biosynthesis and metabolism of endogenous substances, including steroids, fatty acids, phytoalexins, alkaloids, eicosanoids and vitamins[1]. The substrates of P450 also encompass a host of xenobiotics, including those that occur biologically (i.e. antibiotics and phytoestrogens), as well as man-made chemicals such as drugs and environmental pollutants[1]. From a medicinal chemist's point of view, P450s are important, firstly because of their capability to alter pharmacological activity of a drug. Secondly because they provide a gateway to target diseased cells, e.g. by synthesising novel prodrugs that would be selectively bioactivated by a specific P450 that is prevalent in that diseased state. Pathogenic microorganisms could also be targeted using a similar approach and, in theory, the prodrug strategy would offer a better therapeutic window and minimum side-effects as a result of intracellular bioactivation of the non-toxic prodrug to its cytotoxic species selectively within pathogenic cells. This strategy could also be employed in the design of novel pesticides and herbicides for use in agriculture. The selective killing of pest insects and weeds rather than non selective methods of employing toxic substances would have an enormous positive impact on the ecosystem.

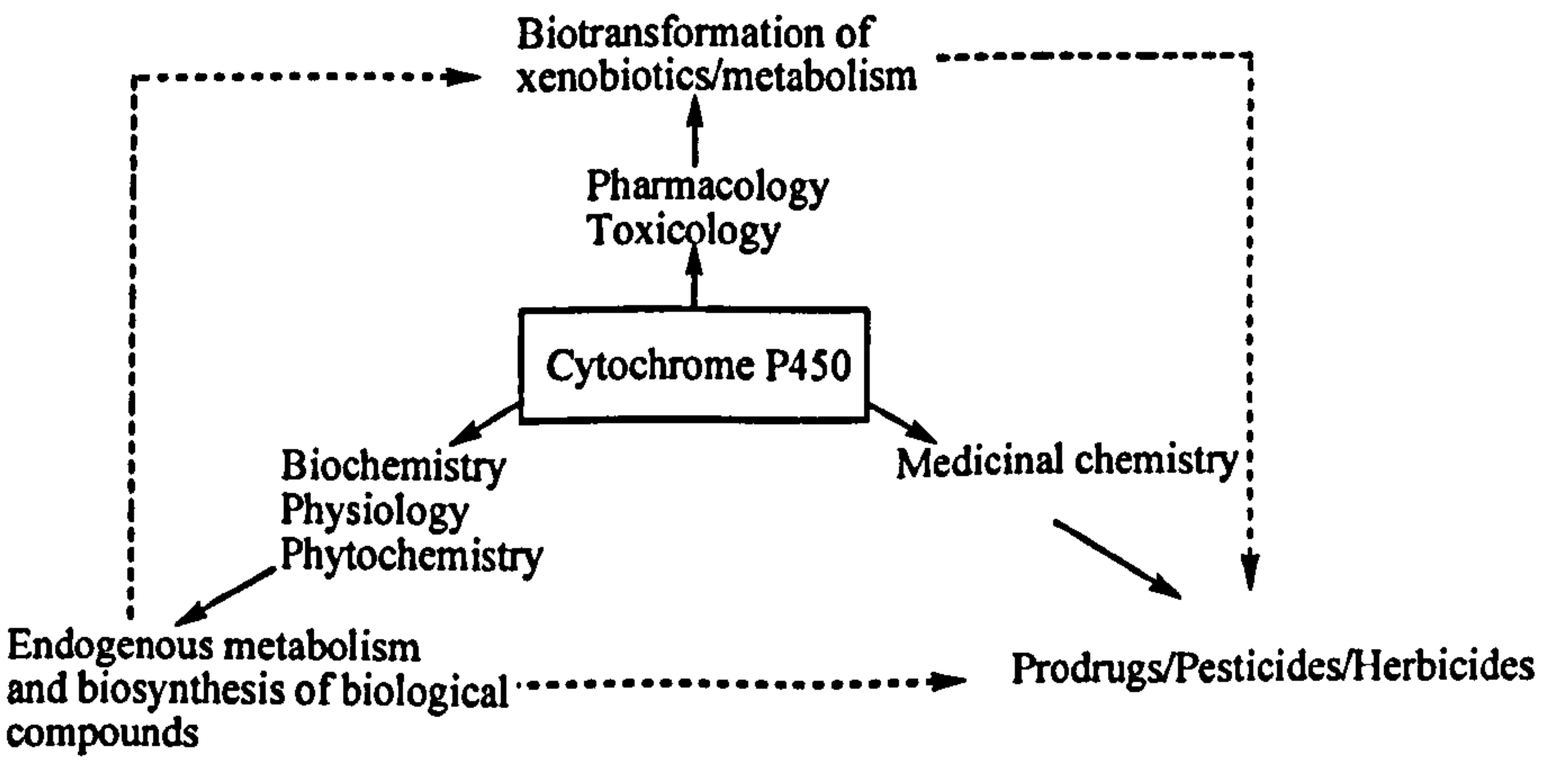

Figure 2: Cytochrome P450 research areas and potential applications

1.1.2 Evolution of cytochrome P450

As more and more genomes from different organisms were sequenced, the number of P450 genes/proteins detected also significantly increased. At the moment of writing, more than 3000 P450 genes have been sequenced[18]. The large number of P450s identified has made the studies on how this superfamily evolved over the last 3.5 billion years[14,15] possible. Using appropriate algorithms, it is feasible to compare two or more proteins sequences and their approximate evolutionary distance can be calculated[22]. The method is based on the specific rate of protein mutation[23] and how mutation rate is associated with the divergence of two related proteins[24]. This led to the unweighted pair group method of phylogenetic analysis (UPGMA)[25,26], a method for the formulation of phylogenetic trees (for example see Figure 3).

The P450 nomenclature devised in 1987[17] is now choking with families as more and more P450 families are discovered and assigned. The explosion of family number has made the nomenclature cumbersome as well as created inconvenience in evolutionary studies. Some families of P450 clearly belong together and therefore, a higher order of nomenclature is necessary to cluster these families collectively. The term used for these clusters is clan. The clan system devised by David Nelson[27], has made the studies of P450 evolution manageable. P450s within a particular clan are diverged from a common P450. Comparisons of different clans have shown that P450s are probably descendants of an ancestral protein present in a prehistoric life form, before the divergence of prokaryotes and eukaryotes. It is interesting to note that the CYP1 family enzymes share a common ancestral root with P450s that are responsible for sex hormone biosynthesis (Figure 3). This indicates the possible endogenous role of CYP1 enzymes in the homeostasis of hormonal level in animals.

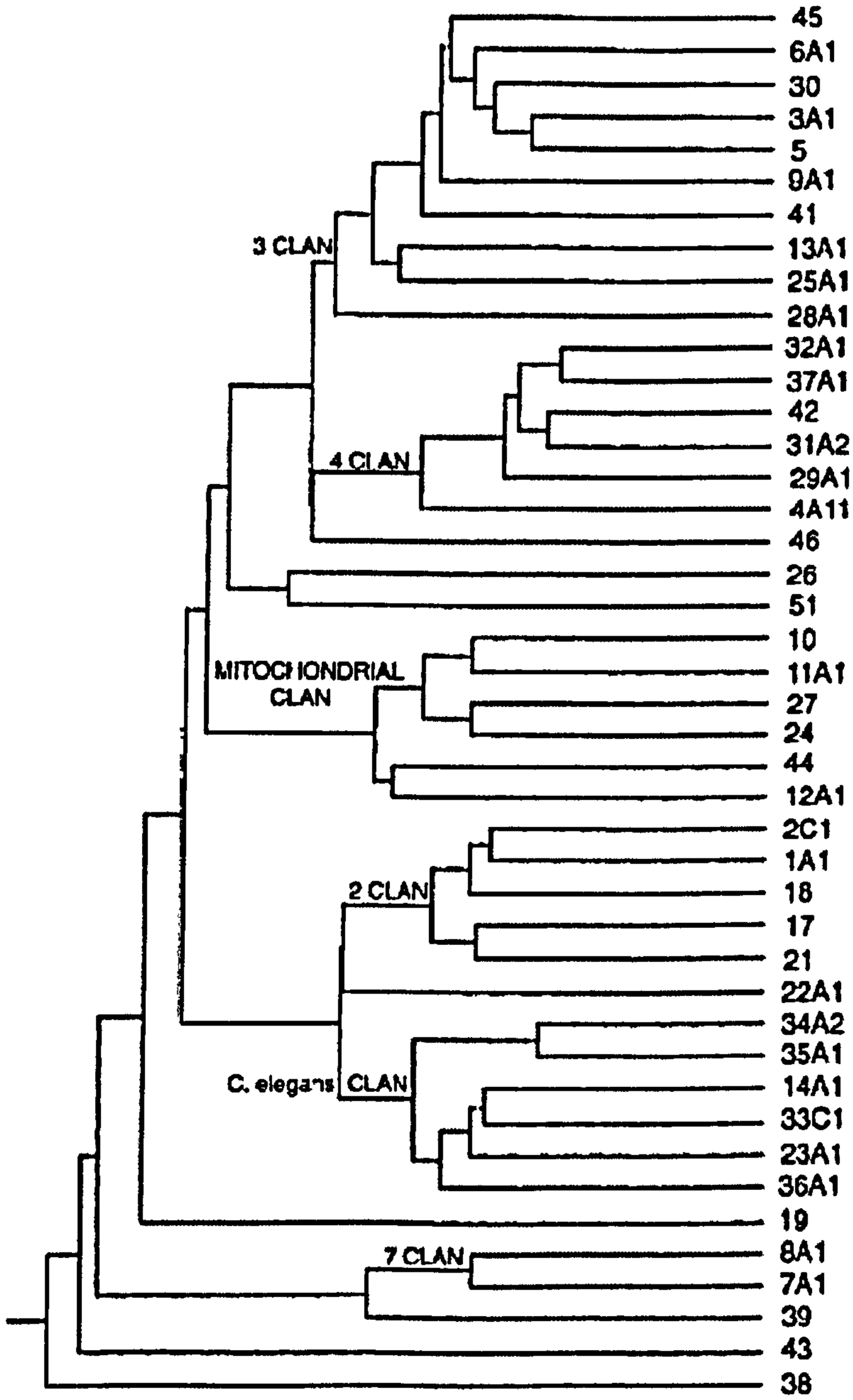

Figure 3: A UPGMA phylogenetic tree of 43 animal P450s

The phylogenetic tree only shows one P450 from each family. Adapted from Nelson[27].

It is thought that the ancestral P450 was developed by ancient thermophilic archaebacteria which occupied the vicinity of deep sea volcanoes[28]. This is a sound hypothesis since there would be a plentiful supply of iron and sulphur, the key elements for P450 and the redoxin redox partner. It has been suggested that the early role of P450 enzymes may have involved detoxification of reactive oxygen species harmful to

anaerobes[29]. As the oxygen level in the earth's atmosphere rose, due to photosynthetic activity of blue-green algae[30], excess oxygen has enabled life to develop from simple single cell organisms to the progressively more complex eukaryotes. As species evolved complexity and multicellularity, ancestral P450s were recruited for new tasks that did not exist before and this could be the driving force of P450 divergence[31].

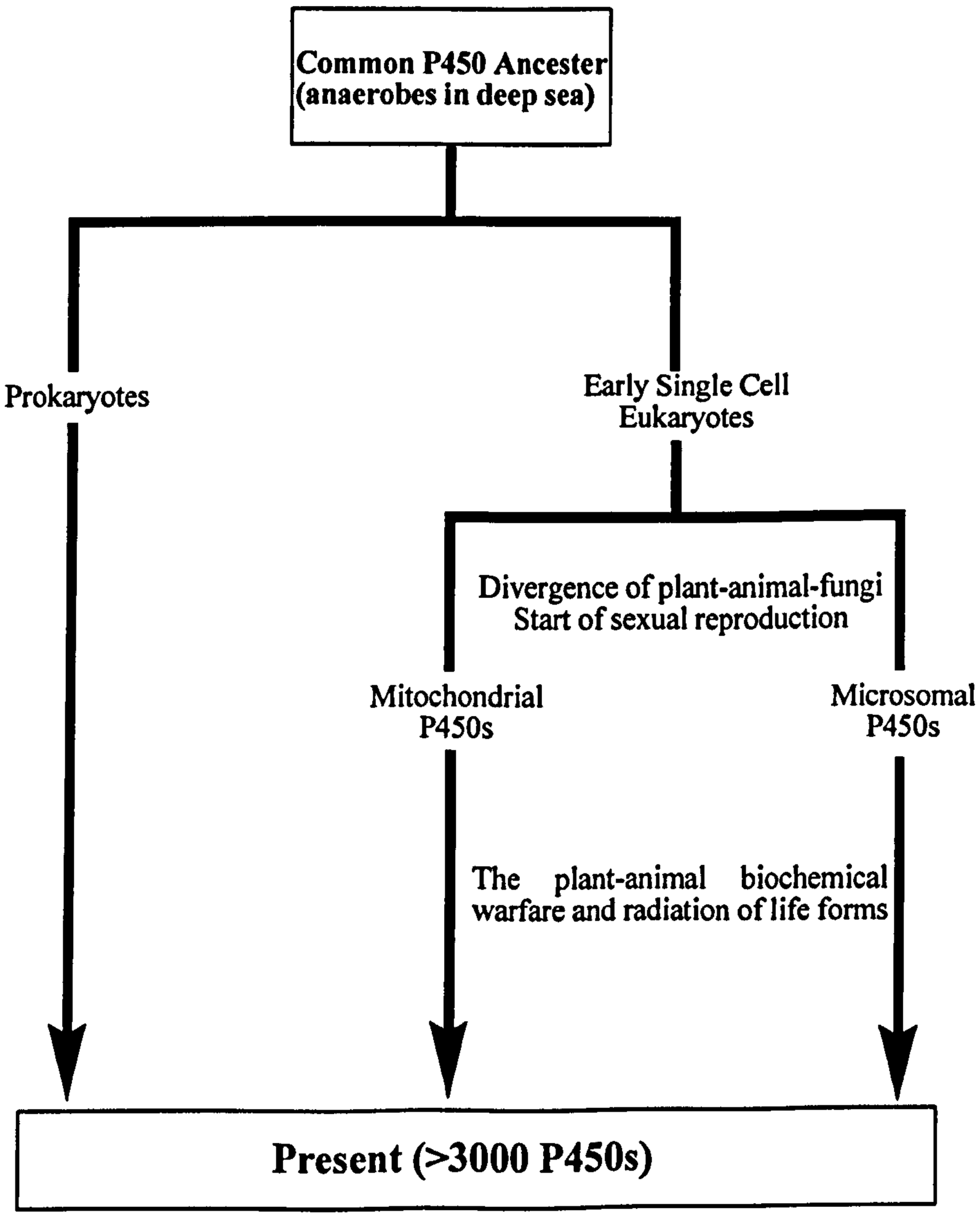

Figure 4: ***Tree diagram summarised the divergences of P450s and the major evolutionary events***

It was postulated by Nelson that the oldest P450 in prokaryotes and eukaryotes is CYP51[27,31]. CYP51 and its homologues are found in most life forms that synthesise sterols, these include bacteria, mammals, fungi and plants. Insects do not have CYP51, since they obtain sterols from their diet. However, the author believed that the remnant of this gene could still be present in the insect genome. CYP51 and its homologues are responsible for 14-α-demethylation of lanosterol skeleton in bacteria, fungi and animals, as well as 14α-demethylation of obtusifoliol skeleton in plants (Figure 5). This is a crucial stage in sterols biosynthesis as evidenced by the absence of a 14α-methyl group in all known functional sterols.

The evolution of life forms, which has progressed to complex multicellular organisms, presumably has necessitated signalling molecules that control inter- and intracellular communications. Ancestral P450s were expanded to accommodate these new roles, as evidenced by the fact that most of these signalling molecules, including steroid hormones and eicosanoids, are synthesised or partially synthesised by P450s.

As the divergence of animal-fungi-plant took place, we can see the beginning of the great animal-plant "biochemical warfare"[32]. P450s were further diverged in plants to synthesise toxic products that would prevent them being consumed by animals but on the other hand, animals also evolved to acquire a battery of P450s that could detoxify these harmful substances. Many plant substances such as flavonoids do possess properties that can alter animals physiological and biochemical processes[33-36]. *Homo sapiens* did not emerge as a distinct species until about 1 million years ago[2] and it is also widely accepted that our evolution was based on a largely vegetarian diet. Therefore, there is an intriguing possibility that plant substances such as flavonoids, could be an integral part of our exo-hormonal system that helps to maintain homeostasis

in our body (Potter and Tan, *unpublished hypothesis*). Animal P450s that evolved to metabolise these exo-hormones may play a regulatory role on exo-hormonal levels, as well as endogenous hormone metabolism.

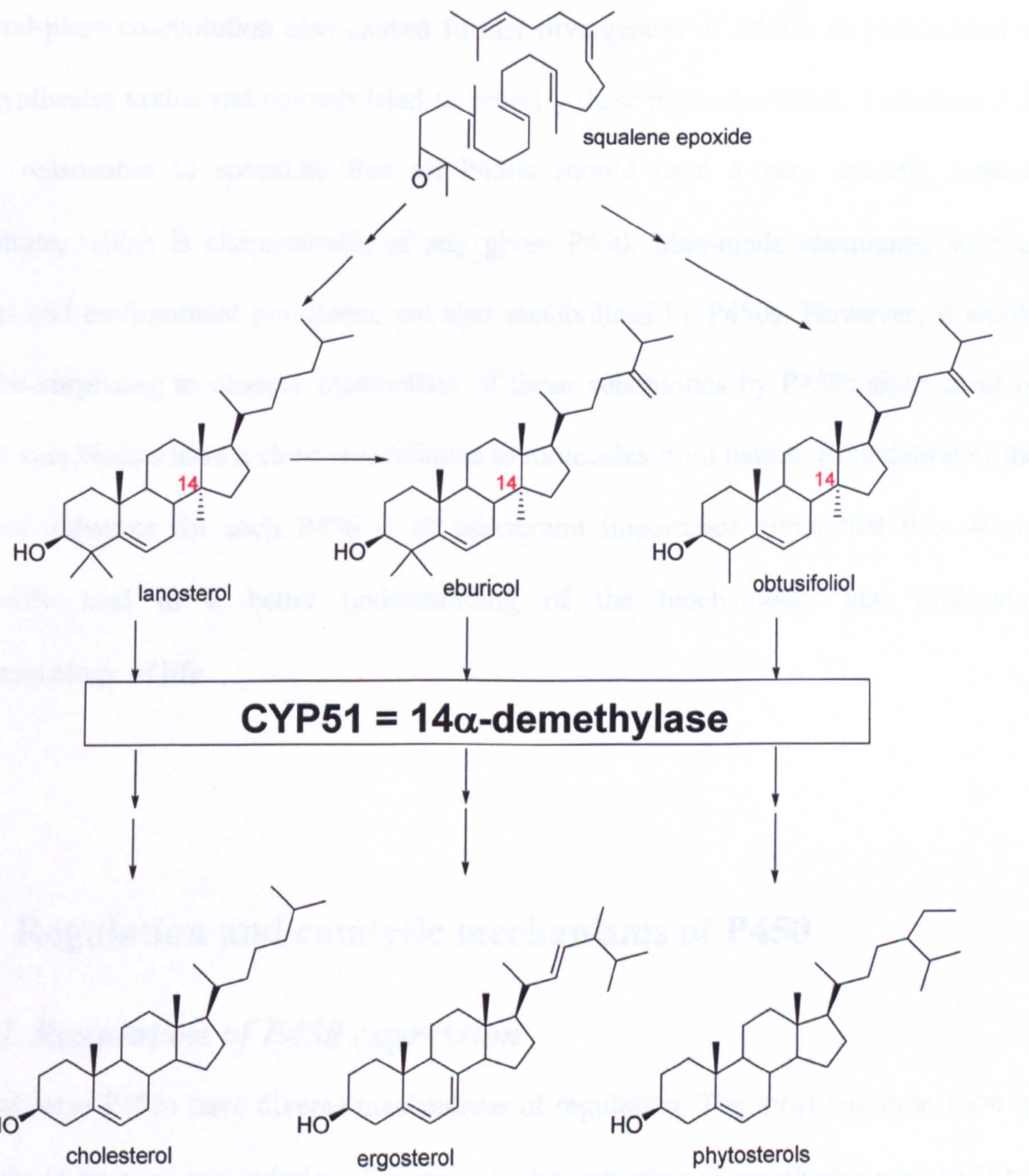

Figure 5: Biosynthesis of sterols from different organisms

Lanosterol is the natural substrate of CYP51 in yeast, bacteria and mammals. Eburicol and obtusifoliol are natural substrate of filamentous fungi and plants CYP51, respectively. The carbon-14 is indicated in red

The cytochrome P450 may have emerged as an enzyme to detoxify reactive oxygen species in anaerobes. As the earth's atmospheric oxygen rose, the enzymes subsequently acquired the ability to harness chemical potential of oxygen to biosynthesise and metabolise endogenous compounds such as steroids, fatty acids and eicosanoids. The animal-plant co-evolution also caused further divergences of P450s, as plants tried to biosynthesise toxins and animals tried to detoxify these phytochemicals. Therefore, it is very reasonable to speculate that all P450s should have a very specific ***natural*** substrate, which is characteristic of any given P450. Man-made chemicals, such as drugs and environment pollutants, are also metabolised by P450s. However, it would not be surprising to observe metabolism of these xenobiotics by P450s since most of these xenobiotics have a close resemblance to molecules from nature. Elucidation of the natural substrate for each P450 is of paramount importance given that this would probably lead to a better understanding of the biochemistry and molecular pharmacology of life.

1.2 Regulation and catalytic mechanisms of P450

1.2.1 Regulation of P450 expression

Cytochrome P450s have diverse mechanisms of regulation. The most common form is thought to be gene transcription, for example the induction of xenobiotic metabolising CYPs (eg. CYP1, CYP2, CYP3 and CYP4) by exogenous ligands[37,38]. Post-transcriptional mechanisms are involved, these include mRNA processing and stabilization. Lastly, post-translational mechanisms are also implicated. These are

thought to be mediated via protein stabilization and degradation through changes in the phosphorylation state of the enzyme.

The most extensively studied and characterised P450 with regard to its regulation is CYP1A1[39]. *CYP1A1* is a member of the polycyclic aromatic hydrocarbon (PAH) inducible gene family. The induction of this P450 involves activation of transcription via the aryl hydrocarbon receptor (AhR). AhR is a cytosolic receptor and is usually complexed with the molecular chaperone heat shock protein 90 (HSP90)[40], co-chaperone p23[41] and a tetratricopeptide repeat protein of the immunophilin family, variously termed as AhR-interacting protein (AIP)[42], AhR-associated protein 9 (ARA9)[43] and hepatitis B virus X-associated protein 2 (XAP2)[44]. The complexation of AhR and its cytosolic factors is thought to be essential to maintain AhR in a latent non-DNA binding mode as well as to maintain a conformational receptive state, ready for the binding of AhR ligands[41,45,46]. The AhR has a basic helix-loop-helix (bHLH) motif near the N-terminus[47]. Close to this motif is a region of around 300 amino acids sequence, referred to as *P*er-ARNT-*S*im (PAS) domain (*P*er and *S*im are *Drosophila* proteins), which ensues protein-protein interactions[48]. The AhR also contains a glutamine-rich C-terminus that is involved in nucleus translocation recognition.

It is generally accepted that upon binding of an AhR ligand, the HSP90 and other cytosolic factors will dissociate from AhR to facilitate nucleus translocation[49]. Inside the nucleus, the AhR-ligand complex dimerises with another bHLH/PAS transcription cofactor, i.e. the AhR nucleus translocator (ARNT), to form a mature transcriptional factor that will bind to DNA recognition site (xenobiotic responsive element, XRE) upstream to the *CYP1A1* gene and initiates gene transcription. However, Lees and Whitelaw[50] have shown that HSP90 only dissociates in the nucleus after secondary

dimerisation between AhR-ligand complex and ARNT. The authors suggested this concerted exchange of AhR partner proteins is necessary to avoid AhR degradation. AhR transcriptional activity is dependent on the phosphorylation state of the AhR itself[51]. Tyrosine phosphorylation, as well as phosphorylation of serine/threonine residues, has been shown to be required in DNA binding and transcriptional activity. The AhR pathway was found to activate gene expression of a factor designated as AhR-repressor[52]. The AhR-repressor competes with AhR for ARNT and this could form part of the regulatory circuit in the AhR pathway.

The AhR is a pleiotropic transcription factor. AhR has been shown to cross-talk with nuclear factor kappa B (NF-κB)[53], which itself also a pleiotropic transcription factor. NF-κB is a key factor in regulating the immune system and inflammatory responses, as well as responding to cellular and oxidative stress[54,55]. AhR has been found to be associated with apoptosis in murine hepatoma 1c1c7 cells by a mechanism that is independent of ARNT and exogenous AhR ligands[56]. AhR also cross-talk with hypoxia inducible signalling pathway in both inhibitory and additive manners[57]. These evidences shows that NF-κB, the AhR and hypoxia inducible pathways are interconnected in the regulation of angiogenesis, apoptosis, immune response as well as metabolism of endo- and exogenous compounds. The precise mechanistic control of these interconnected systems is currently unknown and remains to be fully elucidated.

1.2.2 Mechanism of P450 catalysed reactions

P450s catalyse biosynthesis and metabolism of a wide diversity of chemicals including endogenous substances and xenobiotics (either biological or man-made). Many reactions catalysed by P450s have been demonstrated, these include hydroxylation,

epoxidation, deamination, dealkylation, dehalogenation and even reduction.

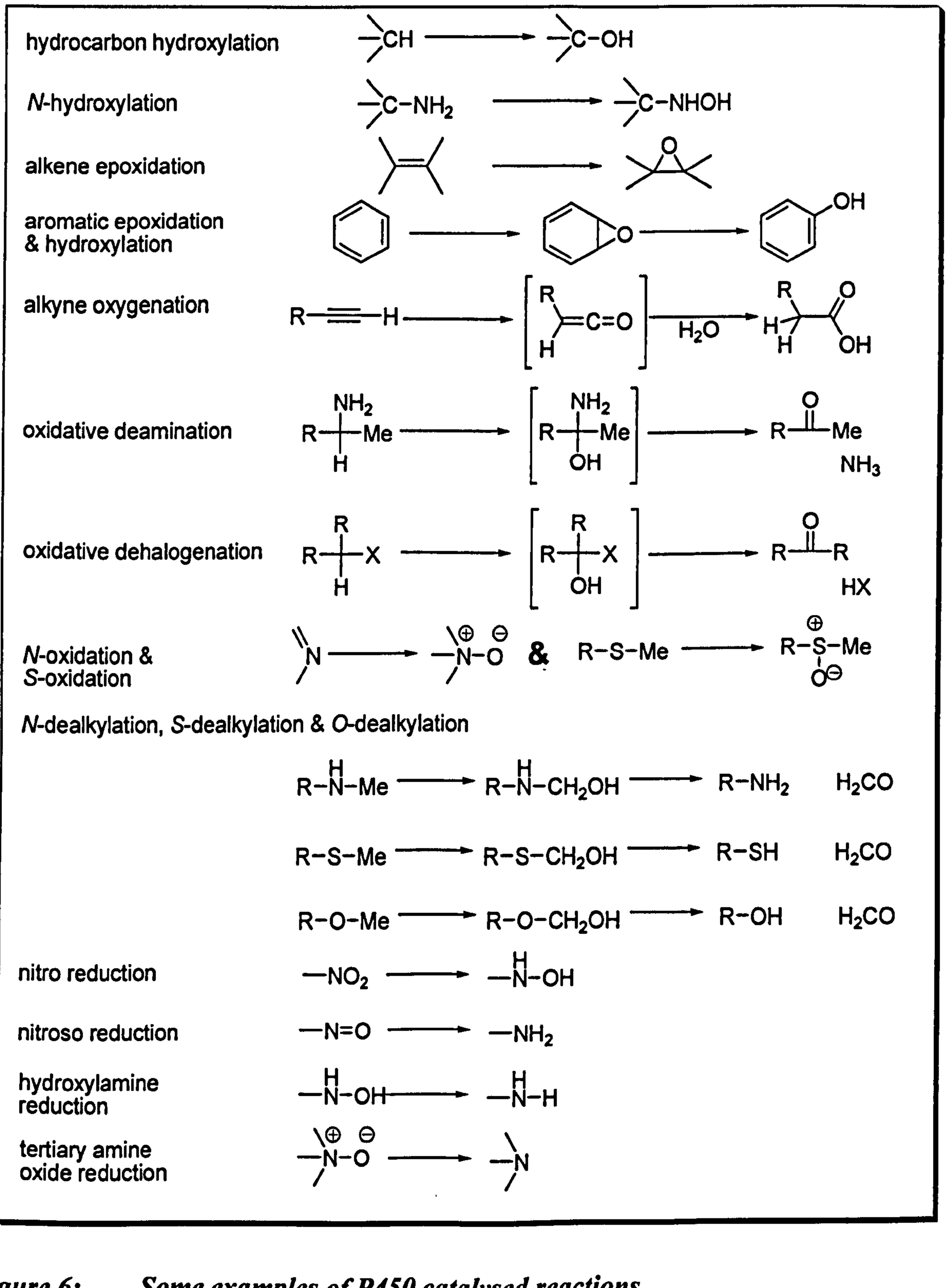

Figure 6: ***Some examples of P450 catalysed reactions***

The active site of P450 contains a *b*-haem, a complex between an iron atom and

protoporphylin IX. The prosthetic group is bound to the protein partly by hydrophobic forces. The fifth ligand of the haem is a thiolate anion provided by a cysteine residue from the apoprotein.

The substrates of P450 can be categorised into 3 main groups[58,59]. The first group termed Type I, are usually hydrophobic compounds. The haem of the P450 in free (resting) state is usually hexa-coordinated, with water molecule occupies the sixth coordinate site (see Figure 7; part (1)). This features a Fe(III) cation in a stable, low spin configuration with very low reduction potential (-300mV). Upon binding of a Type I substrate, the water molecule is lost from the Fe(III) which results in a Fe(III) high spin configuration. The substrate at this stage does not bind to the haem but is held in the substrate binding pocket via various hydrophobic and hydrogen-bonding interactions[60-62]. The high spin configuration increased the cation reduction potential to -170mV which is mandatory for the P450 catalytic reaction. The increase in reduction potential yields a greater electromotive force for the subsequent electron transfer from NADPH-cytochrome P450 reductase (Figure 7; part (A)).

The shift from low to high spin state induced by Type I substrates can be observed in a characteristic UV spectral change, with an absorption maximum at around 390nm and a minimum at around 420nm[59]. Type II substrates however, are mainly nitrogenous bases and are thought to ligate (via the lone pair electrons on the nitrogen atom) to the haem iron of P450. This hexa-coordinate configuration results in a low spin state, with a characteristic UV spectral change with absorption maximum around 430~435nm and minimum around 385~390nm. The third group of P450 substrates are the reverse Type I substrates. They were formerly designated as modified Type II[59], due to the close resemblance of spectral change (maximum at 420nm and a trough at 390) to Type II

compounds. The reserve Type I spectral change is thought to be the result of displacement of the bound endogenous Type I substrate from the P450 binding site[63,64].

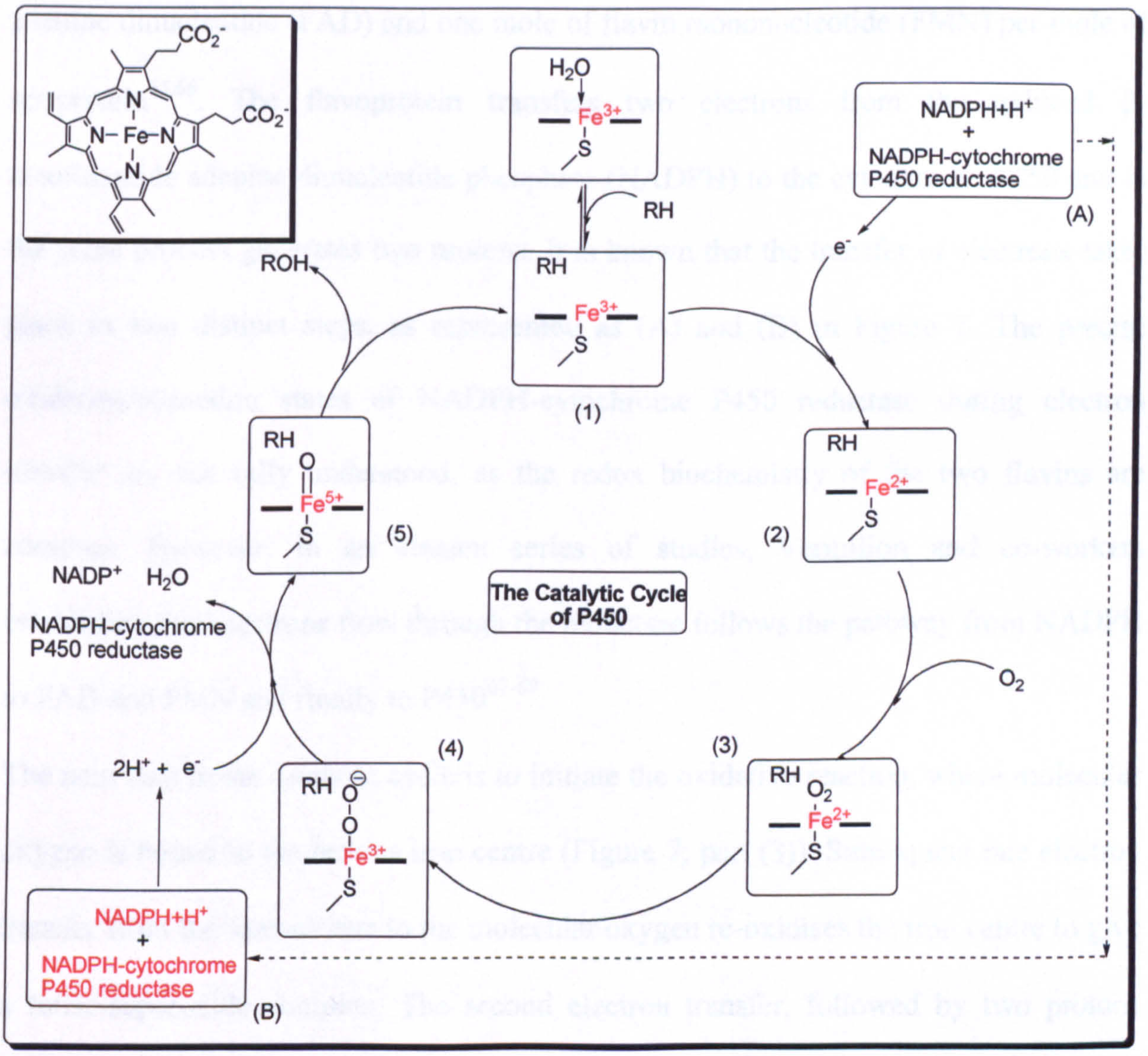

Figure 7: The cytochrome P450 catalytic cycle

The penta-coordinated haem is shown in (1) with its fifth ligand cysteine residue from the P450 apoprotein (shown as -S-). (A) and (B) represent the sequential electrons transfer and (1) to (5) are steps in the P450 oxidation leading to a hydroxylated product. The inlet showed the iron protoporphylin prosthetic group. RH = substrate; ROH = hydroxylated product.

The first electron for the reduction of Fe(III) to Fe(II) is provided by the NADPH-cytochrome P450 reductase. The NADPH-cytochrome P450 reductase is a flavin-containing enzyme. Each one of this flavoprotein is made up with one mole of flavin adenine dinucleotide (FAD) and one mole of flavin mononucleotide (FMN) per mole of apoprotein[65,66]. The flavoprotein transfers two electrons from the reduced β-nicotinamide adenine dinucleotide phosphate (NADPH) to the cytochrome P450 and in the same process generates two protons. It is known that the transfer of electrons takes place in two distinct steps, as represented as (A) and (B) in Figure 7. The precise oxidation/reduction states of NADPH-cytochrome P450 reductase during electron transfer are not fully understood, as the redox biochemistry of the two flavins are complex. However, in an elegant series of studies, Vermilion and co-workers established that electrons flow through the reductase follows the pathway from NADPH to FAD and FMN and finally to P450[67-69].

The next step in the catalytic cycle is to initiate the oxidative reaction, where molecular oxygen is bound to the ferrous iron centre (Figure 7; part (3)). Subsequent one electron transfer from the ferrous iron to the molecular oxygen re-oxidises the iron centre to give a ferric-superoxide complex. The second electron transfer, followed by two protons from the reductase, yields a Fe(V)-oxo complex.

The Fe(V)=O species is highly electrophilic that would react with electron-rich centres of substrates like double bonds of alkenes and arenes, lone pair electrons of heteroatoms, or electrons involved in C-H bond. Oxygen insertion into the substrate is believed to involve hydrogen abstraction from the substrate. Recombination of the resulting transient hydroxyl and carbon radical gives the product and restores the P450 to its starting ferric state (Figure 8) [70].

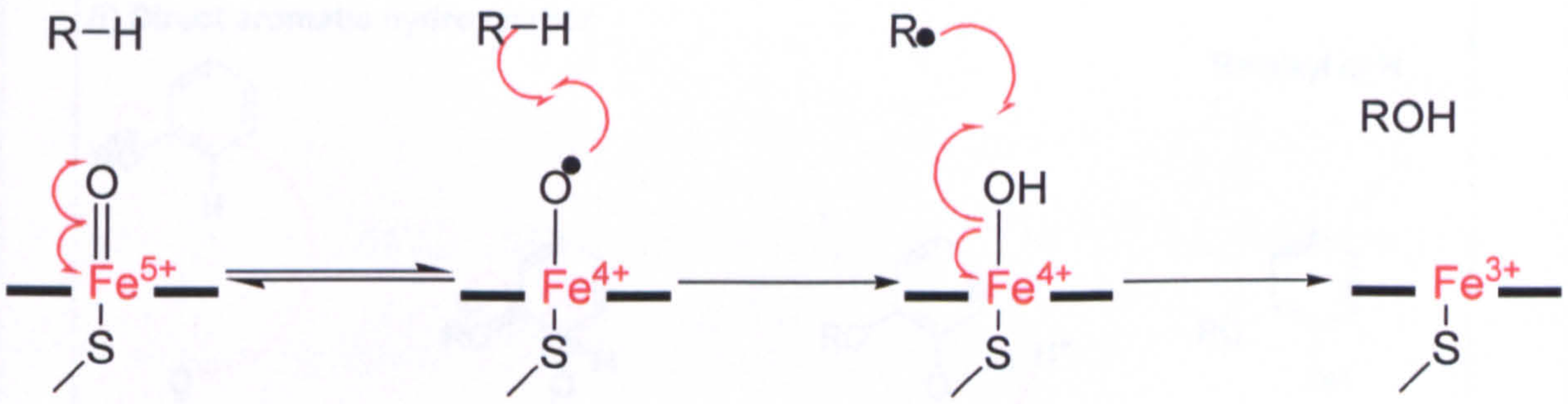

Figure 8: Hydroxylation of substrate (RH) by cytochrome P450

It is thought that a Fe(IV)-O radical is involved. The transient Fe(V) and Fe(IV) equilibrium is believed to be stabilised by the cysteine axial ligand, and by ligand-to-metal charge transfer from the macro cyclic and highly delocalised prophyrin ring.

Potter (*personal communication*, unpublished hypothesis) proposed an alternative mechanism, which was thought to be more energetically favourable, in the final stage of oxygen insertion in P450 catalysed oxidation. The mechanism involved the Fe(V)=O species directly with the aid of mesomeric effects of the lone pair electrons on the oxygen atom (Figure 9; (i)). This requires substrate temporary bound to the ferric haem centre before rearranging to give the hydroxylated product. Direct hydrogen abstraction from aliphatic substrate may also take place since the Fe(V)=O centre is highly electrophilic. In this case, it is best illustrated by *O*-demethylation shown in Figure 9(ii).

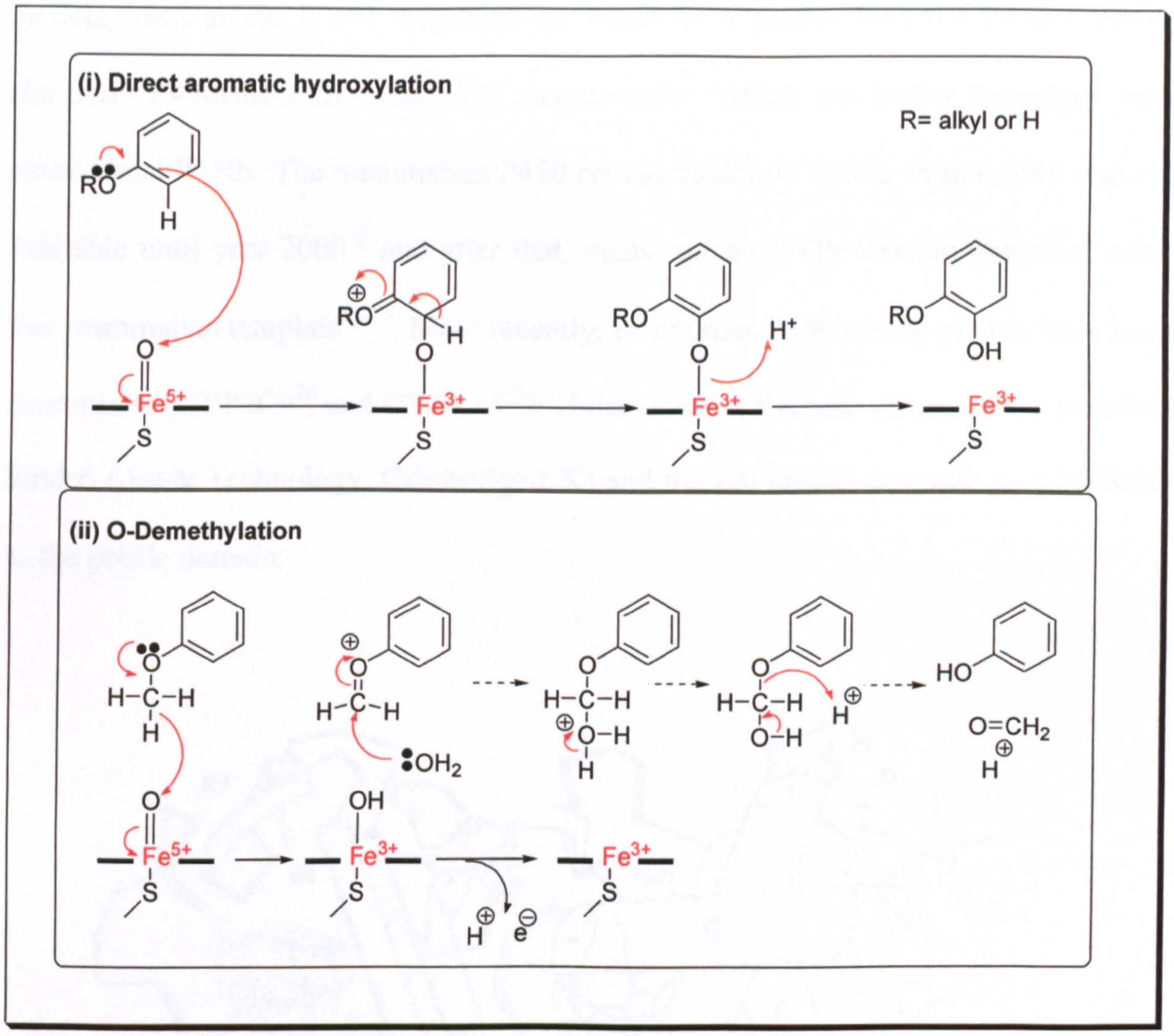

Figure 9: Alternative mechanism in P450 catalysed oxidation

The mechanism proposed by Professor Gerry Potter which involves the Fe(V)=O species directly as opposed to the mechanism shown in Figure 8.

1.2.3 Molecular modelling of P450 enzymes

Earlier studies on the relationships of structure to function in the P450s have been limited by the lack of three-dimensional (3D) crystal structure for a mammalian P450. Older mammalian P450 molecular models are based on the known structure of CYP101 ($P450_{cam}$)[61], a cytosolic bacterial P450 from *Pseudomonas putida* that only shares 10~20% primary sequence homology with its mammalian counterparts[60]. Some other

models, such as the CYP1 enzymes, are based on a unique bacterial P450 CYP102 (formerly P450BM-3 from *Bacillus megaterium*)[71] which has higher homology with microsomal P450s. The mammalian P450 crystal model (CYP2C5 from rabbit) was not available until year 2000[72] and after that, many human CYPs were re-modelled using this mammalian template[73-75]. More recently, two human P450 crystal models have been determined (CYP2C9[76] and CYP3A4[77]). Unfortunately, the both projects were privately funded (Astek Technology, Cambridge UK) and the full crystal structure is unavailable to the public domain.

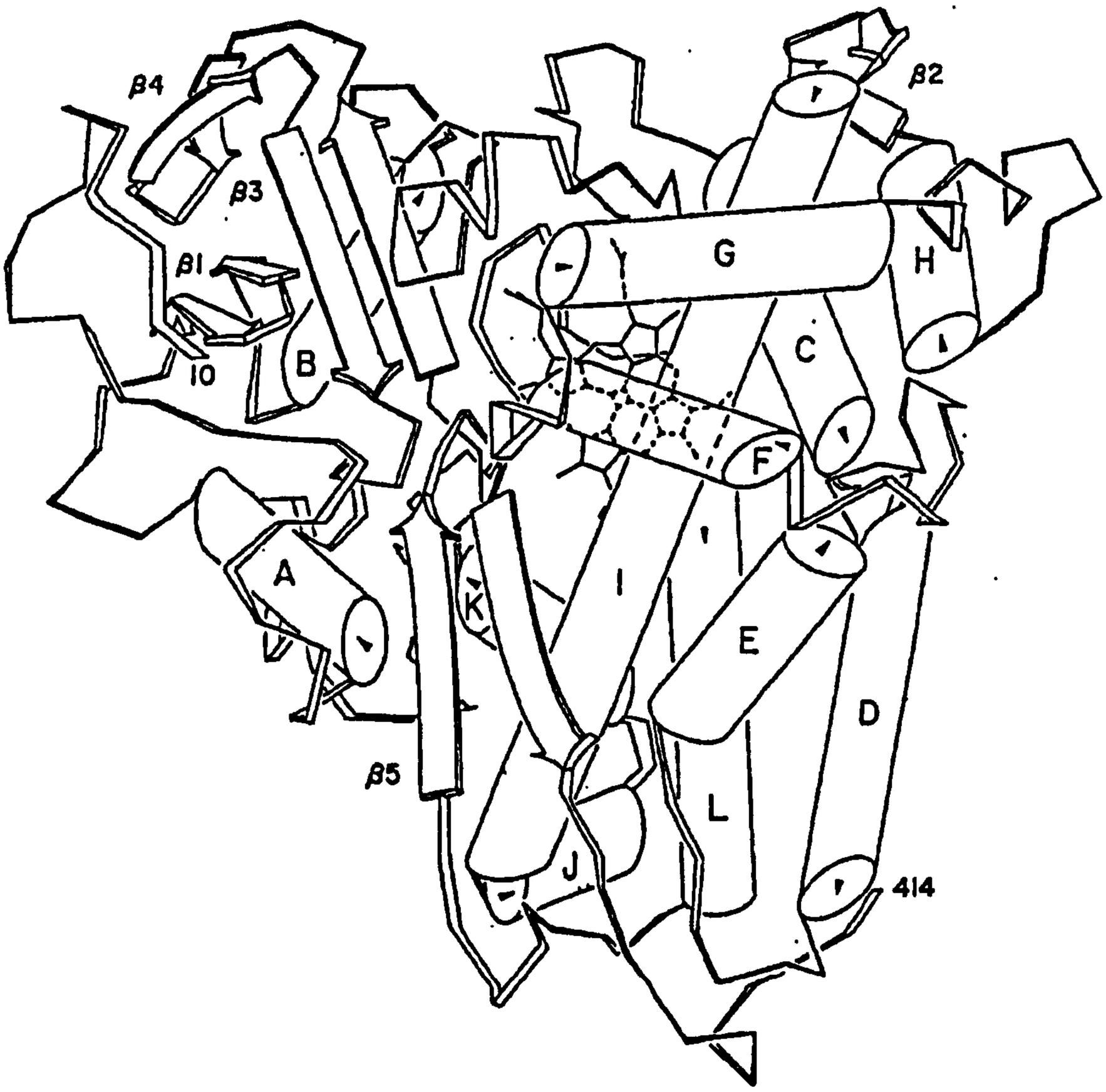

Figure 10: The crystal model of CYP101 ($P450_{cam}$)

The rods labelled A-L are α-helices and the antiparallel β-sheets are represented by broad arrows (β1-β5).

Adapted from Poulos *et al*[61].

Studies on the available P450 crystal models[72,78] demonstrate the dramatic similarity in tertiary structural elements between different P450s, even though these proteins only share very low primary sequence homology, as well as the number of amino acids in each enzymes. The crystal structures of P450s resemble a triangular prism, with approximately 45% α-helices, 15% antiparallel β-sheet structures and the remaining as random loops. Although the α-helices are distributed throughout the polypeptide chain, tertiary structure reveals an asymmetrical arrangement, with helices clustered on one side and the β-sheets located near the N-terminal of the protein (see Figure 10). In microsomal P450s, the N-terminus sequences contain highly hydrophobic amino acids residues, termed the signal-anchor (SA) sequences[79], which are important to afford membrane anchorage[80]. On the contrary, the membrane bound mature mitochondrial P450s do not contain the SA sequence, indicating other hydrophobic surface of the protein responsible for membrane anchorage. The crystal structure of the microsomal P450 CYP2C5 confirmed the above assumption by showing a hydrophobic surface of the P450, formed by non-contiguous portions of the polypeptide chain, interacted with endoplasmic reticulum (ER)[72]. The study also showed that the interaction of the hydrophobic surface with ER places the entrance of the substrate access channel in or near the membrane. This configuration orients the proximal face of the protein and the prosthetic group perpendicular to the plane of ER for interaction with the NADPH-cytochrome P450 reductase (Figure 1; page 19).

As a result of difficulties in obtaining crystal for each individual P450 enzyme, the 3D structure for most of the P450s were constructed based on homology modelling techniques, employing special software packages and specially built computer workstation[71,73-75]. In any homology modelling study, amino acids sequence of the

target protein is aligned with the sequence of the homologue for which the 3D structure is known. This exercise is to identify those residues which comprise secondary structural elements (α-helices and β-sheets) that can be then assembled into a whole 3D structure. However, as a result of different number of amino acid in each individual P450, the assignment of secondary structure is poor. This is compensated by truncation and/or addition of amino acids into the target protein though this exercise has severely compromised the accuracy of the final model.

1.3 Cancer and the P450 CYP1 family enzymes

1.3.1 Cancer

Cancer is a disease that arises from stepwise accumulation of genetic changes in normal cells. These changes liberate neoplastic cells from the homeostatic mechanisms that govern normal cell death and cell proliferation. Cancer can manifest itself in many forms, including both solid tumours and leukaemias. These cancer cells will grow out of control and invade, erode and destroy normal tissues.

Over one in three people will be diagnosed with cancer during their lifetime. In year 2002, more than 270,000 new cases of cancer were diagnosed in the UK[81]. There are over 200 different types of cancer, but the four major types which are lung, breast, prostate and colorectal, account for over half of all cases diagnosed.

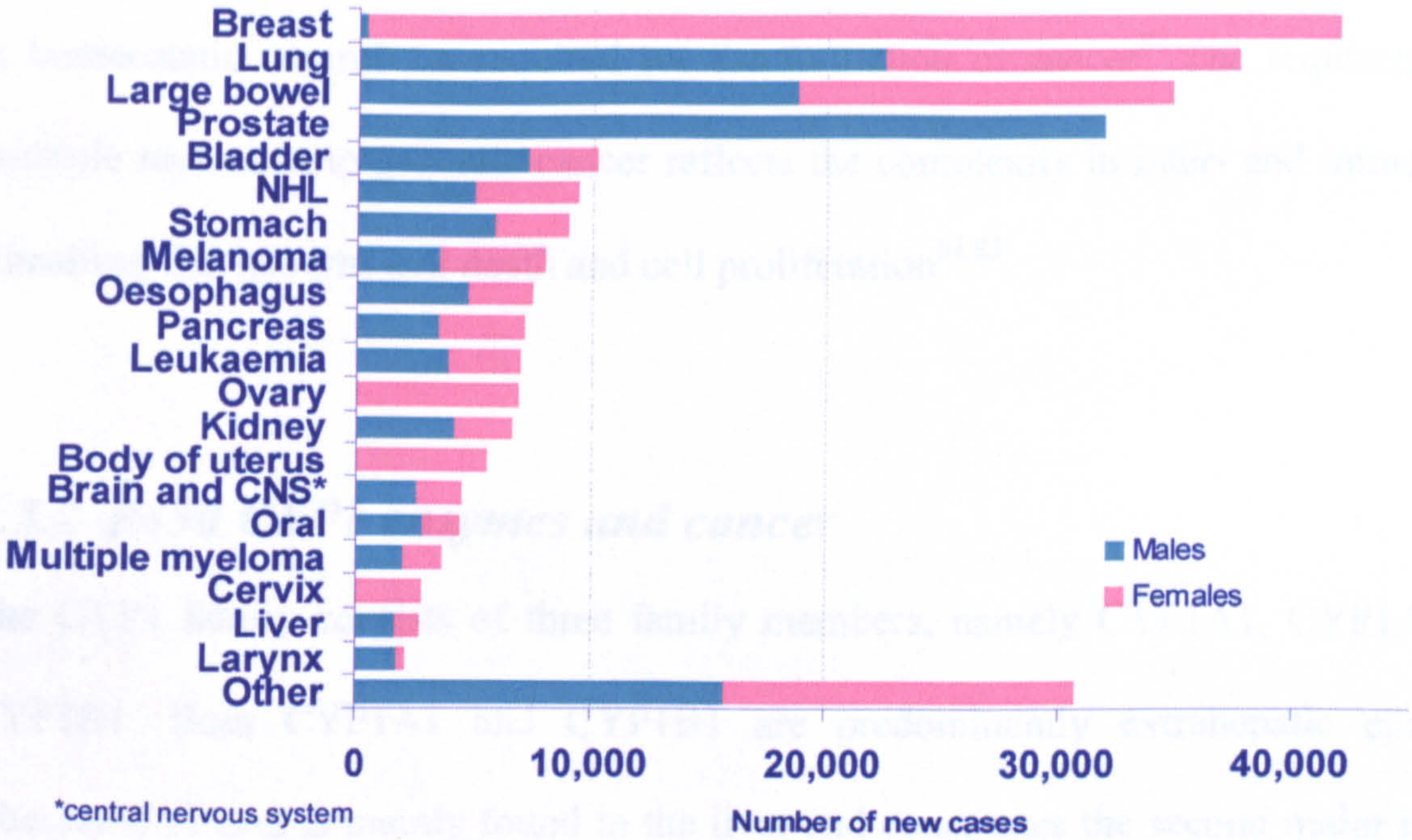

Figure 11: UK Cancer Incidence 2002

The 20 most commonly diagnosed cancer in UK. Adapted from Cancer Research UK[81].

Cancer was the cause of more than a quarter of all deaths in the UK in 2003 and amongst these cases, 22% was caused by cancer of the lung and a quarter from cancers of the large bowel, breast and prostate[82]. Cigarette smoking has been identified as the single most important cause of cancer. Overall, one third of all cancer related deaths, including around 90% of lung cancer deaths, were linked to tobacco smoking. Apart from cigarette smoking, an individual's risk of developing cancer depends on many factors including diet, life style and genetic inheritance.

Carcinogenesis, the process by which cancers are generated, is a multistep mechanism where accumulation of genetic errors affects vital regulatory pathways. Cancer is initiated in a single cell (clonal origin) which then multiplies and acquires further changes that give the population a survival advantage over the normal cells. The altered cells then multiply to generate millions of cells that constitute a clinical cancer. It has

been estimated that in the human population four to six somatic mutations in genes vital in homeostatic control are required for the formation of cancer[83].The requirement of multiple mutations to generate cancer reflects the complexity in inter- and intracellular signalling that governs cell death and cell proliferation[84,85].

1.3.2 P450 CYP1 enzymes and cancer

The CYP1 family consists of three family members, namely CYP1A1, CYP1A2 and CYP1B1. Both CYP1A1 and CYP1B1 are predominantly extrahepatic enzymes, whereas CYP1A2 is mainly found in the liver and constitutes the second major hepatic P450 enzyme after CYP3A4[86]. The CYP1 enzymes are highly conserved in the animal kingdom and are the only few P450s that have retained the same designation in all species.

As a result of their induction by xenobiotics, studies on CYP1 enzymes have mainly focused on their metabolic capabilities to bioactivate carcinogens. One good example is the extrahepatic activation of the steroid hormone 17β-estradiol by CYP1A1 and CYP1A2 to its carcinogenic metabolite 4-hydroxyestradiol (4OH-E2)[87,88]. It is thought that 4OH-E2 exerts its mutagenic effect by undergoing redox cycling that results in the generation of reactive semiquinone/quinone intermediates that damage DNA by alkylation[89-93]. CYP1 enzymes are also capable of bioactivating a wide range polycyclic aromatic hydrocarbons (PAH) and polycyclic aromatic amines (PAA)[94-98]. The enzymes' capabilities to activate procarcinogens to their ultimate mutagenic species have led to CYP1 enzymes being implicated in chemical-induced carcinogenesis.

1.3.3 CYP1B1- The gateway to tumour selective chemotherapy

CYP1B1 was first identified in mouse embryonic fibroblasts[99] and later the human homologue was identified in a keratinocyte cell line treated with 3,4,7,8-tetrachlorodibenzo-*p*-dioxin (TCDD)[100]. Shortly thereafter, the protein was characterised and designation of a new subfamily CYP1B was warranted due to its distinction from the other CYP1A proteins[101].

Many studies on the tissue expression of CYP1B1 have concentrated on the detection of *CYP1B1* mRNA using reverse transcriptase polymerase chain reaction (RT-PCR)[98,102,103] and it is clearly evident that CYP1B1 is expressed extrahepatically. However, these authors did not address the existence of functionally competent CYP1B1 in the tissues they had examined. It has been shown that there is a poor correlation between mRNA and the corresponding protein expression[104-106] and therefore, presence of *CYP1B1* mRNA cannot proof that CYP1B1 protein is also expressed.

Using immunohistochemistry, Murray and co-workers[107] have demonstrated that CYP1B1 protein was present in tumours derived from the bladder, brain, breast, colon, connective tissues, kidney, liver, lung, lymph nodes, oesophagus, ovary, skin, small intestine, stomach, testis and uterus. The presence of CYP1B1 was not detected in corresponding normal tissues though *CYP1B1* mRNA was detectable. This observation has led to believe that regulation of CYP1B1 in tumours is predominantly post-transcriptional and possibly involves the use of alternative polyadenylation sites, resulting in altered mRNA stability[108].

Although CYP1B1 is highly overexpressed in tumours cells[107,109-117], not all tumours contain the enzyme[109,110]. In a study performed by Gibson *et. al.*, CYP1B1 was also

found in tumour-associated smooth muscle, blood vessel pericytes and macrophages[110]. It is possible that, during cancer progression, signalling molecules, produced by cancer cell induce the expression of CYP1B1 in surrounding tissues. Interestingly, CYP1B1 has been demonstrated as an important modulator in mice retinal vascular homeostasis and is required for hypoxia-induced neovascularisation[118]. Moreover, *AhR* knock out experiments in mice have shown abnormal liver growth and poor vascularisation, as well as abnormality in epidermal development[119-121]. These evidences are highly indicative CYP1B1 being involved in angiogenesis and vascularisation during foetal development. Hypoxia inducible pathway has been shown to cross-talk with the AhR pathway[57]. It is probable that during foetal development, hypoxic conditions in rapidly growing tissues induce the expression of CYP1B1 via a still unidentified mechanism. The expressed protein can then metabolise an endogenous substrate to form a pro-angiogenic signalling molecule that directs formation of new blood vessels to the hypoxic tissues. As tumours progress, dedifferentiation of cancer cells regress the cells back to foetal-alike state. Tumour cells may therefore hijack the foetal angiogenic mechanism to counter the hypoxic environment which is usually observed in most solid tumours. Consequently, the above hypothesis may partly explain the tumour selective expression of CYP1B1.

There is indisputable evidence to show that CYP1 enzymes do activate procarcinogens to their ultimate mutagenic metabolites and hence the enzymes are considered to be carcinogenic. However, we have to comprehend that most of these mutagenic compounds are man-made, synthesised perhaps in the past 200 years as a result of industrial revolution and advancement in organic chemistry. Thus, CYP1 enzymes are not evolved to metabolise these xenobiotics. The capabilities of CYP1 enzymes to

metabolise these compounds are probably due to their structural similarity to 17β-estradiol, the only known endogenous substrate for the CYP1 mono-oxygenases.

Contrary to the carcinogenic theory, Potter *et. al.* believe that CYP1B1 maybe functions as tumour specific rescue enzyme, utilised natural anticancer prodrugs in diet to selectively destroy the malignant tumours[122]. The hypothesis is supported by the fact that resveratrol, a dietary phytoestrogen found in grapes and peanuts, was converted to piceatannol *in vitro* by CYP1B1[123]. CYP1B1 also catalysed formation of two more metabolites termed M1 and M3 from resveratrol. The identities of these two metabolites have been recently resolved with authentic standards as trans-3,4,5,4'-tetrahydroxystilbene and trans-3,4,5,3',4'-pentahydroxystilbene, respectively (Potter *et. al.*, unpublished observations; Figure 12). Piceatannol[124-126] and trans-3,4,5,4'-tetrahydroxystilbene[127] are known anticancer agents. M3 may undergo isomerisation to form cis-M3. cis-3,4,5,3',4'-Pentahydroxystilbene may possess similar anti-tumour activity due to its striking resemblance to a highly potent anticancer agent combrestatin A4[128].

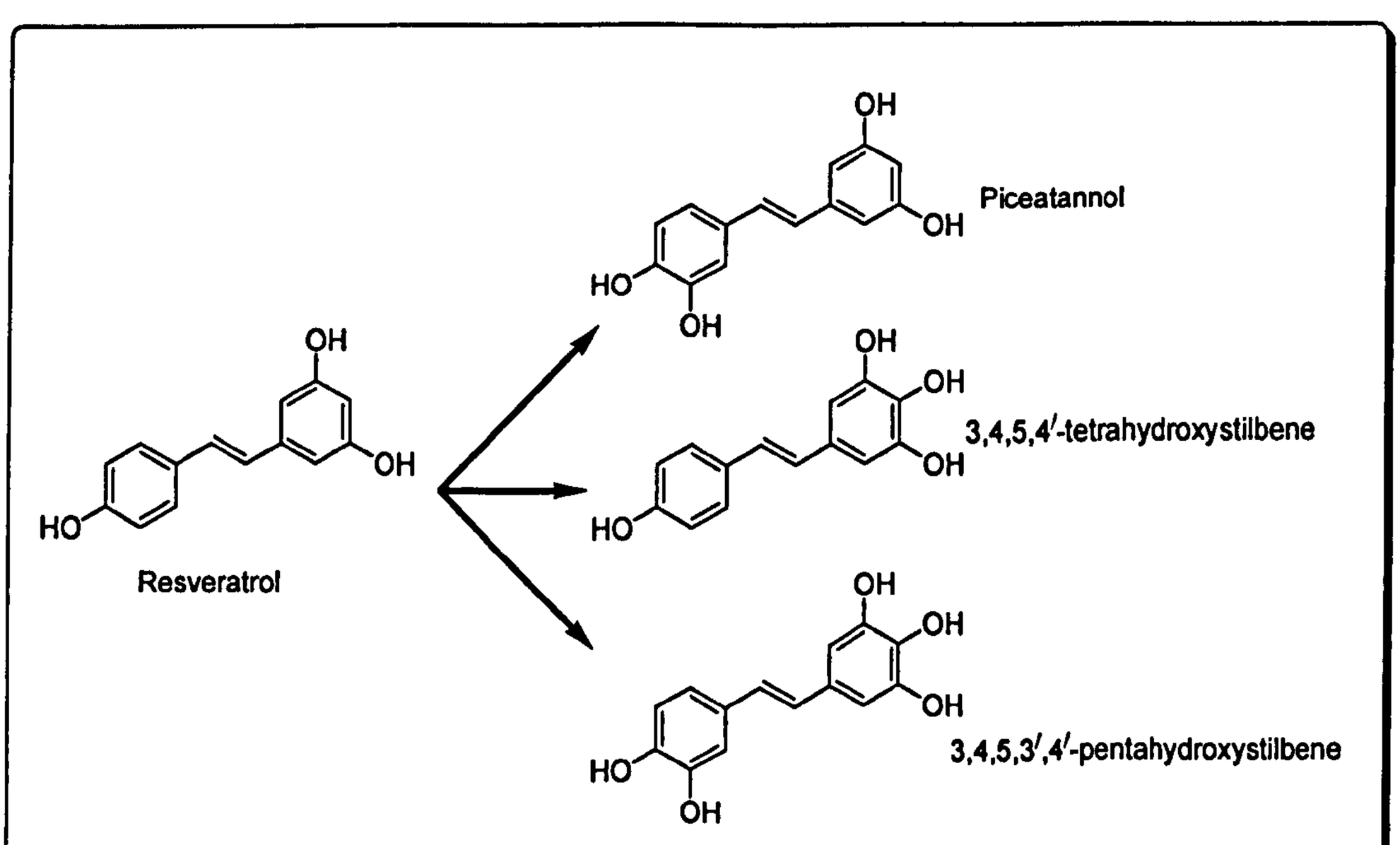

Figure 12: In vitro metabolism of resveratrol by CYP1B1

Most of the current chemotherapeutics in clinical uses are cytotoxic. As a general perception that natural anticancer agents have to be as cytotoxic as their synthetic counterparts, most medicinal phytochemists have so far been searching for more and more cytotoxic natural compounds in the hope that these toxins can be developed into mainstream treatment for cancers. This may lead to novel compounds for cancer treatment but due to the non-specific toxicity of these compounds, patients may suffer from debilitating or even lethal side effects.

The discovery of specific bioactivation of resveratrol by CYP1B1 to cytotoxic species has shown that non toxic natural molecules present in human diet could prevent tumours developing by producing anticancer molecules within the cancer cells. This elegant piece of work has for the first time demonstrated the molecular mechanism on how dietary components can exert their anticancer properties through specific enzyme bioactivation. Since this discovery, more of these beneficial natural molecules have been discovered and they are now collectively called ***Salvestrols*** (Potter *et. al.*, www.naturesdefence.com). These newly identified Salvestrols have turned out to be far more powerful and life-protecting than resveratrol.

Although the exact role of CYP1B1 in carcinogenesis and cancer progression still remains a hotly debated issue, the tumour overexpression of CYP1B1 has provided a gateway to selectively target cancer cells by employing novel anticancer prodrugs that will specifically activated by CYP1B1. The intracellular bioactivation of anticancer prodrug has the advantage of significant reduction in severe side-effects since the anticancer agent would only be produced within cancer cells that expressed CYP1B1.

1.4 Aim of research

As part of the continuing drug discovery programme at Cancer Drug Discovery Group within the Leicester School of Pharmacy, this Ph.D. research is set up to investigate the structure-activity relationships (SAR) of the cytochrome P450 CYP1B1 enzyme. The SAR determined by the inhibitor studies will allow the design of selective substrates for the CYP1 family enzymes. This is important because CYP1A2 is a major hepatic enzyme whereas CYP1B1 is overexpressed in tumours. The SAR information will allow the design of prodrugs that are selectively activated by CYP1B1 in tumours and hence would reduce any potential hepatotoxicity. Furthermore, it is also important to differentiate the active sites of both CYP1A1 and CYP1B1. CYP1A1 expression is highly elevated in cancer of prostate[129], stomach[130,131] and bladder[132]. CYP1A1 protein also highly elevated in some inflammatory diseases[133]. The SAR information on CYP1A1 will allow the design of CYP1A1 selective prodrugs for the treatment of the mentioned ailments.

In summary, the aim of this project is:

- To synthesise a range of potential CYP1B1 inhibitors in order to probe the enzyme's active site.
- To differentiate between the active sites of the CYP1 family enzymes, CYP1A1, CYP1A2 and CYP1B1.
- To use the SAR of CYP1B1 inhibitors to guide future selective prodrug design.

Chapter 2

Probing the Active Site of CYP1 Enzymes Using Nitrogen Heterocyclic Chalcones

2.1 Introduction

2.1.1 Potential application of selective inhibitor of the CYP1 family enzymes

In an effort to improve CYP1B1 selectivity of future prodrugs, this project was commissioned to define the structure-activity relationships (SAR) of the CYP1 mono-oxygenases. The gathered SAR data would aid future prodrug design and the inhibitors identified from this research would potentially have other applications. One such possible use would be as a specific inhibitor to determine substrate selectivity for *in vitro* drug metabolism and pharmacokinetics (DMPK) studies.

CYP1A2 is the main hepatic P450 after CYP3A4 and is responsible for metabolic degradation of many drugs in current clinical use. Selective CYP1A2 inhibitors with low intrinsic toxicity might be co-formulated with these therapeutic agents to improve the half-life of the drugs. This would allow less frequent dosing which would subsequently lead to an increase in patient's compliance, and may also help to reduce possible side-effects associated with frequent repeat dosing. CYP1A1 is mainly an extra-hepatic P450 and a selective CYP1A1 inhibitor could be used in the same way as above to inhibit extra-hepatic metabolism of clinical therapeutics.

Recently, CYP1B1 has been shown to interact with current anticancer agents such as flutamide, docetaxel, paclitaxel, bleomycin, methotrexate, epirubicin and mytomycin C[134,135]. *In vitro* studies have shown that the presence of CYP1B1 reduces the efficacy of docetaxel[135,136]. Specific CYP1B1 inhibitors with favourable toxicological and pharmacological profiles may be co-administered with current chemotherapeutics to enhance their anticancer properties.

2.1.2 Development of CYP1B1 activated anticancer prodrugs

There is an urgent need for more selective anticancer drugs. Current chemotherapeutic agents are cytotoxic to tumours and to normal tissues. Although certain tumours are highly sensitive to chemotherapy, many others are not, and in some cases chemotherapy actually increases morbidity and mortality. A major aim in cancer chemotherapy is to selectively kill cancer cells whilst sparing normal ones. Research into different protein expression patterns in tumour cells will allow the distinction between tumour and normal cells, hence providing targets for new anti-tumour medicines.

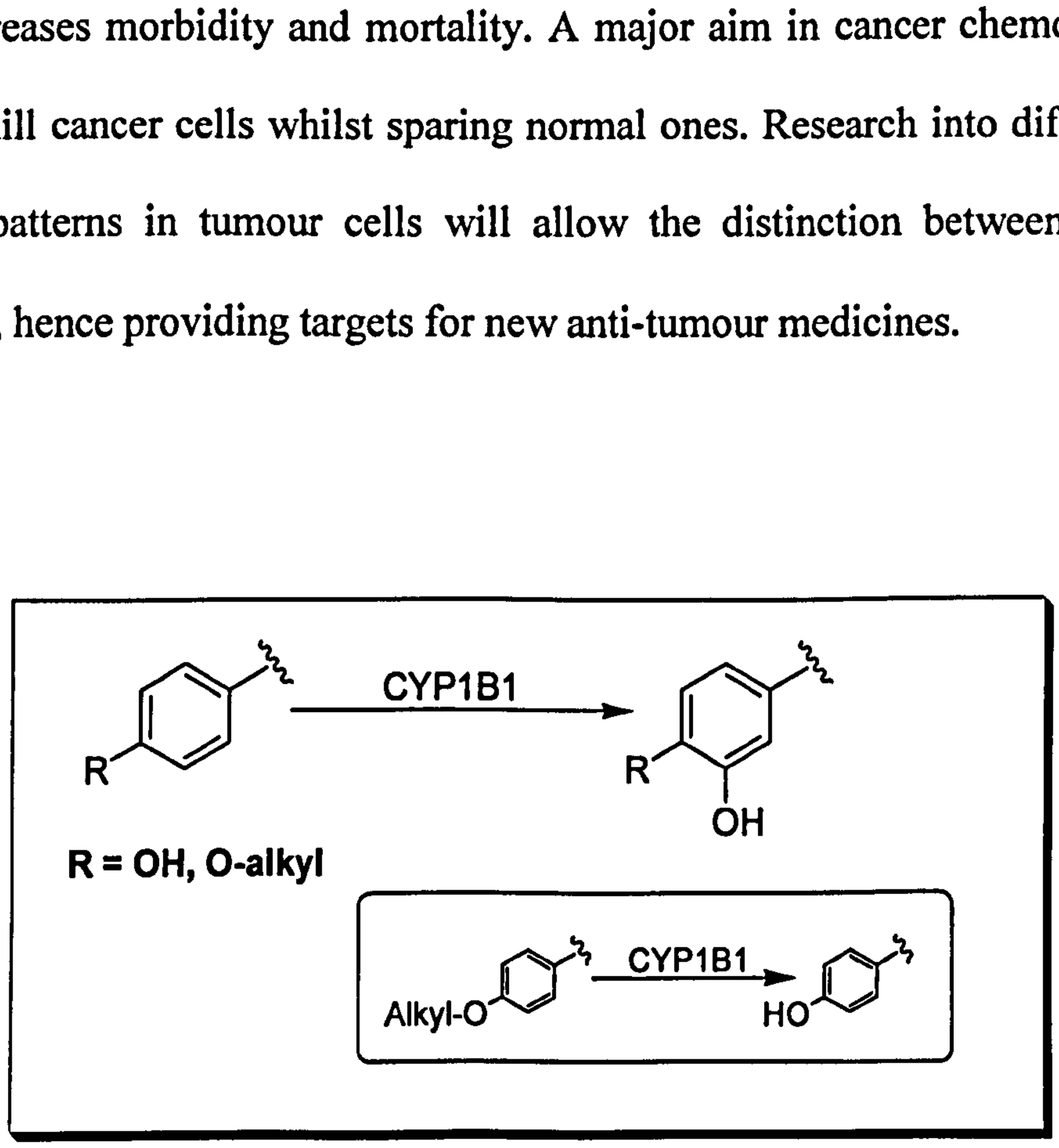

Figure 13: Aromatic hydroxylation reaction catalysed by CYP1B1

Apart from catalysing direct aromatic hydroxylation, CYP1B1 also catalyses *O*-dealkylation reaction (see inlet).

It is no exaggeration to say that the discovery of overexpression of CYP1B1 in tumours[107] is one of the most important revelations in cancer research for the past twenty years. The presence of a specific yet functionally competent enzyme within tumours has provided medicinal chemists a gateway to design prodrugs that would be selectively activated by this enzyme[137,138].

Potter and co-workers have successfully synthesised a range of novel tumour selective anticancer prodrugs that were designed to be activated by CYP1B1 aromatic hydroxylation (Figure 13). One of such novel compounds is DMU212 (Stilserene®), which will enter phase I clinical trial soon. However, this compound is not bioactivated exclusively by CYP1B1[139], in fact, other CYP1 enzymes (CYP1A1 and CYP1A2) also catalysed the same bioactivation as CYP1B1. Nevertheless, DMU212 has shown significant improvement in term of tumour selectivity[140] and has been shown to cause no side effects on animals in toxicology studies[141].

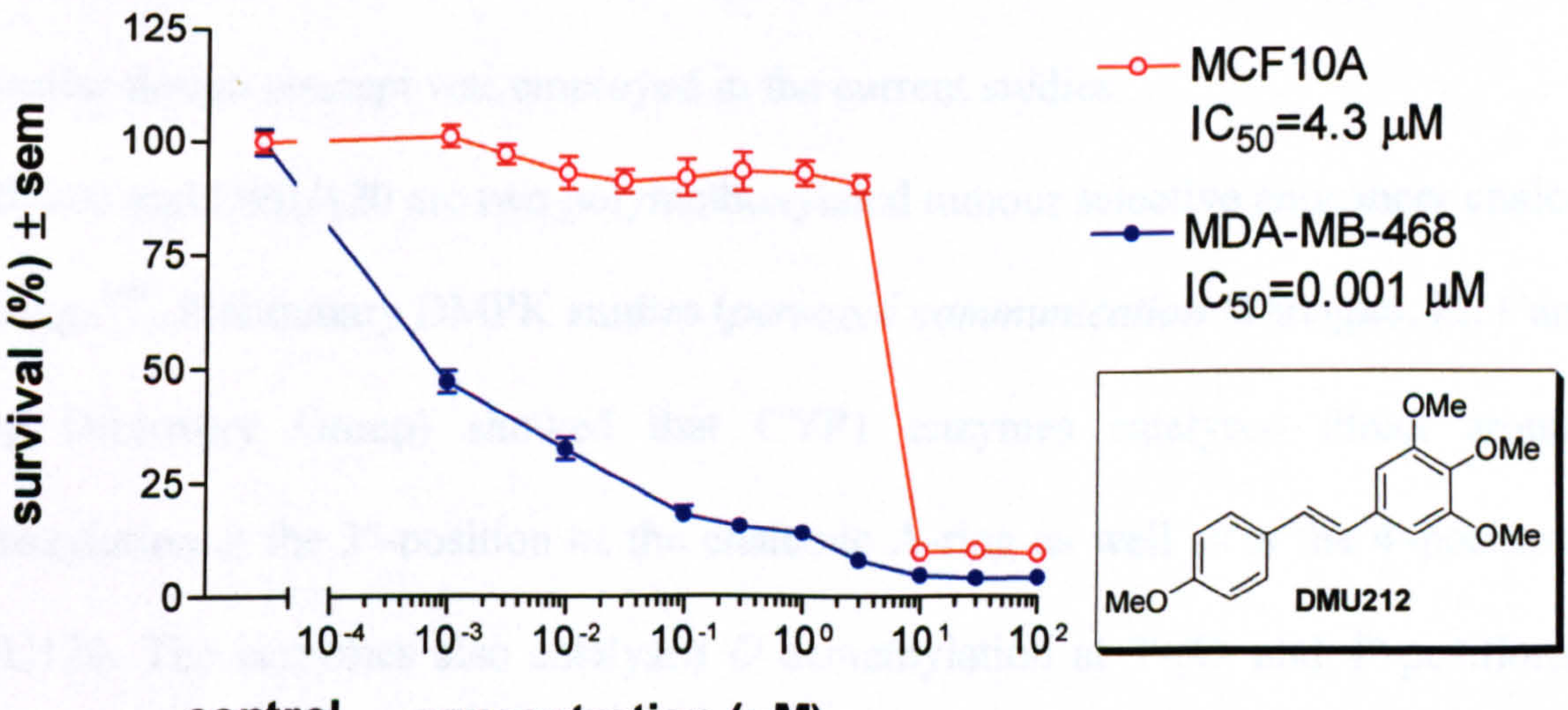

Figure 14: MTT-assay showing cytotoxicity of DMU212 against breast cell lines

MCF10A is a "normal" breast cell line that does not express any CYP1 enzymes. MDA-MB-468 (MDA468) is a highly metastatic and multi-drug resistant human breast tumour model that expresses mainly CYP1B1 (*personal communication* Butler, P. C., Cancer Drug Discovery Group). DMU212 showed 4300-fold tumour selectivity in this *in vitro* assay. (MTT = 3-(4,5-Dimethylthiazol-2-yl)-2,5-diphenyl tetrazolium bromide).

2.1.3 Design of CYP1 enzyme inhibitors

A small range of potential inhibitors (50~100 compounds) has to be synthesised and assayed in order to collect enough information to delineate their SAR with CYP1 family enzymes. Because of constraint in time, the target inhibitors must be easy to synthesise and their corresponding starting materials must also be readily available.

Previously, other Type II P450s inhibitors (see Section 1.2.2) have been identified or synthesised. One example was the P450 CYP17α-hydroxylase inhibitor Abiraterone® and its analogues[142-144]. The nitrogenous bases on these compounds provided strong dative-coordinate bond between the nitrogen lone pair electrons and the P450 haem centre. This interaction will deny the target enzyme from its normal catalytic functions. A similar design concept was employed in the current studies.

DMU102 and DMU120 are two polymethoxylated tumour selective anticancer chalcone prodrugs[145]. Preliminary DMPK studies (*personal communication* Wanogho, E., Cancer Drug Discovery Group) showed that CYP1 enzymes catalysed direct aromatic hydroxylation at the 3"-position of the chalcone A-ring as well as at the 4'-position of DMU120. The isozymes also catalysed *O*-demethylation at 3'-,4'- and 4"-positions of the prodrugs (Figure 15).

Chalcones are relatively easy to synthesise with the Claisen-Schmidt aldol condensation reaction. Combining previous experience on CYP17α inhibitors and the knowledge of substituted chalcone metabolism by CYP1 enzymes, six chalcones with heterocyclic A-rings were designed to investigate the effectiveness of this group of compounds as potential CYP1 enzyme inhibitors (Figure 16). The first three of these chalcones consisted of a pyridyl A-ring, whilst the remaining chalcones have a smaller five-membered imidazolyl A-ring. Differences in the position of the lone pair of electrons on

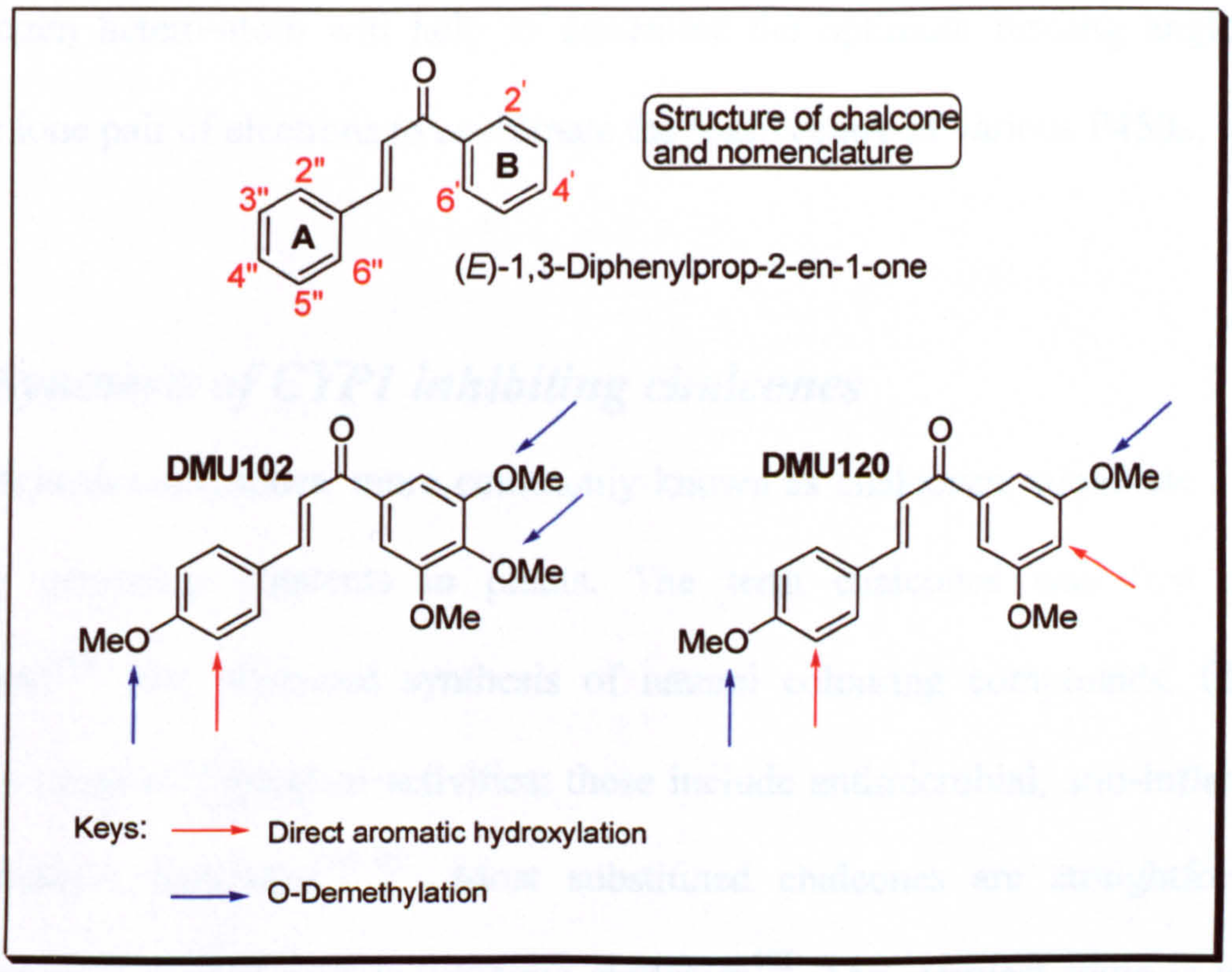

Figure 15: The structure and nomenclature of chalcone

The above figure shows the hydroxylation and *O*-demethylation of chalcone prodrugs DMU102 and DMU120 (*personal communication* Wanogho, E., Cancer Drug Discovery Group).

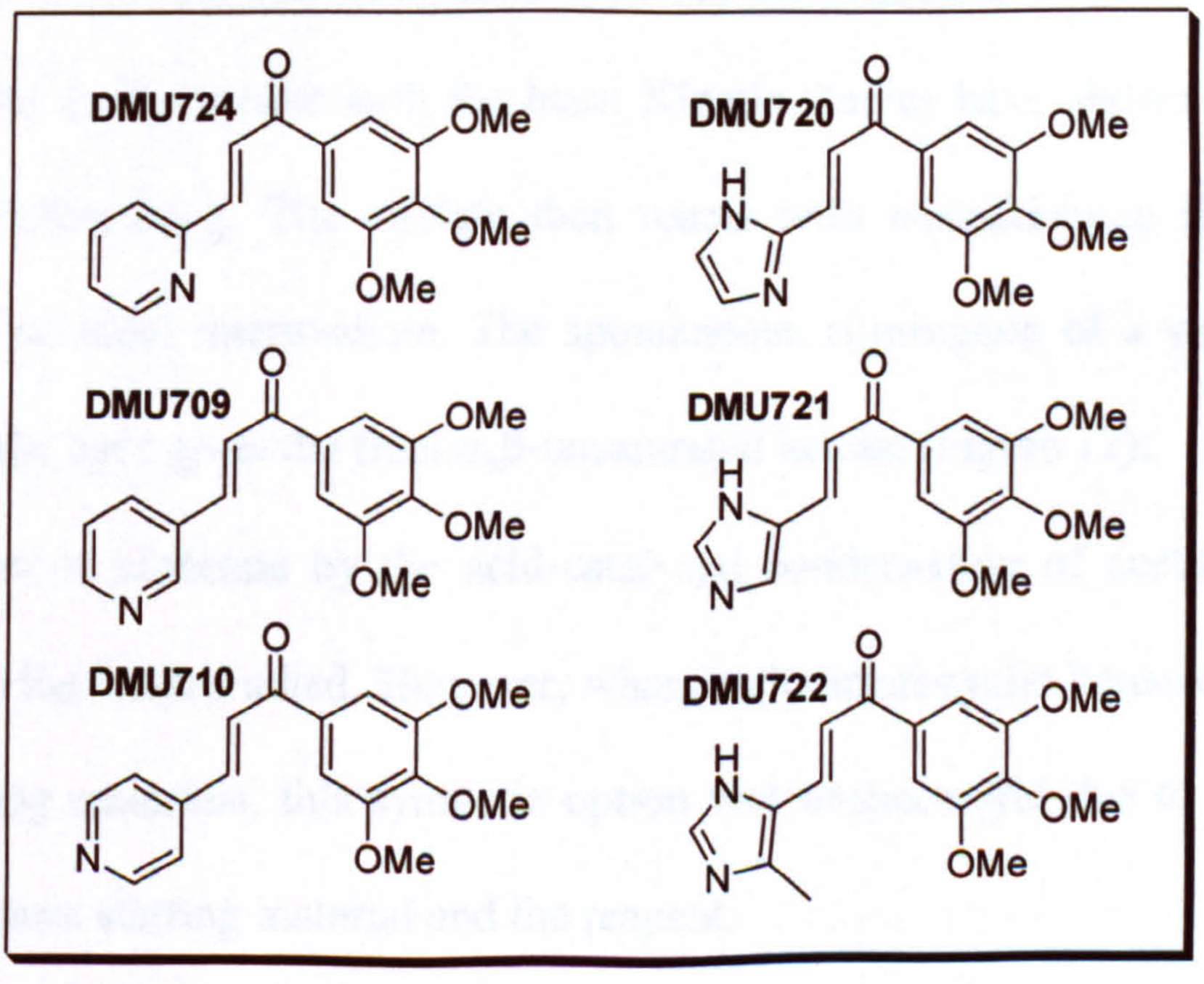

Figure 16: Chemical structure of potential CYP1 mono-oxygenases inhibitors

the nitrogen hetero-atom will help to determine the optimum binding angle for the nitrogen lone pair of electrons to coordinate the haem centre of various P450s.

2.1.4 Synthesis of CYP1 inhibiting chalcones

Benzylideneacetophenones, more commonly known as chalcones, constitute a class of naturally occurring pigments in plants. The term chalcones was first used by Kostanecki[146] who pioneered synthesis of natural colouring compounds. Chalcones possess a range of biological activities; these include antimicrobial, anti-inflammatory and anticancer properties[147-151]. Most substituted chalcones are straightforward to synthesise with several proven synthetic strategies[152]. The simplest route is the base-catalysed Claisen-Schmidt aldol condensation using either methanol (MeOH) or ethanol (EtOH) as solvent and 50% w/v sodium hydroxide (NaOH) solution as base. Kinetic studies have been reported for the base-catalysed formation of chalcones[153].

The first step of the reaction mechanism involves the formation of an enolate from the reaction of the acetophenone with the base. Kinetic studies have shown that this first step is rate-determining. The enolate then reacts with benzaldehyde leading to the formation of an aldol intermediate. The spontaneous elimination of a water molecule catalysed by the base gives the final α,β-unsaturated ketone (Figure 17).

The formation of chalcone by the acid-catalysed condensation of acetophenone and benzaldehyde has been studied. However, when basic heterocyclic benzaldehydes were used as starting materials, this synthetic option was unsuccessful due to side-reaction between the basic starting material and the reagent.

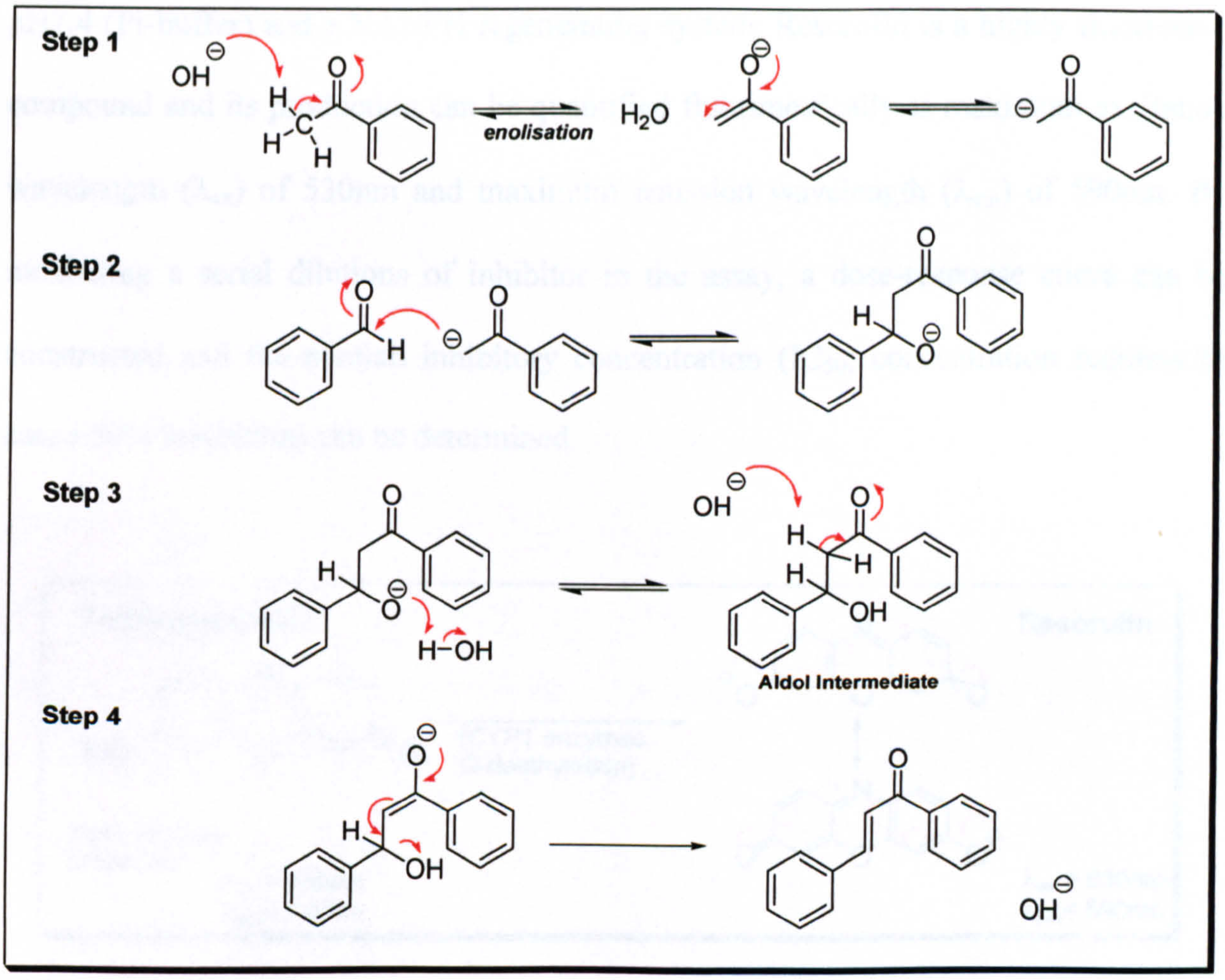

Figure 17: Reaction mechanism of Claisen-Schmidt aldol condensation

Anhydrous reaction conditions can increase the rate of formation of enolate in the rate-determining Step 1 by shifting the reaction equilibrium to the right through the removal of water. This can be achieved by using anhydrous solvent and concentrated NaOH solution.

2.1.5 Biological evaluation of potential CYP1 enzyme inhibitors

The inhibitors were assayed using the 7-ethoxyresorufin-*O*-deethylase (EROD) assay originally described by Burke[154]. As the name implies, the experiment relies on the ability of P450 to deethylate 7-ethoxyresorufin (7ER) to form resorufin. The experiment involves incubation of 7ER, the inhibitor and the cytochrome P450 (in the form of microsomes) in EROD buffer at physiological temperature (37°C) for a pre-determined incubation time. The EROD buffer consists of deionised water, phosphate buffer at

pH7.4 (Pi-buffer) and a NADPH regenerating system. Resorufin is a highly fluorescent compound and its production can be quantified fluorimetrically at maximum excitation wavelength (λ_{ex}) of 530nm and maximum emission wavelength (λ_{em}) of 590nm. By incubating a serial dilutions of inhibitor in the assay, a dose-response curve can be constructed and the median inhibitory concentration (IC_{50}; concentration requires to cause 50% inhibition) can be determined.

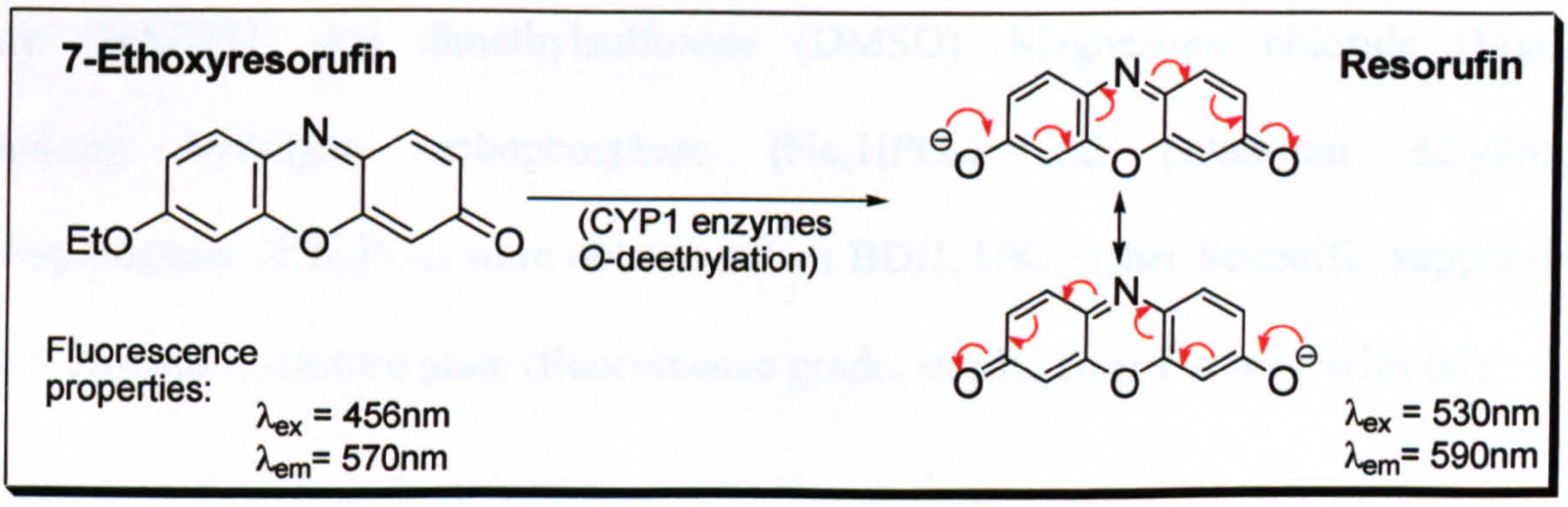

Figure 18: The principle of EROD assay

The EROD assay relies on CYP1 enzymes to deethylate 7ER to form resorufin. As a result of distinct λ_{ex} and λ_{em} for both 7ER and resorufin, the fluorescence intensity of resorufin can be reliably measured without interference from 7ER.

2.2 Reagents and methods

2.2.1 Materials

All chemical reagents and starting materials used in synthesis were purchased from either Lancaster Synthesis Ltd (UK) or Aldrich Chemical Co. Ltd (UK). Thin layer chromatography (TLC) was performed on silica gel sheet supplied by Merck (TLC Aluminium Sheet- Silica Gel $60F_{254}$). TLC was monitored sequentially with UV light

and was stained with 2,4-dinitrophenylhydrazine (2,4-DNP; to stain for the carbonyl group). Purification of synthetic compounds was carried out using flash column chromatography with silica gel, supplied by Fisher Scientific, UK.

The following reagents for EROD assay were obtained from Sigma Chemical Co.: α-naphthaflavone, 7-ethoxyresorufin (7ER), resorufin, β-nicotinamide adenine dinucleotide phosphate ($NADP^+$), glucose-6-phosphate dehydrogenase (G6PD), glucose-6-phosphate (G6P), β-nicotinamide adenine dinucleotide phosphate reduced form (NADPH) and dimethylsulfoxide (DMSO). Magnesium chloride ($MgCl_2$), disodium hydrogen orthophosphate (Na_2HPO_4) and potassium dihydrogen orthophosphate (KH_2PO_4) were obtained from BDH, UK. Fisher Scientific supplied the black 96-well microtitre plate (fluorescence grade, sterile, clear flat base with lid).

2.2.2 Synthetic strategy

The target inhibitors were synthesised using the Claisen-Schmidt aldol condensation:

To an equimolar (eq) of the corresponding acetophenone and benzaldehyde in MeOH was added 5eq of NaOH 50% w/v solution. The resulting mixture was monitored by TLC until all starting materials have been consumed. The reaction was quenched with 50ml of distilled water and extracted with ethyl acetate (3 X 150ml). The combined organic layers were washed with saturated brine (20ml), dried with anhydrous magnesium sulfate and concentrated under *vacuo*. The resulting concentrate was purified by flash column chromatography to afford the pure target compound.

2.2.3 Buffer preparation

100mM Pi-buffer was prepared by the addition of 8.375g of Na_2HPO_4 and 5.579g of KH_2PO_4 to 900ml of deionised water. Depending on the initial pH, either 1M NaOH or 1M hydrochloric acid (HCl) was used to adjust the pH to 7.4. The buffer volume was then adjusted to 1L, the pH re-checked and re-adjusted if necessary. The buffer was stored at 4°C for up to six months.

2.2.4 Preparation of Solution A

Solution A is a component of the NADPH regenerating system in EROD buffer and was prepared according to Gentest Corporation[155]. $NADP^+$ (200mg), G6P (200mg) and $MgCl_2$ (133mg) were weighed out, dissolved and made up to 10ml with deionised water. This was stored in aliquots of 200µL at -20°C for up to six months.

2.2.5 Preparation of Solution B

Solution B is a component of the NADPH regenerating system in EROD buffer and was prepared according to Gentest Corporation[155]. G6PD (250 units) was dissolved with 6.25ml of PO_4 buffer. This was stored in aliquots of 100µL at -20°C for up to six months.

2.2.6 Preparation of NADPH regenerating system

The NADPH regenerating system was prepared immediately prior to use according to Gentest method[155]. 1.5mL of Solution A, 1.5mL of Pi-buffer and 0.3mL Solution B was made up to 15mL with deionised water (or scale to required volume).

2.2.7 Preparation of other solutions for EROD assay

7ER and resorufin stock solutions (1mM) were prepared in DMSO and were stored at 4°C for up to one year. Inhibitor stock solutions (5mM) were prepared by dissolving the respective inhibitor in DMSO and stored at -20°C for up to six months. 7ER and resorufin stock solutions were diluted to appropriate concentration with 10% DMSO in deionised water prior to EROD assay. Serial dilution of inhibitor was carried out in a clear 96-well microtitre plate (supplied by Fisher Scientific) with 10% DMSO pre-warmed to 37°C (to ensure complete solubility) to give concentrations of 0.5, 0.05, 0.005 and 0.0005mM. 5µL of these dilutions was transferred to the fluorescence grade 96-well microtitre plate with EROD buffer to give final inhibitor concentrations of 25, 2.5, 0.25 and 0.025µM. The top concentration of the inhibitor was halved if the inhibitor was not soluble at 25µM and this would give final inhibitor concentrations of 12.5, 1.25, 0.125 and 0.0125µM.

2.2.8 Recombinant human cytochrome P450 isozymes

Microsomes prepared from insect cells transformed using a baculovirus and expressing human cytochrome P450 CYP1A1, CYP1A2 and CYP1B1 with co-expression of human NADPH-cytochrome P450 reductase (Supersomes™) were obtained from Gentest Corporation, USA *via* Cambridge Biosciences, UK. Supersomes™ were stored at -80°C until required. When required, Supersomes™ were rapidly thawed at 37°C and then stored on ice. Supersomes™ were diluted in ice-cold phosphate buffer (100mM) at pH 7.4 to the appropriate concentration immediately prior to use.

2.2.9 Microsomal incubation- EROD assay

The high throughput EROD assay was carried out as described by Gentest Corporation[155] with modification. The modification was to prepare serial dilutions of inhibitors in a separate 96-well microtitre plate instead of in the fluorescence grade 96-well microtitre plate i.e. to check whether inhibitors were completely dissolved in the aqueous environment.

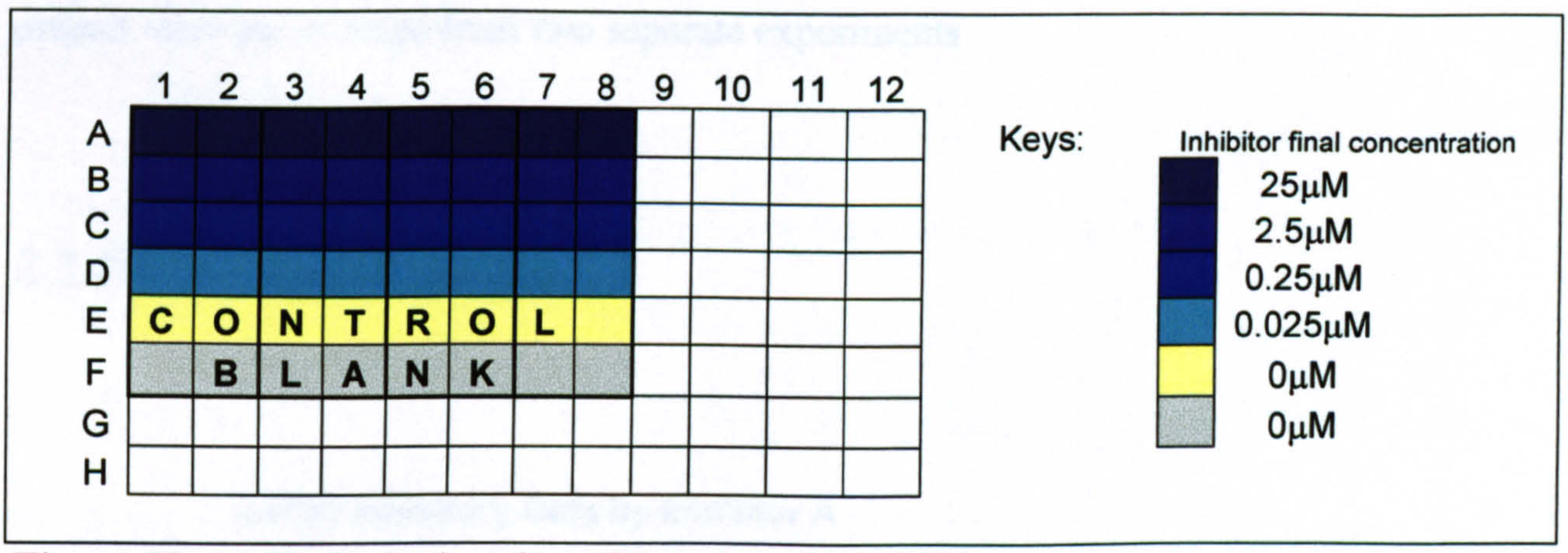

Figure 19: Typical microtitre plate set up for EROD assay

Each well contains 30µL of Pi-buffer, 5µL of 0.1mM 7ER solution (final concentration of 5µM), 50µL of NADPH regenerating system (final concentration: $NADP^+$ = 1.3µM; G6P and $MgCl_2$ = 3.3µM; 0.04U/mL of G6PD), 10µL of diluted Supersome™ (final concentration of 0.5pmol/mL) and 5µL of the inhibitor serial dilution. 5µL of 10% v/v DMSO in deionised water was used as control and in the blank. Columns 1-2, 3-4, 5-6 and 7-8 were duplicates.

For economic reasons and to reduce wastage, only five concentration points were used to construct the IC_{50} curves. Four compounds were assayed per plate per P450 in duplicate. The EROD assay was carried out in a humidified incubator at 37°C under subdued lighting, in a final volume of 100µL. The reaction was initiated by addition of the Supersome™ and was terminated after 30 minutes by addition of 100µL ice-cold

MeOH. The blank was the same as the control except Supersome™ was added at the end of the experiment, after addition of ice-cold MeOH (enzyme attenuated by cold MeOH). Fluorescence was quantified with a fluorescence plate reader (GeminiXS, Molecular Devices) and data was collected using Softmax Pro (version 3.1.2, Molecular Devices). The EROD assay was performed twice for each inhibitor on separate occasions. This was to ensure the quality of data collected and to identify any potential operator errors that may give rise to false information. The IC_{50} values presented in this project were the average from two separate experiments

2.2.10 Data analysis

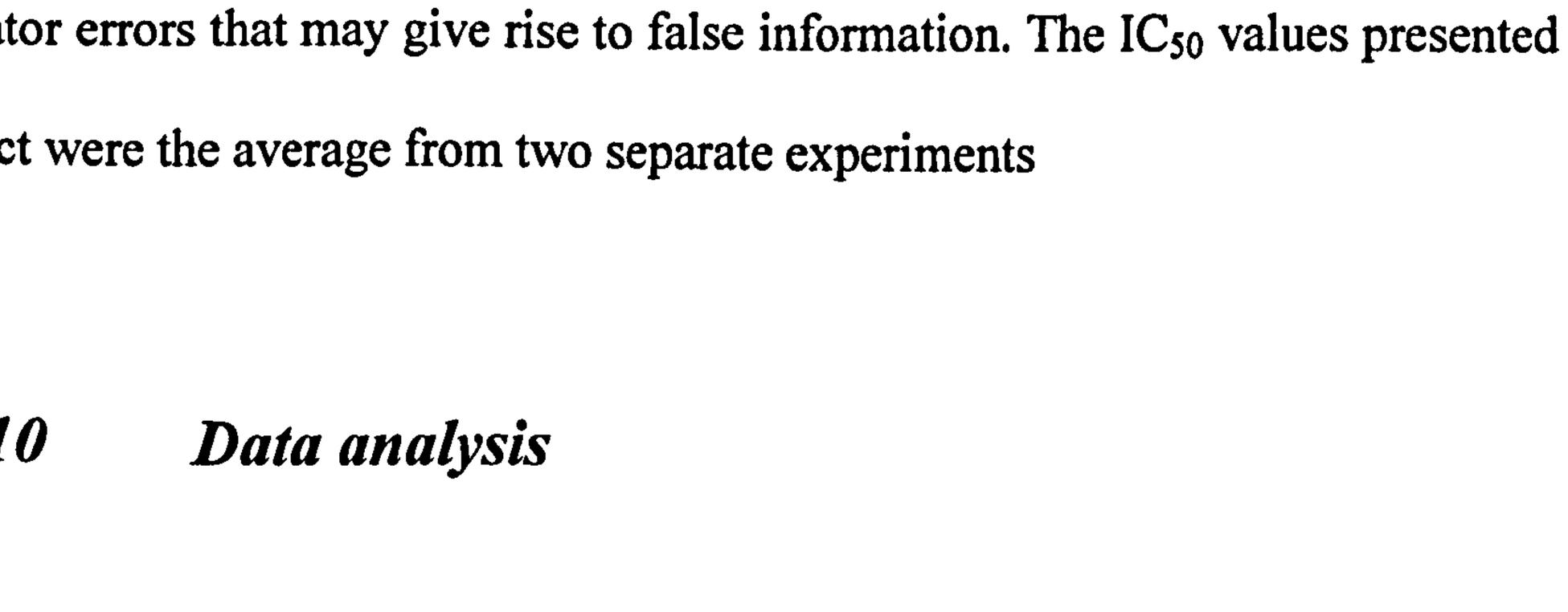

Figure 20: Estimation of IC_{50} values from dose-response curve

The IC_{50} values for inhibitor were estimated manually as shown above. IC_{50} value for CYP1A2 was estimated by extrapolating the curve (dotted line). The IC_{50} values calculated by Prism using non-linear regression curve fit for CYP1A1, CYP1A2 and CYP1B1 were 4.45, 3175 and 0.47μM, respectively.

Data collected from EROD was processed by Prism, version 4.02 (GraphPad Software

Inc.). A dose-response curve was constructed and the IC_{50} value was obtained manually from the curve. This was necessary because the calculated IC_{50} value from Prism, using non-linear regression curve fit, was often inaccurate. IC_{50} values over 25μM (most concentrated point) but less than 100μM were estimated by extrapolation. Inhibitor with equal or more than ten-fold potency over other CYP1 enzymes will be consider as more selective inhbitor.

2.3 Results

2.3.1 Synthetic methods used to synthesise inhibitors

The synthetic method described in Section 2.2.2 was used in an attempt to synthesise the target heterocyclic chalcone inhibitors, but without formation of the desired chalcones. TLC monitoring showed that a new spot formed within two minutes after addition of NaOH solution. The new spot stained deep-red with 2,4-DNP, indicative the formation of a new carbonyl compounds. However, the product broke down if the reaction was permitted to proceed to completion.

Another synthetic approach, described by Chan[156], was used which gave the desired products. This involved the use of lithium diisopropylamide (LDA) as base, generated at low temperature (-78°C) from 1eq of diisopropylamine and n-butyl lithium (nBuLi) under anhydrous conditions and nitrogen atmosphere (this synthetic route is referred as Synthetic Method 1 thereafter). DMU709 and DMU710 (structure see Section 2.1.3) were synthesised with good yield (40% and 36%, respectively) by employing this method.

The Claisen-Schmidt aldol condensation is an exothermic reaction. The rapid

degradation of product using the synthetic method described in Section 2.2.2 could probably be due to instability of the product and the heterocyclic benzaldehyde under heat.

DMU724 was synthesised using a modification of the method described in Section 2.2.2. The procedure involved cooling down the solution of starting materials in MeOH to around 0°C before the addition of 2eq 50% w/v NaOH solution (instead of 5eq previously). The mixture was stirred on ice at around 0°C for a further 2 hours before warming up to room temperature overnight (this synthetic route is referred as Synthetic Method 2). DMU724 was afforded with high yield (79%).

A third method was used to synthesise the imidazolyl chalcones DMU720, DMU721 and DMU722. This solvent-free Claisen-Schmidt condensation was developed by Mogilaiah and Bao[157] for the synthesis of α,β-unsaturated ketones. The method involved grinding the starting materials with powdered NaOH (2eq) using a pestle and mortar (this synthetic route is referred as Synthetic Method 3). DMU720, DMU721 and DMU722 were afforded by this method in good yields (30%, 27% and 32%, respectively).

2.3.2 Validation of the high throughput EROD assay

The modified high throughput EROD assay was validated by comparison with α-naphthaflavone EROD IC_{50} values for CYP1 mono-oxygenases reported by Shimada *et. al.*[158].The final concentration points employed for the in-house method were half of the values described in Figure 20 due to the low solubility of α-naphthaflavone. No apparent differences were detected between the two sets of results (Table 2).

Table 2: α-Naphthaflavone EROD IC_{50} values obtained using in house high throughput EROD assay compared with data from Shimada[158]

	IC_{50} (μM)		
Method	CYP1A1	CYP1A2	CYP1B1
Shimada *et. al.*	0.06	0.006	0.005
In-house method*	0.04	0.009	0.002

*Results presented were means of two independent experiments on different occasions. Each experiment was carried out in duplicate.

2.3.3 Identification of lead inhibitors

Table 3: Nitrogen heterocyclic chalcones inhibitory activities against CYP1 catalysed EROD reaction

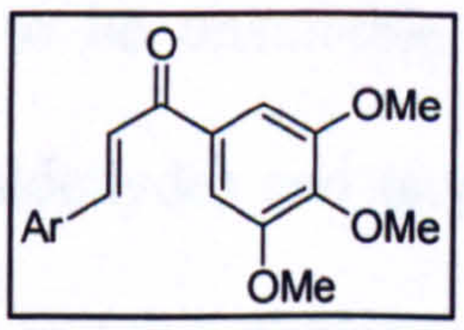

		IC_{50} (μM)		
Inhibitors	Ar	CYP1A1	CYP1A2	CYP1B1
DMU709	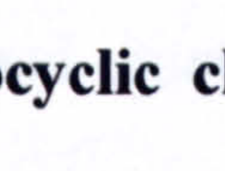	0.3	25	7
DMU710	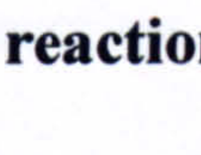	0.5	4	19
DMU720		39	>100	>100
DMU721		12	49	7
DMU722	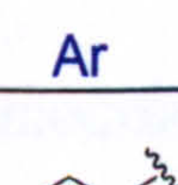	30	>100	90
DMU724	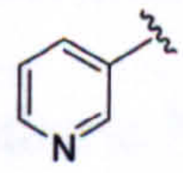	13	>100	>100

Results presented were means of two independent experiments. Each experiment was carried out in duplicate.

The pyridyl chalcones DMU709 and DMU710 were identified as more selective CYP1A1 inhibitors with sub-micro molar IC_{50} values. Both inhibitors were approximately at least 10-fold more selective against CYP1A1 catalysed EROD reaction. DMU720 and DMU724 have shown weak but selective inhibition of CYP1A1. IC_{50} values for DMU722 were obtained by extrapolation from the dose-response curve. The imidazolyl chalcone DMU721 showed only weak inhibition activities against CYP1A1 and CYP1B1 catalysed EROD reaction.

2.4 Discussion

Six inhibitors were synthesised successfully with good yield. Claisen-Schmidt condensation is an exothermic reaction. The method intended to be used for synthesis (Section 2.2.2) was found to be unsuitable probably due to degradation of starting material (heterocyclic benzaldehyde) and target compounds under heat. The suspicion was confirmed when the 2-pyridyl chalcone DMU724 was successfully synthesised with high yield (79%) using a modified version of the method described in Section 2.2.2. The modified method (Synthetic Method 2; Section 2.5.2) involved cooling down the solution of 2-pyridylcarboxaldehyde and 3,4,5-trimethoxyacetophenone in MeOH to approximately 0°C before addition of base. The amount of base used in Synthetic Method 2 was less than the amount proposed in the original method. The effect of the amount of base used in Synthetic Method 2 on product stability was not investigated. DMU709 and DMU710 were synthesised using LDA as base (Section 2.5.2). However, this method involved several steps and was time-consuming. In view of limited time, a more versatile method was sought to synthesise the target compounds.

The solvent-free Synthetic Method 3 (Section 2.5.2) was used to synthesise the imidazolyl chalcones DMU720, DMU721 and DMU722. All three compounds were afforded in good yield (27-32%). The method involved grinding the starting materials with 2eq of powdered NaOH using a pestle and mortar. It is noteworthy to mention that this simple and easily reproducible technique in the solid/semi-solid state, affords target compounds in a shorter reaction period compared with Synthetic Method 1 and 2. Moreover, the condensation takes place at room temperature, in the absence of solvent and with a reasonable yield. Synthetic Method 3 was more economical since less solvent was used. However, it involved a more labour intensive grinding process.

The in-house high throughput EROD assay was validated using the known CYP1 enzyme inhibitor α-naphthaflavone. Incubation time of 30 minutes was selected as opposed to 5-10 minutes reported elsewhere. The longer incubation time was necessary because any potential inhibitors identified by this EROD assay would be used in the cell culture assay that can last up to 96-hours. The inhibitors would be useless if they could not survive 30 minutes of potential metabolic degradation by the very enzyme that is the target of inhibition.

Either NADPH or a NADPH regenerating system can be used in the assay. However, since 30 minutes incubation time was used in the EROD assay, the regenerating system allowed a constant level of NADPH and ensured that no NADPH depletion would occur over the longer incubation period.

DMU709 and DMU710 were identified as more selective inhibitors of CYP1A1 with sub-micro molar IC_{50} values (Table 3). The 3-pyridyl and 4-pyridyl A-ring of DMU709 and DMU710, respectively, inhibited their target enzyme as predicted from preliminary metabolism studies on chalcone prodrugs DMU102 and DMU120 (Figure 15).

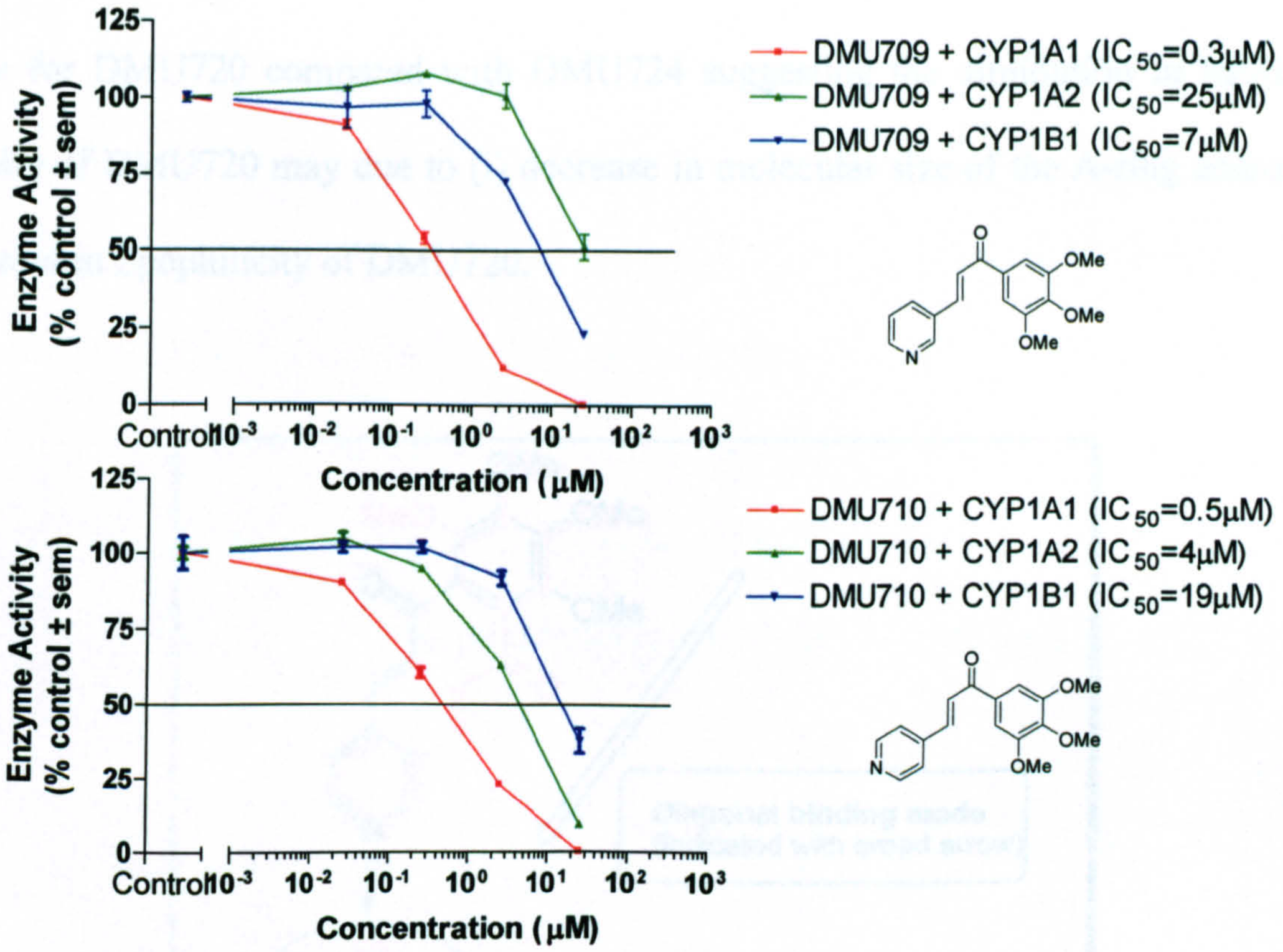

Figure 21: DMU709 and DMU710 inhibition towards CYP1 catalysed EROD activity

DMU709 has a better inhibition window at 1μM concentration. Results presented were means of two independent experiments. Each experiment was carried out in duplicate.

Although the 2-pyridyl chalcone DMU724 also selectively inhibited CYP1A1, its inhibition was probably via a Type I interaction (Section 1.2.2). In this case a Type II interaction was not possible due to the nitrogen lone pair electrons from the 2-pyridyl A-ring being too sterically hindered to perform Type II binding interaction with the CYP1A1 haem centre.

Compared to the six-membered pyridyl A-ring chalcones, the smaller five membered heterocyclic A-ring chalcone DMU720 was less capable to inhibit CYP1 enzymes. Similar to DMU724, the nitrogen lone pair electrons on DMU720 were too sterically

hindered to provide interaction with the P450 haem. A 3-fold increase in CYP1A1 IC_{50} value for DMU720 compared with DMU724 suggesting the diminution in inhibitory activity of DMU720 may due to (i) decrease in molecular size of the A-ring and/or (ii) decrease in lipophilicity of DMU720.

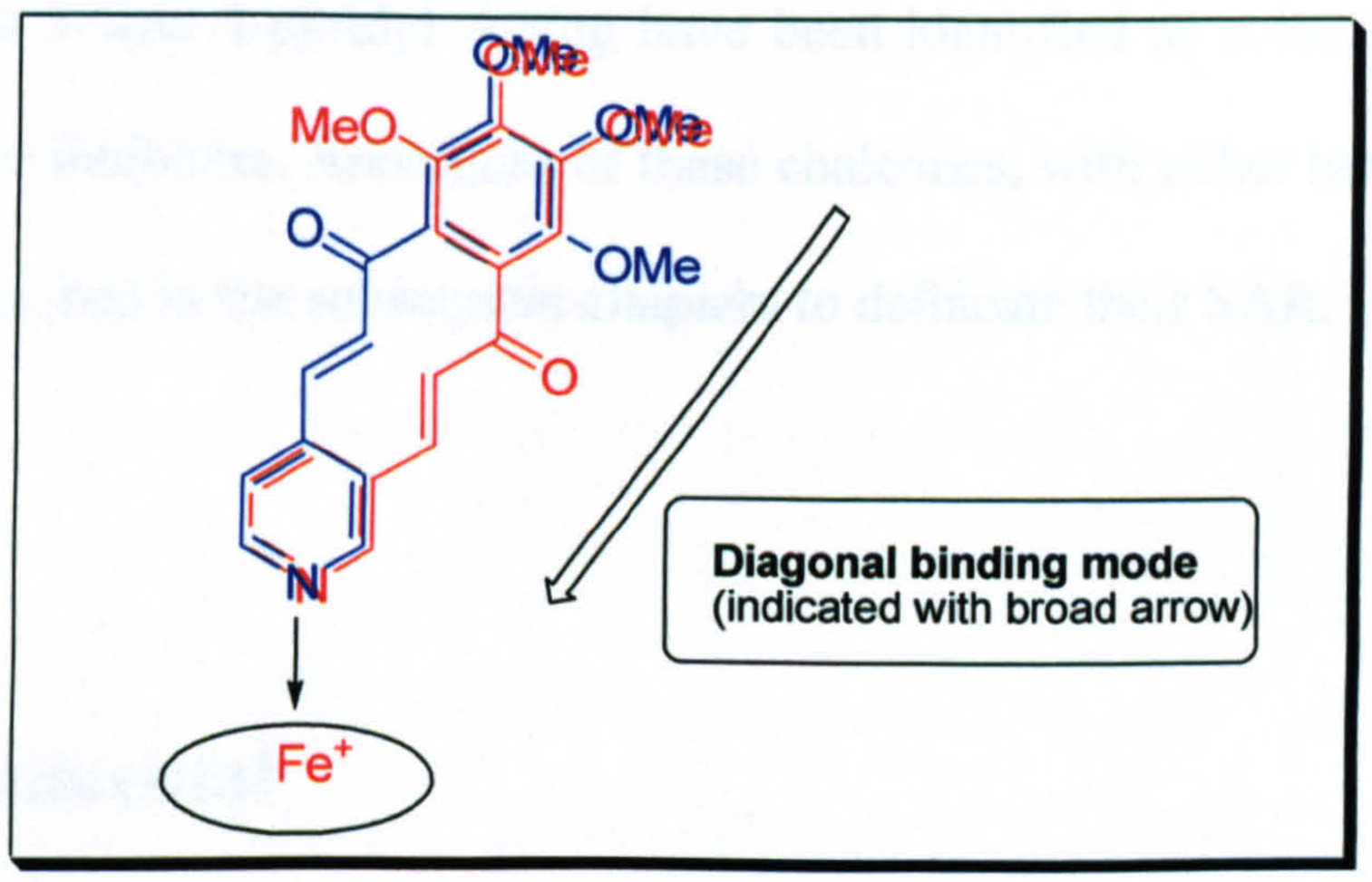

Figure 22: Possible Type II binding interaction between DMU709 and DMU710 with the CYP1A1 haem centre

The above figure illustrates the possible binding orientation of both DMU709 (red) and DMU710 (blue) within the CYP1A1 active site. Both inhibitors interact in a diagonal binding mode.

Although the nitrogen lone pair electrons on DMU721 and DMU722 were not sterically hindered, both DMU721 and DMU722 were less potent inhibitor than DMU709 and DMU710. The diminution of inhibitory activity of the imidazolyl chalcones was due to the decrease in lipopholicity. Using CambridgeSoft ChemDraw® Ultra software version 8, the LogP values of DMU709, DMU710, DMU720, DMU721 and DMU722 were estimated (Crippen's fragmentation method[159]). All imidazolyl chalcones have lower LogP values compared with their pyridyl chalcone analogues (LogP 0.5~1.3 for imidazolyl chalcones DMU720, DMU721 and DMU722; LogP 1.9 for both DMU709

and DMU710). Mammalian P450s are membrane bound enzyme system (Figure 1). Williams *et. al.*[72] have shown that the interaction of the P450 enzyme and the hydrophobic membrane places the entrance of the substrate access channel in or near the membrane. Consequently, the more hydrophilic imidazolyl chalcones are less likely to enter the enzyme to elicit their inhibitory activities.

Chalcones with 3- and 4-pyridyl A-ring have been identified as suitable templates for designing future inhibitors. Analogues of these chalcones, with either heterocyclic A- or B-ring, are described in the subsequent chapters to delineate their SAR.

2.5 Experimental

2.5.1 Analytical methods

The ^{1}H- and ^{13}C-NMR spectra were recorded by Mike Needham on a 400MHz super-conducting Bruker Spectrometer. Infrared spectra were recorded in potassium bromide disk on a Shimadzu Spectrophotometer (model FTIR-8300). The mass spectra were obtained with a VG 70SEQ spectrometer or with a MALDI spectrometer (Lasermat 2000, Finnigan MAT Ltd) without using any matrix. Melting points were recorded using a Gallenkamp melting point apparatus (model number: MPD350.BM2.5) and were not corrected.

2.5.2 General methods for chalcone synthesis

Synthetic Method 1: (The LDA method) To a stirred and cold (-78°C) anhydrous tetrahydrofuran (THF) was added diisopropylamine (1eq) followed by nBuLi (1eq)

dropwise over 5 minutes in a nitrogen atmosphere. The mixture was stirred at –78°C for 30 minutes before a solution of acetophenone (1eq) in anhydrous tetrahydrofuran (THF) was added slowly. The resulting mixture was stirred for 10 minutes followed by addition of a solution of aldehyde (1eq) in anhydrous THF. The mixture was stirred and allowed to warm up to room temperature overnight. The reaction was quenched with water and neutralised to pH7 with 1M HCl. The mixture was extracted with ethyl acetate (3 X 100ml). The combined organic layers were washed with saturated brine, dried over magnesium sulphate and concentrated under *vacuo*. The crude compound was purified by column chromatography with increasing solvent system polarity (hexane: ethyl acetate: triethylamine (5%); with increasing ethyl acetate from 10~80%).

Synthetic Method 2: (The NaOH method with cooling) To a stirred and cooled (0°C) solution of acetophenone and benzaldehyde in MeOH was added 2eq of 50% w/v NaOH solution. The resulting mixture was stirred at 0°C for another two hours before warming up to room temperature overnight. Standard work up as described in Synthetic Method 1.

Synthetic Method 3: (The solvent-free method) Acetophenone and benzaldehyde were mixed and ground with powdered NaOH using pestle and mortar. The mixing and grinding stopped when no further changes in consistency and colour of the mixture was observed. The resulting mixture was dissolved with 3 X 100ml ethyl acetate:water mixture (3:1). The organic layer was partitioned, washed with saturated brine, dried over magnesium sulphate and concentrated under *vacuo*. The crude compound was purified by column chromatography with increasing solvent system polarity (hexane: ethyl acetate: triethylamine (5%); with increasing ethyl acetate from 10~80%).

(*E*)-1-(3',4',5'-Trimethoxyphenyl)-3-(3-pyridyl)prop-2-en-1-one (DMU709)

Synthetic Method 1; ^{1}H-NMR ($CDCl_3$) δ 3.85 (3H, s, OMe), 3.95 (6H, s, OMe), 7.45 (2H, s), 7.52 (1H, m), 7.80 (1H, d, *J*=16.7Hz), , 7.94 (1H, d, *J*=16.7), 8.30 (1H, d), 8.56 (1H, d), 8.89 (1H, s); ^{13}C-NMR ($CDCl_3$) δ 57.33, 61.62, 108.11, 125.86, 125.94, 133.92, 134.78, 137.41, 141.91, 144.70, 151.09, 151.73, 155.11, 190.70; IR Spectrum V_{max} (KBr)/cm^{-1} 1660 (C=O); Mass Spectrum (FAB) m/z 300 (M^+ + 1, 100%); mp 131°C.

(*E*)-1-(3',4',5'-Trimethoxyphenyl)-3-(4-pyridyl)prop-2-en-1-one (DMU710)

Synthetic Method 1; ^{1}H-NMR ($CDCl_3$) δ 3.90 (3H, s, OMe), 3.96 (6H, s, OMe), 7.44 (2H, s), 7.72 (1H, d, *J*=16.4Hz), 7.78 (2H, m), 8.00 (1H, d, *J*=16.4Hz), 8.63 (2H, m); ^{13}C-NMR ($CDCl_3$) δ 55.99, 60.32, 106.77, 123.07, 125.99, 126.93, 133.12, 141.09, 143.78, 149.89, 153.68, 189.39; IR Spectrum V_{max} (KBr)/cm^{-1} 1658 (C=O); Mass Spectrum (FAB) m/z 300 (M^+ + 1, 100%); mp 120°C.

(*E*)-1-(3',4',5'-Trimethoxyphenyl)-3-(1*H*-2-imidazolyl)prop-2-en-1-one (DMU720)

Synthetic Method 3; ^{1}H-NMR (CD_3OD) δ 3.75 (3H, s, OMe), 3.85 (6H, s, OMe), 7.20 (2H, s), 7.30 (2H, s, imidazolyl), 7.50 (1H, d, *J*=15.6Hz), 7.82 (1H, d, *J*=15.6Hz), 13.4 (1H, s, imidazolyl); ^{13}C-NMR (CD3OD) δ 49.39, 50.04, 57.23, 61.63, 107.77, 124.03, 131.98, 134.79, 144.62, 145.69, 155.11, 190.23; IR Spectrum V_{max} (KBr)/cm^{-1} 1658 (C=O); Mass Spectrum (FAB) m/z 289 (M^+ + 1, 100%); mp 202°C.

(*E*)-1-(3',4',5'-Trimethoxyphenyl)-3-(1*H*-4-imidazolyl)prop-2-en-1-one (DMU721)

Synthetic Method 3; ^{1}H-NMR ($CDCl_3$) δ 3.90 (3H, s, OMe), 3.95 (6H, s, OMe), 7.27

(1H, s), 7.33 (2H, s), 7.37 (1H, s), 7.70 (1H, d, *J*=15.3Hz), 7.78 (1H, d, *J*=15.3Hz), 7.81 (1H, s); ^{13}C-NMR ($CDCl_3$) δ 49.58, 50.23, 56.74, 61.34, 106.55, 120.19, 123.02, 133.86, 134.86, 137.8, 142.89, 153.52, 189.47; IR Spectrum V_{max} (KBr)/cm^{-1} 1666 (C=O); Mass Spectrum (MALDI) m/z 288.22 (M^+, 100%); mp 119-120°C.

(*E*)-1-(3',4',5'-Trimethoxyphenyl)-3-(5''-methyl-1*H*-4-imidazolyl)prop-2-en-1-one (DMU722)

Synthetic Method 3; ^{1}H-NMR ($CDCl_3$) δ 2.10 (3H, s), 3.90 (3H, s), 3.95 (6H, s), 7.35 (2H, s), 7.62 (1H, d, *J*=15.1Hz), 7.71 (1H,d), 7.78 (1H, d, *J*=15.1Hz), 13.2 (1H, d); ^{13}C-NMR ($CDCl_3$) δ 49.38, 50.23, 56.71, 61.33, 106.50, 118.69, 132.17, 133.87, 136.17, 142.81, 153.50, 175.53, 189.33; IR Spectrum V_{max} (KBr)/cm^{-1} 1651 (C=O); Mass Spectrum (MALDI) m/z 302.23 (M^+, 100%); mp 106-108°C.

(*E*)-1-(3',4',5'-Trimethoxyphenyl)-3-(2-pyridyl)prop-2-en-1-one (DMU724)

Synthetic Method 2; ^{1}H-NMR δ ($CDCl_3$) 3.85(3H, s, OMe), 3.95(6H, s, OMe), 7.34(2H, s), 7.52(1H, m), 7.79(1H, d, *J*=15.5Hz), 8.09 (1H, d, *J*=15.5Hz), 8.3(1H, d), 8.56(1H, d), 8.90(1H, s); ^{13}C-NMR ($CDCl_3$) δ 49.98, 50.68, 56.51, 61.01, 99.64, 106.49, 124.43, 125.26, 133.20, 136.93, 142.71, 150.19, 153.26, 189.11; IR Spectrum V_{max} (KBr)/cm^{-1} 1666 (C=O); Mass Spectrum (MALDI) m/z 299 (M^+, 100%); mp 99°C.

Summary of Structures

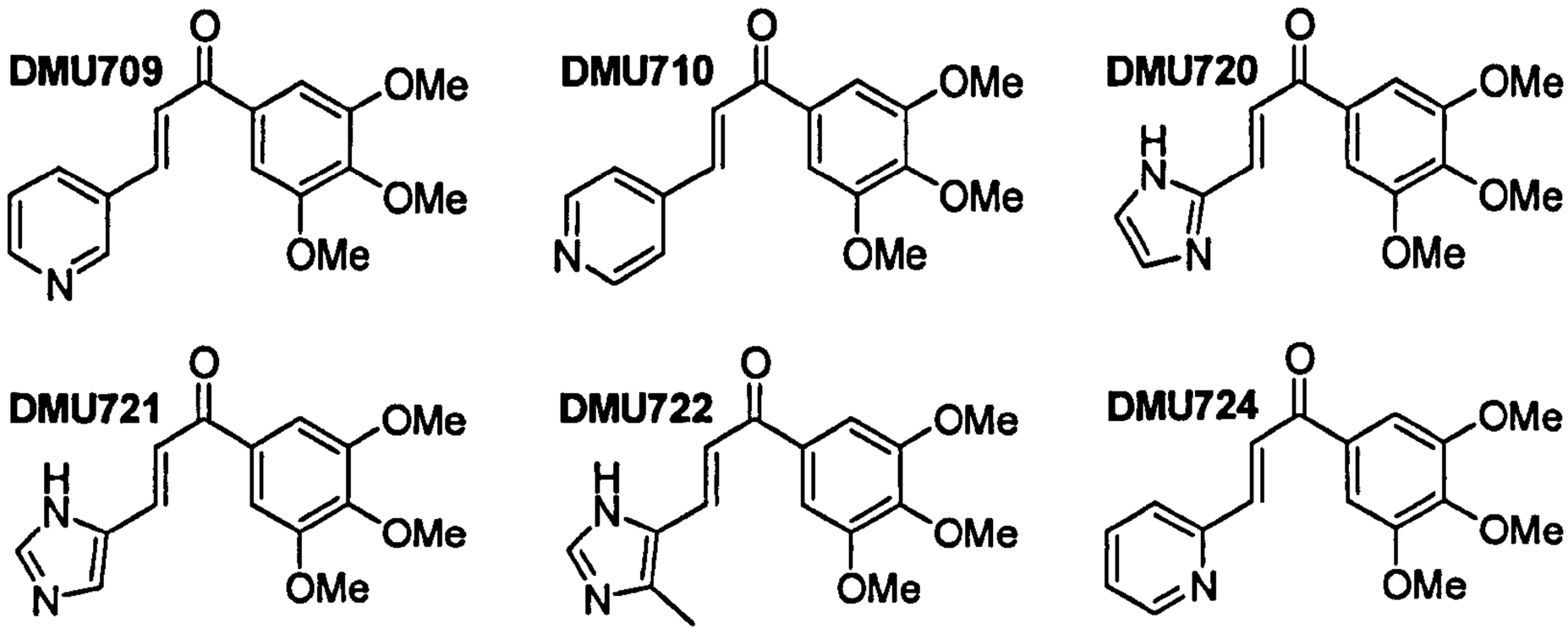

Chapter 3

3-Pyridyl Chalcones As Selective CYP1 Enzyme Inhibitors

3.1 Introduction

Previously, two heterocyclic chalcones, namely DMU709 and DMU710, have been identified as more selective CYP1A1 inhibitors (Chapter 2). Both compounds have a pyridine A-ring in the chalcone core structure (Section 2.4; Figure 21) and it is thought that inhibition of the P450 enzyme is via interaction between the lone pair electrons from the nitrogenous heterocycle and the P450 haem.

In order to further define the SAR of the CYP1 enzyme inhibitors, analogues of DMU709 will be synthesised and studied in this chapter. These analogues of DMU709 will share the similar 3-pyridyl A-ring core structure but with varying number and type of functional groups on the chalcone B-ring. Assuming the 3-pyridyl ring is fixed in position to the haem, the variation on the chalcone B-ring will allow delineation of hydrogen-bonding interactions within the enzyme active sites. A few 3-pyridyl chalcones with polycyclic fused-ring system in substitution of the chalcone B-ring will also be synthesised. These bulky molecules will help to determine the maximum molecular size that the isozyme active sites will tolerate and to probe the hydrophobic nature of the enzyme-substrate binding pockets.

As both the A- and B-ring of the chalcones can orientate to face the P450 haem centre in the active site, another group of DMU709 analogues with 3-pyridyl B-ring were synthesised. These are discussed in Chapter 4. The latter group of chalcones with heterocyclic B-ring is referred to as the "reversed" 3-pyridyl chalcones (Figure 23). The 4-pyridyl and reversed 4-pyridyl analogues of DMU710 will also be discussed in Chapter 4.

The 4(5)-imidazolyl chalcone inhibitor DMU721 has shown some inhibition activity towards CYP1 enzymes catalysed EROD reaction, with EROD IC_{50} values of 12, 49

and 7μM for CYP1A1, CYP1A2 and CYP1B1, respectively. Two DMU721 analogues, DMU744 and DMU2120, will be characterised in this chapter to further investigate chalcone compounds with a 4(5)-imidazolyl A-ring.

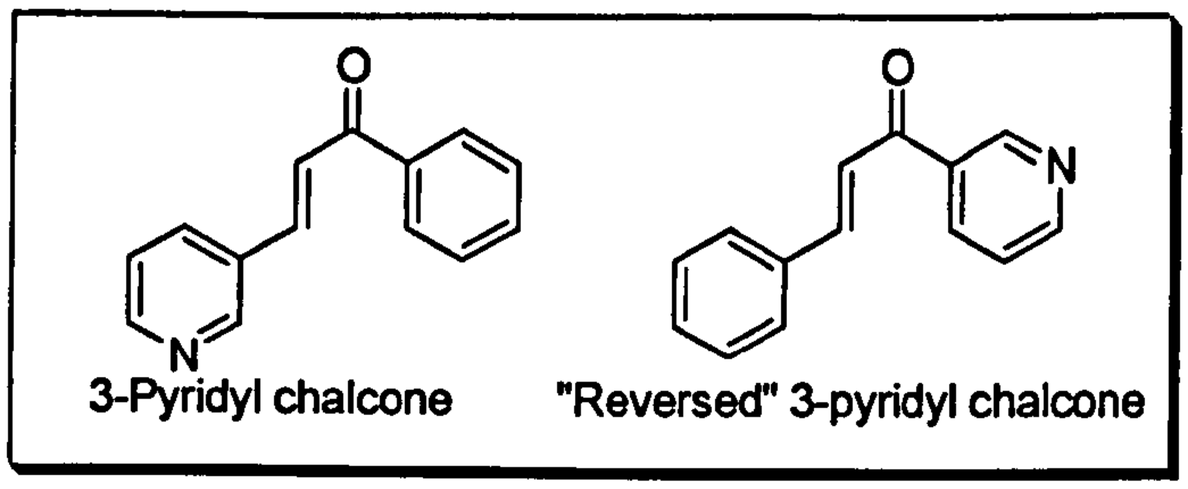

Figure 23: ***The structures of 3-pyridyl chalcones and its analogue the "reversed" 3-pyridyl chalcone***

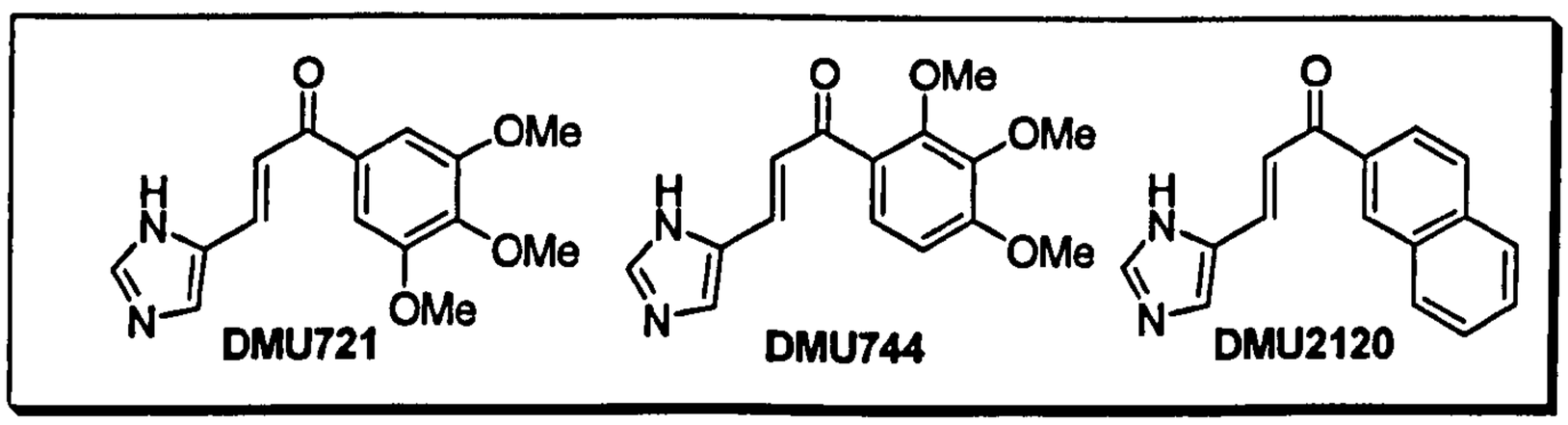

Figure 24: ***The 4(5)-imidazolyl chalcone DMU721 and its analogues***

3.2 Reagents and methods

3.2.1 Materials

All reagents and starting materials for synthesis were purchased from either Lancaster Synthesis (UK) or Aldrich Chemical Co. Ltd (UK). Reactions were followed and monitored with TLC as described in Section 2.2.1. Purification of the synthesised compounds was carried out using flash column chromatography with silica gel (supplied by Fisher Scientific, UK) unless otherwise stated.

Reagents and plasticware for the EROD assay were obtained from Sigma Chemical Co. and Fisher Scientific (see Section 2.2.1). Furafylline was supplied by Ultrafine Chemical Ltd, UK. Microsomes expressing human cytochrome P450 CYP1A1, CYP1A2 and CYP1B1 with co-expression of human NADPH-cytochrome P450 reductase (Supersomes™) were obtained from Gentest Corporation, USA *via* Cambridge Biosciences, UK. Control microsomes (Gentest Corporation) prepared from insect cells treated with the vector plasmid but without the human CYP cDNA is referred to as inactive microsomes.

3.2.2 Synthetic strategies

Details for each synthetic method are described in Section 2.5.2.

3.2.3 Microsomal incubation- EROD assay

The EROD assay was conducted as described in Section 2.2.9. The preparation of different solutions used in the EROD assay can be found from Section 2.2.3 to Section 2.2.7.

3.3 Results

3.3.1 Synthesis of heterocyclic chalcone inhibitors

A total of 34 potential CYP1 enzyme inhibitors has been synthesised. Their chemical structures, synthetic method, physical characteristics and yields are presented in Table 4-6.

All compounds were synthesised successfully and with reasonable yield. As a result of poor solubility of some polycyclic acetophenone in MeOH (see Table 5 notes), acetone or a MeOH:dichloromethane mixture were used as solvent for the reaction.

DMU2123, DMU2124 and DMU2127 were initially synthesised using Synthetic Method 2. In these cases, the reactions did not lead to the target compounds but instead generated unexpected triaryl compounds (Figure 25). DMU2123, DMU2124 and DMU2127 were synthesised successfully employing Synthetic Method 3.

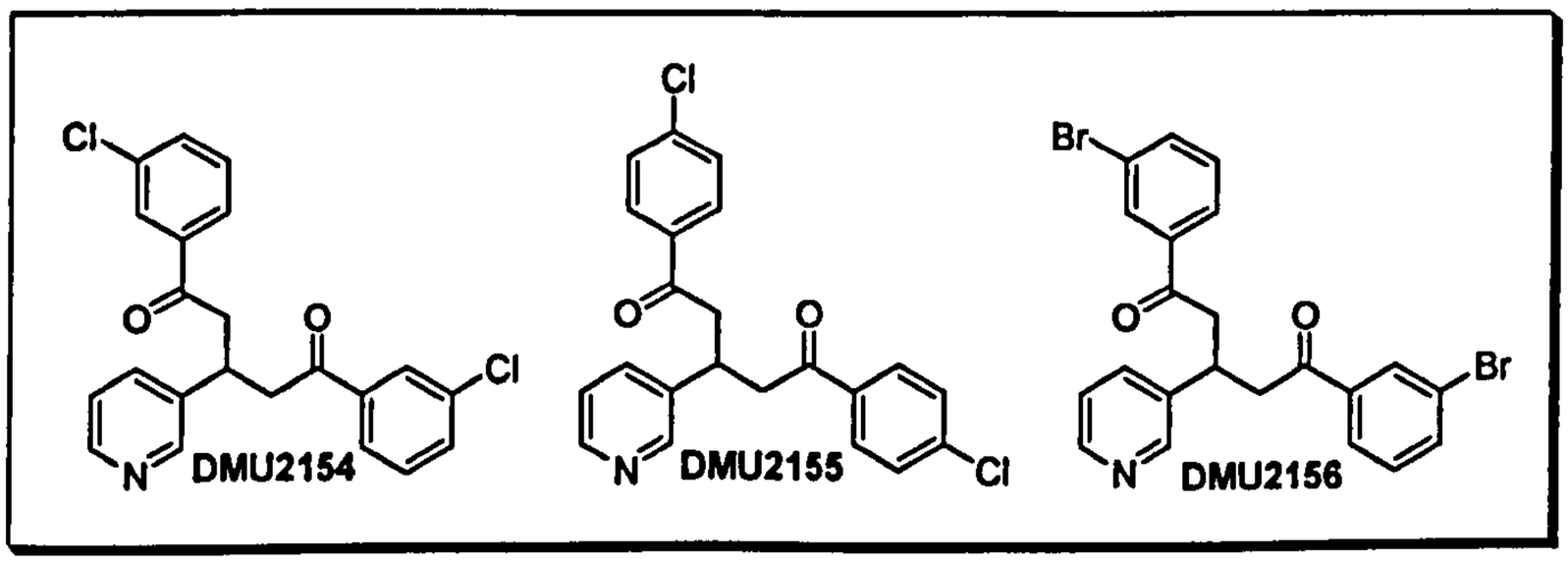

Figure 25: Chemical structure of the triaryl compounds DMU2154, DMU2155 and DMU2156

Table 4: Chemical structures and physical characteristics of 4(5)-imidazolyl chalcones

Inhibitors	Structure	Physical characteristics (yield%)	Method
DMU744	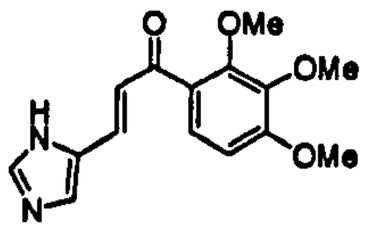	fine yellow powder (18%)	2**
DMU2120	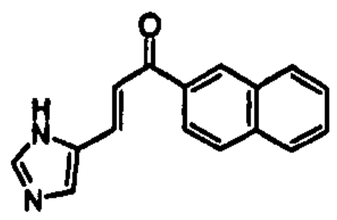	yellow powder (33%)	2**

Notes: Method (see Section 2.5.2); 2** as Synthetic Method 2 but the reaction was refluxed at 50°C for 2 days after the initial 24 hours where cooling and warming up to room temperature occurred.

Table 5: Chemical structures and physical characteristics of the 3-pyridyl chalcone inhibitors

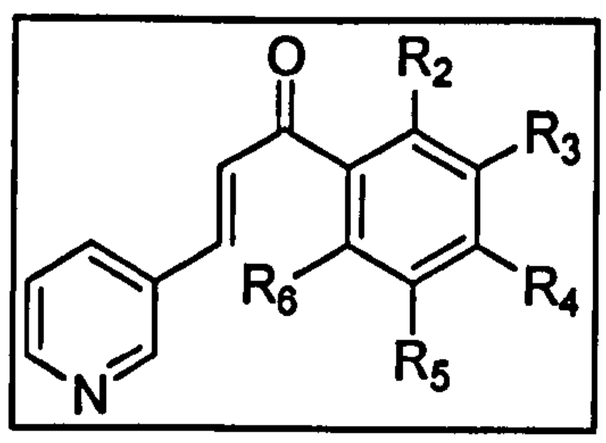

Inhibitors	R_2	R_3	R_4	R_5	R_6	Physical chracterictics (yield %)	Method
DMU709*	H	OMe	OMe	OMe	H	fine yellow powder (40%)	1
DMU711	H	H	H	H	H	dark yellow solid (35%)	1
DMU712	OMe	H	H	H	H	pale yellow crystals (52%)	1
DMU713	H	OMe	H	H	H	light brown powder (25%)	1
DMU714	H	H	OMe	H	H	yellow powder (48%)	1
DMU715	OMe	H	OMe	H	H	bright yellow powder (55%)	1
DMU716	H	OMe	OMe	H	H	fine light brown crystals (37%)	1
DMU717	H	OMe	H	OMe	H	yellow powder (34%)	1
DMU718	OMe	OMe	OMe	H	H	yellow crystals (51%)	1
DMU757*	OH	H	OH	H	H	~~ see note ~~	
DMU760*	H	OH	H	OH	H	~~ see note ~~	
DMU763*	OH	H	H	H	H	~~ see note ~~	
DMU764*	H	OH	H	H	H	~~ see note ~~	
DMU765*	H	H	OH	H	H	~~ see note ~~	
DMU782	OMe	H	H	OMe	H	yellow solid (64%)	2
DMU785*	H	Cl	Cl	H	H	~~ see note ~~	
DMU786*	Cl	H	Cl	H	H	~~ see note ~~	
DMU2123	H	Cl	H	H	H	pale yellow powder (52%)	3
DMU2124	H	H	Cl	H	H	pale yellow powder (61%)	3
DMU2127	H	Br	H	H	H	fine pale yellow powder (39%)	3
DMU2151	H	F	F	H	H	pale apple green crystals (48%)	2

Notes:

Method (see Section 2.5.2).

* Synthesised previously in Chapter 2

* Synthesised by Mussarath Walji as part of her undergraduate final year project; Synthetic Method 3 employed for the synthesis of all three compounds. * Synthesised by Leena Lakdawala as part of her undergraduate final year project; Synthetic Method 3 employed for the synthesis of all four compounds.

Table 6: Chemical structures and physical characteristics of 3-pyridyl chalcone inhibitors with polycyclic fused-ring system

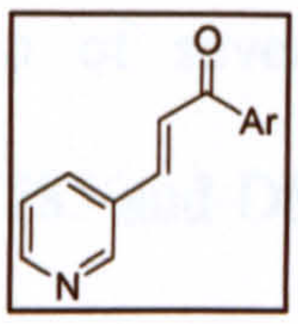

Inhibitors	Ar	Physical characteristics (yield%)	Method
DMU745	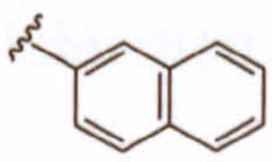	pale brown crystals (52%)	1
DMU746	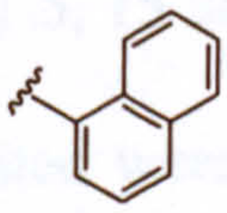	brown waxy solid (88%)	1
DMU762	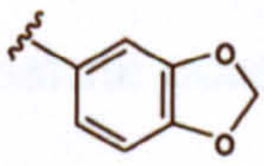	pale yellow powder (60%)	2
DMU2133	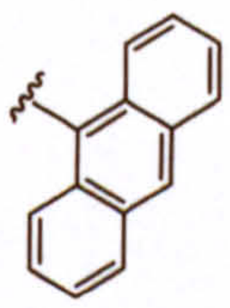	fine yellow powder (28%)	2*
DMU2134	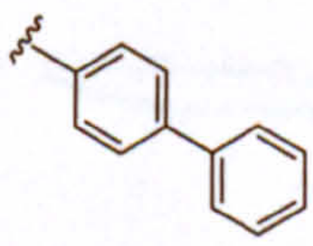	yellow powder (27%)	2
DMU2136	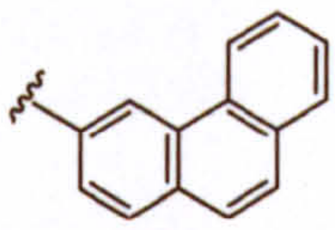	bright yellow solid (61%)	2#
DMU2137	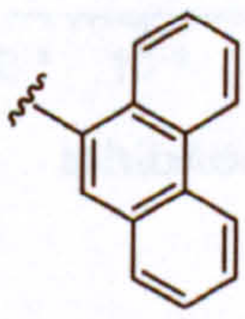	fine yellow crystals (61%)	2#
DMU2139	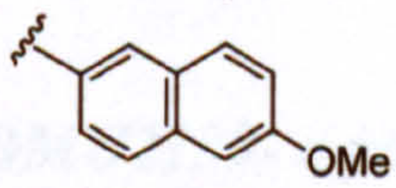	pale yellow needles (8%)	2
DMU2140	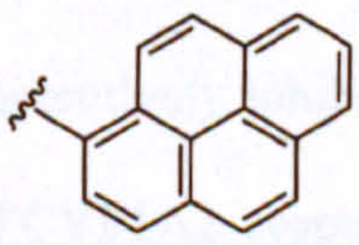	bright yellow solid (54%)	2

Notes: Method (see Section 2.5.2); 2* = as Synthetic Method 2 but acetone was used as solvent for the reaction; 2# = as Synthetic Method 2 but MeOH:dichloromethane mixture was used as solvent (MeOH 75% v/v).

3.3.2 Identification of CYP1B1 inhibitors

The EROD assay performed on 3-pyridyl chalcones and the triaryl compounds led to the identification of several CYP1B1 inhibitors. DMU713, DMU716, DMU745, DMU746, DMU785 and DMU2139 are more selective inhibitors of CYP1B1 with sub micro molar IC_{50} and with at least 10-fold enzyme selectivity ratio (eSR). Amongst the identified CYP1B1 inhibitors, DMU2139 was the most potent with highest eSR compared with inhibition to other CYP1 enzymes. The EROD IC_{50} values for DMU2139 were 1.5, 15 and 0.08μM for CYP1A1, CYP1A2 and CYP1B1, respectively. All results presented were means of two individual experiments. Each experiment was carried out on separate occasions in duplicate.

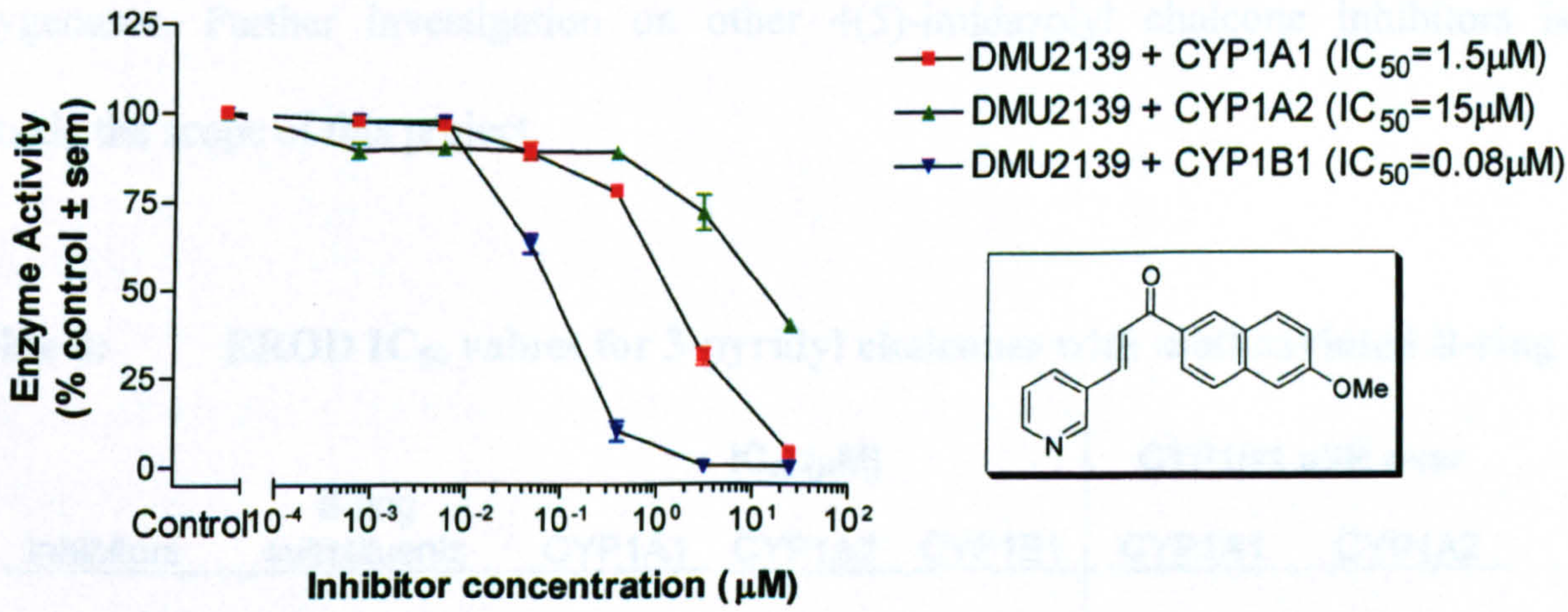

Figure 26: DMU2139- a potent and selective inhibitor of CYP1B1

DMU2139 more selectively inhibits CYP1B1 catalysed EROD reaction. It is 19- and 188-fold selective than CYP1A1 and CYP1A2, respectively. eSR of DMU2139 was calculated using this formula:

IC_{50} (*other isoform*)**/ IC_{50}** (*CYP1B1*)

Table 7: 4(5)-Imidazolyl chalcones inhibitory activities against EROD reaction

Inhibitors	B-ring substituents	IC_{50} (μM) CYP1A1	CYP1A2	CYP1B1
DMU721*	3,4,5-$(OMe)_3$	12	49	7
DMU744	2,3,4-$(OMe)_3$	70	70	10
DMU2120	2-naphthyl	0.7	3	0.5

* Synthesised previously in Chapter 2.

The EROD IC_{50} values for the two 4(5)-imidazolyl chalcones have also been determined. DMU744 more selectively inhibits CYP1B1 with an IC_{50} of 10μM. DMU2120 more selectively inhibits the extrahepatic CYP1 enzymes. These 4(5)-imidazolyl chalcones have shown some inhibitory activities against CYP1 mono-oxygenases. Further investigation on other 4(5)-imidazolyl chalcone inhibitors is outside the scope of this project.

Table 8: EROD IC_{50} values for 3-pyridyl chalcones with methoxylated B-ring

Inhibitors	B-ring substituents	IC_{50} (μM) CYP1A1	CYP1A2	CYP1B1	CYP1B1 eSR over CYP1A1	CYP1A2
DMU709*	3,4,5-$(OMe)_3$	0.3	25	7	0.04	4
DMU711	phenyl	25	30	3.5	7	9
DMU712	2-(OMe)	6	9	3	2	3
DMU713	3-(OMe)	4	5	0.4	10	13
DMU714	4-(OMe)	7.5	18	3	3	6
DMU715	2,4-$(OMe)_2$	2	3	0.4	5	8
DMU716	3,4-$(OMe)_2$	7	8	0.6	12	13
DMU717	3,5-$(OMe)_2$	0.6	4	0.2	3	20
DMU718	2,3,4-$(OMe)_3$	4	2	0.5	8	4
DMU782	2,5-$(OMe)_2$	3	2	18	0.2	0.1

Note: Chemical structures see Table 5. DMU713 and DMU716 are more selective inhibitors of CYP1B1 which have shown at least 10-fold eSR over the CYP1A enzymes. * Synthesised previously in Chapter 2.

Table 9: EROD IC_{50} values for 3-pyridyl chalcones with hydroxylated B-ring

Inhibitors	B-ring substituents	IC_{50} (μM) CYP1A1	CYP1A2	CYP1B1	CYP1B1 eSR over CYP1A1	CYP1A2
DMU757	2,4-$(OH)_2$	59	NI	>100	nd	nd
DMU760	3,5-$(OH)_2$	NI	NI	NI	nd	nd
DMU763	2-(OH)	13	7	0.8	16	9
DMU764	3-(OH)	20	>100	6	3	>17
DMU765	4-(OH)	NI	NI	NI	nd	nd

Note: Chemical structures see Table 5. DMU763 has shown CYP1B1 selectivity over CYP1A1 and CYP1A2, with eSR of 16 and 9, respectively. NI = no inhibition; nd = not determined.

Table 10: EROD IC_{50} values for 3-pyridyl chalcones with halogenated B-ring

Inhibitors	B-ring substituents	IC_{50} (μM) CYP1A1	CYP1A2	CYP1B1	CYP1B1 eSR over CYP1A1	CYP1A2
DMU785	3,4-$(Cl)_2$	1.5	1.5	0.15	10	10
DMU786	2,4-$(Cl)_2$	16	7	5	3	1
DMU2123	3-(Cl)	4	1	0.5	8	2
DMU2124	4-(Cl)	6	10	1.5	4	7
DMU2127	3-(Br)	3	0.4	0.2	15	2
DMU2151	3,4-$(F)_2$	15	3	5	3	0.6

Note: Chemical structures see Table 5. DMU785 has shown a 10-fold selectivity over CYP1A enzymes in the EROD assay.

Table 11: EROD IC_{50} values for the tricyclic compounds DMU2154, DMU2155 and DMU2156

Inhibitors	IC_{50} (μM) CYP1A1	CYP1A2	CYP1B1	eSR of inhibitor over CYP1A1	CYP1A2
DMU2154	NI	NI	NI	nd	nd
DMU2155	NI	NI	50	nd	nd
DMU2156	30	>100	7	4	>14

Note: Full chemical structures see Figure 25. NI = no inhibition; nd = not determined.

Table 12: EROD IC_{50} values for 3-pyridyl chalcones with polycyclic B-ring

Inhibitors	B-ring substitunets	IC_{50} (μM)			eSR of inhibitor over	
		CYP1A1	CYP1A2	CYP1B1	CYP1A1	CYP1A2
DMU745	2-naphthyl	0.3	2	0.02	15	100
DMU746	1-naphthyl	1	3	0.09	11	33
DMU762	3,4-MDO	2	11	0.8	3	14
DMU2133	9-anthracenyl	15	8	9	2	0.9
DMU2134	4-biphenyl	3	NI	0.5	6	nd
DMU2136	3-phenanthrenyl	0.1	1.5	0.02	5	75
DMU2137	9-phenanthrenyl	0.05	1	0.07	0.7	14
DMU2139	6-OMe-2-naphthyl	1.5	15	0.08	19	188
DMU2140	1-pyrenyl	0.3	5	0.12	3	42

Note: Full chemical structures see Table 6. DMU745, DMU746 and DMU2139 have been shown to be highly selective against CYP1 catalysed EROD reaction. nd = not determined; MDO = methylenedioxyyphenyl.

3.4 Discussion

All target compounds have been synthesised successfully using different synthetic methods (see Table 4-6). The hydroxylated 3-pyridyl chalcones was synthesised using Synthetic Method 3 as described by Mogilaiah and Bao[157]. This solvent-free method offers a convenient way to synthesise hydroxylated chalcone without the need to employ a hydroxy protective group.

The triaryl compounds DMU2154, DMU2155 and DMU2156 were unexpected products generated during the attempted synthesis of DMU2123, DMU2124 and DMU2127, respectively, using the solution phase Synthetic Method 2. The chemical structures of these triaryl compounds were first evidenced by the unique aliphatic proton chemical shift signatures (Figure 27) detected by proton nuclear magnetic

resonance (NMR) spectroscopy. The chemical structures were finally confirmed by carbon NMR spectroscopy and mass spectroscopy (MS) (see Section 3.5).

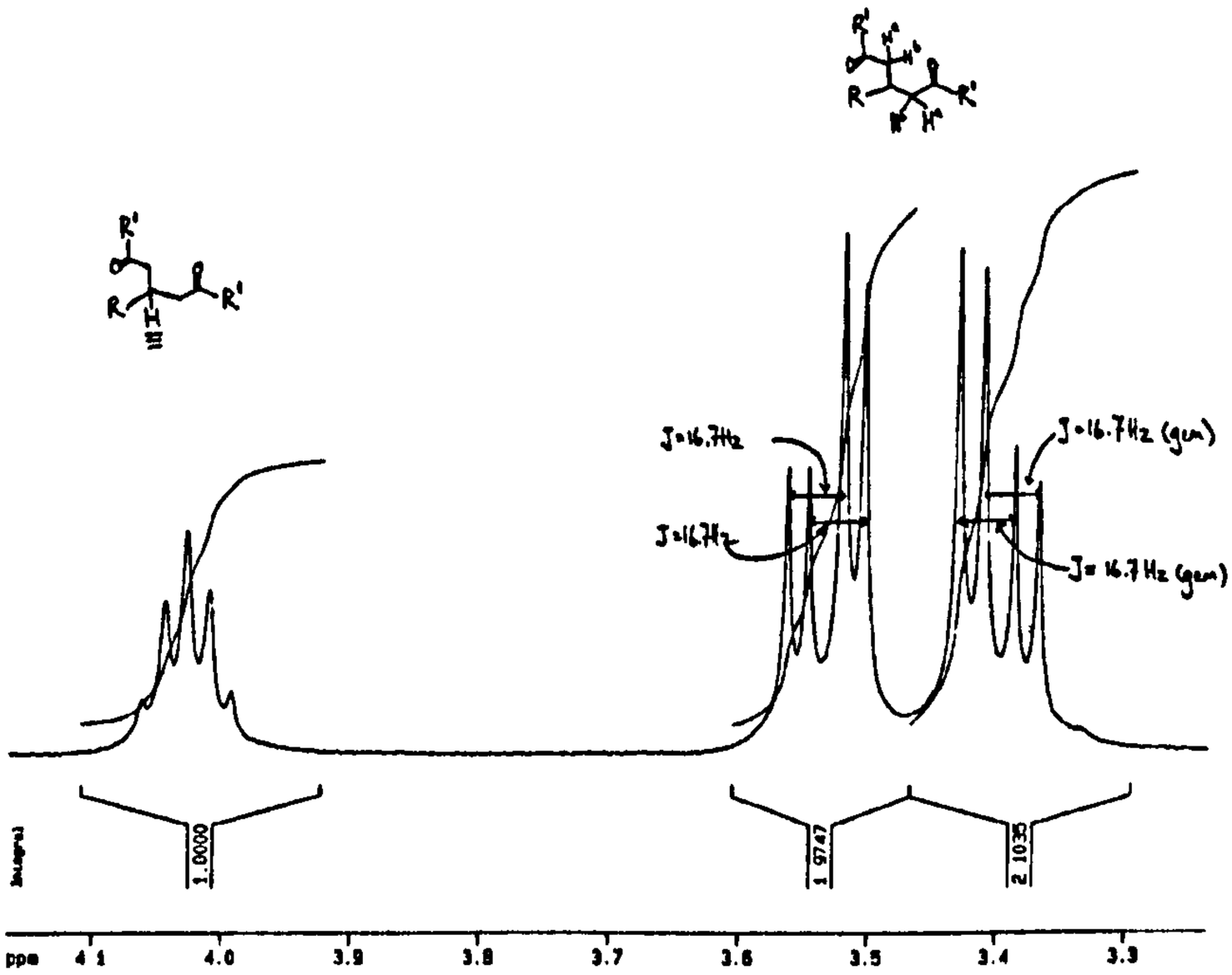

Figure 27: Proton NMR spectrum of DMU2154 aliphatic protons

DMU2155 and DMU2156 proton NMR spectra have also shown similar aliphatic proton chemical shifts and proton-proton coupling patterns.

The formation of these triaryl compounds was due to a secondary Michael conjugation after the target chalcones have been formed initially in the reaction. Unreacted acetophenone enolate can attack the chalcone in a Michael addition reaction. This addition is facilitated by the electron withdrawing halogen substituent which renders the enone carbon atom more susceptible to nucleophilic attack (Figure 28). As the conjugated triaryl product was more stable than the pyridyl chalcone, it eventually became the main product in the reaction. No conjugated product was formed when the solvent-free Synthetic Method 3 was used to synthesise pyridyl chalcones with halogen substituents in the B-ring. This was probably due to the inability of chalcone to form an enolate in solid phase.

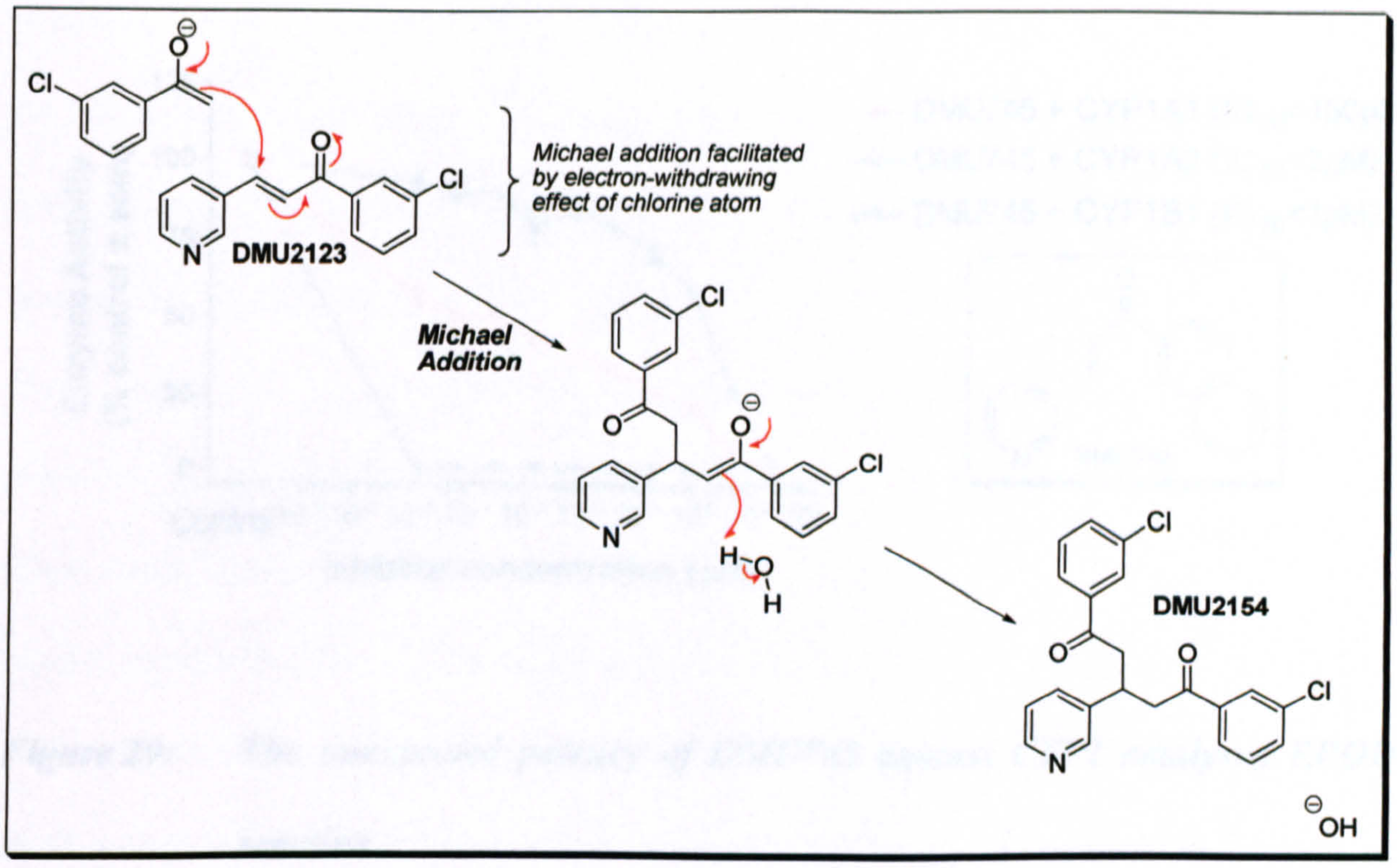

Figure 28: Formation of Michael conjugate DMU2154 from DMU2123

The Michael addition reaction only proceeded in solution phase reaction with pyridyl chalcones that consisted electron-withdrawing substituent group on the B-ring.

In the initial screening of the 3-pyridyl chalcone inhibitors, DMU745, DMU785, DMU2136, DMU2137, DMU2139 and DMU2140 have shown very potent activities against CYP1 catalysed EROD reaction with IC_{50} of less than 1nM (Table 14). Assuming the inhibitors inhibit their target enzyme in a competitive manner i.e. one molecule of inhibitor inhibits one enzyme particle (competitive inhibition); therefore, a recorded IC_{50} value of less than 1nM was not possible since the concentration of enzyme (5nM) used was higher than the concentration of inhibitor in the EROD assay.

A few possibilities that can explain the unusual potency of these inhibitors. First, there could be a tightly controlled allosteric site on the enzyme and the inhibitors could cause a conformational change in the enzyme 3D structure, via interaction with the allosteric site, leading to the total shut down of the P450.

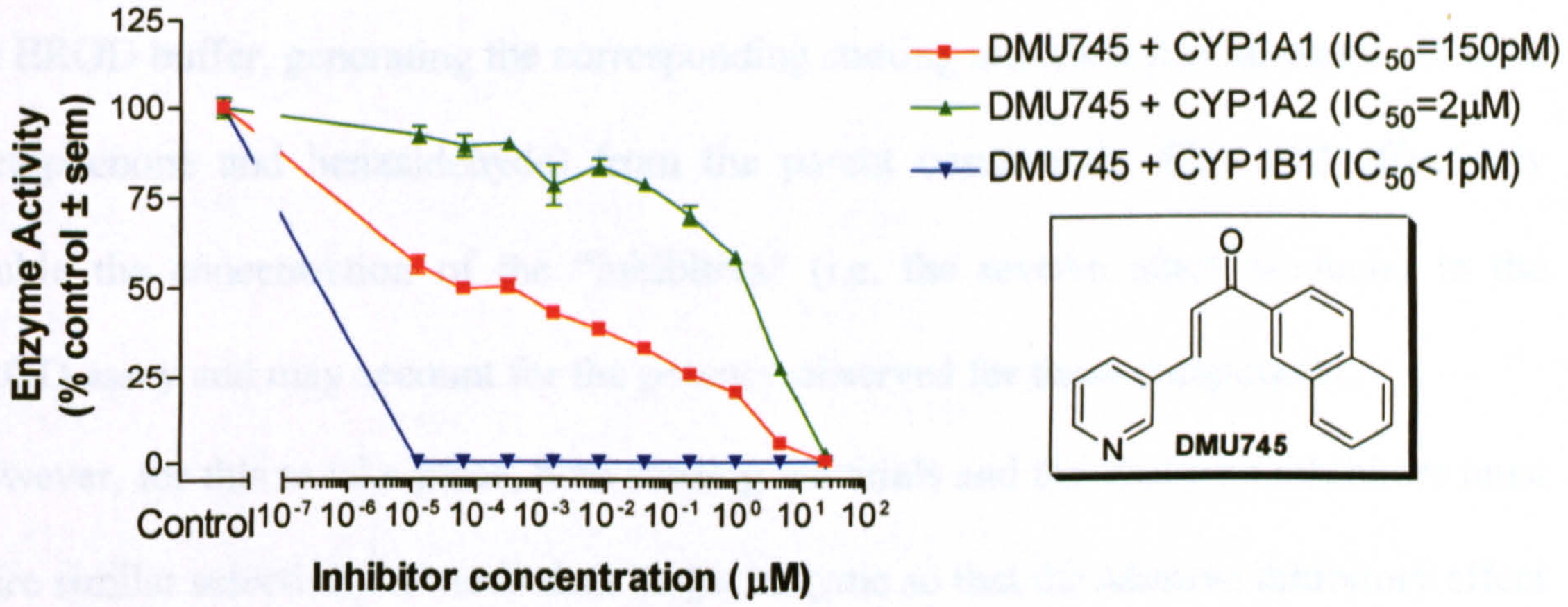

Figure 29: The unexpected potency of DMU745 against CYP1 catalysed EROD reaction

Initially, DMU745 was thought to cause total inhibition of CYP1B1 at 13pM concentration, as opposed to data listed in Table 12. This is unlikely since the amount of P450 present in the assay is more than 100-fold (5nM) of the lowest inhibitor concentration. Further investigation has shown that this anomaly was a result of pipetor tips interaction with DMU745.

7ER, resorufin, components responsible for generating NADPH (i.e. $NADP^+$, glucose-6-phosphate and glucose-6-phospahte dehydrogenase) and NADPH itself can precipitate due to their poor solubility and competition for solubilisation with other organic compounds in the aqueous EROD buffer. Precipitation of these reagents in the EROD buffer during incubation could lead to erroneous conclusion such as those observed with DMU745, DMU785, DMU2136, DMU2137, DMU2139 and DMU2140. Further investigations have shown that there was no precipitation of these reagents during EROD assay. The apparent potency of the inhibitors concerned therefore was not due to precipitation of the reagents used in the EROD assay.

Another possibility to explain the unusual potency of DMU745, DMU785, DMU2136,

DMU2137, DMU2139 and DMU2140 is the inhibitors undergo reverse aldol reaction in the EROD buffer, generating the corresponding starting materials (i.e. an equal molar of acetophenone and benzaldehyde) from the parent compounds. This will effectively double the concentration of the "inhibitors" (i.e. the reverse aldol products) in the EROD assay and may account for the potency observed for these compounds.

However, for this to take place, both starting materials and the chalcone inhibitors must share similar selectivity towards their target enzyme so that the additive inhibitory effect would account for the high potency observed. In order to investigate this possibility, four acetophenones were screened for their EROD inhibitory activity and the results were compared with chalcone inhibitors that were synthesised using these starting materials (Figure 30).

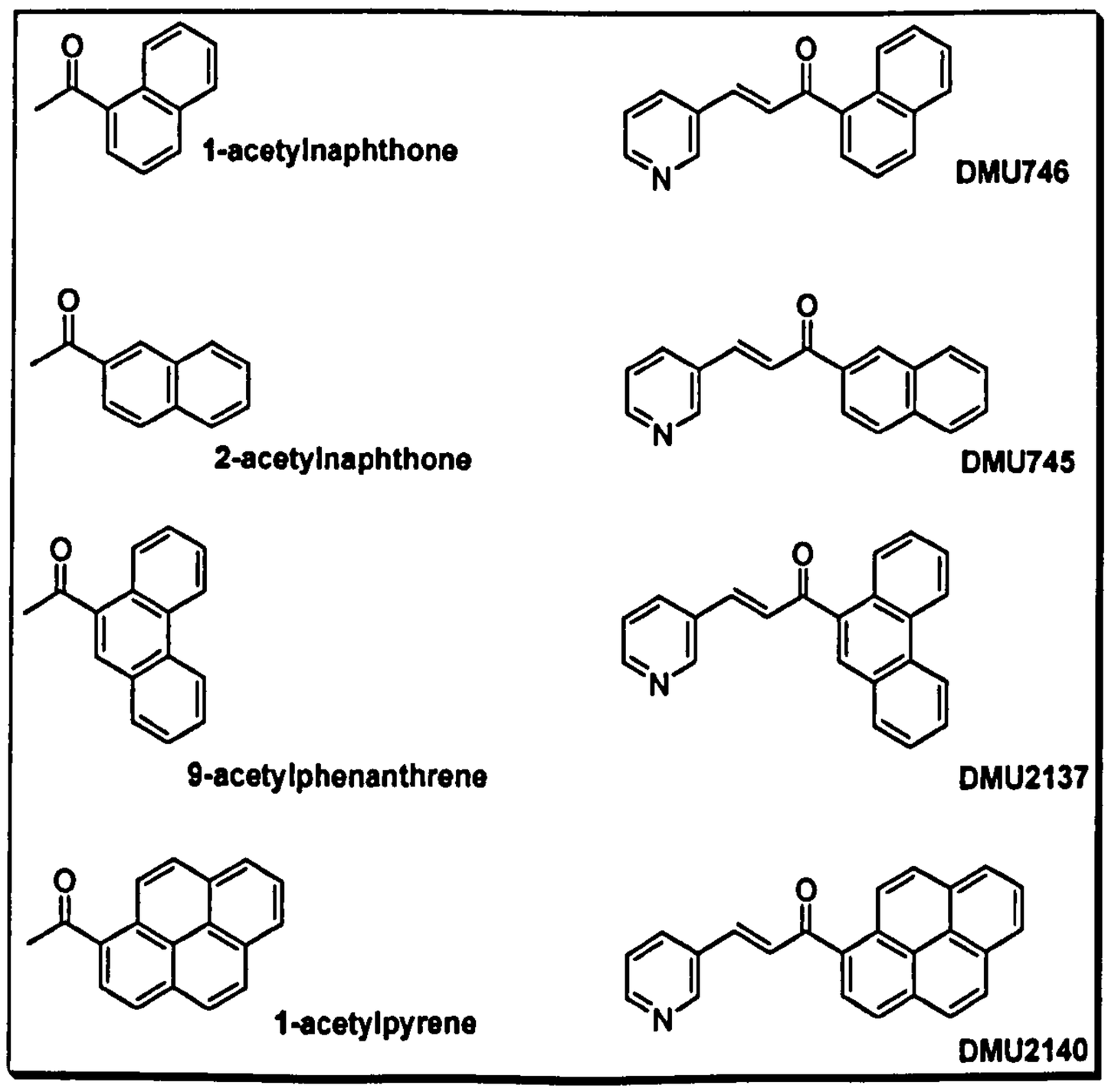

Figure 30: ***Chalcone inhibitors and their corresponding acetophenone starting materials***

Table 13: Chalcone inhibitors and their corresponding starting materials against CYP1 catalysed EROD activity

Inhibitors	IC_{50} (μM) CYP1A1	CYP1A2	CYP1B1	Inhibitors	IC_{50} (μM) CYP1A1	CYP1A2	CYP1B1
1-NAP	NI	100	NI	DMU746	1	3	0.09
2-NAP	NI	14	NI	DMU745	<0.001	4.5	<0.001
9-Phen	15	0.06	1.7	DMU2137	<0.001	0.5	<0.001
1-AcPy	2.5	0.18	0.18	DMU2140	0.2	5	0.008

Note: 1-NAP = 1-acetylnaphthone; 2-NAP = 2-acetylnaphthone; 9-Phen = 9-acetylphenanthrene and 1-AcPy = 1-acetylpyrene; NI = no inhibition. Full chemical structures see Figure 30.

The contrast in potency and selectivity of the 3-pyridyl chalcones and their corresponding starting materials (Table 13) indicated that the suggested reverse aldol reaction did not take place during the EROD assay. The unusual potency for DMU745 to inhibit both CYP1A1 and CYP1B1 with less than 1nM IC_{50} values could not be a result of the combined effects of the products from the reverse aldol reaction. 2-Acetylnaphthone, the starting material of DMU745, did not inhibit either CYP1A1 or CYP1B1. Furthermore, 1-acetylpyrene and 9-acetylphenanthrene, both were starting materials for DMU2140 and DMU2137, respectively, have shown different selectivity against CYP1 catalysed EROD activity. These results have shown that the inhibitors concerned were stable under incubation condition and the apparent potency was not the combined effects of the reverse aldol products.

During the above investigation, a previously unreported CYP1A2 inhibitor has been identified. 9-Acetylphenanthrene is a more potent and more selective inhibitor of CYP1A2 than furafylline[160,161]. Furafylline, as a mechanism based inhibitor, pre-incubation is a necessity. Whereas for 9-acetylphenanthrene, pre-incubation is not required before EROD experiment.

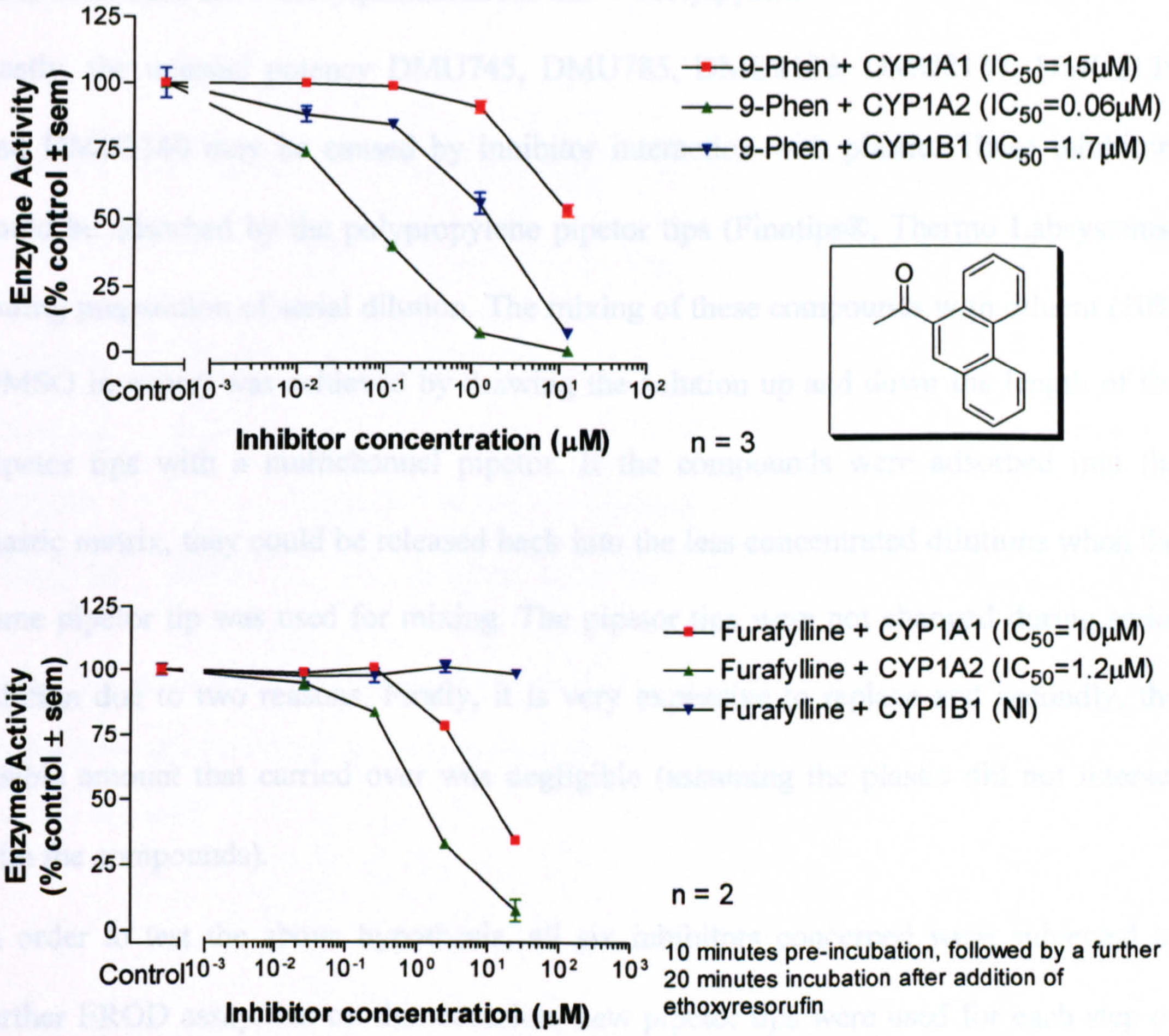

Figure 31: Selective inhibitors of CYP1A2

9-Acetylphenanthrene is a better selective CYP1A2 inhibitor compared to furafylline. 9-Acetylphenanthrene has higher potency and the lack of the need to pre-incubate the inhibitor prior to experiment. NI = no inhibition. 9-Phen = 9-acetylphenanthrene.

The screening of the above acetophenones has also provided some SAR information for the CYP1 enzymes. CYP1 enzymes favour aromatic polycyclic compounds. This is evidenced by the fact that as the size of the aromatic fused-ring increased, the EROD IC_{50} values for all CYP1 family enzymes were generally decreased (Table 13). CYP1A2 may not favour bulkier aromatic group. This has been shown by the 3-fold increase in

IC_{50} value between 9-acetylphenanthrene and 1-acetylpyrene.

Lastly, the unusual potency DMU745, DMU785, DMU2136, DMU2137, DMU2139 and DMU2140 may be caused by inhibitor interaction with plastic. These inhibitors could be adsorbed by the polypropylene pipetor tips (Finntips®, Thermo Labsystems) during preparation of serial dilution. The mixing of these compounds with diluent (10% DMSO in water) was achieved by drawing the solution up and down the length of the pipetor tips with a multichannel pipetor. If the compounds were adsorbed into the plastic matrix, they could be released back into the less concentrated dilutions when the same pipetor tip was used for mixing. The pipetor tips were not changed during serial dilution due to two reasons. Firstly, it is very expensive to replace and secondly, the visible amount that carried over was negligible (assuming the plastic did not interact with the compounds).

In order to test the above hypothesis, all six inhibitors concerned were subjected to further EROD assay, but on this occasion, new pipetor tips were used for each step of serial dilution. It was found that the apparent potency of these inhibitors was due to the interaction of the inhibitors with the pipetor tips as described above. It is thought that high retention of inhibitors by the plastic allowed only small amount of inhibitor being released back into each subsequent dilution, but the amount released sufficient to cause potent inhibition of their target enzymes.

Caution should be exercised when interpreting results for DMU745, DMU785, DMU2136, DMU2137, DMU2139 and DMU2140 in Table 14 (values in red) since adsorption of these inhibitors by the plastic still took place when solutions of these compounds were handled by the Finntips®. It was possible that the plastic 96-well microplate used in the assays could also interact with these inhibitors. The actual IC_{50}

values for these inhibitors could therefore be well less than what have been recorded.

Table 14: Results showing the interaction of plastic with some potent inhibitors of CYP1 enzymes

Inhibitors	IC_{50} (μM) CYP1A1	CYP1A2	CYP1B1	Inhibitors	IC_{50} (μM) CYP1A1	CYP1A2	CYP1B1
DMU745	<0.001	4.5	<0.001	DMU2137	<0.001	0.5	<0.001
	0.3	2	0.02		0.05	1	0.07
DMU785	3	2.3	<0.001	DMU2139	1	20	<0.001
	1.5	1.5	0.15		1.5	15	0.08
DMU2136	<0.001	1	<0.001	DMU2140	0.2	5	0.008
	0.1	1.3	0.02		0.3	5	0.12

The IC_{50} values recorded in red were data from experiments where new pipetor tips were used for mixing.

The inhibitors still showed similar selectively against their target CYP1 enzymes even the potency have markedly decreased.

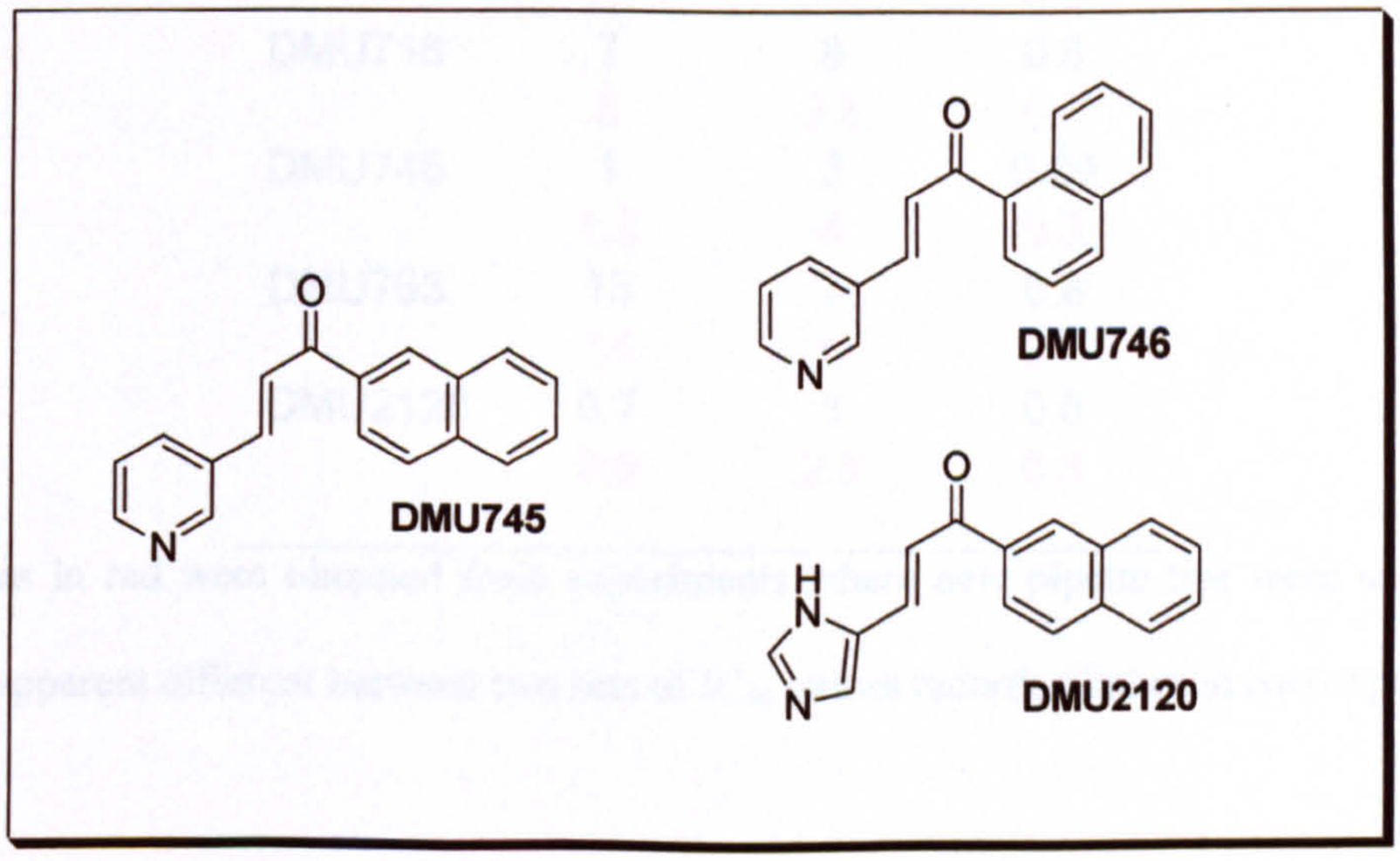

Figure 32: Chemical structure of DMU745 and its analogues

In view of the observations that some compounds do interact with the Finntips®, six 3-pyridyl chalcones were chosen to investigate whether this phenomenon is only limited to the few compounds listed in Table 14. This was achieved by repeating EROD assay

where new pipetor tips were used in each serial dilution mixing steps. It was found that no apparent plastic interaction was observed with these 6 compounds (see Table 15). The regio-isomer of DMU745, namely DMU746, and the imidazolyl analogue DMU2120, did not interact with the plastic pipetor tips (Figure 32). This evidence strongly suggests the polypropylene used in this particular brand of pipette tips interacts with 3-pyridyl chalcone inhibitors in a compound specific manner.

Table 15: EROD results showing no interaction of plastic with other inhibitors of CYP1 enzymes

Inhibitors	IC_{50} (μM) CYP1A1	CYP1A2	CYP1B1
DMU709	0.3	25	7
	0.5	13	2.5
DMU713	4	5	0.4
	6	2.5	0.3
DMU716	7	8	0.6
	8	6.5	0.5
DMU746	1	3	0.09
	1.3	4	0.3
DMU763	13	7	0.8
	14	6	0.7
DMU2120	0.7	3	0.5
	0.8	2.5	0.3

The IC_{50} values in red were obtained from experiments where new pipette tips were used for mixing. There was no apparent different between two sets of IC_{50} values recorded between two experiments.

The pharmacophores for the CYP1 ienzymes were constructed by mapping different inhibitors molecules together, using the coordination of the pyridyl lone pair electrons to the P450 haem as anchorage point. This type of mapping was pioneered in drug design by McCague and Potter, which led to the successful design of anticancer agents

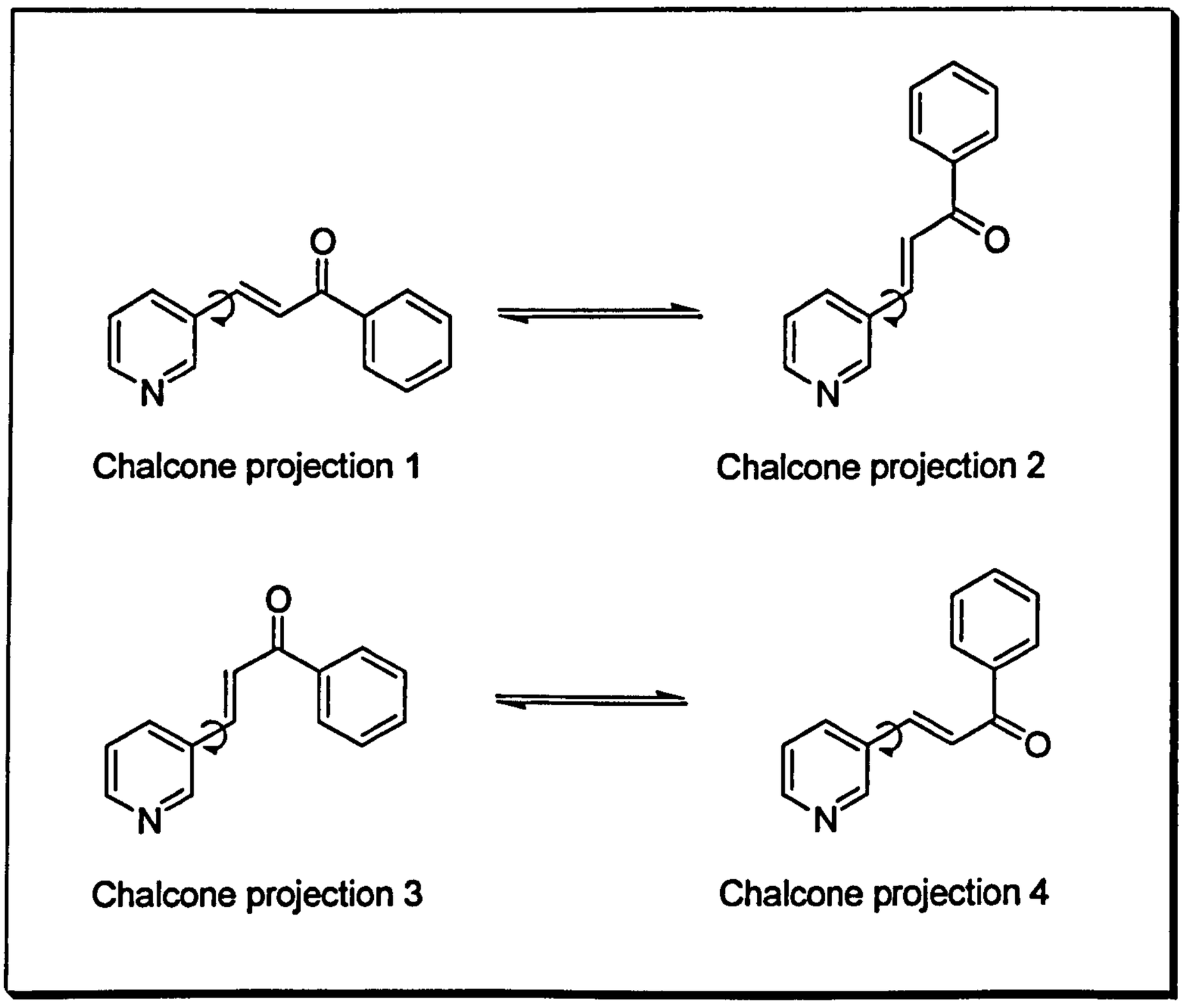

Figure 33: Four possible spatial orientations of 3-pyridyl chalcone

Tamandron[162], Idoxifene[163] and Abiraterone[164]. The inhibitors molecules were mapped out following two rules: (i) minimal space and (ii) mapping the inhibitor molecules all to one side to reduce complexity of the model. Chalcone has four spatial projections (Figure 33). Projection 1 and 2 occupy more 3D space than projection 3 and 4. Therefore, projection 3 and 4 were preferably used for mapping.

The mapping of chalcone can be arbitrarily chosen to the left or right of the haem, where the haem is located at the base of the model. Both mapping to the left or to the right are equally valid since they are relative to the haem. In this project, the chalcone inhibitors were mapped by projection of the chalcones to the right, such as shown in Figure 34.

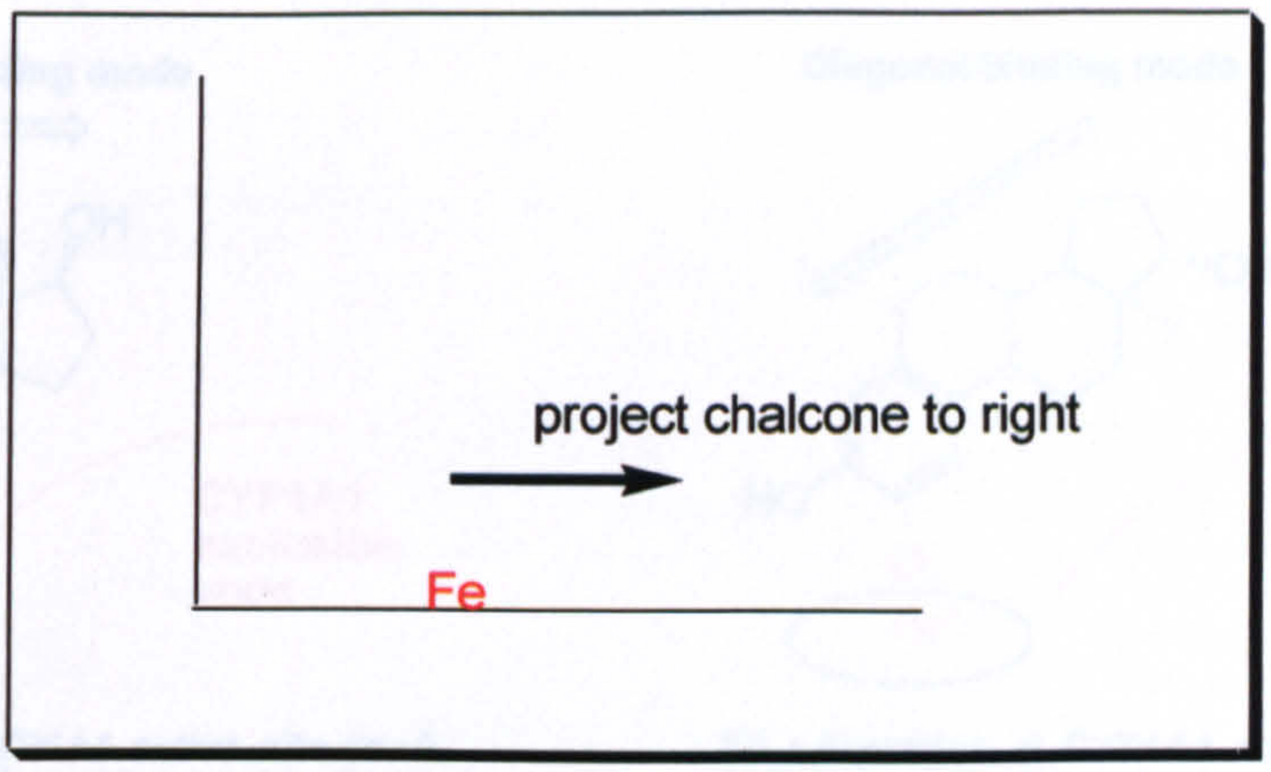

Figure 34: Projection of the chalcone molecule to the right of the pharmacophore model.

The mapping to one side rule reduces the variability of molecular mapping and hence resulted in a less complex pharmacophore model.

To construct CYP1A1 pharmacophore, first the orientation of the chalcone inhibitors within CYP1A1 active site has to be determined. Badawi *et. al.*[88] have shown that CYP1A1 preferentially metabolised estradiol (E2) to 2-hydroxy estradiol (2OH-E2). The formation of 4-hydroxy estradiol (4OH-E2) by CYP1A1 only at approximately 0.25 nmol/min/nmol P450 compared with formation of 2OH-E2 at approximately 8 nmol/min/nmol P450. This indicated that E2 has to orientate itself diagonally in CYP1A1 active site to undergo 2-hydroxylation (Figure 35). 4-Hydroxylation of E2 is not favoured by CYP1A1 indicative the presence of an exlusion zone to the right of the haem (Figure 35). Since the 3-pyridyl chalcone projection 4 has a better mapping onto the E2 molecule, this projection was used to construct CYP1A1 pharmacophore model. The presence of a hydrogen bonding interaction near the exclusion may help to anchor the E2 and chalcone molecules in the enzyme active site.

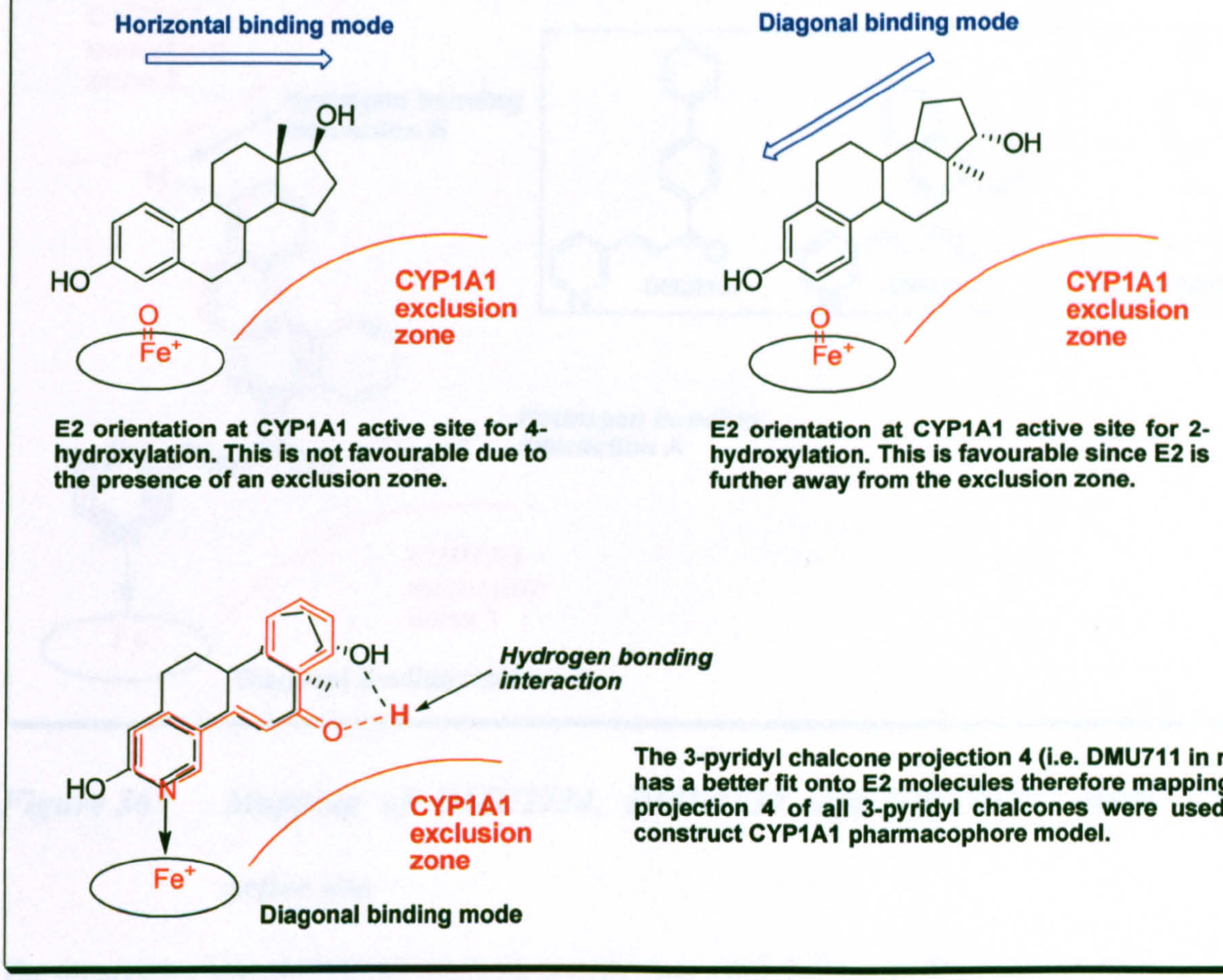

Figure 35: Possible orientation of estradiol and DMU711 in CYP1A1 active site

The presence of a second exclusion zone in CYP1A1 pharmacophore is evidenced by the decrease in CYP1A1 selectivity from DMU2137 (IC_{50} 0.05μM)→ DMU2139 (IC_{50} 1.5μM)→ DMU2134 (IC_{50} 3μM). These inhibitors have progressively longer B-ring structures that extend towards the apex of the model (Figure 36). DMU2134 is 60-fold less selective than DMU2137 probably because the bi-phenyl ring system in DMU2134 is too close to exclusion zone 2. Although the lengths of molecule between DMU2134 and DMU2139 are more or less the same, DMU2139 selectivity is twice of DMU2134. This observation suggested that there is a hydrogen binding interaction between the methoxy oxygen and an amino acid residue.

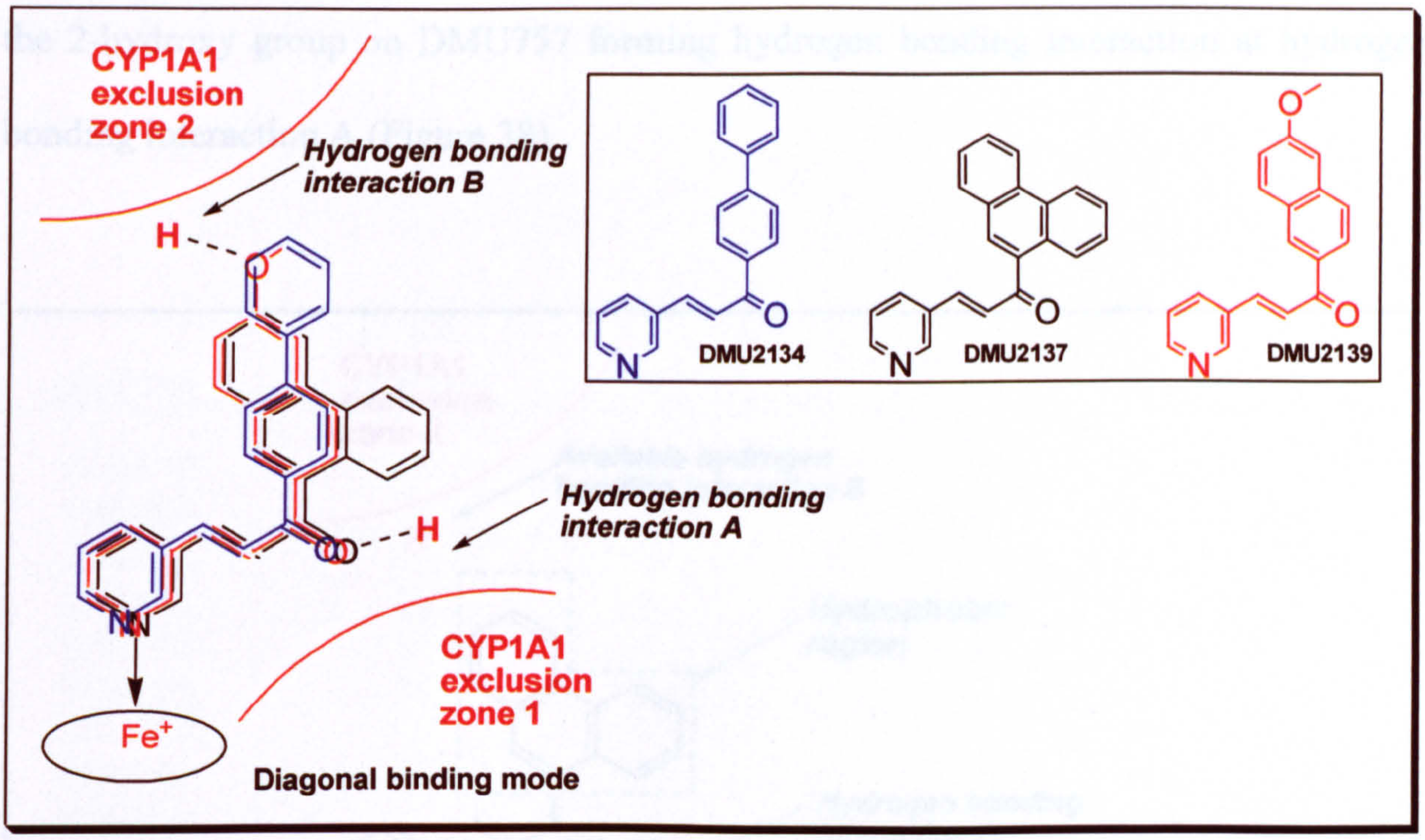

Figure 36: Mapping of DMU2134, DMU2137 and DMU2139 within CYP1A1 active site

The progressive loss of CYP1A1 inhbitory activity from DMU2137 to DMU2139 to DMU2134 indicates the presence of a second exclusion zone.

Amongst all the 3-pyridyl chalcones with polycyclic B-ring substituent, the 9-phenanthrenyl-3-pyridyl chalcone has the strongest inhibitory activity towards CYP1A1 catalysed EROD reaction. This indicates the presence of a specifically shaped hydrophobic region in the active site (Figure 37). The existence of the hydrophobic region is supported by the fact that the mono-methoxylated 3-pyridyl chalcones (DMU712, DMU713 and DMU714) are more potent CYP1A1 inhibitors than their mono-hydroxylated counterparts (DMU763, DMU764 and DMU756; see Table 16). The 3,5-dihydroxy-3-pyridyl chalcone (DMU760) has no inhibitory activity on CYP1A1 because both of its hydroxy groups were mapped within the hydrophobic region. DMU757 has weak inhibitory activity on CYP1A1 probably due to the ability of

the 2-hydroxy group on DMU757 forming hydrogen bonding interaction at hydrogen bonding interaction A (Figure 38).

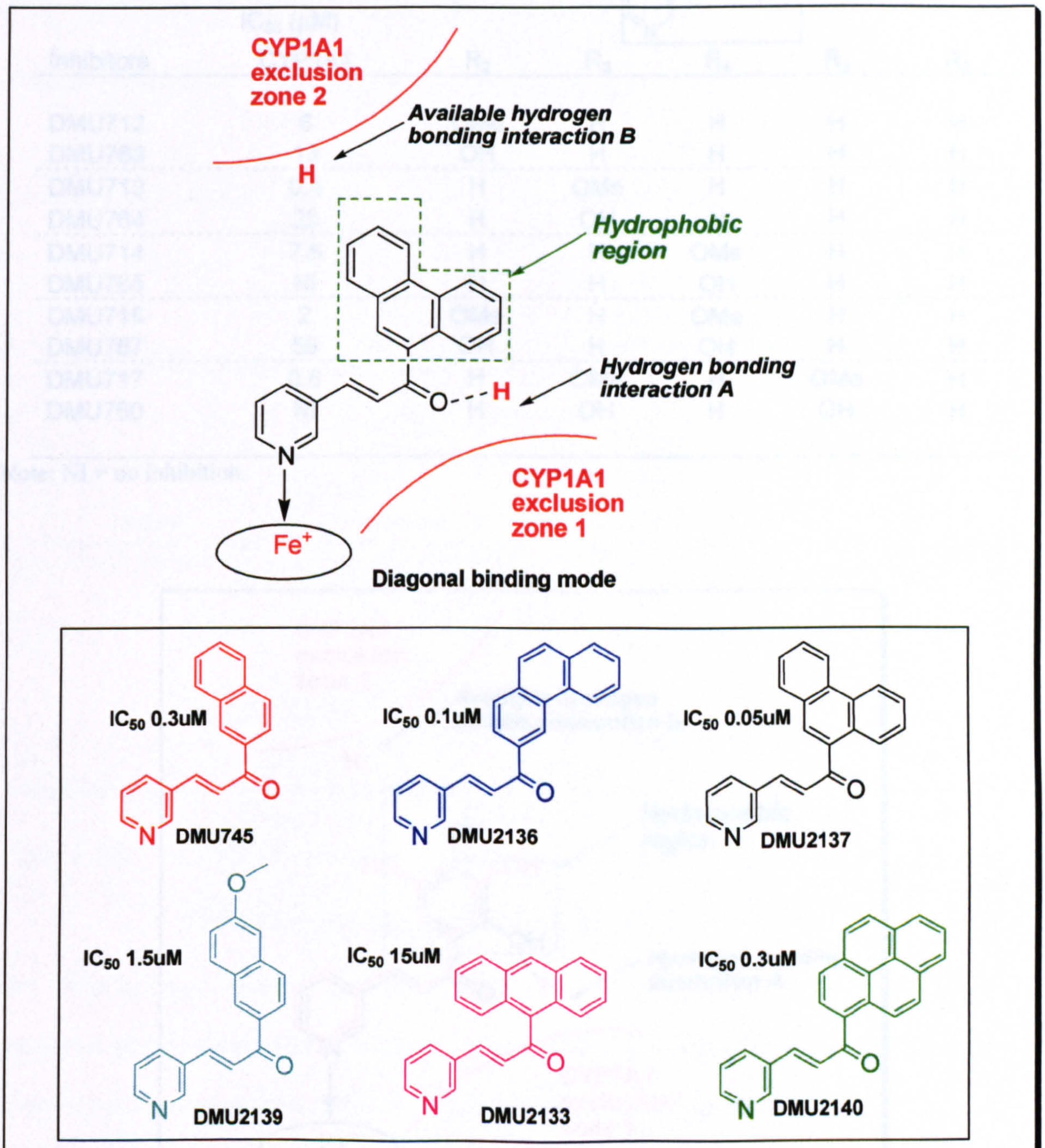

Figure 37: ***CYP1A1 pharmacophore model showing a hydrophobic region in the diagonal binding pocket***

Table 16: EROD results showing the hydrophobic nature of CYP1A1 active site

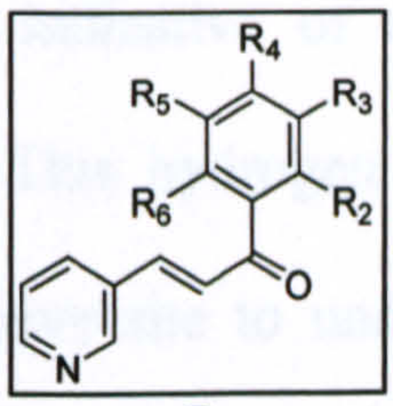

Inhibitors	IC_{50} (μM) CYP1A1	R_2	R_3	R_4	R_5	R_6
DMU712	6	OMe	H	H	H	H
DMU763	13	OH	H	H	H	H
DMU713	0.4	H	OMe	H	H	H
DMU764	20	H	OH	H	H	H
DMU714	7.5	H	H	OMe	H	H
DMU765	NI	H	H	OH	H	H
DMU715	2	OMe	H	OMe	H	H
DMU757	59	OH	H	OH	H	H
DMU717	0.6	H	OMe	H	OMe	H
DMU760	NI	H	OH	H	OH	H

Note: NI = no inhibition.

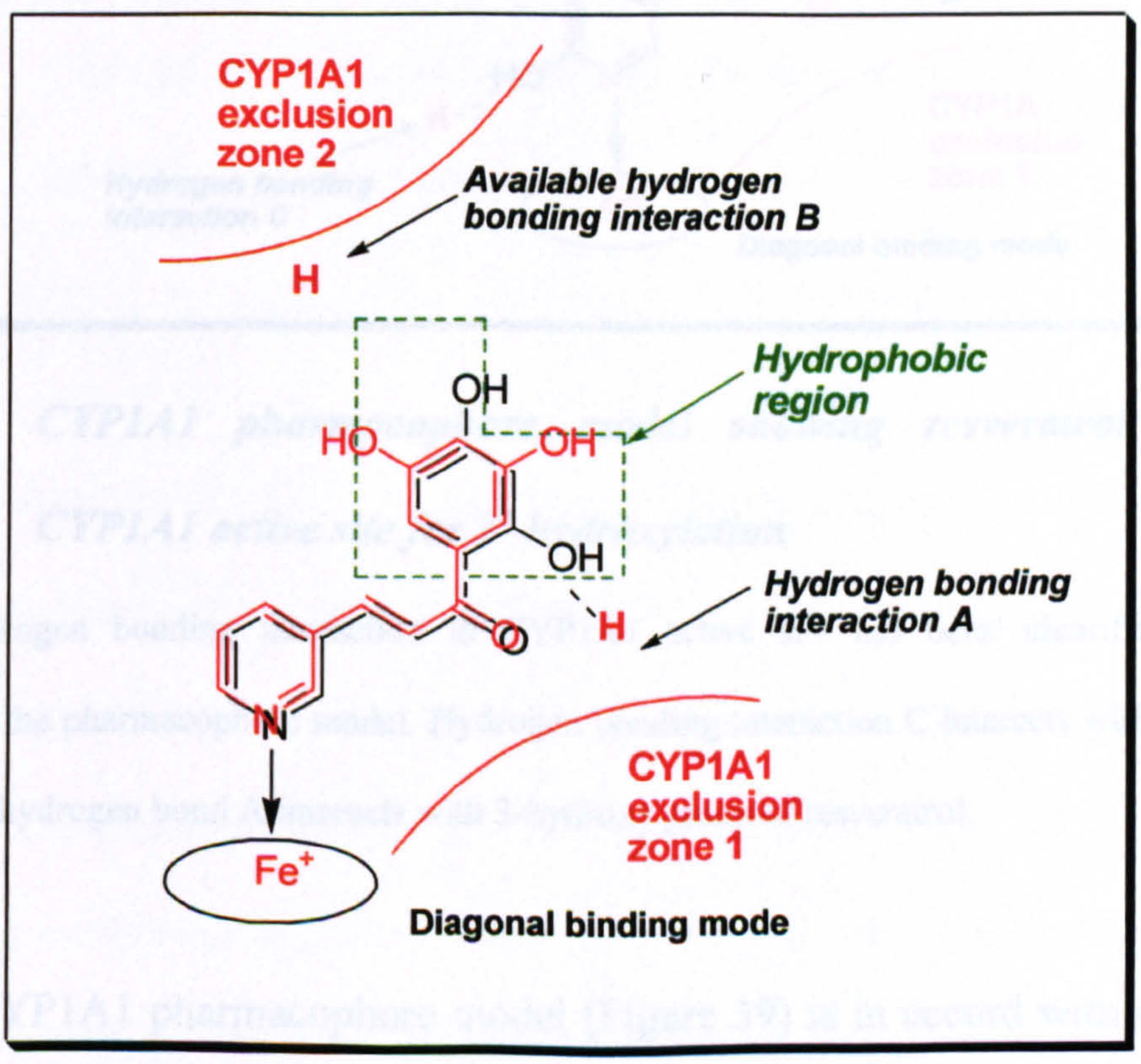

Figure 38: CYP1A1 pharmacophore model showing the mapping of DMU757 (black) and DMU760 (red)

CYP1A1 catalysed metabolism of resveratrol to piceatannol more efficiently compared with other CYP1 enzymes[139] and this result is indicative of a hydrogen-bonding interaction near the CYP1A1 haem (Figure 39). This hydrogen bonding interaction helps anchoring resveratrol within the enzyme active site to undergo metabolism to form piceatannol.

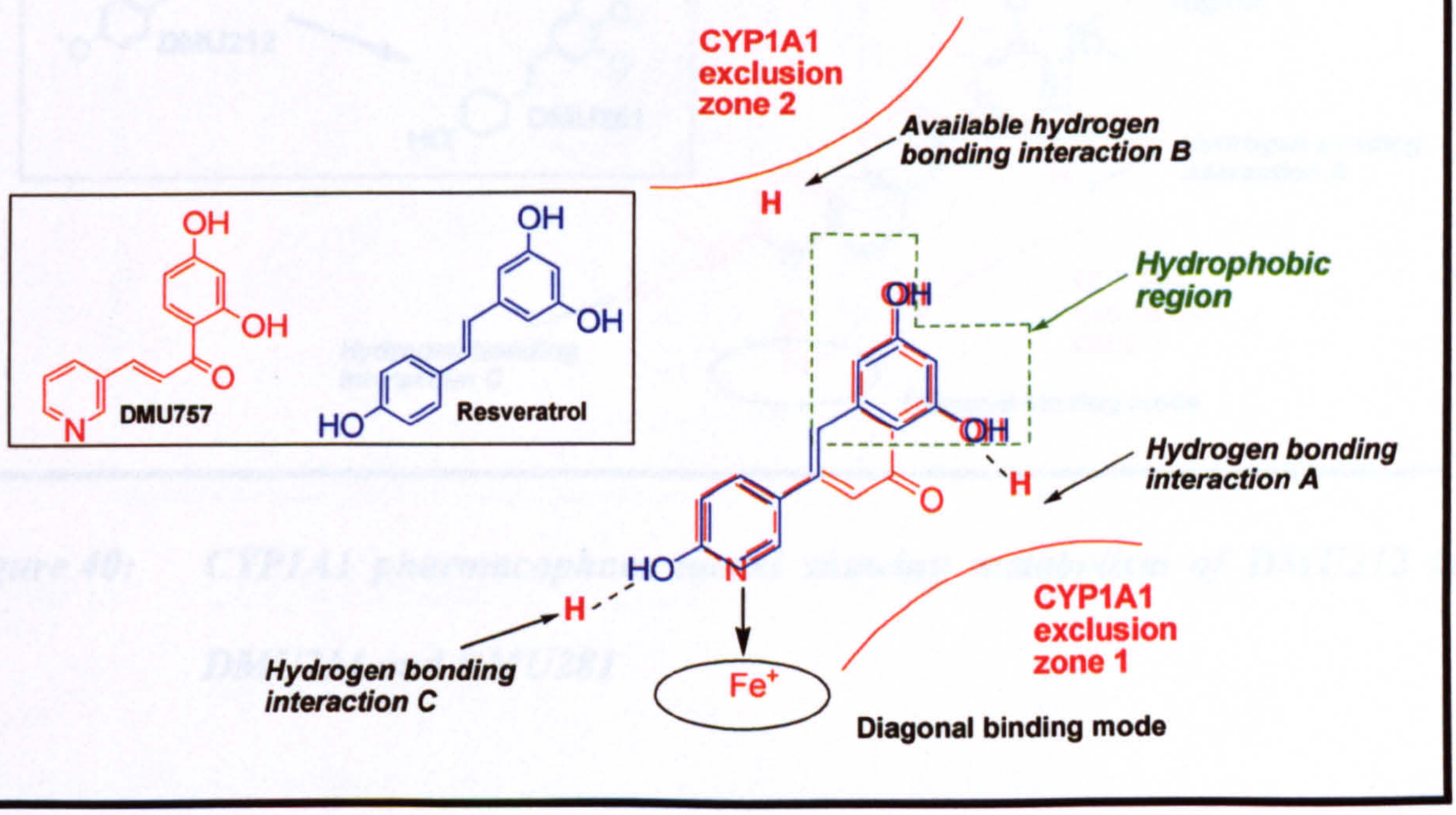

Figure 39: CYP1A1 pharmacophore model showing resveratrol binding in CYP1A1 active site for 3'-hydroxylation

One extra hydrogen bonding interaction in CYP1A1 active site has been identified by mapping resveratrol into the pharmacophore model. Hydrogen bonding interaction C interacts with the 4'-hydroxy substituent and hydrogen bond A interacts with 3-hydroxy group of resveratrol.

The above CYP1A1 pharmacophore model (Figure 39) is in accord with the pattern of metabolism of DMU212 by CYP1A1[139]. CYP1A1 preferably metabolised DMU212 to DMU214 and DMU281 (Figure 40). Mapping of DMU212 onto the constructed

CYP1A1 pharmacophore model has shown how DMU212 orientated itself to form DMU214 and DMU281.

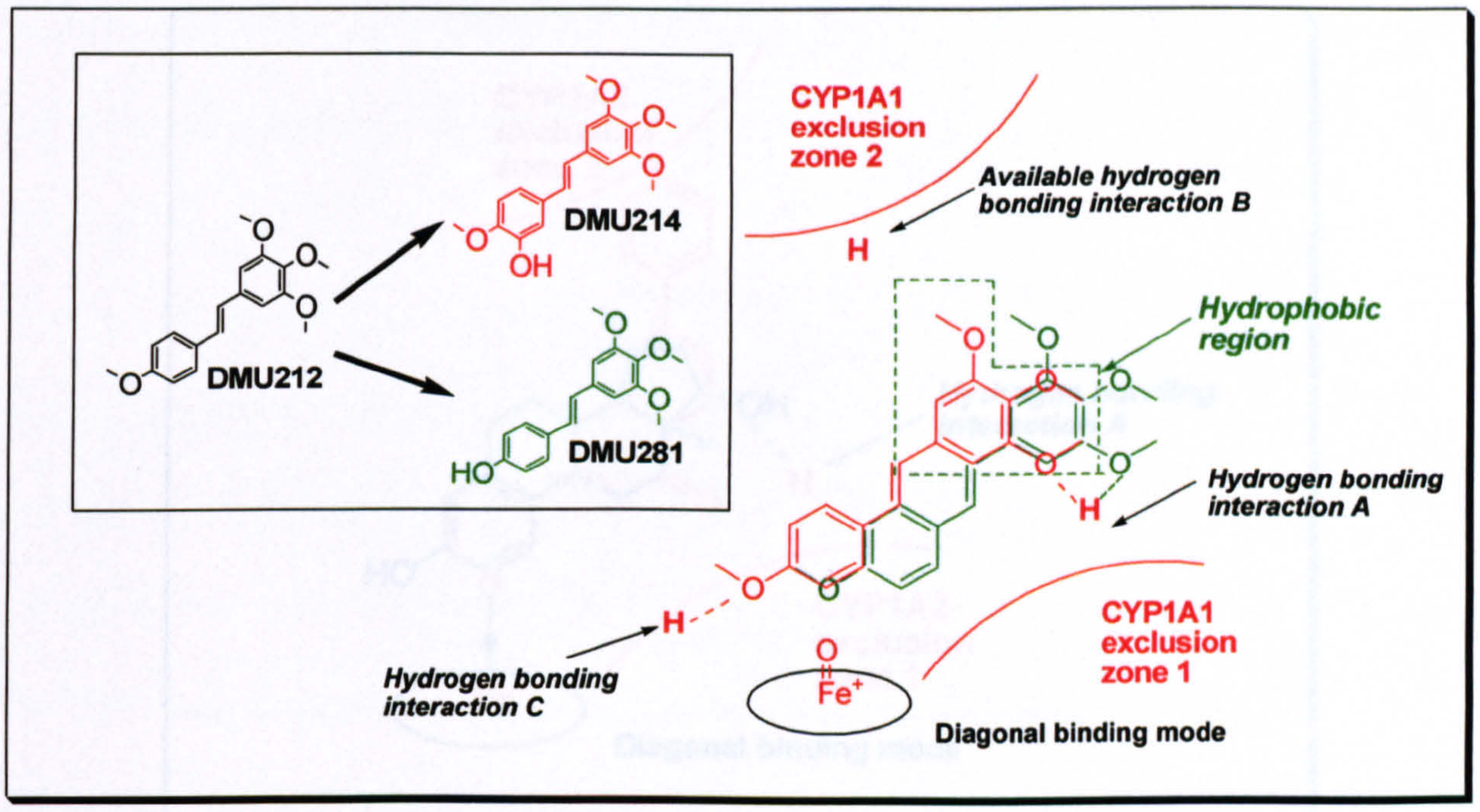

Figure 40: CYP1A1 pharmacophore model showing metabolism of DMU212 to DMU214 and DMU281

A close inspection on CYP1A2 IC_{50} values of the compounds used to generate CYP1A1 pharmacophore model, the potency of these compounds to inhibit CYP1A2 are slightly decreased. Since CYP1A2 is the most efficient CYP1 enzyme to catalyse the formation of 2OH-E2[88], it was thought that CYP1A2 also has a similar diagonal binding pocket as CYP1A1. The 4-biphenyl-3-pyridyl chalcone DMU2134 did not inhibit CYP1A2 at all, which indicated that the bi-phenyl B-ring of DMU2134 is too bulky for CYP1A2 active site (Figure 41). The CYP1A2 exclusion zone 2 could be closer to the haem and therefore reducing the overall size of the active site pocket. A hydrogen binding

interaction near the exclusion zone 1 may have help to anchor E2 molecule within the active site by interacting with the 17β-hydroxy group.

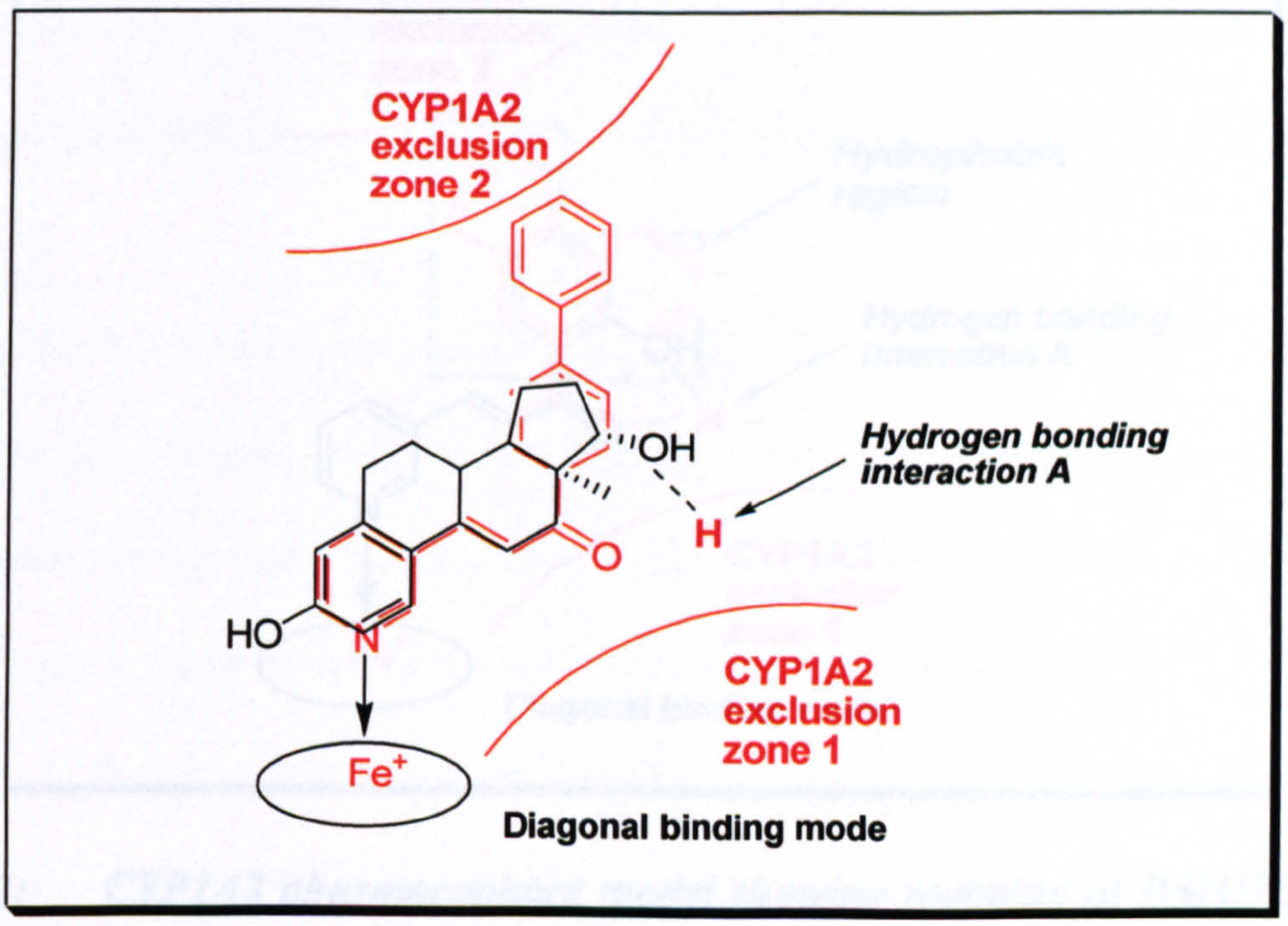

Figure 41: CYP1A2 pharmacophore model showing mapping of DMU2134 (red) and estradiol (black)

The exclusion zone 2 is closer to the haem and effectively reduces the size of the active site pocket. DMU2134 is too bulky to fit into the binding pocket hence its inability to inhibit CYP1A2.

DMU763 inhibits CYP1A2 with IC_{50} of 7μM, DMU764 inhibits the P450 with IC_{50} more than 100μM and DMU765 does not inhibit CYP1A2 (Table 9). These observations confirm the presence of hydrogen bonding interaction at point A, which interacts with the 2-hydroxy group on DMU763. The inability for both dihydroxy 3-pyridyl chalcones (DMU757 and DMU760) to inhibit CYP1A2 indicates the presence of hydrophobic region. Since not much differences in data were observed to delineate the size and shape of CYP1A2 hydrophobic region, it is temporary assigned similar as

with CYP1A1 (Figure 42).

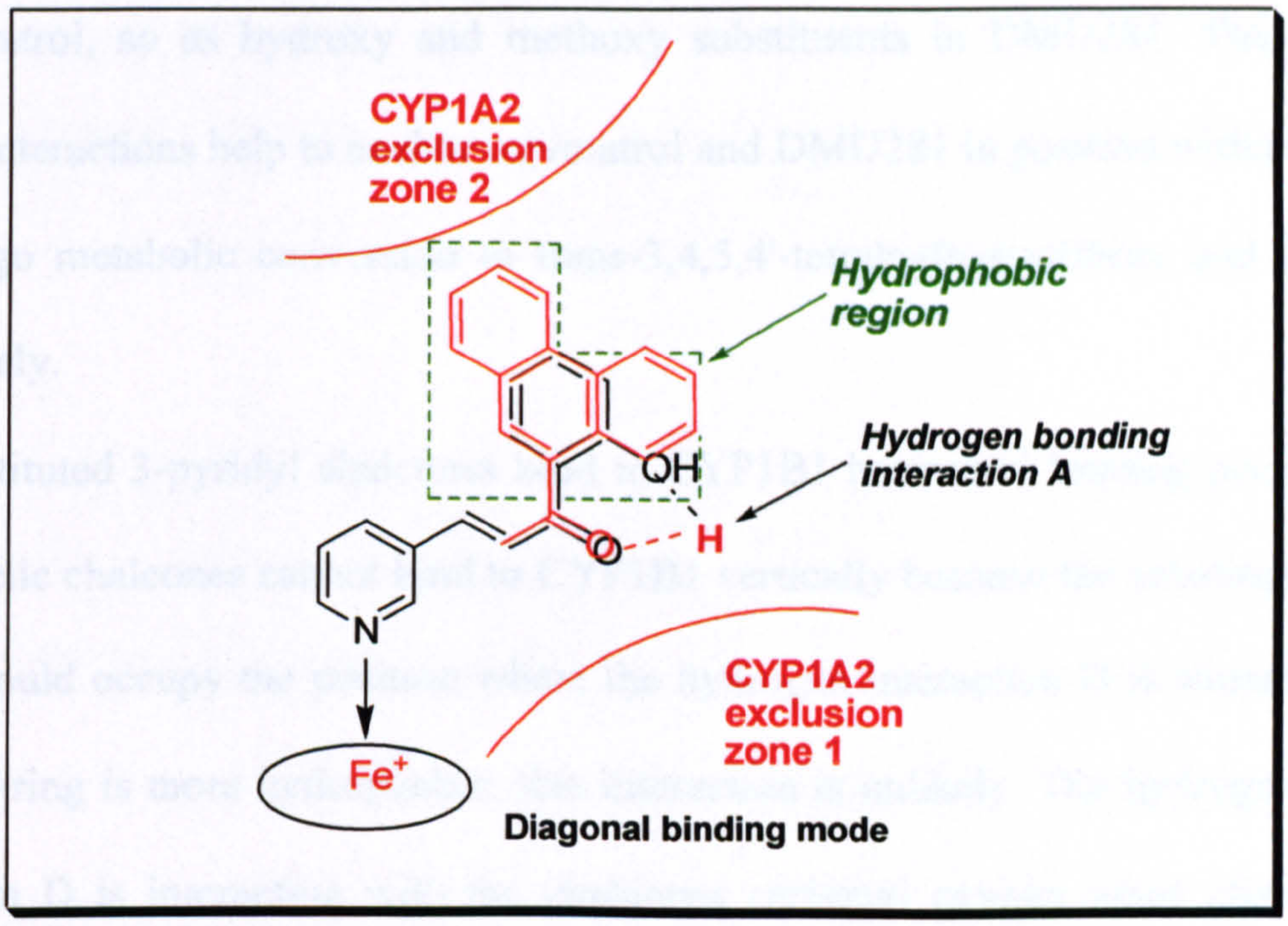

Figure 42: CYP1A2 pharmacophore model showing mapping of DMU763 (black) and the selective CYP1A2 inhibitor 9-acetylphenanthrene (red)

Although CYP1B1 catalyses the formation of piceatannol from resveratrol, Wilsher has found that CYP1B1 is more efficient in converting resveratrol to trans-3,4,5,4'-tetrahydroxystilbene[139]. The same author also found that DMU212 is metabolised to DMU281 by CYP1B1, but the metabolite is further metabolised by CYP1B1 exclusively to give DMU295 (trans-4,4'-dihydroxy-3,5-dimethoxystilbene). Since resveratrol, as well as DMU212 and DMU281, have to orientate within CYP1B1 binding pocket in different way accordingly to facilitate metabolism to form the respective metabolites, CYP1B1 therefore must have 2 distinct binding pockets within the active site.

Figure 43 shows resveratrol orientating itself in CYP1B1 active site ready for 3'- (red)

and 4-hydroxylation (black). Three hydrogen bonding interactions have been assigned to the vertical binding pocket. These hydrogen bonds interact with hydroxy substituents in resveratrol, so as hydroxy and methoxy substituents in DMU281. The hydrogen binding interactions help to anchor resveratrol and DMU281 in position within CYP1B1 to undergo metabolic conversion to trans-3,4,5,4'-tetrahydroxystilbene and DMU295, respectively.

The substituted 3-pyridyl chalcones bind to CYP1B1 horizontal binding pocket. These heterocyclic chalcones cannot bind to CYP1B1 vertically because the substituted phenyl B-ring would occupy the position where the hydrogen interaction D is situated. As the phenyl B-ring is more hydrophobic, this interaction is unlikely. The hydrogen bonding interaction D is interacting with the chalcones carbonyl oxygen when chalcones are bound to CYP1B1 horizontal pocket (Figure 44).

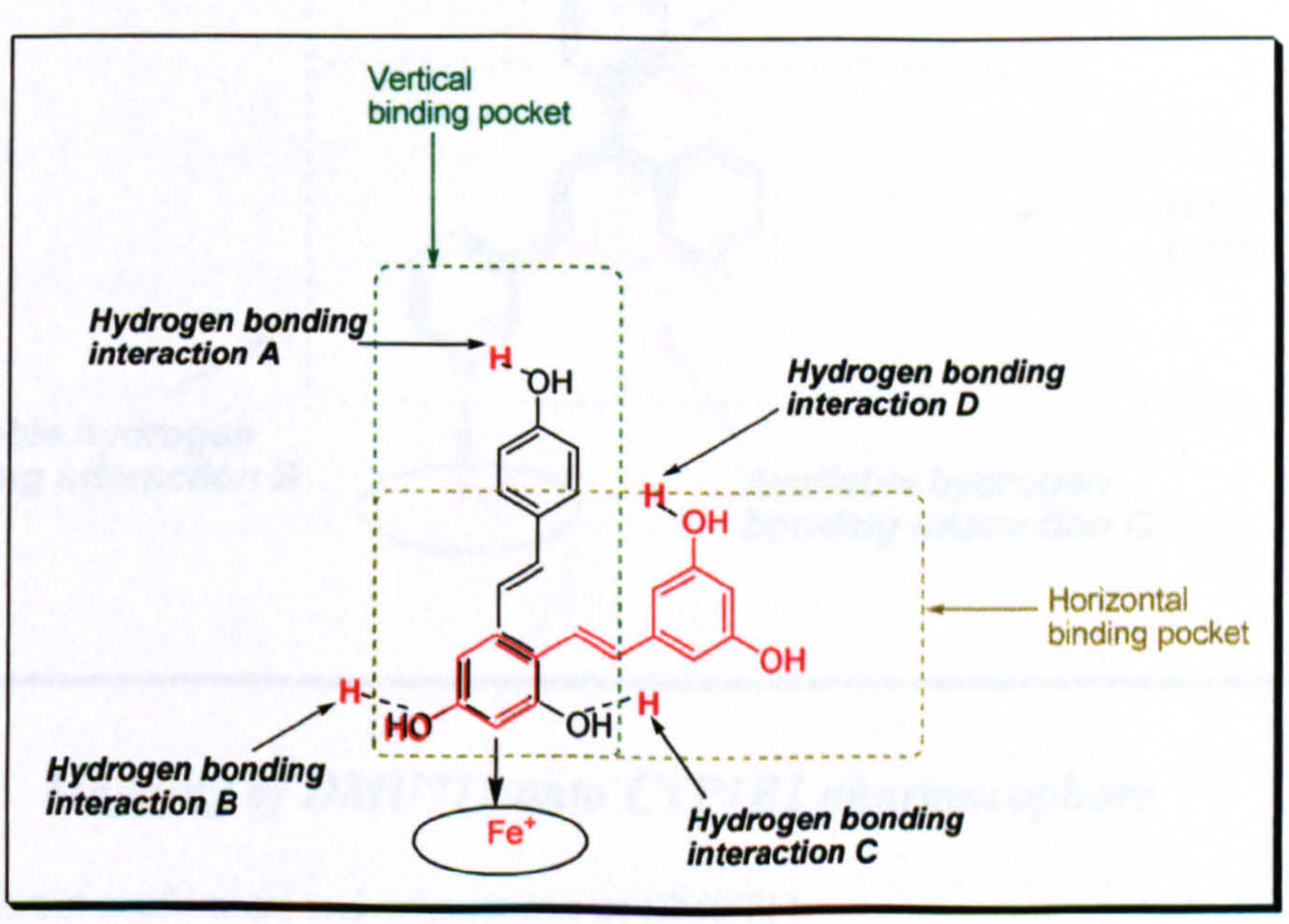

Figure 43: CYP1B1 pharmacophore model showing the vertical and horizontal binding modes of resveratrol

Resveratrol undergoing 3'-hydroxylation (red) in the horizontal binding pocket. The above figure also shows resveratrol undergoing 4-hydroxylation (black) in the vertical binding pocket.

A number of the 3-pyridyl chalcones with a polycyclic aromatic B-ring have shown high selectivity and potency for CYP1B1, with recorded IC_{50} values of less than 100nM (Table 12). IC_{50} values for DMU762, DMU2134 and DMU2140 are ranging from 0.12 μM to 0.8μM and DMU2133 IC_{50} value for CYP1B1 is 9μM. These findings indicate the presence of a hydrophobic region in the CYP1B1 horizontal binding pocket (Figure 45).

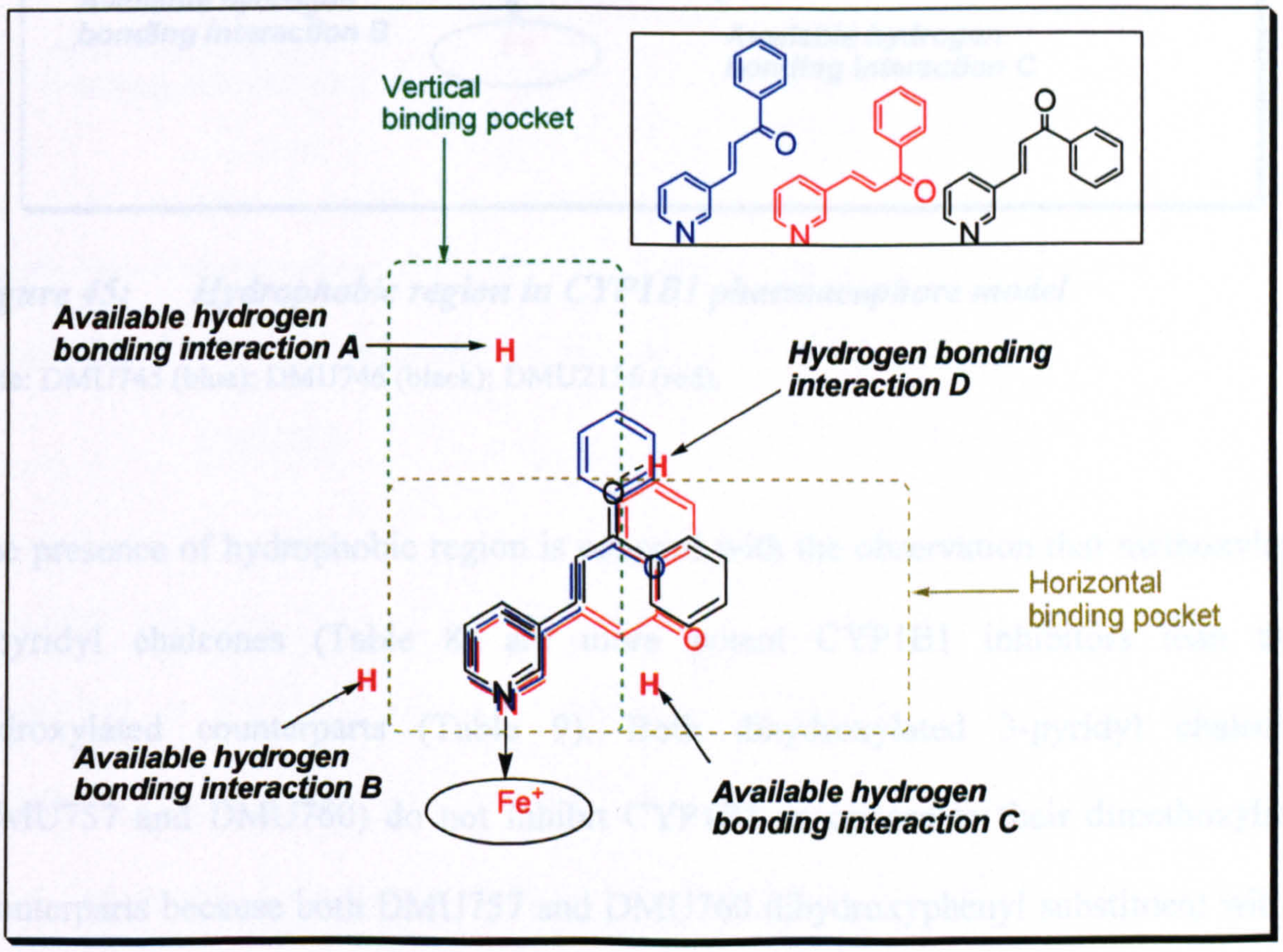

Figure 44: Mapping of DMU711 onto CYP1B1 pharmacophore

Inlet shows different conformers and orientations of DMU711.

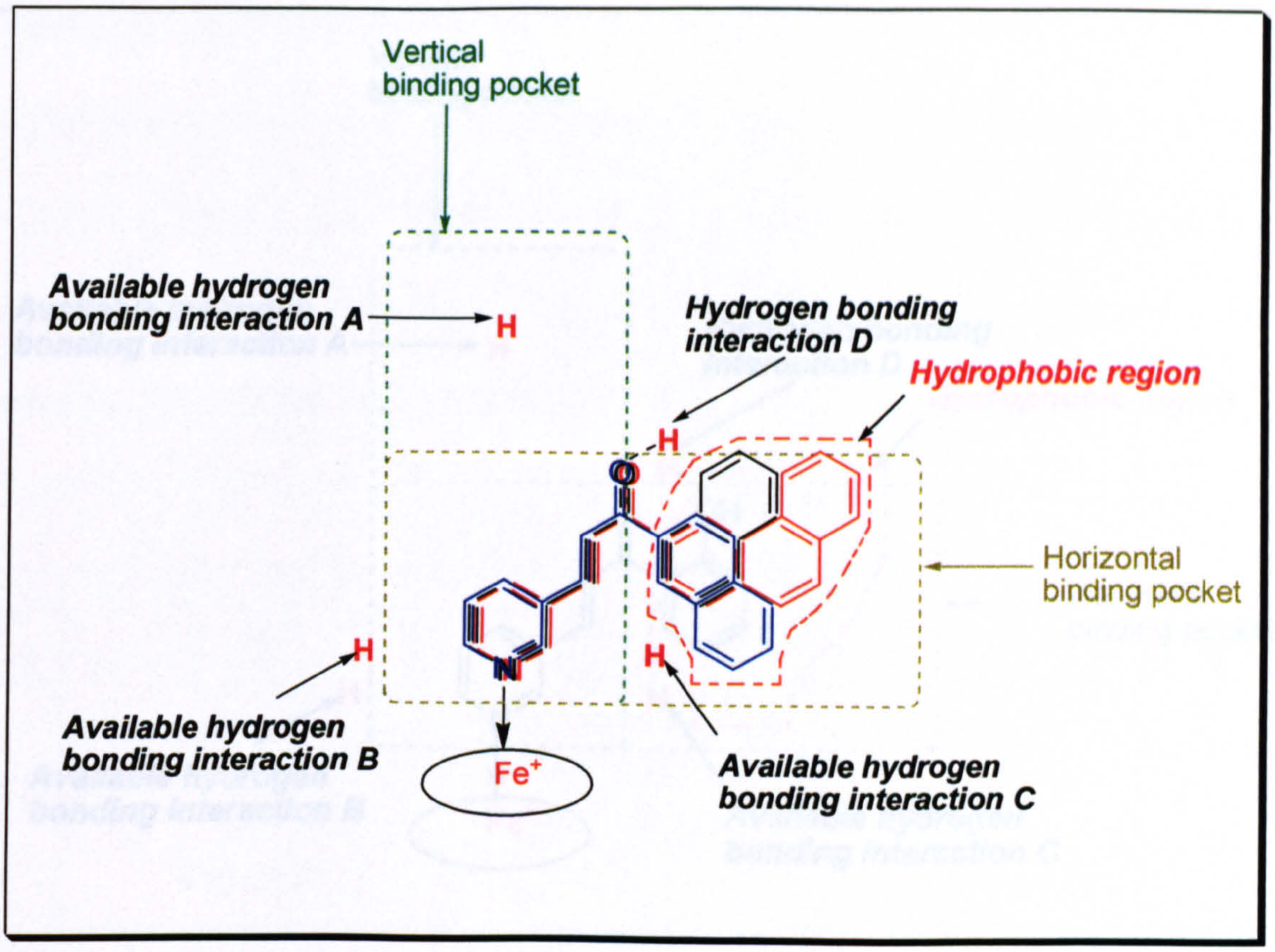

Figure 45: Hydrophobic region in CYP1B1 pharmacophore model

Note: DMU745 (blue); DMU746 (black); DMU2136 (red).

The presence of hydrophobic region is concord with the observation that methoxylated 3-pyridyl chalcones (Table 8) are more potent CYP1B1 inhibitors than their hydroxylated counterparts (Table 9). Both dihydroxylated 3-pyridyl chalcones (DMU757 and DMU760) do not inhibit CYP1B1 as oppose to their dimethoxylated counterparts because both DMU757 and DMU760 dihydroxyphenyl substituent will be rejected by the hydrophobic region. Interestingly, the 2-hydroxylated 3-pyridyl chalcone (DMU763) has shown more CYP1B1 selectivity with a recorded IC_{50} value of 0.8μM. This is probably due to the 2-hydroxy group in DMU763 able to form a hydrogen bond at hydrogen bonding interaction D.

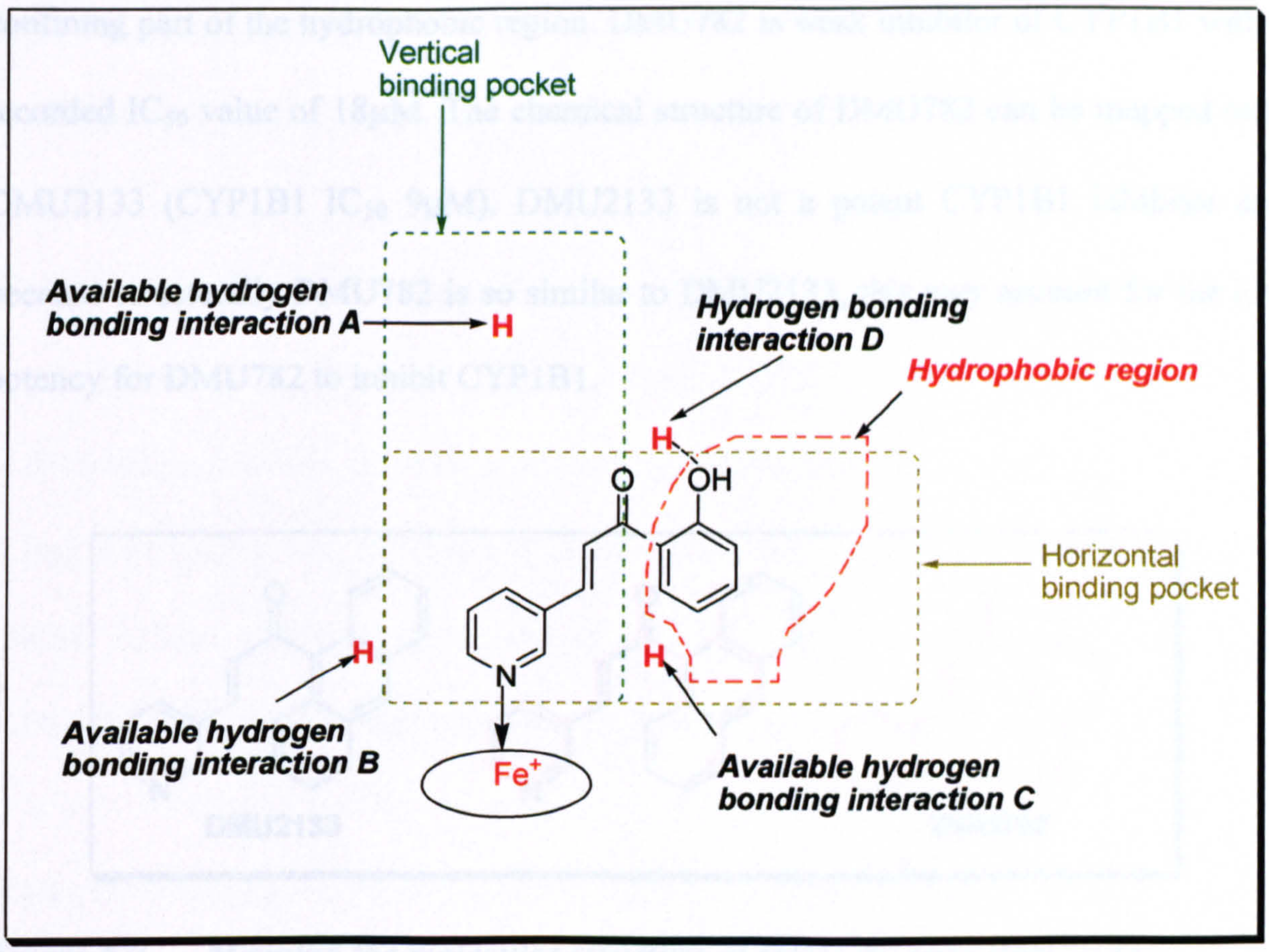

Figure 46: CYP1B1 pharmacophore model showing inhibition of CYP1B1 by DMU763

DMU709 (Chapter 2) is a CYP1A1 inhibitor but its 2,3,4-trimethoxy analogue (DMU718) is CYP1B1 selective. The unique chemical structure of the 3,4,5-trimethoxyphenyl moiety on DMU709 forces the middle methoxy group to occupy space that is out of the planar plane of the phenyl ring. This orientation will occupy more room in 3D space. The hydrophobic region in CYP1B1 may be formed by two groups of hydrophobic amino acid residues in a sandwich formation. This is in accord with the homology model published by Lewis[74]. The bulky trimethoxyphenyl moiety may not favour to be sandwiched between these hydrophobic amino acid residues. DMU718 is 14-fold better CYP1B1 inhibitor than DMU709. Although DMU718 contains a trimethoxyphenyl moiety, its methoxy groups may be out of the more space

confining part of the hydrophobic region. DMU782 is weak inhibitor of CYP1B1 with a recorded IC_{50} value of 18μM. The chemical structure of DMU782 can be mapped onto DMU2133 (CYP1B1 IC_{50} 9μM). DMU2133 is not a potent CYP1B1 inhibitor and because structurally DMU782 is so similar to DMU2133, this may account for the low potency for DMU782 to inhibit CYP1B1.

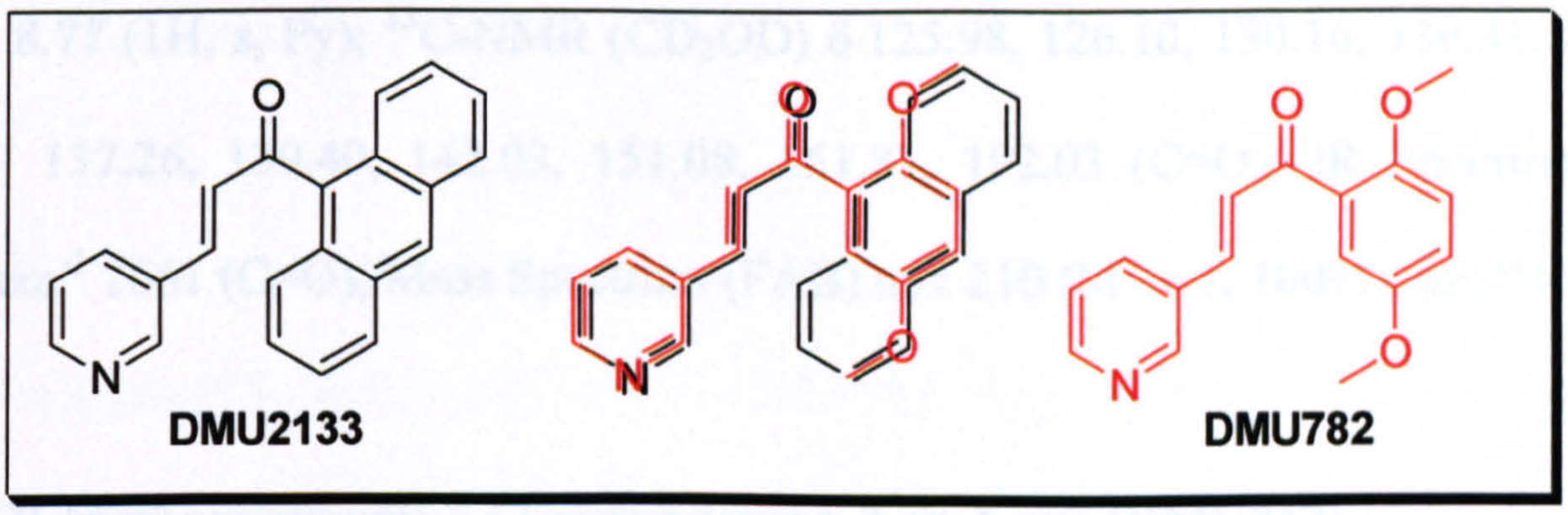

Figure 47: Mapping the molecular structure of DMU782 onto DMU2133

Amongst the synthesised 3-pyridyl chalcones, DMU709 has been found to be the most selective inhibitor for CYP1A1. 9-Acetylphenanthrene, the starting material for the synthesis of DMU2137, has been identified as more selective inhibitor of CYP1A2 with better selectivity and potency compared with the known CYP1A2 mechanistic based inhibitor furafylline. Several more selective inhibitors of CYP1B1 have been discovered. Of these, DMU2139 offers the best selectivity and potency. The pharmacophore models for the CYP1A1, CYP1A2 and CYP1B1 (Figure 40, 42 and 46, respectively) are preliminary and would be further refined in Chapter 4.

3.5 Experimental

Synthetic methods and analytical methods see Section 2.5.1 to 2.5.2.

(*E*)-1-(Phenyl)-3-(3-pyridyl)prop-2-en-1-one (DMU711)

Synthetic Method 1; ^{1}H-NMR (CD_3OD) δ 7.42 (3H, m), 7.55 (1H, t, benzyl), 7.69 (1H, d, *J*=16.8Hz), 7.81 (1H, d, *J*=16.8Hz), 8.02 (2H, d, benzyl), 8.17 (1H, d, Py), 8.46 (1H, d, Py), 8.77 (1H, s, Py); ^{13}C-NMR (CD_3OD) δ 125.98, 126.10, 130.16, 130.31, 133.31, 134.84, 137.26, 139.40, 142.03, 151.08, 151.81, 192.03 (C=O); IR Spectrum V_{max} (KBr)/cm^{-1} 1661 (C=O); Mass Spectrum (FAB) m/z 210 (M^+ + 1, 100%); mp 94°C.

(*E*)-1-(2'-Methoxyphenyl)-3-(3-pyridyl)prop-2-en-1-one (DMU712)

Synthetic Method 1; ^{1}H-NMR (CD_3OD) δ 3.80 (3H, s, OMe), 6.95 (1H, t, benzyl), 7.06 (1H, d, benzyl), 7.35-7.50 (5H, m), 8.04 (1H, d, Py), 8.43 (1H, d, Py), 8.66 (1H, s, Py); ^{13}C-NMR (CD_3OD) δ 56.76, 113.60, 122.24, 125.98, 130.25, 130.93, 131.63, 133.39, 135.22, 137.01, 140.27, 150.82, 151.66, 160.37, 194.69 (C=O); IR Spectrum V_{max} (KBr)/cm^{-1} 1657 (C=O); Mass Spectrum (FAB) m/z 240 (M^+ + 1, 100%); mp 91°C.

(*E*)-1-(3'-Methoxyphenyl)-3-(3-pyridyl)prop-2-en-1-one (DMU713)

Synthetic Method 1; ^{1}H-NMR (CD_3OD) δ 3.75 (3H, s, OMe), 7.10 (1H, d, benzyl), 7.32-7.42 (2H, m), 7.50 (1H, s, benzyl), 7.60 (1H, d, benzyl), 7.68 (1H, d, *J*=16.1Hz), 7.77 (1H, d, *J*=16.1Hz), 8.16 (1H, d, Py), 8.46 (1H, d, Py), 8.77 (1H, s, Py); ^{13}C-NMR (CD_3OD) δ 56.38, 114.61, 121.02, 122.74, 125.96, 126.12, 131.60, 133.29, 137.27, 140.76, 142.04, 150.97, 171.80, 162.00, 191.75 (C=O); IR Spectrum V_{max} (KBr)/cm^{-1} 1664 (C=O); Mass Spectrum (FAB) m/z 240 (M^+ + 1, 100%); mp 82°C.

(*E*)-1-(4'-Methoxyphenyl)-3-(3-pyridyl)prop-2-en-1-one (DMU714)

Synthetic Method 1; ^{1}H-NMR (CD_3OD) δ 4.05 (3H, s, OMe), 7.30 (2H, d, benzyl), 7.74 (1H, m, Py), 7.95 (1H, d, *J*=15.5Hz), 8.15 (1H, d, *J*=15.5Hz), 8.35 (2H, d, benzyl), 8.49 (1H, d, Py), 8.78 (1H, d, Py), 9.08 (1H, s, Py); ^{13}C-NMR (CD_3OD) δ 56.06, 114.62, 123.06, 129.08, 129.31, 130.78, 131.68, 132.71, 142.89, 148.85, 149.70, 167.85, 189.56 (C=O); IR Spectrum V_{max} (KBr)/cm^{-1} 1664 (C=O); Mass Spectrum (FAB) m/z 240 (M^+ + 1, 100%); mp 105-107°C.

(*E*)-1-(2',4'-Dimethoxyphenyl)-3-(3-pyridyl)prop-2-en-1-one (DMU715)

Synthetic Method 1; ^{1}H-NMR (CD_3OD) δ 3.88 (6H, s, OMe), 6.69 (1H, d, benzyl), 7.14 (2H, d, benzyl), 7.38 (1H, m, Py), 7.52 (1H, d, *J*=15.9Hz), 7.78 (1H, d, *J*=15.9Hz), 7.94 (1H, d, Py), 8.62 (1H, d, Py), 8.85 (1H, s, Py); ^{13}C-NMR (CD_3OD) δ 55.96, 56.16, 99.07, 105.89, 122.17, 124.03, 129.49, 131.75, 133.52, 134.98, 138.16, 150.10, 150.88, 161.03, 164.98, 189.94 (C=O); IR Spectrum V_{max} (KBr)/cm^{-1} 1659 (C=O); Mass Spectrum (FAB) m/z 270 (M^+ + 1, 100%); mp 93-95°C.

(*E*)-1-(3',4'-Dimethoxyphenyl)-3-(3-pyridyl)prop-2-en-1-one (DMU716)

Synthetic Method 1; ^{1}H-NMR ($CDCl_3$) δ 3.90 (6H, s, OMe), 6.95 (1H, d, benzyl), 7.37 (1H, m, Py), 7.57-7.71 (3H, m), 7.79 (1H, d, *J*=15.7Hz), 7.94 (1H, d, Py), 8.62 (1H, d, Py), 8.87 (1H, s, Py); ^{13}C-NMR ($CDCl_3$) δ 56.06, 56.11, 110.01, 110.76, 123.16, 123.51, 123.71, 130.88, 134.56, 140.05, 149.38, 149.83, 150.91, 153.58, 158.12, 187.56 (C=O); IR Spectrum V_{max} (KBr)/cm^{-1} 1655 (C=O); Mass Spectrum (FAB) m/z 270 (M^+ + 1, 100%); mp 91-93°C.

(*E*)-1-(3',5'-Dimethoxyphenyl)-3-(3-pyridyl)prop-2-en-1-one (DMU717)

Synthetic Method 1; ^{1}H-NMR ($CDCl_3$) δ 3.85 (6H, s, OMe), 6.68 (1H, t, benzyl), 7.14 (2H, s, benzyl), 7.35 (1H, t, Py), 7.52 (1H, d, *J*=14.7Hz), 7.78 (1H, d, *J*=14.7Hz), 7.94 (1H, d, Py), 8.63 (1H, d, Py), 8.85 (1H, s, Py); ^{13}C-NMR ($CDCl_3$) δ 55.68, 105.34, 106.50, 123.78, 124.00, 130.72, 134.53, 139.78, 141.01, 150.07, 151.17, 161.07, 189.47 (C=O); IR Spectrum V_{max} (KBr)/cm^{-1} 1666 (C=O); Mass Spectrum (FAB) m/z 270 (M^+ + 1, 100%); mp 90-91°C.

(*E*)-1-(2',3',4'-Trimethoxyphenyl)-3-(3-pyridyl)prop-2-en-1-one (DMU718)

Synthetic Method 1; ^{1}H-NMR ($CDCl_3$) δ 3.90-3.95 (9H, OMe), 6.78 (1H, d, benzyl), 7.35 (1H, m, Py), 7.53 (1H, d, *J*=15.7Hz), 7.63 (1H, d, *J*=15.7Hz), 7.78 (1H, d, benzyl), 7.93 (1H, m, Py), 8.61 (1H, d, Py), 8.84 (1H, s, Py); ^{13}C-NMR ($CDCl_3$) δ 56.13, 61.04, 62.06, 107.46, 123.71, 126.01, 128.43, 131.03, 134.43, 138.70, 142.15, 149.93, 150.75, 153.95, 157.45, 189.96 (C=O); IR Spectrum V_{max} (KBr)/cm^{-1} 1666 (C=O); Mass Spectrum (MALDI) m/z 299.7 (M^+, 100%); mp 77°C.

(*E*)-1-(2',3',4'-Trimethoxyphenyl)-3-(1*H*-4-imidazolyl)prop-2-en-1-one (DMU744)

Synthetic Method 3; ^{1}H-NMR (DMSO) δ 3.85 (3H, s, OMe), 3.90 (3H, s, OMe), 3.95 (3H, s, OMe), 6.72 (1H, d, benzyl), 7.28 (1H, s, imidazolyl), 7.45-7.60 (3H, m), 7.71 (1H, d, *J*=17.5Hz), 9.02 (1H, broad, imidazolyl); ^{13}C-NMR (DMSO) δ 56.32, 60.70, 62.02, 108.06, 121.92, 125.43, 125.73, 127.4, 128.37, 129.56, 136.47, 141.82, 153.14, 157.15, 189.53 (C=O); IR Spectrum V_{max} (KBr)/cm^{-1} 1662 (C=O); Mass Spectrum (MALDI) m/z 287.9 (M^+, 100%); mp 182-183°C.

(*E*)-1-(2-Naphthyl)-3-(3-pyridyl)prop-2-en-1-one (DMU745)

Synthetic Method 1; ^{1}H-NMR ($CDCl_3$) δ 7.32 (1H, t, naphthyl), 7.59 (2H, m, naphthyl), 7.69-8.01 (6H, m), 8.10 (1H, d, *J*=16.3Hz), 8.52 (1H, d, Py), 8.62 (1H, d, Py), 8.90 (1H, s, Py); ^{13}C-NMR ($CDCl_3$) δ 123.80, 123.93, 124.39, 126.95, 127.89, 128.63, 128.77, 129.59, 130.15, 130.80, 132.58, 134.63, 135.16, 135.65, 140.85, 150.07, 151.15, 189.56 (C=O); IR Spectrum V_{max} (KBr)/cm^{-1} 1651 (C=O); Mass Spectrum (MALDI) m/z 259.2 (M^+, 100%); mp 117°C.

(*E*)-1-(1-Naphthyl)-3-(3-pyridyl)prop-2-en-1-one (DMU746)

Synthetic Method 1; ^{1}H-NMR ($CDCl_3$) δ 7.33 (1H, m, naphthyl), 7.38 (1H, d, *J*=16.2Hz), 7.51-7.64 (4H, m), 7.78-8.04 (4H, m), 8.37 (1H, d, Py), 8.62 (1H, d, Py), 8.77 (1H, s, Py); ^{13}C-NMR ($CDCl_3$) δ 124.28, 124.79, 125.83, 126.06, 127.82, 128.13, 129.06, 130.87, 132.48, 134.30, 134.90, 136.90, 142.13, 150.32, 150.60, 151.47, 151.80, 195.08 (C=O); IR Spectrum V_{max} (KBr)/cm^{-1} 1662 (C=O); Mass Spectrum (MALDI) m/z 259.1 (M^+, 100%); mp 123-124°C.

(*E*)-1-(3,4-Methylenedioxyphenyl)-3-(3-pyridyl)prop-2-en-1-one (DMU762)

Synthetic Method 2; ^{1}H-NMR ($CDCl_3$) δ 6.07 (2H, s, methylenedioxy), 6.74 (1H, d, benzyl), 6.90 (1H, d, benzyl), 7.49-7.59 (2H, m), 7.75 (1H, d, *J*=16.8Hz), 7.92 (1H, d, Py), 8.39 (1H, m, Py), 8.63 (1H, d, Py), 8.88 (1H, s, Py); ^{13}C-NMR ($CDCl_3$) δ 101.99, 108.02, 108.45, 123.65, 123.76, 124.88, 130.83, 132.61, 134.54, 140.35, 148.48, 149.93, 151.02, 152.04, 187.59 (C=O); IR Spectrum V_{max} (KBr)/cm^{-1} 1658 (C=O); Mass Spectrum (MALDI) m/z 253.3 (M^+, 100%); mp 138-139°C.

(*E*)-1-(2',5'-Dimethoxyphenyl)-3-(3-pyridyl)prop-2-en-1-one (DMU782)

Synthetic Method 2; ^{1}H-NMR ($CDCl_3$) δ 3.80 (3H, s, OMe), 3.90 (3H, s, OMe), 6.95 (1H, d, benzyl), 7.07 (1H, d, benzyl), 7.23 (1H, s, benzyl), 7.33 (1H, t, Py), 7.54 (1H, d, *J*=15.8Hz), 7.64 (1H, d, *J*=15.8Hz), 7.90 (1H, d, Py), 8.60 (1H, d, Py), 8.72 (1H, s, Py); ^{13}C-NMR ($CDCl_3$) δ 55.80, 56.40, 113.39, 114.49, 119.71, 123.66, 128.65, 129.03, 130.97, 134.51, 138.78, 149.84, 150.72, 152.79, 153.68, 191.35 (C=O); IR Spectrum V_{max} (KBr)/cm^{-1} 1662 (C=O); Mass Spectrum (MALDI) m/z 269.6 (M^+, 100%); mp 169-170°C.

(*E*)-1-(2-Naphthyl)-3-(1*H*-4-imidazolyl)prop-2-en-1-one (DMU2120)

Synthetic Method 2; ^{1}H-NMR (DMSO) δ 6.58-6.69 (2H, m, naphthyl), 7.73 (1H, s, imidazolyl), 7.77 (1H, d, *J*=16.5Hz), 7.86 (1H, d, *J*=16.5Hz), 7.92 (1H, s, naphthyl), 8.00 (1H, d, naphthyl), 8.03-8.10 (2H, m, naphthyl), 8.17 (1H, d, naphthyl), 8.72 (1H, s, imidazolyl); ^{13}C-NMR (DMSO) δ 118.24, 124.24, 127.03, 127.80, 128.58, 129.66, 129.70, 130.06, 132.16, 132.46, 134.66, 135.02, 135.52, 189.03 (C=O); IR Spectrum V_{max} (KBr)/cm^{-1} 1647 (C=O); Mass Spectrum (MALDI) m/z 248.2 (M^+, 100%); mp 139-140°C.

(*E*)-1-(3'-Chlorophenyl)-3-(3-pyridyl)prop-2-en-1-one (DMU2123)

Synthetic Method 3; ^{1}H-NMR ($CDCl_3$) δ 7.38 (1H, t, benzyl), 7.46 (1H, t, Py), 7.58 (1H, d, benzyl), 7.55 (1H, d, *J*=16.1Hz), 7.80 (1H, d, *J*=16.1Hz), 7.89 (1H, d, benzyl), 7.96 (1H, d, Py), 7.99 (1H, s, benzyl), 8.64 (1H, d, Py), 8.87 (1H, s, Py); ^{13}C-NMR ($CDCl_3$) δ 123.24, 123.77, 126.54, 128.57, 130.03, 130.40, 132.97, 133.23, 134.58, 139.00, 141.70, 150.06, 151.32, 188.40 (C=O); IR Spectrum V_{max} (KBr)/cm^{-1} 1666

(C=O); Mass Spectrum (MALDI) m/z 243.9 (M^+, 100%); mp 128-129°C.

(*E*)-1-(4'-Chlorophenyl)-3-(3-pyridyl)prop-2-en-1-one (DMU2124)

Synthetic Method 3; ^{1}H-NMR ($CDCl_3$) δ 7.36 (1H, t, Py), 7.48 (2H, d, benzyl), 7.55 (1H, d, *J*=16.3Hz), 7.79 (1H, d, *J*=16.3Hz), 7.91-8.00 (3H, m), 8.64 (1H, d, Py), 8.85 (1H, s, Py); ^{13}C-NMR ($CDCl_3$) δ 123.32, 123.81, 129.08, 129.96, 130.53, 134.63, 136.07, 139.62, 141.42, 150.02, 151.29, 188.46 (C=O); IR Spectrum V_{max} (KBr)/cm^{-1} 1666 (C=O); Mass Spectrum (MALDI) m/z 243.3 (M^+, 100%); mp 111-112°C.

(*E*)-1-(3'-Bromophenyl)-3-(3-pyridinyl)prop-2-en-1-one (DMU2127)

Synthetic Method 3; ^{1}H-NMR ($CDCl_3$) δ 7.34-7.42 (2H, m), 7.53 (1H, d, *J*=15.8Hz), 7.72 (1H, d, benzyl), 7.80 (1H, d, *J*=15.8Hz), 7.91-7.97 (2H, m), 8.15 (1H, s, benzyl), 8.65 (1H, d, Py), 8.88 (1H, s, Py); ^{13}C-NMR ($CDCl_3$) δ 118.02, 118.15, 118.72, 121.94, 125.23, 125.34, 126.46, 129.54, 130.85, 134.45, 136.68, 145.03, 146.29, 183.26 (C=O); IR Spectrum V_{max} (KBr)/cm^{-1} 1662 (C=O); Mass Spectrum (MALDI) m/z 288.8 (M^+, 100%); mp 127°C.

(*E*)-1-(9-Anthracenyl)-3-(3-pyridinyl)prop-2-en-1-one (DMU2133)

Synthetic Method 2; ^{1}H-NMR ($CDCl_3$) δ 7.18-7.23 (2H, m), 7.33 (1H, d, *J*=14.9Hz), 7.45 (2H, d, anthracenyl), 7.47 (2H, d, anthracenyl), 7.63 (1H, d, Py), 7.85-7.91 (2H, m), 7.79-8.05 (2H, m), 8.52 (1H, s, anthracenyl), 8.55 (1H, s, Py); ^{13}C-NMR ($CDCl_3$) δ 123.69, 125.01, 125.57, 126.82, 128.38, 128.75, 130.04, 130.73, 131.10, 133.99, 134.49, 143.58, 150.13, 151.44, 199.47 (C=O); IR Spectrum V_{max} (KBr)/cm^{-1} 1631 (C=O); Mass Spectrum (MALDI) m/z 309.1 (M^+, 100%); mp 172-173°C.

(*E*)-1-(4-Biphenyl)-3-(3-pyridyl)prop-2-en-1-one (DMU2134)

Synthetic Method 2; ^{1}H-NMR ($CDCl_3$) δ 7.34-7.43 (2H, m), 7.49 (2H, t, biphenyl), 7.61-7.68 (3H, m), 7.75 (2H, d, biphenyl), 7.82 (1H, d, *J*=16.1Hz), 7.77 (1H, d, Py), 8.11 (2H, d, biphenyl), 8.64 (1H, d, Py), 8.88 (1H, s, Py); ^{13}C-NMR ($CDCl_3$) δ 123.75, 123.86, 127.27, 12.737, 128.28, 128.96, 129.15, 130.73, 134.58, 136.43, 139.80, 140.79, 145.87, 149.97, 151.09, 189.21 (C=O); IR Spectrum V_{max} (KBr)/cm^{-1} 1659 (C=O); Mass Spectrum (MALDI) m/z 285.5 (M^+, 100%); mp 140°C.

(*E*)-1-(3-Phenanthrenyl)-3-(3-pyridinyl)prop-2-en-1-one (DMU2136)

Synthetic Method 2; ^{1}H-NMR ($CDCl_3$) δ 7.28 (1H, t, phenanthrenyl), 7.53-7.91 (9H, m), 8.09 (1H, d, phenanthrenyl), 8.60 (1H, d, Py), 8.68 (1H, d, Py), 8.85 (1H, s, phenanthrenyl), 9.22 (1H, s, Py); ^{13}C-NMR ($CDCl_3$) δ 122.69, 123.71, 123.82, 124.00, 125.49, 126.19, 127.19, 127.25, 128.78, 128.93, 129.75, 129.76, 130.49, 130.69, 132.11, 134.55, 134.90, 135.27, 140.75, 150.00, 151.04, 189.41 (C=O); IR Spectrum V_{max} (KBr)/cm^{-1} 1655 (C=O); Mass Spectrum (MALDI) m/z 309.1 (M^+, 100%); mp 113°C.

(*E*)-1-(9-Phenanthrenyl)-3-(3-pyridinyl)prop-2-en-1-one (DMU2137)

Synthetic Method 2; ^{1}H-NMR ($CDCl_3$) δ 7.30 (1H, t, Py), 7.39 (1H, d, J=16.1Hz), 7.59-7.77 (5H, m), 7.87 (1H, d, Py), 7.93 (1H, d, phenanthrenyl), 8.03 (1H, s, phenanthrenyl), 8.34 (1H, d, phenanthrenyl), 8.60 (1H, d, Py), 8.68 (1H, d, phenanthrenyl), 8.72 (1H, d, phenanthrenyl), 8.77 (1H, s, Py); ^{13}C-NMR ($CDCl_3$) δ 122.73, 123.00, 123.75, 126.43, 127.20, 127.29, 127.40, 128.71, 128.73, 129.12, 129.64, 129.88, 130.05, 130.38, 130.77, 131.59, 134.47, 135.52, 141.92, 150.12,

151.27, 194.77 (C=O); IR Spectrum V_{max} (KBr)/cm^{-1} 1651 (C=O); Mass Spectrum (MALDI) m/z 309.6 (M^+, 100%); mp 120°C.

(*E*)-1-(6'-Methoxy-2-naphthyl)-3-(3-pyridyl)prop-2-en-1-one (DMU2139)

Synthetic Method 2; ^{1}H-NMR ($CDCl_3$) δ 3.95 (3H, s, OMe), 7.17 (1H, s, naphthyl), 7.22 (1H, m, naphthyl), 7.36 (1H, t, Py), 7.73 (1H, d, J=15.8Hz), 7.78-7.90 (3H, m), 7.98 (1H, d, Py), 8.08 (1H, m, naphthyl), 8.47 (1H, s, naphthyl), 8.63 (1H, d, Py), 8.89 (1H, s, Py); ^{13}C-NMR ($CDCl_3$) δ 55.40, 105.87, 119.81, 123.71, 123.83, 125.05, 127.38, 127.83, 130.03, 130.85, 131.13, 133.08, 134.55, 137.34, 140.32, 149.94, 150.95, 159.91, 189.03 (C=O); IR Spectrum V_{max} (KBr)/cm^{-1} 1643 (C=O); Mass Spectrum (MALDI) m/z 289.4 (M^+, 100%); mp 133°C.

(*E*)-1-(1-Pyrenyl)-3-(3-pyridyl)prop-2-en-1-one (DMU2140)

Synthetic Method 2; ^{1}H-NMR ($CDCl_3$) δ 7.38 (1H, t, Py), 7.50 (1H, d, *J*=14.9Hz), 7.62 (1H, d, *J*=14.9Hz), 7.87 (1H, d, Py), 7.98-8.07 (2H, m), 8.10-8.25 (6H, m), 8.59 (1H, d, Py), 8.63 (1H, d, prenyl), 8.78 (1H, s, Py); ^{13}C-NMR ($CDCl_3$) δ 123.74, 124.00, 124.27, 124.53, 124.85, 126.05, 126.24, 126.30, 126.41, 127.07, 128.91, 129.38, 129.51, 130.54, 131.04, 132.97, 133.51, 134.45, 141.52, 149.97, 151.07, 194.67 (C=O); IR Spectrum V_{max} (KBr)/cm^{-1} 1620 (C=O); Mass Spectrum (MALDI) m/z 333.4 (M^+, 100%); mp 113°C.

(*E*)-1-(3',4'-Difluorophenyl)-3-(3-pyridyl)prop-2-en-1-one (DMU2151)

Synthetic Method 2; ^{1}H-NMR ($CDCl_3$) δ 7.30 (1H, m, benzyl), 7.38 (1H, t, Py), 7.54 (1H, d, *J*=16.0Hz), 7.78-7.90 (3H, m), 7.97 (1H, d, Py), 8.65 (1H, d, Py), 8.88 (1H, s,

Py); ^{13}C-NMR ($CDCl_3$) δ 117.47, 117.99, 118.02, 122.66, 123.77, 125.43, 125.48, 130.32, 134.60, 134.76, 141.82, 150.01, 151.38, 186.96 (C=O); IR Spectrum V_{max} (KBr)/cm^{-1} 1662 (C=O); Mass Spectrum (MALDI) m/z 245.5 (M^+, 100%); mp 119°C.

1,5-bis(3'-Chlorophenyl)-3-(3-pyridyl)pentane-1,5-dione (DMU2154)

Synthetic Method 2; ^{1}H-NMR ($CDCl_3$) δ 3.33 (1H, d, J=17Hz$_{gem}$), 3.38 (1H, d, J=17Hz$_{gem}$), 3.49 (1H, d, J=17Hz$_{gem}$), 3.52 (1H, d, J=17Hz$_{gem}$), 4.08 (1H, p), 7.21 (1H, t, Py), 7.39 (2H, t, benzyl), 7.51 (2H, d, benzyl), 7.65 (1H, d, Py), 7.80 (2H, d, benzyl), 7.89 (2H, s, ben),8.45 (1H, d, Py), 8.59 (1H, s, Py); ^{13}C-NMR ($CDCl_3$) δ 32.65, 42.59, 114.34, 121.82, 124.47, 126.52, 128.37, 131.61, 133.41, 136.46, 137.21, 146.66, 147.54, 194.82 (C=O); IR Spectrum V_{max} (KBr)/cm^{-1} 1678 (C=O); Mass Spectrum (MALDI) m/z 398.3 (M^+, 100%); mp 146°C.

1,5-bis(4'-Chlorophenyl)-3-(3-pyridyl)pentane-1,5-dione (DMU2155)

Synthetic Method 2; ^{1}H-NMR (DMSO) δ 3.38 (1H, d, J=16.7Hz$_{gem}$), 3.42 (1H, d, J=16.7Hz$_{gem}$), 3.52 (1H, d, J=16.7Hz$_{gem}$), 3.56 (1H, d, J=16.7Hz$_{gem}$), 4.03 (1H, p), 7.22 (1H, t, Py), 7.44 (4H, d, benzyl), 7.69 (1H, d, Py), 7.91 (4H, d, benzyl), 8.39 (1H, d, Py), 8.57 (1H, s, Py); ^{13}C-NMR (DMSO) δ 34.06, 43.94, 123.35, 128.88, 129.90, 135.08, 135.29, 138.25, 139.47, 147.49, 149.52, 197.49 (C=O); IR Spectrum V_{max} (KBr)/cm^{-1} 1681 (C=O); Mass Spectrum (MALDI) m/z 398.8 (M^+, 100%); mp 154°C.

1,5-bis(3'-Bromophenyl)-3-(3-pyridyl)pentane-1,5-dione (DMU2156)

Synthetic Method 2; ^{1}H-NMR ($CDCl_3$) δ 3.33 (1H, d, J=16.8Hz$_{gem}$), 3.37 (1H, d, J=16.8Hz$_{gem}$), 3.48 (1H, d, J=16.8Hz$_{gem}$), 3.53 (1H, d, J=16.8Hz$_{gem}$), 4.08 (1H, p), 7.22

(1H, t, Py), 7.33 (2H, t, benzyl), 7.63-7.70 (3H, m), 7.85 (2H, d, benzyl), 8.04 (2H, s, benzyl), 8.45 (1H, d, Py), 8.57 (1H, s, Py); ^{13}C-NMR ($CDCl_3$) δ 32.63, 42.55, 121.42, 121.83, 124.91, 128.63, 129.47, 133.64, 134.54, 136.65, 137.20, 146.67, 147.53, 194.72 (C=O); IR Spectrum V_{max} (KBr)/cm^{-1} 1678 (C=O); Mass Spectrum (MALDI) m/z 487.1 (M^+, 100%); mp 154°C.

Summary of Structures

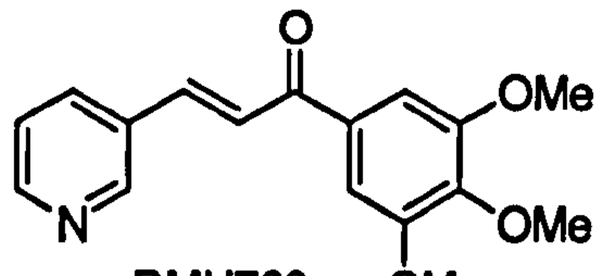

DMU709

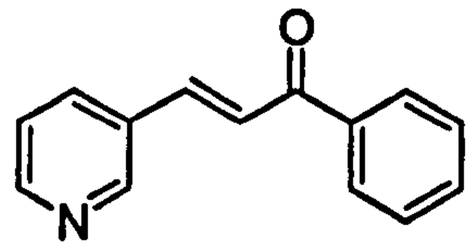

DMU711

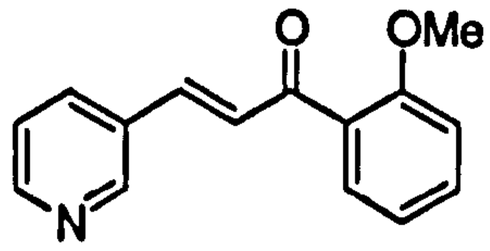

DMU712

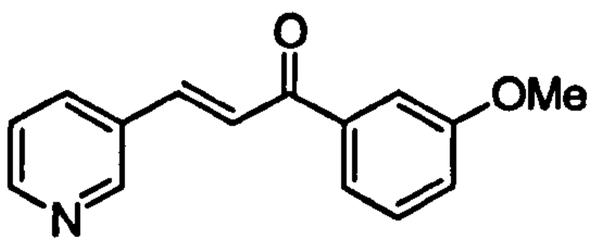

DMU713

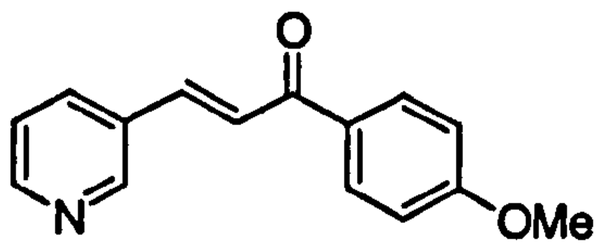

DMU714

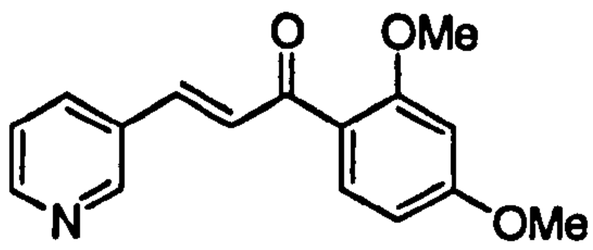

DMU715

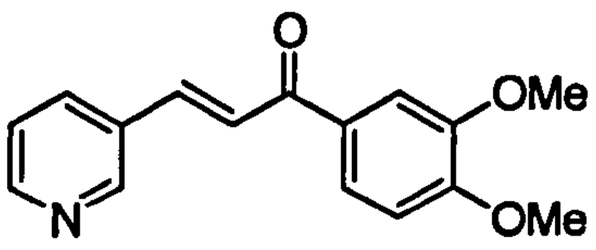

DMU716

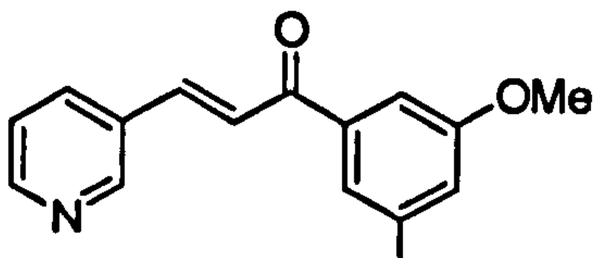

DMU717

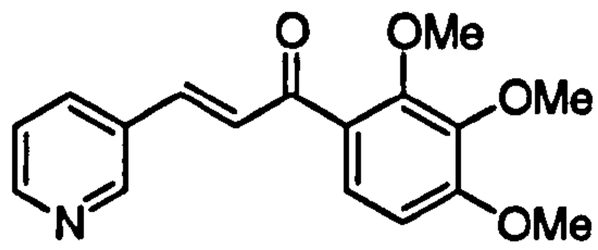

DMU718

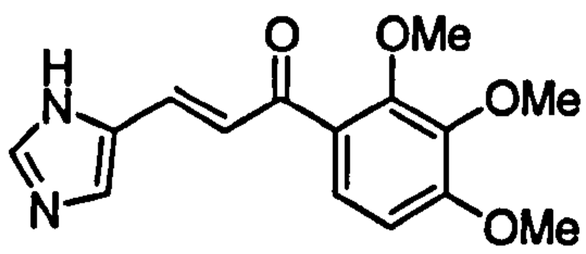

DMU744

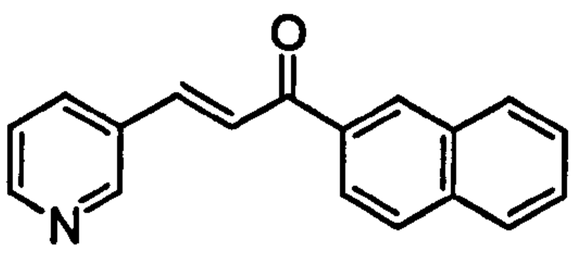

DMU745

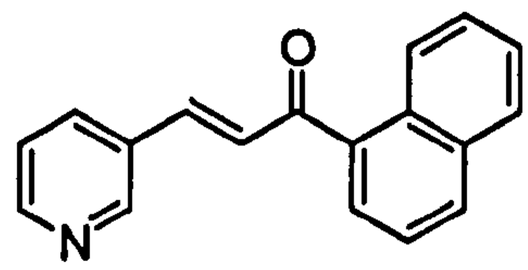

DMU746

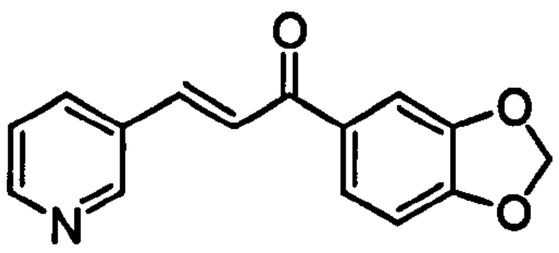

DMU762

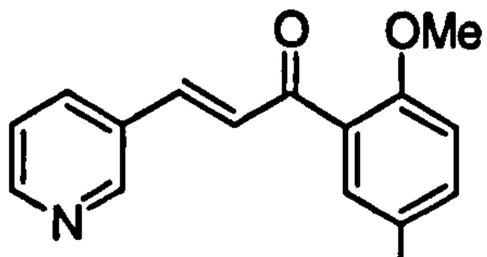

DMU782

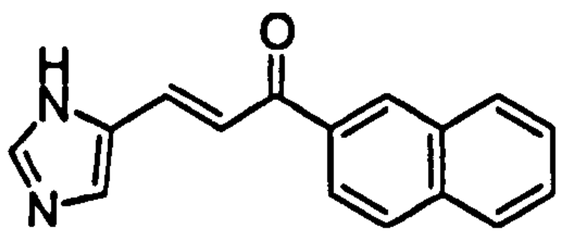

DMU2120

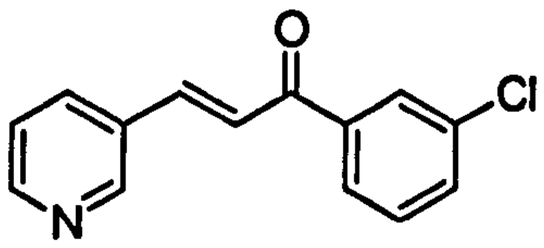

DMU2123

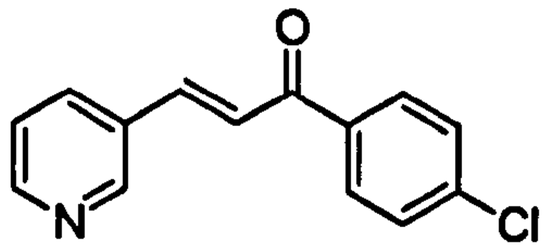

DMU2124

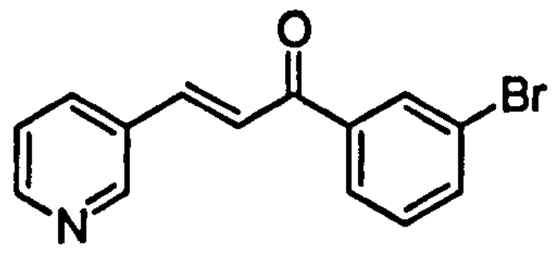

DMU2127

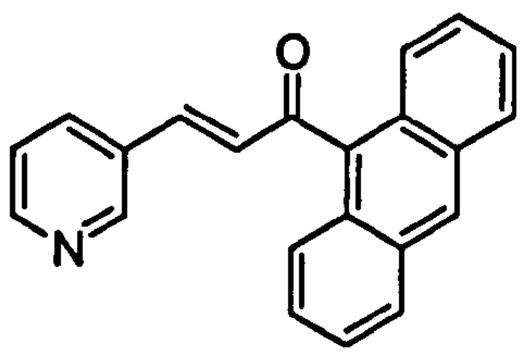

DMU2133

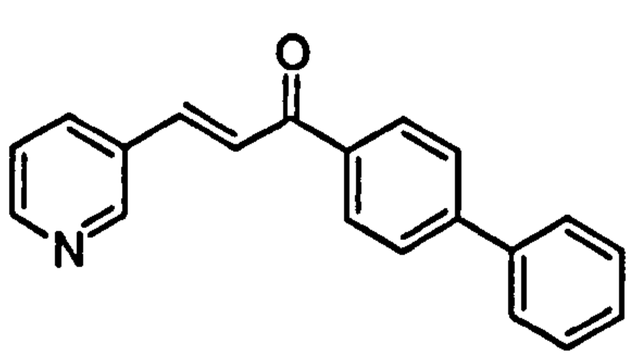

DMU2134

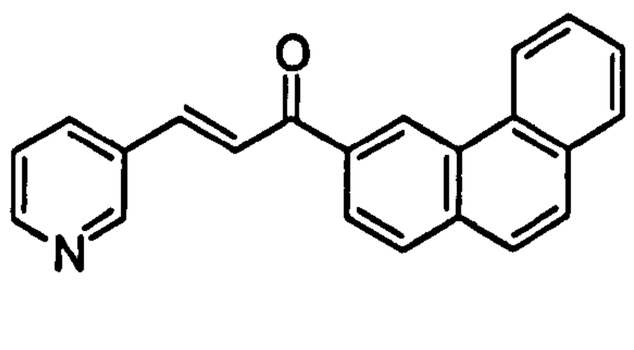

DMU2136

3-Pyridyl chalcones as selective CYP1 enzyme inhibitors

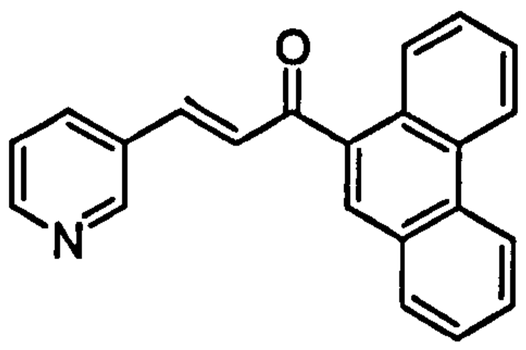

DMU2137

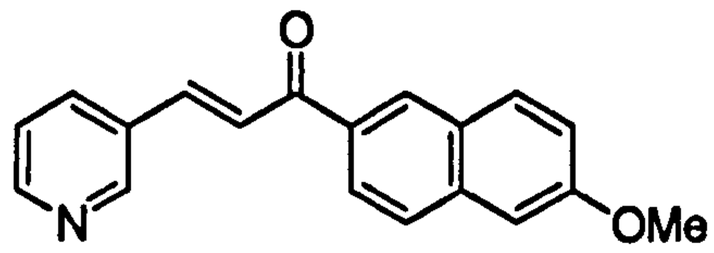

DMU2139

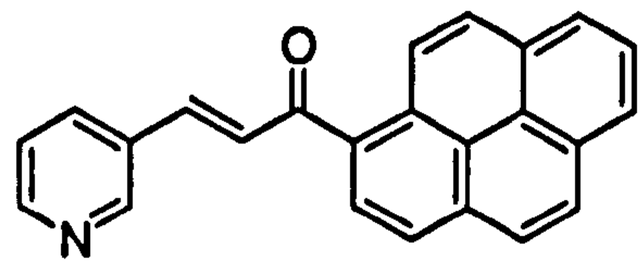

DMU2140

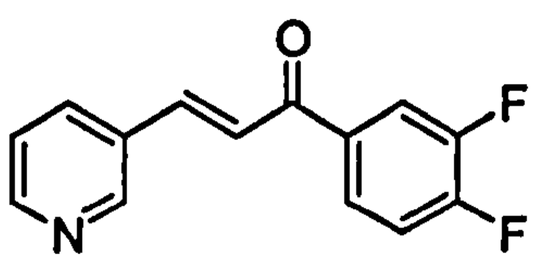

DMU2151

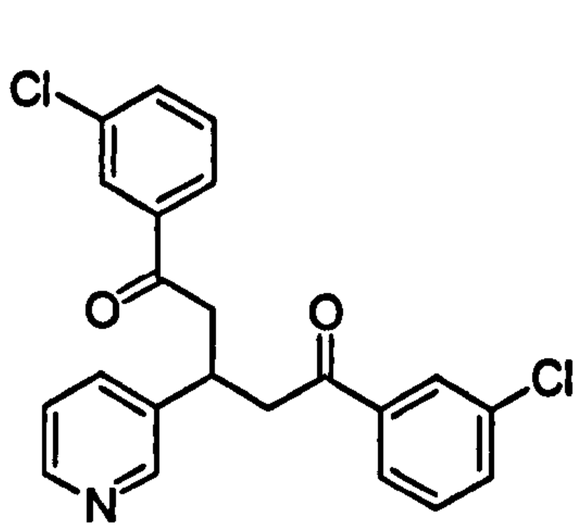

DMU2154

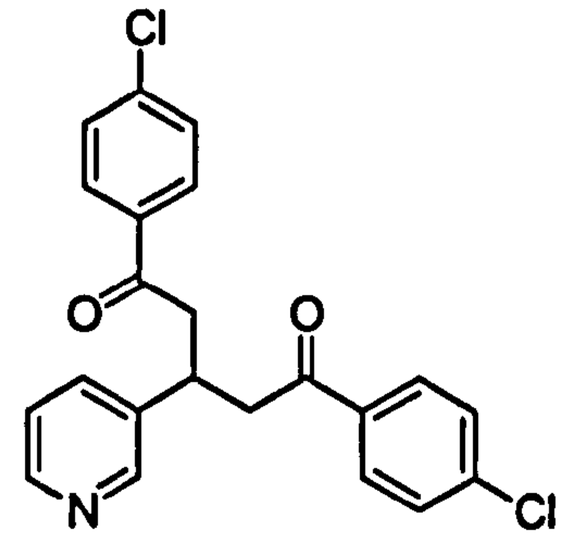

DMU2155

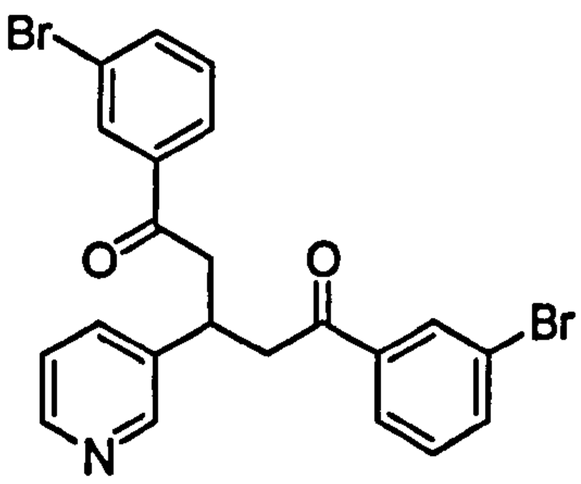

DMU2156

Chapter 4

CYP1 Enzyme Inhibition by "Reverse" 3- & 4-Pyridyl Chalcones

4.1 Introduction

The 3-chloro and 3-bromo 3-pyridyl chalcones DMU2123 and DMU2127, respectively, are both inhibitors of CYP1B1 (Table 10). Surprisingly, both inhibitors are bioactivated in the induced MCF7 and MDA-MB-468 (MDA468) cell lines, making them potential prodrug candidates for further pre-clinical studies (see Chapter 5). One may have concluded that, since these molecules have inhibition activity against CYP1B1, their bioactivation to the cytotoxic species would not be catalysed by the same CYP enzyme. Indeed, preliminary drug metabolism studies have shown that the bioactivation of these potential anticancer agents was mainly by CYP1A1, though an unidentified residue insect CYP presence in other Supersomes™ and the control microsomes also catalysed the same process, but to a lesser extent (Chapter 5).

The bioactivation of DMU2123 and DMU2127 has shown that the 3-pyridyl chalcones can align themselves in the P450s in two orientations. The pyridyl A-ring of these compounds can bind to the haem to cause enzyme inhibition, or the substituted B-ring can face the haem ready to undergo metabolic oxidation.

To further investigate the structure-activity relationships (SAR) of CYP1 enzymes, a range of reverse 3-pyridyl chalcones has been synthesised and examined. Nine 4-pyridyl analogues of DMU710 (see Chapter 2) have also been made and their SAR will be discussed in this chapter. The reverse 3-pyridyl chalcones will help to determine which end of the chalcone molecule preferably binds to the surface of the haem, by comparing the EROD inhibitory data between the 3-pyridyl and the reverse 3-pyridyl chalcones. The combined EROD data from all the synthesised chalcones would help to refine the pharmacophore models constructed in the previous chapter.

4.2 Reagents and methods

4.2.1 Materials

All chemical reagents and starting materials for synthesis were purchased from either Lancaster Synthesis (UK) or Aldrich Chemical Co. Ltd (UK). Reactions were followed and monitored with TLC as described in Section 2.2.1 with 2,4-DNP. Purification of the synthesised compounds was carried out using flash column chromatography with silica gel (supplied by Fisher Scientific, UK) unless otherwise stated.

Reagents and plasticware for the EROD assay were obtained from Sigma Chemical Co. Ltd and Fisher Scientific (see Section 2.1.1). Microsomes prepared from insect cells transformed using a baculovirus expressing human cytochrome P450 CYP1A1, CYP1A2 and CYP1B1 with co-expression of human NADPH-cytochrome P450 reductase (Supersomes™) were obtained from Gentest Corporation, USA *via* Cambridge Biosciences, UK. Handling of Supersomes™ was previously described in Section 2.2.8.

4.2.2 Synthetic strategies

All target inhibitors were synthesised using the Claisen-Schmidt aldol condensation with a base as catalyst. All three methods described in Section 2.5.2 were employed. Synthetic Method 1 uses lithium diisopropylamide as base. Method 2 is carried out with 50% w/v NaOH solution as base and with cooling. Synthetic Method 3 is a solvent-free method involved grinding the starting materials and powdered NaOH with a pestle and mortar. Details for each synthetic method can be found in Section 2.5.2.

4.2.3 Microsomal incubation- EROD assay

The EROD assay was conducted as described in Section 2.2.9. The method of preparation of different solutions used in the EROD assay can be found from Section 2.2.3 to Section 2.2.7.

4.3 Results

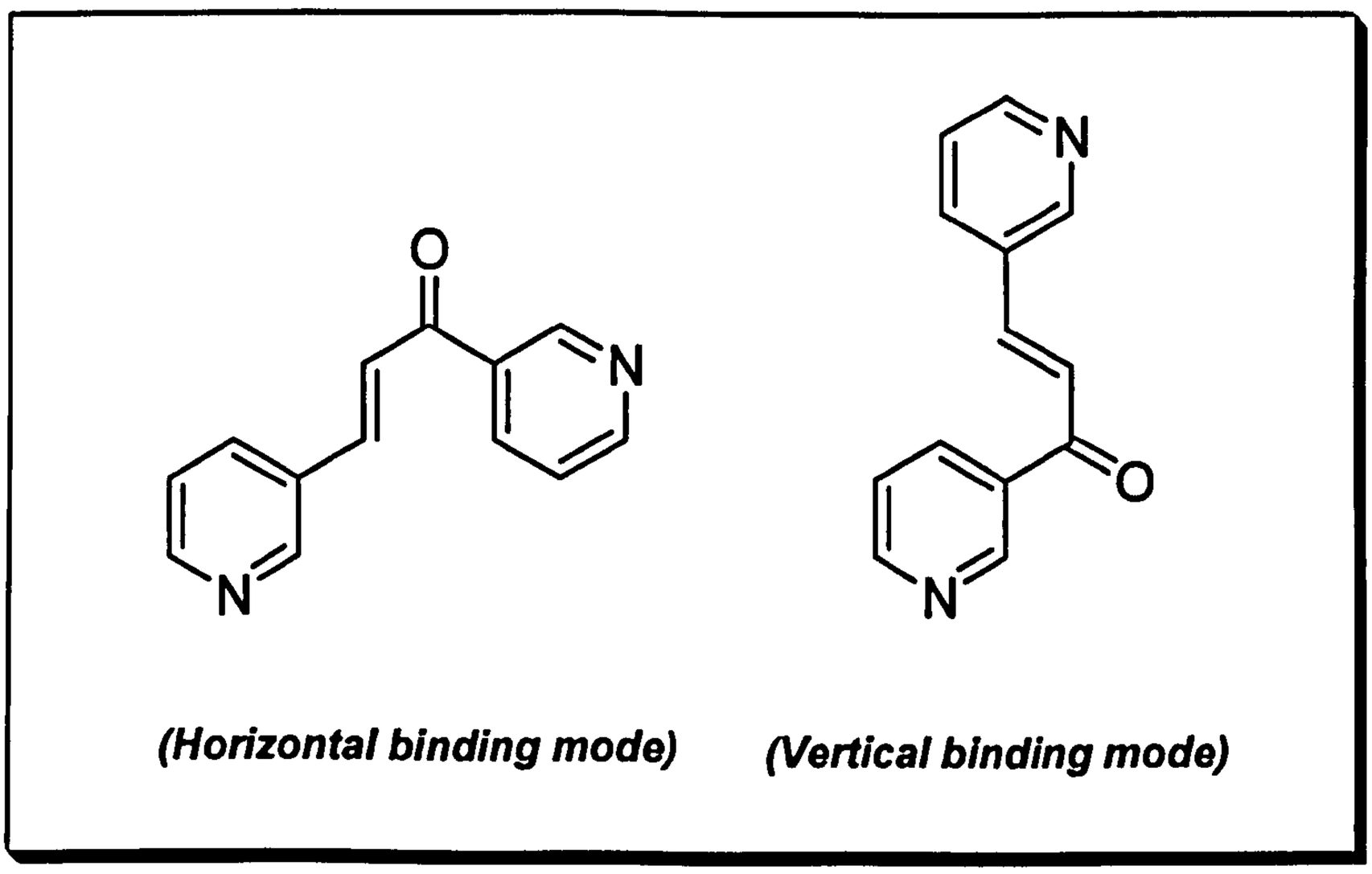

Figure 48: ***Chemical structure of the di-3-pyridyl chalcone DMU2141 in the horizontal and vertical binding mode projections***

A total of 19 reverse 3-pyridyl chalcones have been synthesised. As a result of the lack of readily available starting materials, only 3 polycyclic compounds have been made for the reverse 3-pyridyl series of chalcones. (*E*)-1,3-di(3-pyridyl)prop-2-en-1-one (refer to

as di-3-pyridyl chalcone) has also been synthesised.

Table 17: Chemical structure and physical characteristics of some reverse 3-pyridyl chalcones

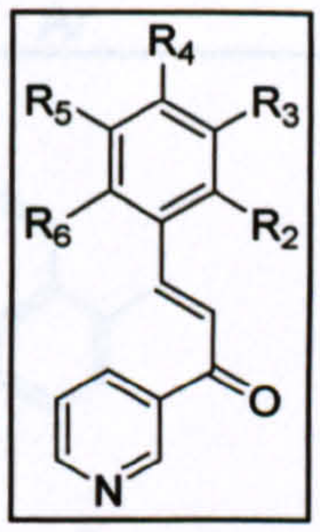

Inhibitors	R_2	R_3	R_4	R_5	R_6	Physical chracterictics (yield %)	Method
DMU729	H	H	OMe	H	H	fine yellow needle (49%)	2
DMU766	OH	H	H	H	H	apple green crystal (9%)	3
DMU767	H	OH	H	H	H	yellow powder (17%)	3
DMU768	H	H	OH	H	H	yellow crystal (13%)	3
DMU774	H	OMe	OMe	H	H	yellow waxy solid (15%)	3
DMU775*	OMe	H	OMe	H	H	~~ see note ~~	
DMU776*	OMe	H	H	OMe	H	~~ see note ~~	
DMU777*	H	OMe	H	OMe	H	~~ see note ~~	
DMU778	H	Cl	Cl	H	H	fine yellow crystal (70%)	2
DMU789	H	OMe	H	H	H	light brown crystal (33%)	2
DMU790	OMe	H	H	H	H	yellow powder (50%)	2
DMU2101	H	F	F	H	H	off white powder (13%)	2
DMU2103	H	OH	OMe	H	H	bright yellow powder (13%)	3
DMU2114	H	OMe	OMe	OMe	H	bright yellow powder (37%)	2
DMU2117	OMe	OMe	OMe	H	H	bright yellow solid (57%)	2
DMU2118	H	H	H	H	H	yellow waxy solid (29%)	2

Note: * Synthesised by Nishad Rajabali as part of her undergraduate final year project; Method (see Section 4.5).

Table 18: Physical characteristics of the polycyclic reverse 3-pyridyl and the di-3-pyridyl chalcones

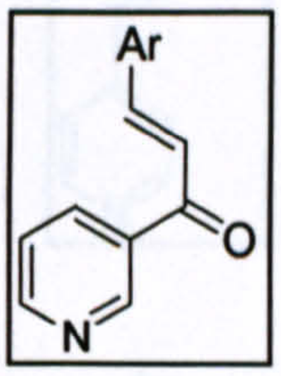

Inhibitors	Ar	Physical chracterictics (yield %)	Method
DMU756	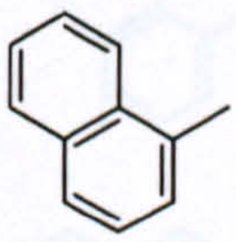	pale yellow solid (5%)	3
DMU769	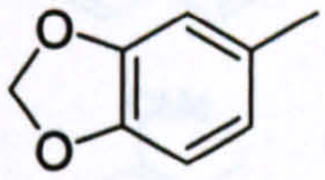	bright yellow powder (76%)	2
DMU2105	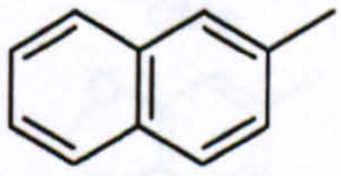	fine yellow crystal (29%)	3
DMU2141	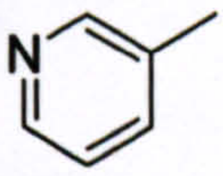	pale yellow powder (14%)	2

Note: Method see section 4.5.

Nine analogues of the CYP1A1 inhibitor DMU710 (Chapter 2) were made. Four of these compounds were 4-pyridyl chalcones and the remaining were the reverse 4-pyridyl analogues. The chemical structure and physical characteristics of these heterocyclic 4-pyridyl chalcones are tabulated in Table 19 and Table 20.

Table 19: Physical characteristics of the synthesised 4-pyridyl chalcones

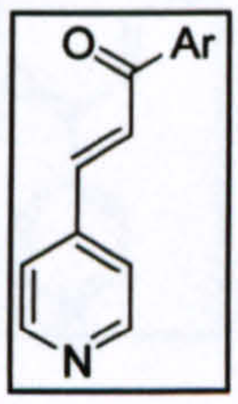

Inhibitors	Ar	Physical chracterictics (yield %)	Method
DMU779	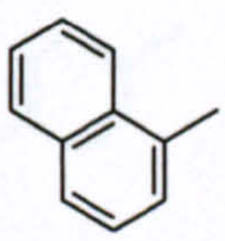	light brown oil (18%)	3
DMU780	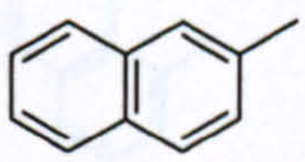	yellow powder (39%)	3
DMU781	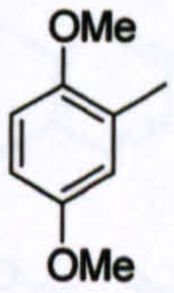	dark yellow solid (43%)	3
DMU2143	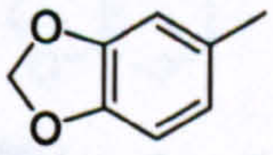	fine off white crystal (40%)	2

Note: Method see section 4.5.

DMU2114 and DMU2157, the reverse 3-pyridyl analogue of DMU709 and the reverse 4-pyridyl analogue of DMU710 (see Chapter 2), respectively, were found to be more selective against CYP1A1 catalysed EROD reaction. Several more selective inhibitors of CYP1B1 have also been identified in the reverse 3-pyridyl chalcone series. DMU774, DMU775, DMU776, DMU777, DMU778, DMU2103 and DMU2105 all have been found to be more CYP1B1 selective with at least 10-fold selectivity ratio over the CYP1A enzymes. The EROD IC_{50} data are tabulated in Table 21-25. The CYP1B1 enzyme selectivity ratio (eSR) was calculated with this formula: $\mathbf{IC_{50(CYP1A)}}$ / $\mathbf{IC_{50(CYP1B1)}}$.

Table 20: Chemical structure of reverse 4-pyridyl chalcones

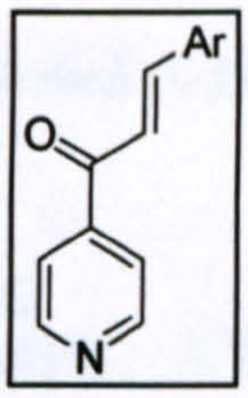

Inhibitors	Ar	Physical chracterictics (yield %)	Method
DMU730	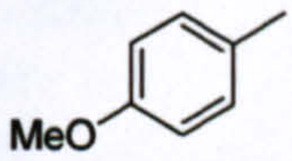	fine yellow crystal (32%)	2
DMU755	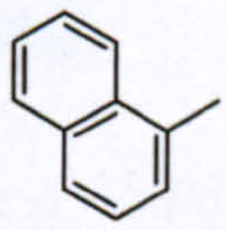	yellow crystal (8%)	1
DMU2106	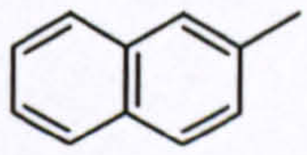	fine yellow crystal (42%)	3
DMU2144	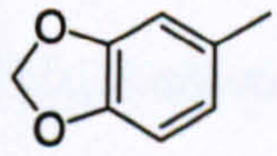	bright yellow powder (26%)	2
DMU2157	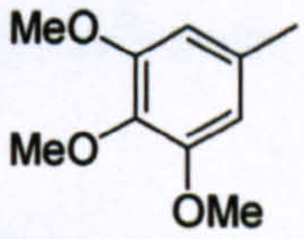	light brown solid (17%)	2

Note: Method see section 4.5.

Table 21: EROD IC_{50} values for reverse 3-pyridyl chalcones with hydroxylated and halogenated A-ring

Inhibitors	A-ring Substituents	IC_{50} (μM) CYP1A1	CYP1A2	CYP1B1	CYP1B1 eSR over CYP1A1	CYP1A2
DMU766	2-OH	11	6	0.8	14	8
DMU767	3-OH	20	35	3	7	12
DMU768	4-OH	50	NI	5	10	nd
DMU778	3,4-$(Cl)_2$	20	20	0.4	50	50
DMU2101	3,4-$(F)_2$	20	4	0.7	29	6
DMU2103	3-OH,4-OMe	7	70	0.7	10	100

Note: NI = no inhibition; nd = not determined.

Table 22: EROD IC_{50} values for reverse 3-pyridyl chalcones with methoxylated A-ring

Inhibitors	A-ring Substituents	IC_{50} (μM) CYP1A1	CYP1A2	CYP1B1	CYP1B1 eSR over CYP1A1	CYP1A2
DMU729	4-OMe	8.5	16	1.5	6	11
DMU774	3,4-$(OMe)_2$	4	2	0.2	20	10
DMU775	2,4-$(OMe)_2$	1.6	0.9	0.07	23	13
DMU776	2,5-$(OMe)_2$	1.8	1.5	0.07	26	21
DMU777	3,5-$(OMe)_2$	2	4	0.07	29	57
DMU789	3-OMe	5.5	1	0.4	14	3
DMU790	2-OMe	3.5	0.8	0.4	9	2
DMU2114	3,4,5-$(OMe)_3$	0.6	8	3	0.2	3
DMU2117	2,3,4-$(OMe)_3$	2.5	0.7	0.25	10	3
DMU2118	phenyl	70	10	4	18	3

Table 23: EROD IC_{50} values for the polycyclic reverse 3-pyridyl and the di-3-pyridyl chalcones

Inhibitors	A-ring Substituents	IC_{50} (μM) CYP1A1	CYP1A2	CYP1B1	CYP1B1 eSR over CYP1A1	CYP1A2
DMU756	1-naphthyl	1	2	0.3	3	7
DMU769	3,4-MDO	1	8	0.8	1	10
DMU2105	2-naphthyl	5	8	0.15	33	53
DMU2141	3-pyridyl	NI	NI	19	nd	nd

Note: NI = no inhibition; nd = not determined; MDO = methylenedioxyphenyl.

The 4-pyridyl and reverse 4-pyridyl chalcones generally are more CYP1A selective except DMU779 and DMU780 (Table 24). DMU2144 is a better CYP1A1 inhibitor with eSR of 5- and 8-fold over CYP1A2 and CYP1B1, respectively.

Table 24: EROD IC_{50} values for 4-pyridyl chalcones

Inhibitors	B-ring Substituents	IC_{50} (μM) CYP1A1	CYP1A2	CYP1B1	CYP1B1 eSR over CYP1A1	CYP1A2
DMU710*	3,4,5-$(OMe)_3$	0.5	4	9	0.06	0.1
DMU779	1-naphthyl	2	0.5	0.3	7	2
DMU780	2-naphthyl	1.3	1.3	0.35	4	4
DMU781	2,5-$(OMe)_2$	6	4	12	0.5	0.3
DMU2143	3,4-MDO	2	6	9	0.2	0.7

Note: MDO = methylenedioxyphenyl; * see Chapter 2

Table 25: EROD IC_{50} values for reverse 4-pyridyl chalcones

Inhibitors	A-ring Substituents	IC_{50} (μM) CYP1A1	CYP1A2	CYP1B1	CYP1B1 eSR over CYP1A1	CYP1A2
DMU730	4-OMe	8	14	12	0.7	1
DMU755	1-naphthyl	0.4	0.35	0.2	2	2
DMU2106	2-naphthyl	2	50	4	0.5	13
DMU2144	3,4-MDO	0.8	4	6	0.1	0.7
DMU2157	3,4,5-$(OMe)_3$	0.3	5	9	0.03	0.6

Note: MDO = methylenedioxyphenyl.

4.4 Discussion

Unlike the previous series of 3-pyridyl chalcones (Chapter 3), only two pyridyl chalcones synthesised in this chapter, namely DMU780 and DMU2105, were found to interact with the plasticware. DMU785 (Chapter 3) and DMU780 were found to interact with the plastic pipetor tips but their reverse analogues DMU778 and DMU2106, respectively, were found to be inert to plastic. These results reaffirmed that the polypropylene pipetor tips (Finntips®, Thermo Labsystems) interact with heterocyclic

chalcones in a compound specific manner.

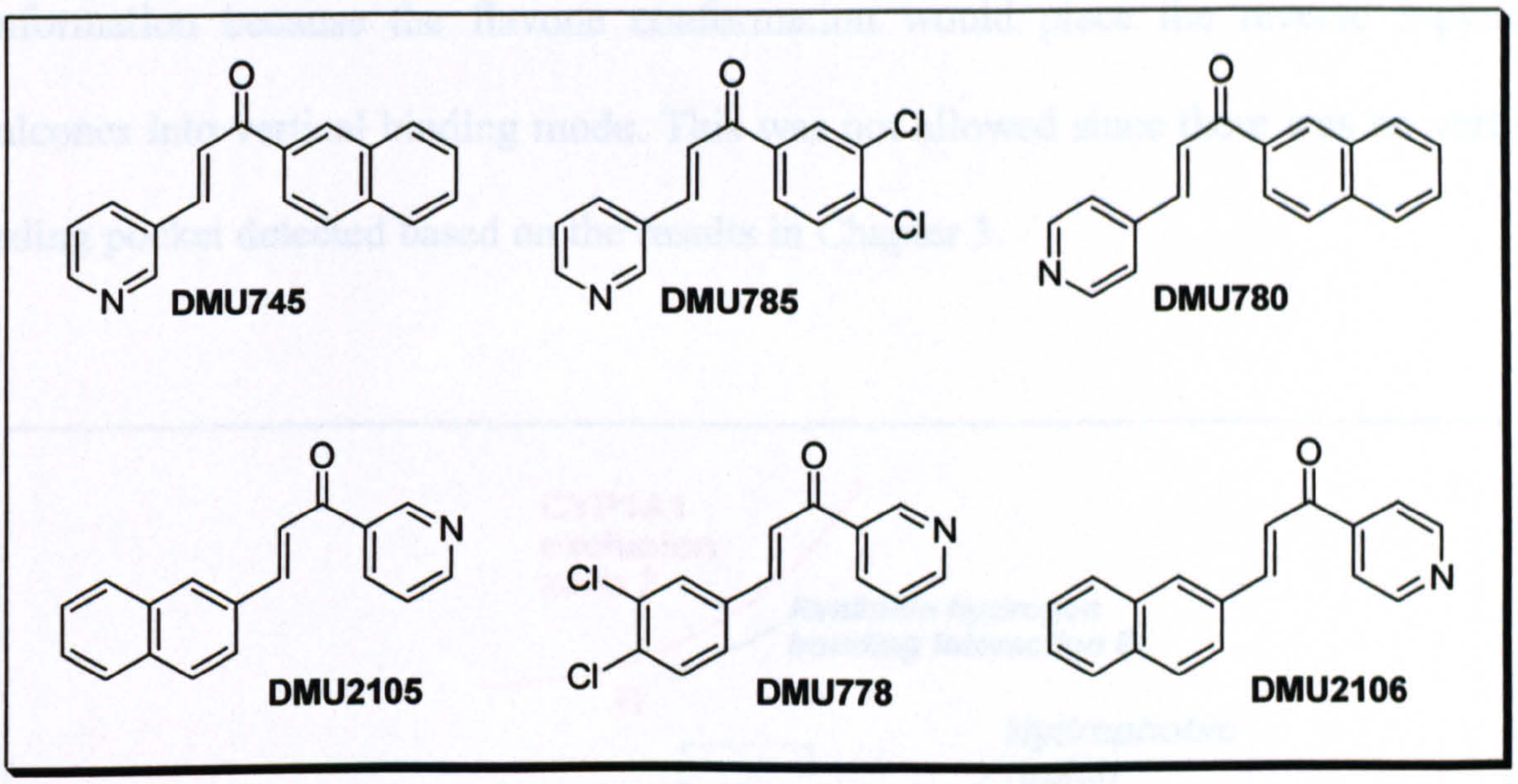

Figure 49: Chemical structure of DMU745, DMU780, DMU785 and their reverse analogues

DMU778 and DMU2106 are inert to plastic showing that the plastic-chalcone interaction is compound specific.

Table 26: Results showing the interaction of plastic pipette tips with DMU780 and DMU2105

Inhibitors	IC_{50} (μM) CYP1A1	CYP1A2	CYP1B1
DMU780	1.2	3	<0.0001
	1.3	1.3	0.35
DMU2105	6	23	<0.0001
	5	8	0.15

The IC_{50} values recorded in red were data from experiments where new pipetor tips were used for mixing.

The inhibitors still showed similar selectively against their target CYP1 enzymes even the potency have markedly decreased.

From Chapter 3, it has been found that CYP1A1 has a diagonal binding pocket. The reverse 3-pyridyl chalcones have to bind to the CYP1A1 haem in chalcone conformation because the flavone conformation would place the reverse 3-pyridyl chalcones into vertical binding mode. This was not allowed since there was no vertical binding pocket detected based on the results in Chapter 3.

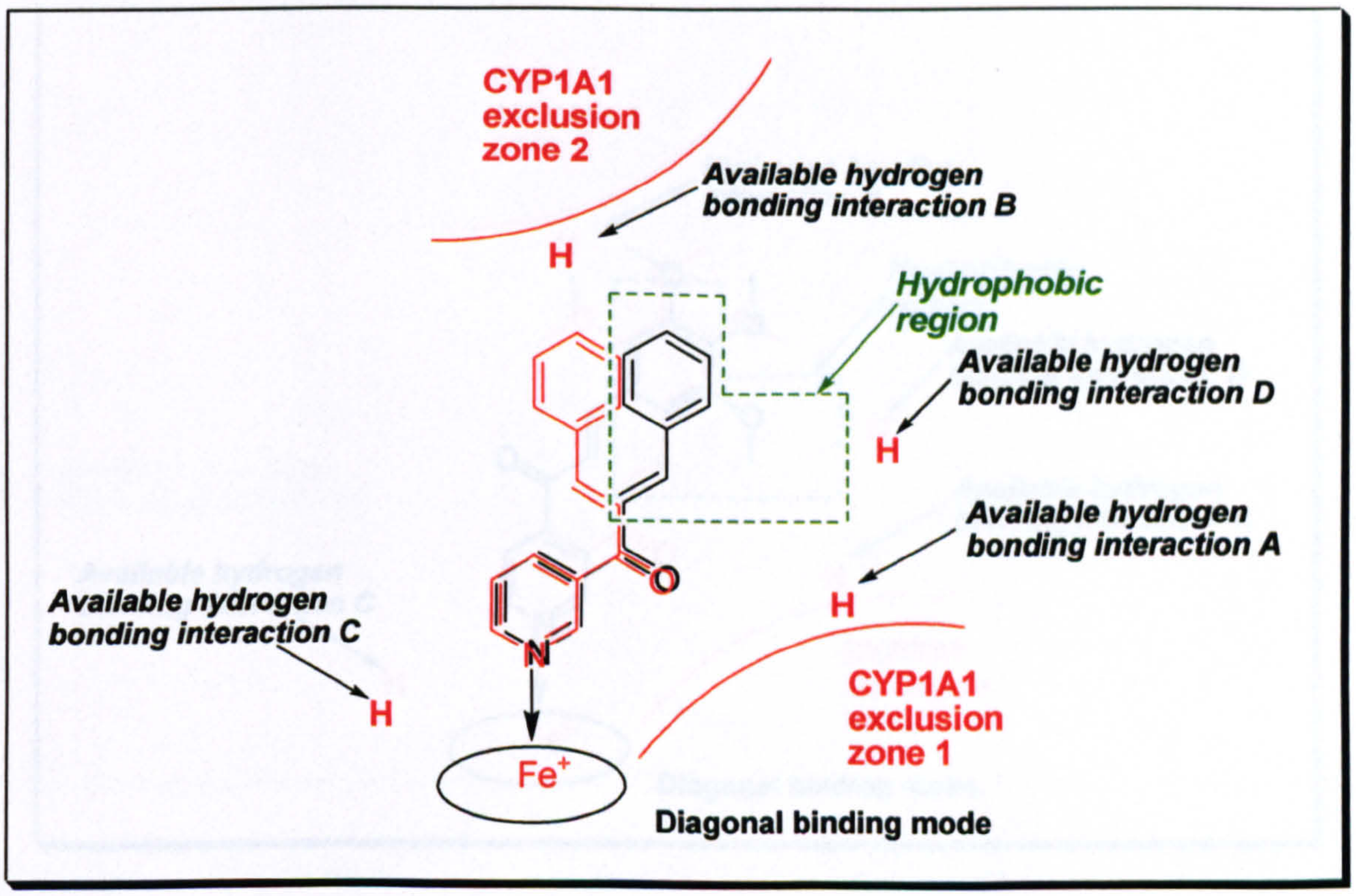

Figure 50: ***CYP1A1 pharmacophore model showing the binding of reverse 3-pyridyl chalcone in chalcone conformation (black) and flavone conformation (red)***

The flavone conformation will place the reverse 3-pyridyl chalcone into vertical binding mode. This is not allowed because there was no evidence of vertical binding pocket detected, based on the observations in Chapter 3.

The only identified CYP1A1 inhibitor in the reverse 3-pyridyl chalcone series was DMU2114. The reverse analogue of the CYP1A1 inhibitor 3,4,5-trimethoxy-4-pyridyl

chalcone (DMU710) also found to be more CYP1A1 selective. Figure 51 shows the mapping of both inhibitors onto the CYP1A1 pharmacophore model where the lipophilic 3,4,5-trimethoxyphenyl moiety of each compound fits well into the hydrophobic region.

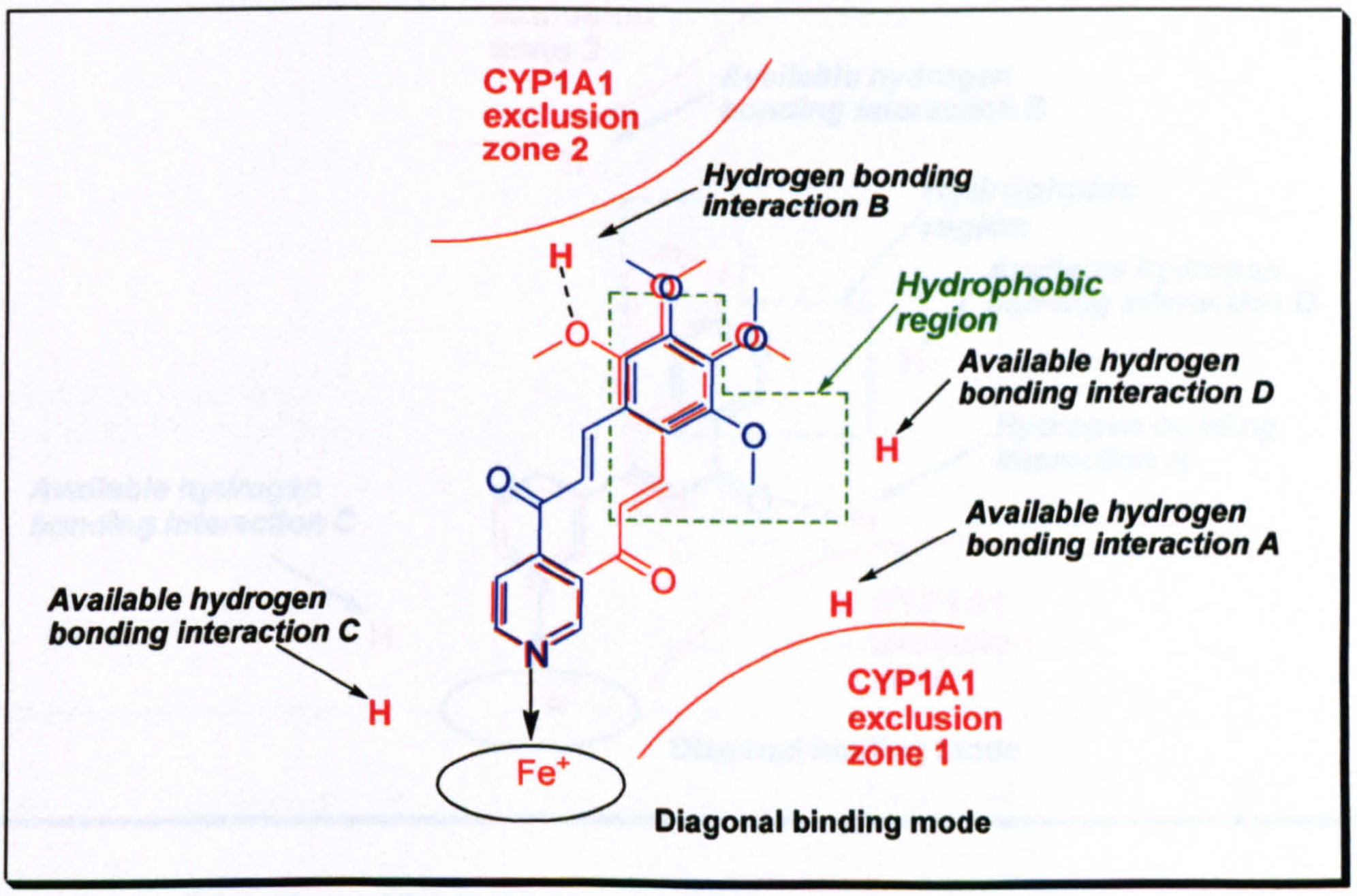

Figure 51: CYP1A1 pharmacophore model showing the mapping of CYP1A1 selective inhibitor DMU2114 (red) and DMU2157 (blue)

The presence of the hydrophobic region within CYP1A1 active site is further consolidated by the fact that the di-3-pyridyl chalcone DMU2141 does not inhibit CYP1A1 at all. The 3-pyridyl A- and B-ring of DMU2141 can face the P450 haem so that the nitrogen lone pair of electrons can coordinate to the haem, causing inhibition of the enzyme. However, regardless which molecular orientation DMU2141 binds to the CYP1A1 haem (Figure 55), one of its more hydrophilic 3-pyridyl ring would have to be

mapped onto the CYP1A1 hydrophobic zone. The CYP1A1 hydrophobic region will simply reject DMU2141 hence the compound is inactive against CYP1A1 catalysed EROD reaction.

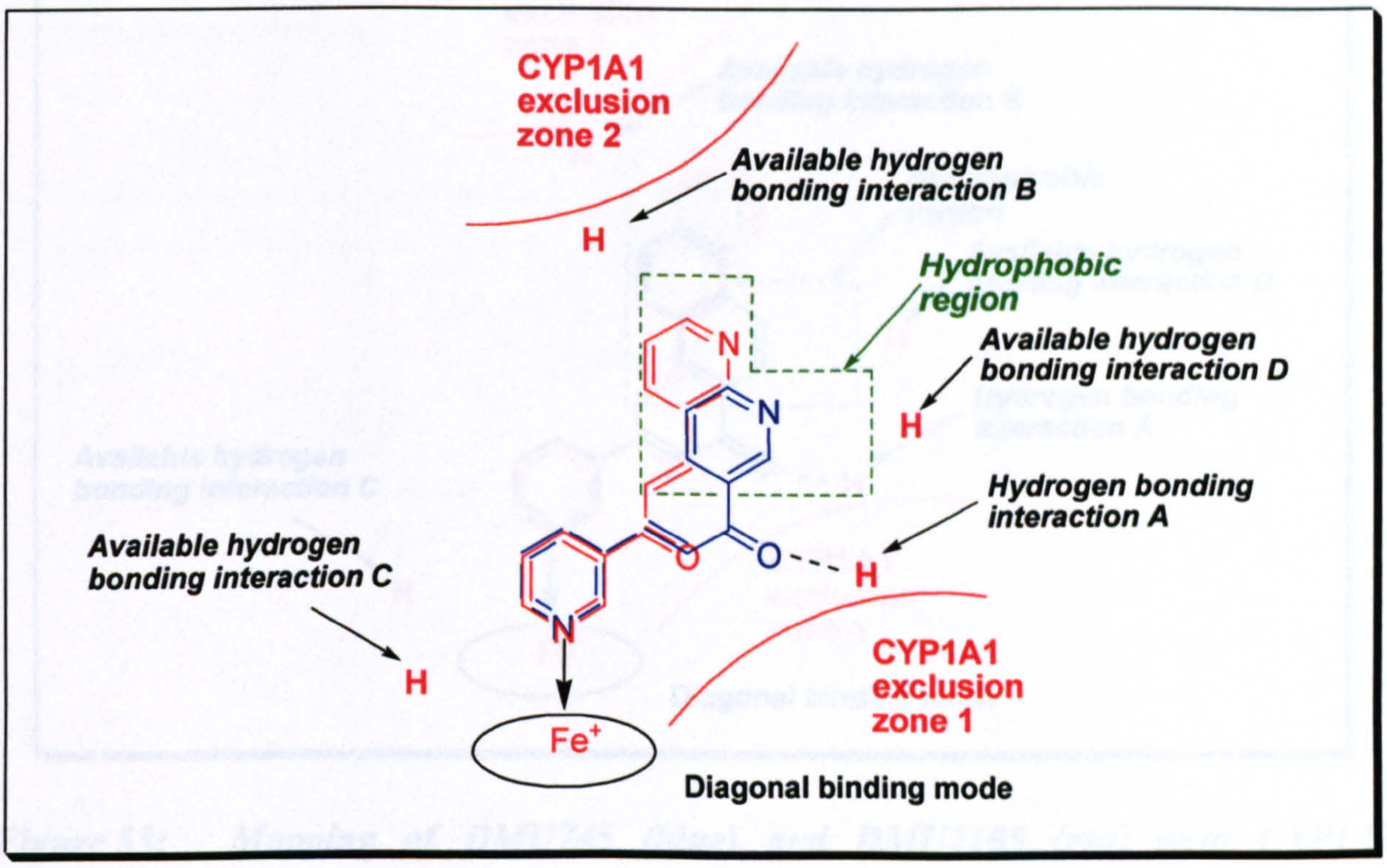

Figure 52: Mapping of DMU2141 onto CYP1A1 pharmacophore model

Regardless of either the 3-pyridyl A-ring (blue) or 3-pyridyl B-ring (red) facing the haem, the other hydrophilic pyridyl ring in DMU2141 would be forced into CYP1A1 hydrophobic region. These molecular orientations are unlikely therefore DMU2141 does not inhibit CYP1A1.

There is no apparent difference for the 1-naphthyl-3-pyridyl chalcone DMU746 and 1-naphthyl reverse 3-pyridyl chalcone DMU756 in the inhibition of CYP1A1 catalysed EROD reaction (IC_{50} 1μM). However, the 2-naphthyl reverse 3-pyridyl chalcone (DMU2105; IC_{50} 5μM) shows a ~17-fold decrease in the inhibition of CYP1A1 when compared with its 3-pyridyl analogue (DMU745; IC_{50} 0.3μM). Given that both

molecules occupy very similar 3D space (Figure 53), the difference in their potency for CYP1A1 inhibition may be due to the interaction of the naphthyl group with the hydrophobic region.

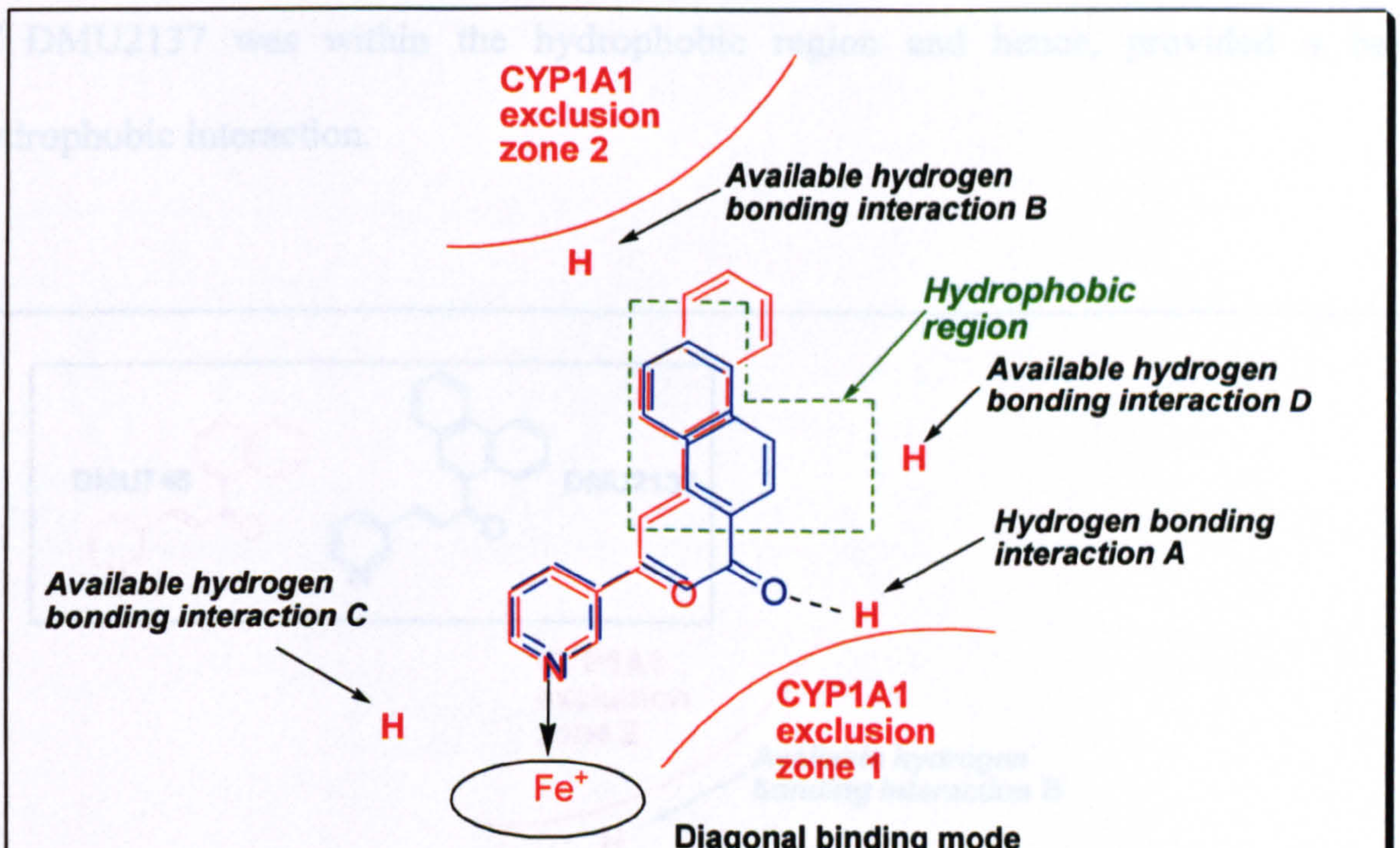

Figure 53: Mapping of DMU745 (blue) and DMU2105 (red) onto CYP1A1 pharmacophore model

The exclusion zone 1 is not the factor that causes a 17-fold reduction in CYP1A1 inhibition potency for DMU2105 compared with its 3-pyridyl analogue. In fact, the hydrogen bonding between the carbonyl oxygen and hydrogen bonding A plays an important role.

The 17-fold reduction in CYP1A1 inhibition potency for DMU2105 suggested CYP1A1 hydrophobic region was smaller. The 2-naphthyl ring of DMU2105 was outside the hydrophobic region, hence a lower inhibition potency compared with it 3-pyridyl analogue (DMU745). The presence of a small hydrophobic region in CYP1A1 was further supported by 20-fold reduction in inhibition potency of 1-naphthyl-3-pyridyl

chalcone DMU746 (IC_{50} 1μM) compared with the 9-phenanthrenyl-3-pyridyl chalcone DMU2137 (IC_{50} 0.05μM). Although DMU746 could be mapped onto the more potent CYP1A1 inhibitor DMU2137, the 1-naphthyl group of DMU746 only partially mapped into the hydrophobic region (Figure 54). In contrast, most of the 9-phenanthrenyl group of DMU2137 was within the hydrophobic region and hence, provided a better hydrophobic interaction.

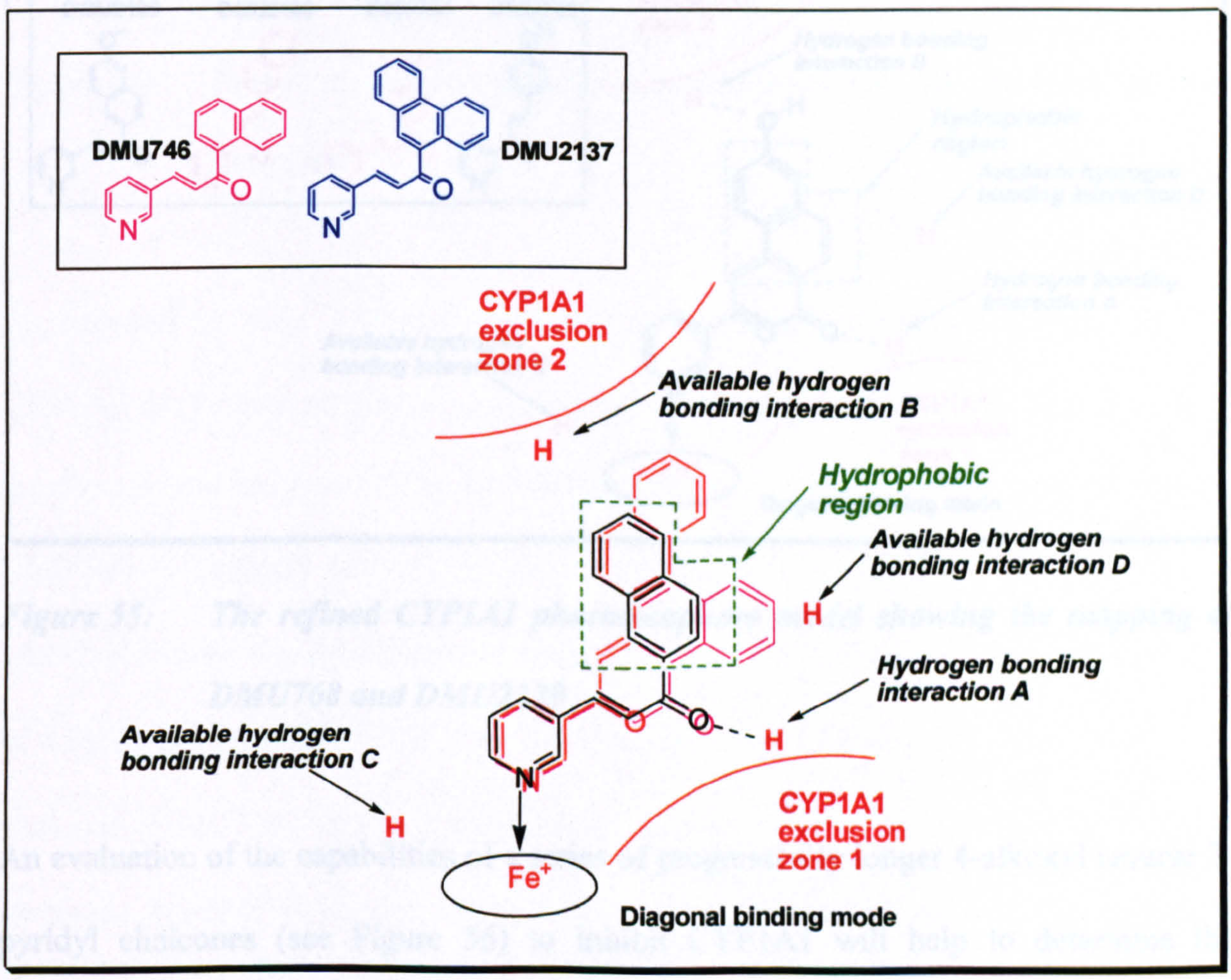

Figure 54: The refined CYP1A1 pharmacophore model with a smaller hydrophobic region

The above figure shows the mapping of DMU745 (black), DMU2105 (red) and DMU746 (magenta) on the pharmacophore model. The naphthyl rings of DMU746 and DMU2105 only partially mapped into the hydrophobic region.

The 4-hydroxy-3-pyridyl chalcone DMU765 did not inhibit CYP1A1 but its reverse 3-pyridyl analogue was a weak CYP1A1 inhibitor with an IC_{50} of 50μM. These observations supported the presence of hydrogen bonding interaction at point B. The 3-fold increase in potency from DMU2105 to DMU2139 also concords with the above observation (see Figure 55).

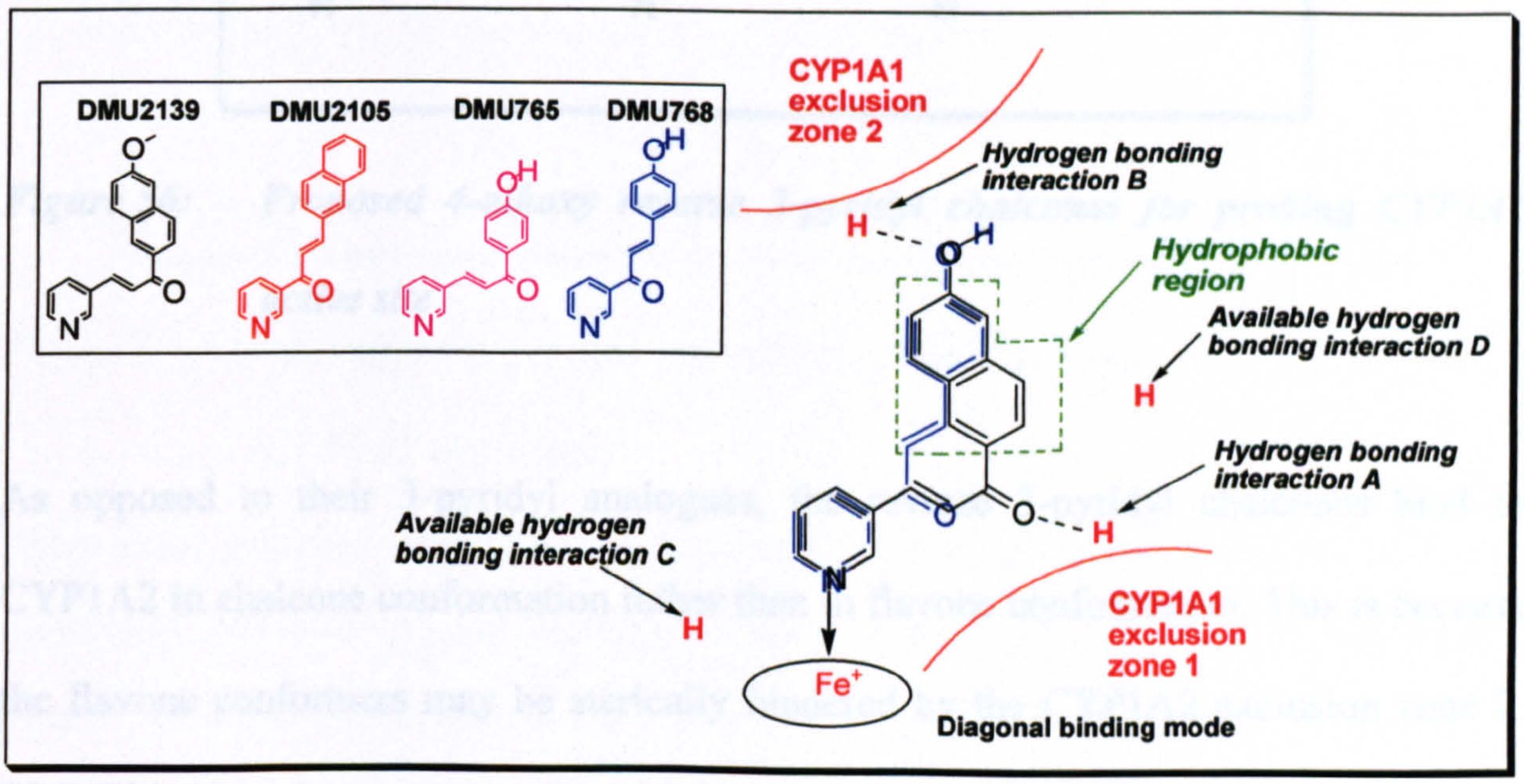

Figure 55: The refined CYP1A1 pharmacophore model showing the mapping of DMU768 and DMU2139

An evaluation of the capabilities of a series of progressively longer 4-alkoxyl reverse 3-pyridyl chalcones (see Figure 56) to inhibit CYP1A1 will help to determine the maximum molecular length that the CYP1A1 active site would tolerate. Unfortunately, the starting materials (i.e. 4-alkoxybenzaldehyde) are not readily available. Thus, the synthesis and evaluation of these proposed inhibitors is outside the scope of this project.

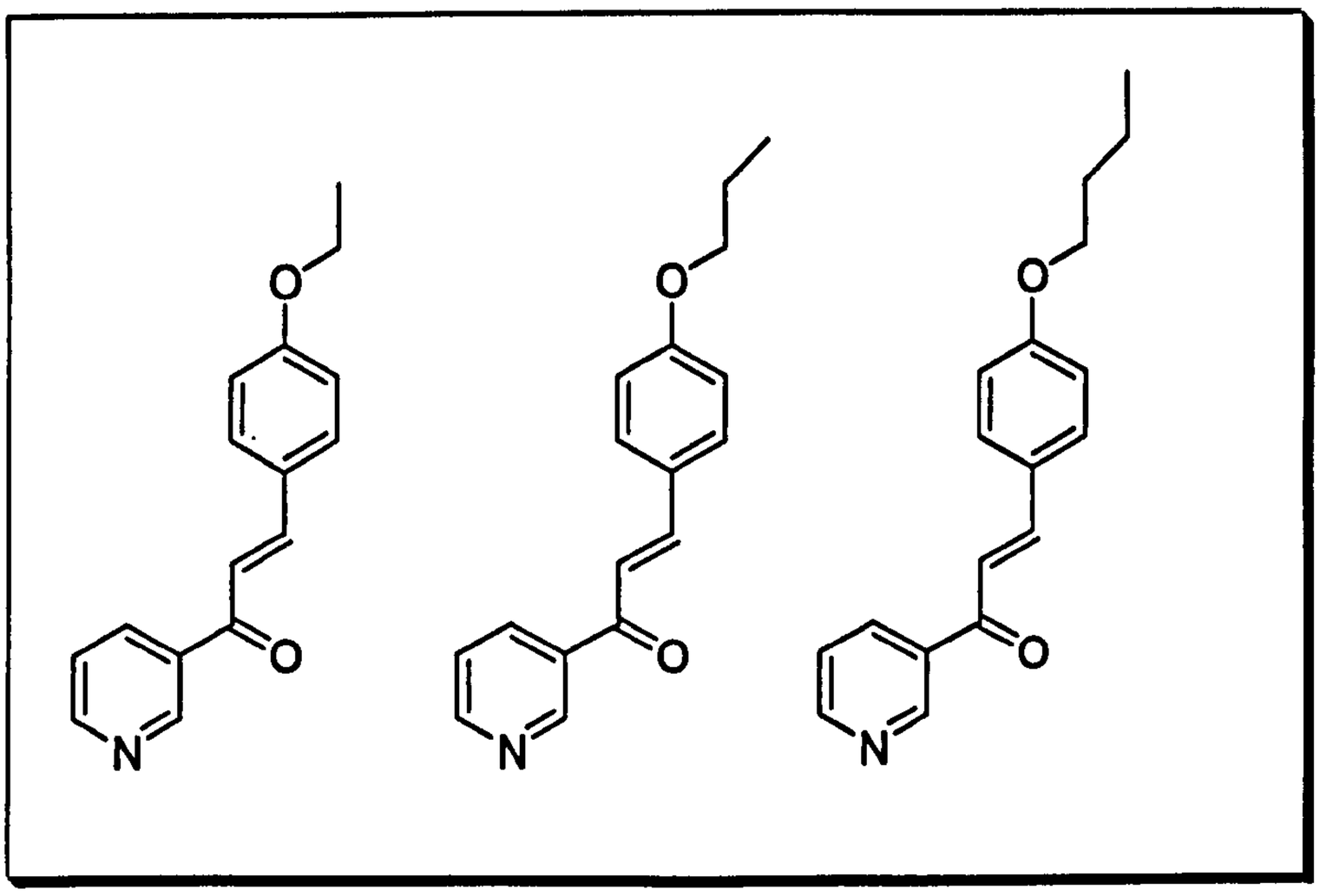

Figure 56: ***Proposed 4-alkoxy reverse 3-pyridyl chalcones for probing CYP1A1 active site***

As opposed to their 3-pyridyl analogues, the reverse 3-pyridyl chalcones bind to CYP1A2 in chalcone conformation rather than in flavone conformation. This is because the flavone conformers may be sterically hindered by the CYP1A2 exclusion zone 2. DMU729 (4-methoxy reverse 3-pyridyl chalcone) inhibits CYP1A2 with an IC_{50} of 16μM. However, the 2,4-dimethoxy analogue (DMU775) inhibits CYP1A2 with an IC_{50} of 0.9μM. The potency of DMU775 is very close to that of 2-methoxy reverse 3-pyridyl chalcone (DMU790; IC_{50} of 0.8μM). These results indicate the presence of a second hydrogen bonding interaction within CYP1A2 active site (Figure 57). The hydrogen bonding interaction at point B in CYP1A2 must be a prominent feature. The interaction of the 2-methoxy group of DMU775 with this hydrogen bonding could override the unfavourable effect of the 4-methoxy group present in the same molecule.

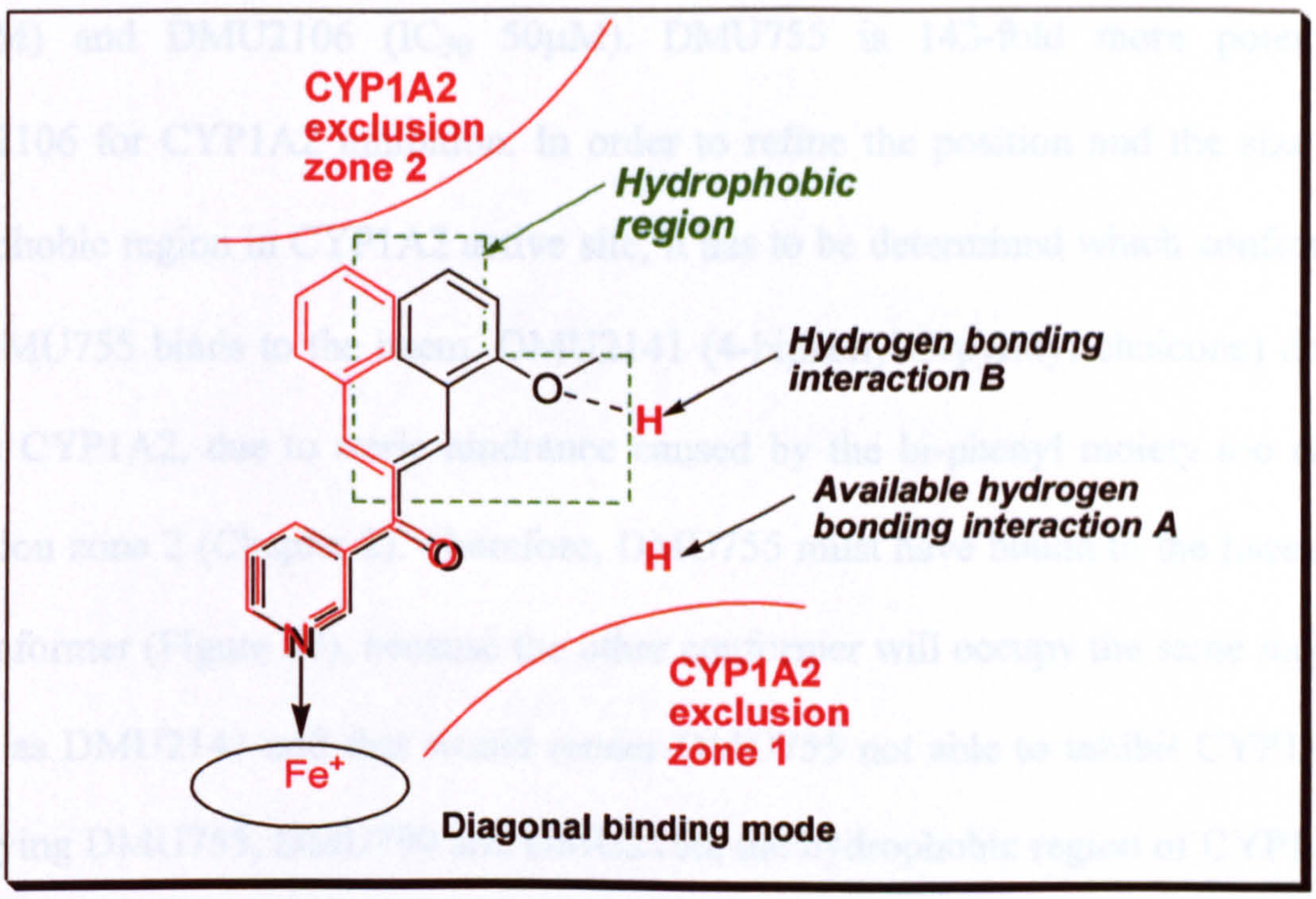

Figure 57: Identification of a second hydrogen bonding interaction within CYP1A2 active site

Figure above shows the mapping of DMU790 (black) onto the pharmacophore model in chalcone conformation. The reverse 3-pyridyl chalcones are thought to bind to CYP1A2 in chalcone conformation since the flavone conformation (red) could be sterically unfavourable due to the close proximity to exclusion zone 2.

Previously, due to lack of significant differences in data generated by the 3-pyridyl chalcones (Chapter 3), the hydrophobic region of CYP1A2 was assumed as similar to that of CYP1A1, based on the same selectivity pattern observed for both CYP1A enzymes. The presence of a hydrophobic region in CYP1A2 is confirmed by the inability of the di-3-pyridyl chalcone (DMU2141) to inhibit CYP1A2. DMU2141 does not inhibit CYP1A2 because, regardless of which 3-pyridyl ring facing the haem, the other more hydrophilic pyridyl ring would map onto the hydrophobic region.

There is a significant difference in CYP1A2 inhibition potency between DMU755 (IC_{50}

0.35μM) and DMU2106 (IC_{50} 50μM). DMU755 is 143-fold more potent than DMU2106 for CYP1A2 inhibition. In order to refine the position and the size of the hydrophobic region in CYP1A2 active site, it has to be determined which conformation that DMU755 binds to the haem. DMU2141 (4-biphenyl-3-pyridyl chalcone) does not inhibit CYP1A2, due to steric hindrance caused by the bi-phenyl moiety too close to exclusion zone 2 (Chapter 2). Therefore, DMU755 must have bound to the haem as the C2 conformer (Figure 58), because the other conformer will occupy the same molecular length as DMU2141 and that would render DMU755 not able to inhibit CYP1A2. By overlaying DMU755, DMU790 and DMU2106, the hydrophobic region of CYP1A2 has been refined. The hydrophobic region in CYP1A2 is considerably smaller compared with CYP1A1; encompassing space just enough to cover a naphthyl group (Figure 59).

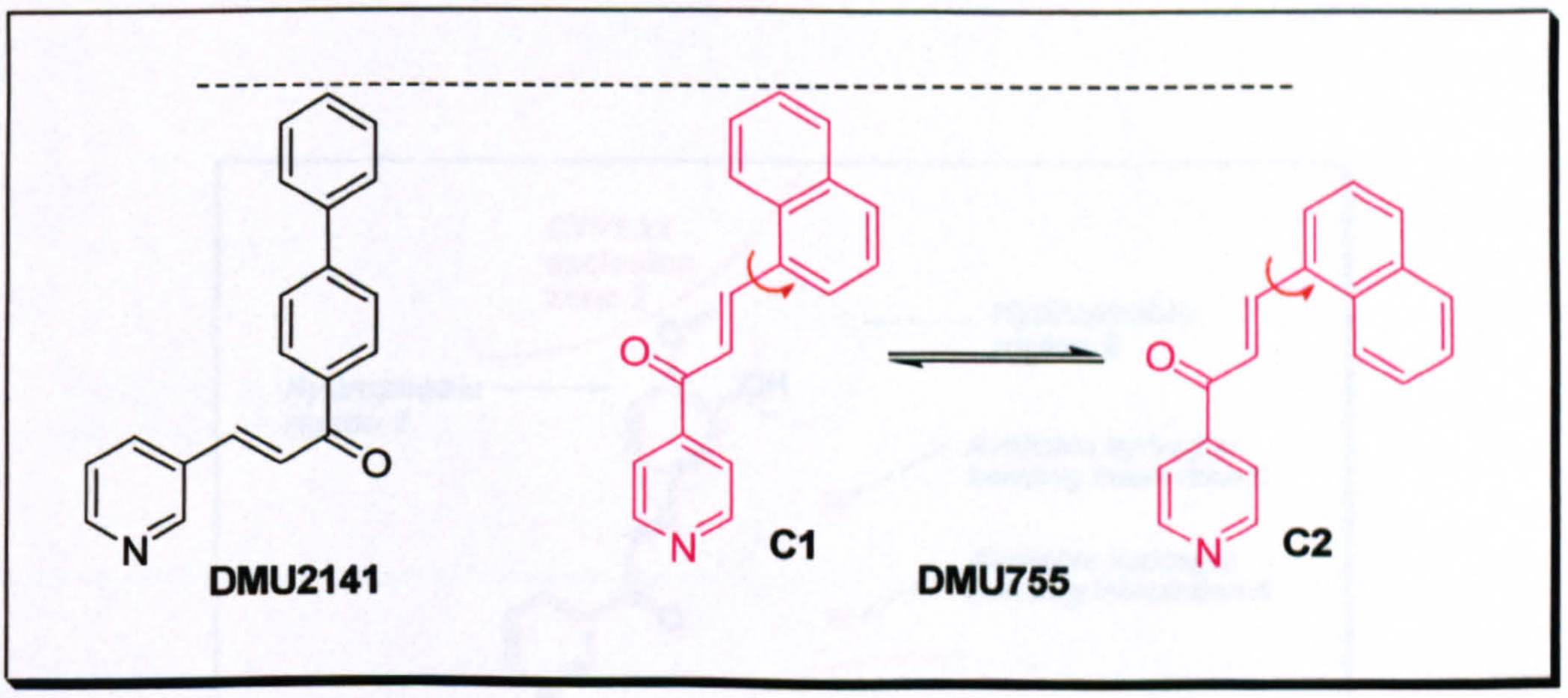

Figure 58: Possible molecular orientation of DMU755 within CYP1A2 active site

DMU755 probably binds to CYP1A2 as C2 conformer since the C1 conformer will be sterically hindered by the exclusion zone 2.

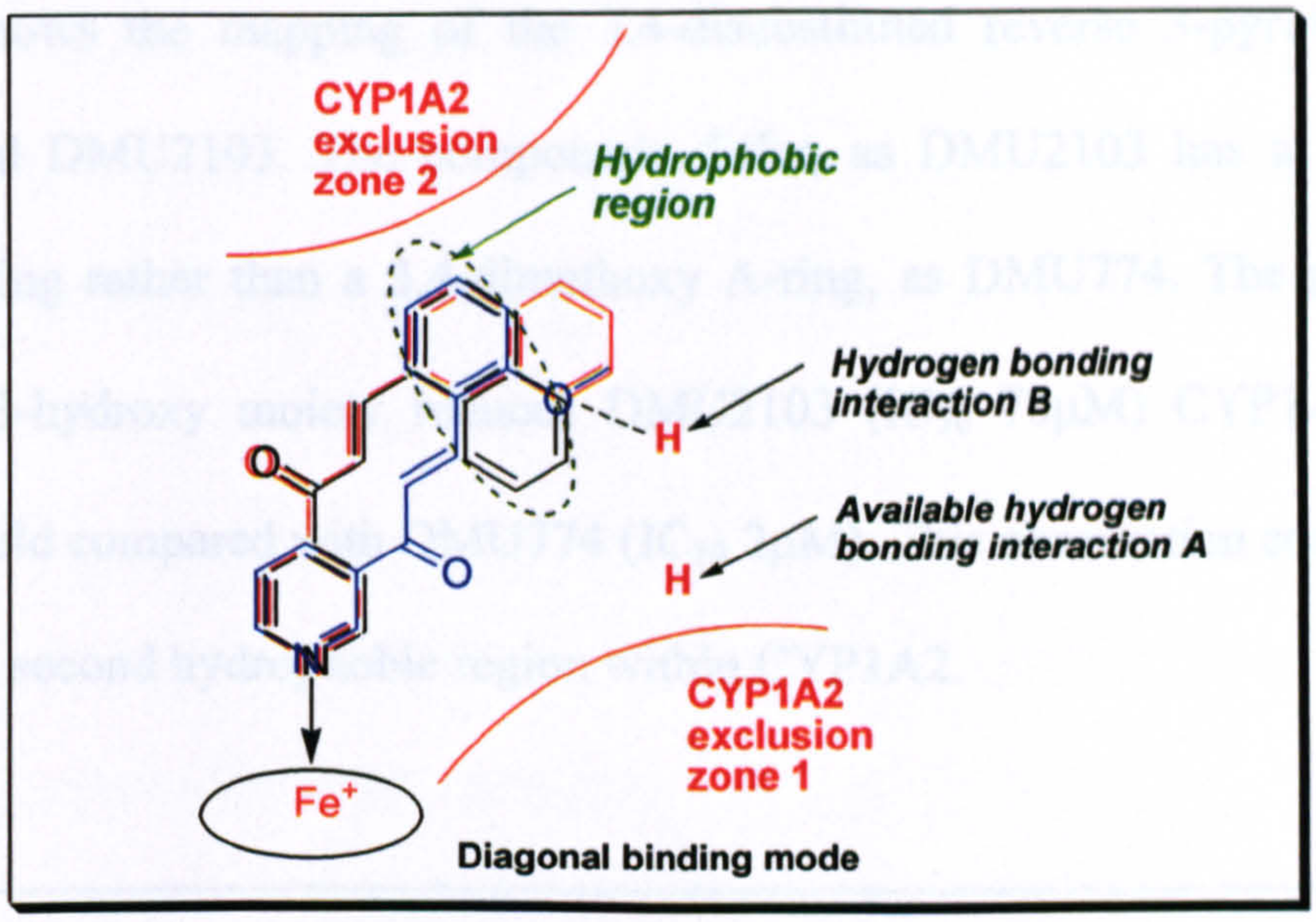

Figure 59: CYP1A2 pharmacophore model with refined hydrophobic region

By mapping DMU755 (black), DMU790 (blue) and DMU2106 (red), the hydrophobic region of CYP1A2 has been defined. The hydrophobic region is not as big as it was thought to be and it encompassed space for a naphthyl group.

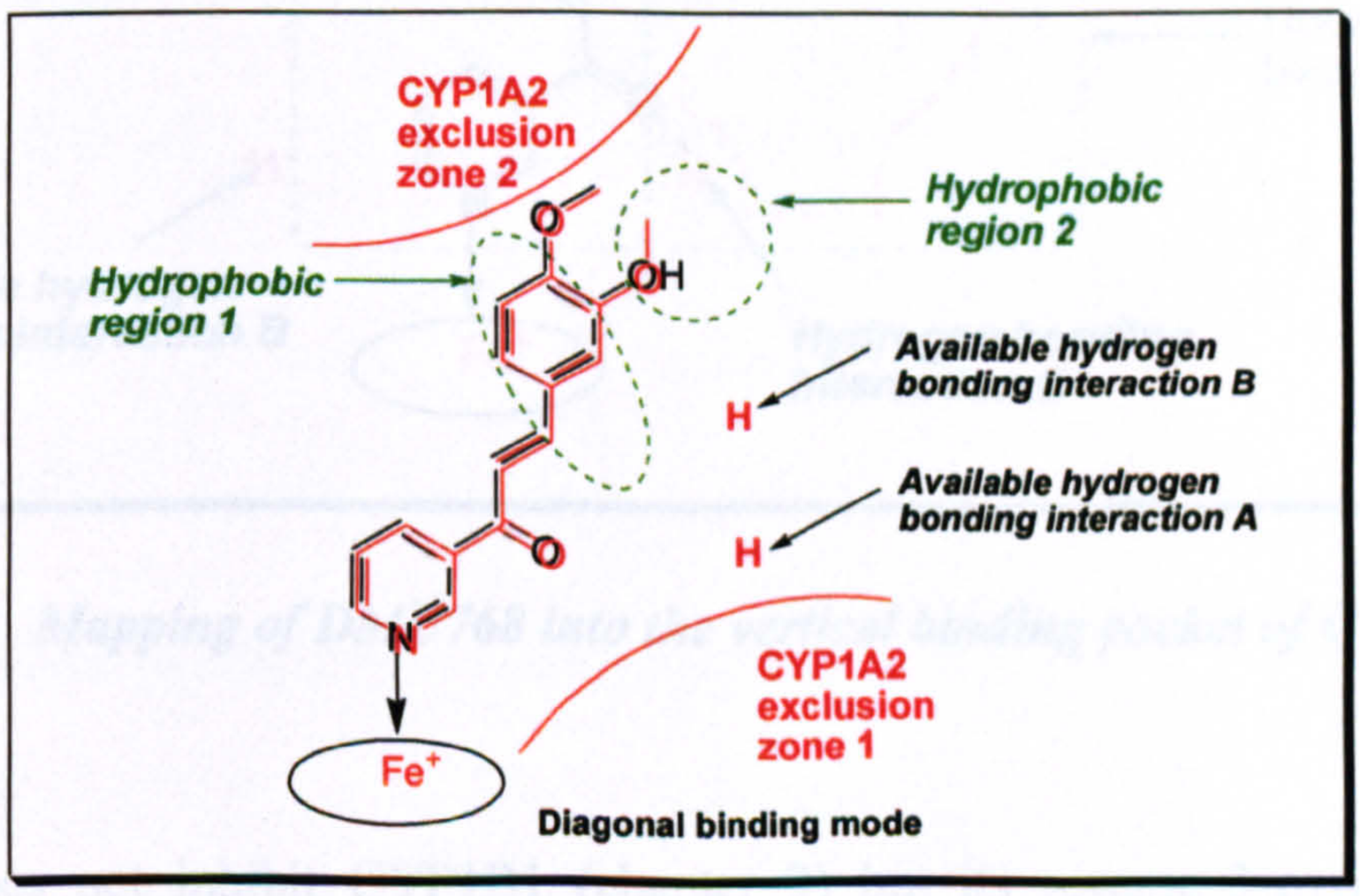

Figure 60: The refined CYP1A2 pharmacophore model showing a second hydrophobic region

Figure above shows the mapping of DMU774 (red) and DMU2103 (black). The presence of a second hydrophobic region reduces DMU2103 potency by 35-fold compared with DMU774.

Figure 60 shows the mapping of the 3,4-disubstituted reverse 3-pyridyl chalcones DMU774 and DMU2103. The compounds differ, as DMU2103 has a 3-hydroxy-4-methoxy A-ring rather than a 3,4-dimethoxy A-ring, as DMU774. The presence of a hydrophilic 3-hydroxy moiety reduces DMU2103 (IC_{50} 70μM) CYP1A2 inhibition potency 35-fold compared with DMU774 (IC_{50} 2μM). This observation corroborates the presence of a second hydrophobic region within CYP1A2.

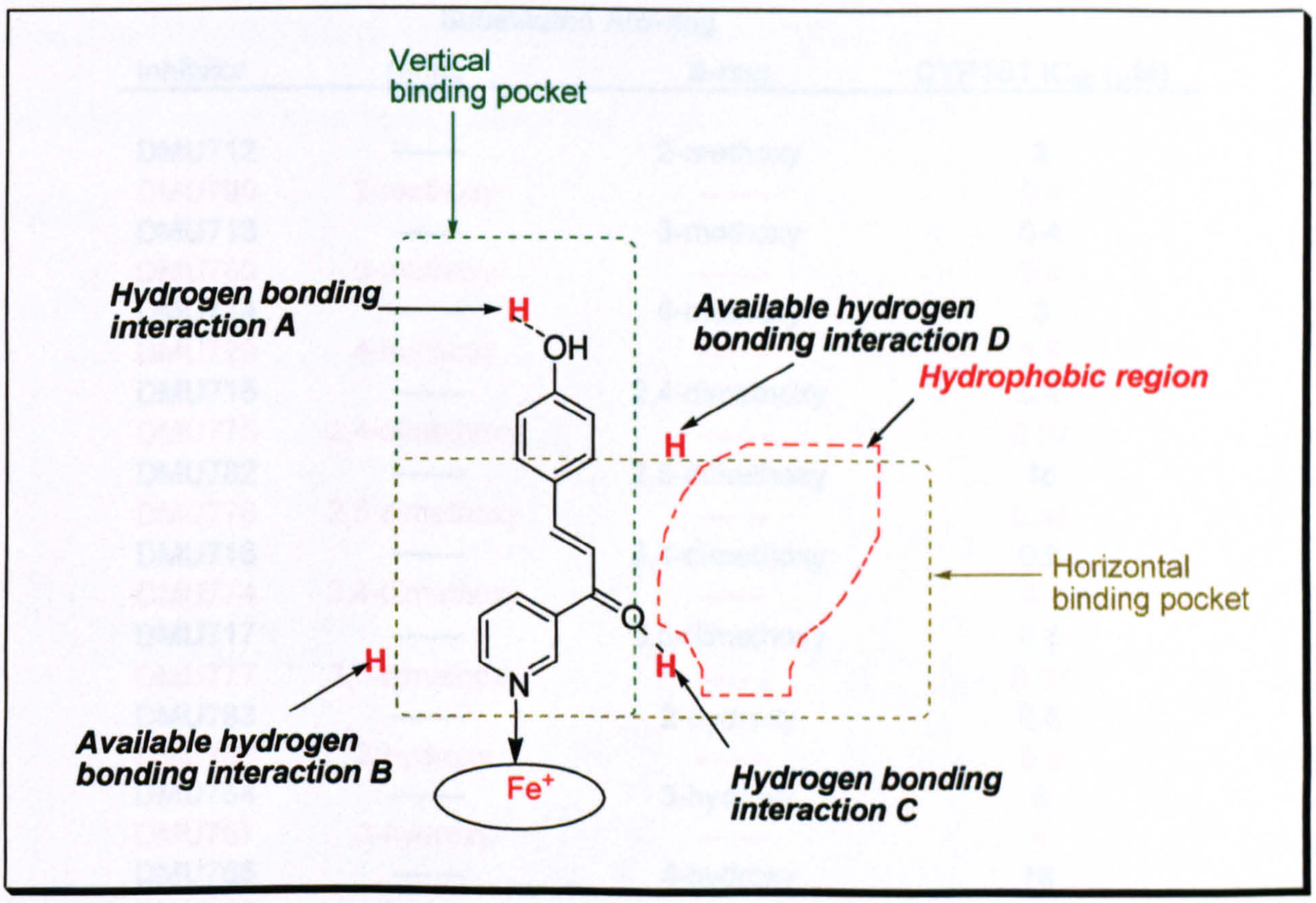

Figure 61: Mapping of DMU768 into the vertical binding pocket of CYP1B1

DMU765 does not inhibit CYP1B1 (chapter 3) but its reverse 3-pyridyl analogue DMU768 inhibits CYP1B1 with an IC_{50} of 5μM. DMU768 binds to CYP1B1 via the vertical binding pocket, since the binding of DMU768 to the horizontal pocket will place the hydrophilic phenol substituent into the hydrophobic zone (Figure 61). In fact it

is thought that all reverse 3-pyridyl chalcones with substituted functional groups on the A-ring are preferably bind to CYP1B1 via the vertical binding pocket. This is evidenced by most substituted A-ring reverse 3-pyridyl chalcones showing an improved potency for CYP1B1 inhibition.

Table 27: Comparison of CYP1B1 EROD IC_{50} of 3-pyridyl chalcones and their reverse 3-pyridyl analogues

	Substituted A/B-ring		
Inhibitor	A-ring	B-ring	CYP1B1 IC_{50} (μM)
DMU712	-------	2-methoxy	3
DMU790	2-methoxy	-------	0.4
DMU713	-------	3-methoxy	0.4
DMU789	3-methoxy	-------	0.4
DMU714	-------	4-methoxy	3
DMU729	4-methoxy	-------	1.5
DMU715	-------	2,4-dimethoxy	0.4
DMU775	2,4-dimethoxy	-------	0.07
DMU782	-------	2,5-dimethoxy	18
DMU776	2,5-dimethoxy	-------	0.07
DMU716	-------	3,4-dimethoxy	0.6
DMU774	3,4-dimethoxy	-------	0.2
DMU717	-------	3,5-dimethoxy	0.2
DMU777	3,5-dimethoxy	-------	0.07
DMU763	-------	2-hydroxy	0.8
DMU766	2-hydroxy	-------	0.8
DMU764	-------	3-hydroxy	6
DMU767	3-hydroxy	-------	4
DMU765	-------	4-hydroxy	NI
DMU768	4-hydroxy	-------	5

Note: 3-pyridyl chalcones (black); reverse 3-pyridyl chalcones (red).

The 1- and 2-naphthyl reverse 3-pyridyl chalcones (DMU756 and DMU2105, respectively) probably bind to CYP1B1 via the horizontal binding pocket as chalcone conformers. The planar naphthyl substituents afford a strong lipophilic interaction with the hydrophobic region.

DMU776 and DMU777 show potent inhibition of CYP1B1, with a recorded IC_{50} of 0.07μM for both inhibitors. This indicates the presence of a second hydrogen bonding interaction at the top of the vertical binding pocket. The evidence for the presence of a second hydrogen bonding interaction at the top of the vertical binding pocket is corroborated by the selective metabolism of DMU214 to DMU293[139] by CYP1B1 (Figure 63).

DMU2141 selectively inhibits CYP1B1 with an IC_{50} of 19μM. DMU2141 must have bound to CYP1B1 in the vertical binding pocket. DMU2141 cannot bind to CYP1B1 horizontal pocket because its hydrophilic 3-pyridyl rings cannot fit into the hydrophobic region.

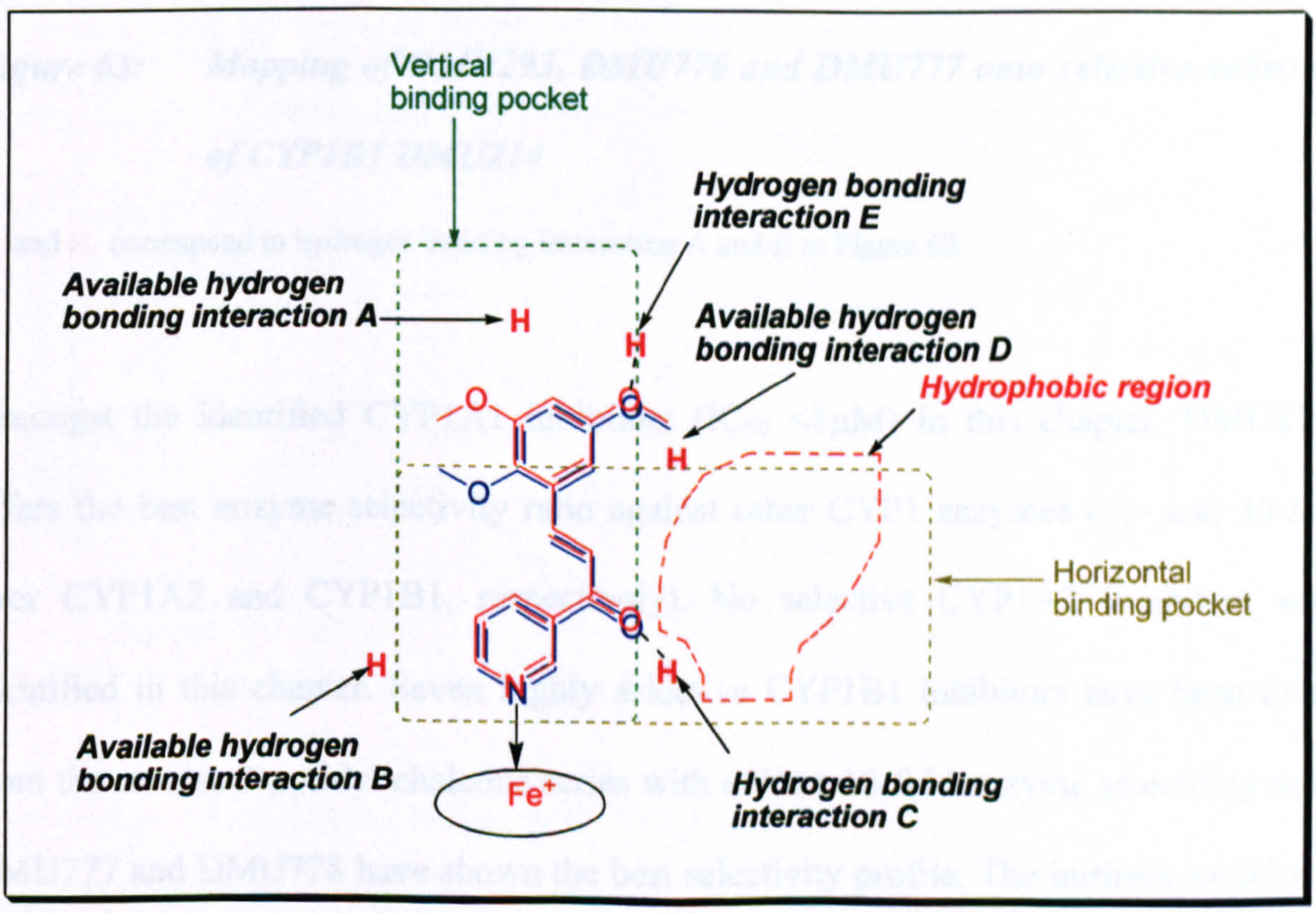

Figure 62: Identification of the fifth hydrogen binding interaction for CYP1B1 pharmacophore model

Note: DMU776 (blue); DMU777 (red).

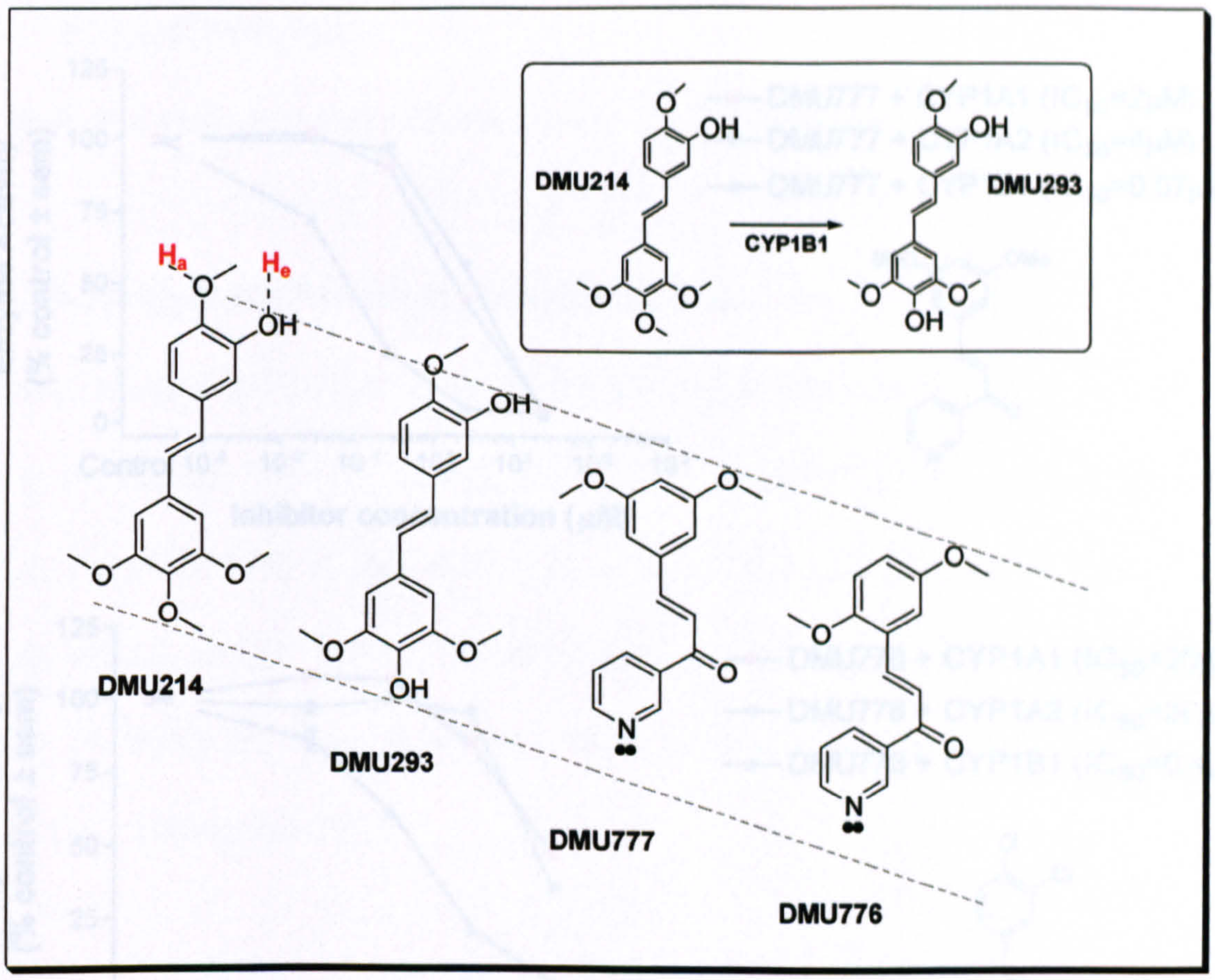

Figure 63: Mapping of DMU293, DMU776 and DMU777 onto selective substrate of CYP1B1 DMU214

H_a and H_e correspond to hydrogen bonding interaction A and E in Figure 62.

Amongst the identified CYP1A1 inhibitors (IC_{50} <1μM) in this chapter, DMU2157 offers the best enzyme selectivity ratio against other CYP1 enzymes (17- and 30-fold over CYP1A2 and CYP1B1, respectively). No selective CYP1A2 inhibitors were identified in this chapter. Seven highly selective CYP1B1 inhibitors have been found from the reverse 3-pyridyl chalcone series with at least 10-fold enzyme selectivity ratio. DMU777 and DMU778 have shown the best selectivity profile. The intrinsic toxicity of all identified inhibitors has to be determined to assess their suitability for cell culture or *in vivo* experiments. This will be discussed in Chapter 5.

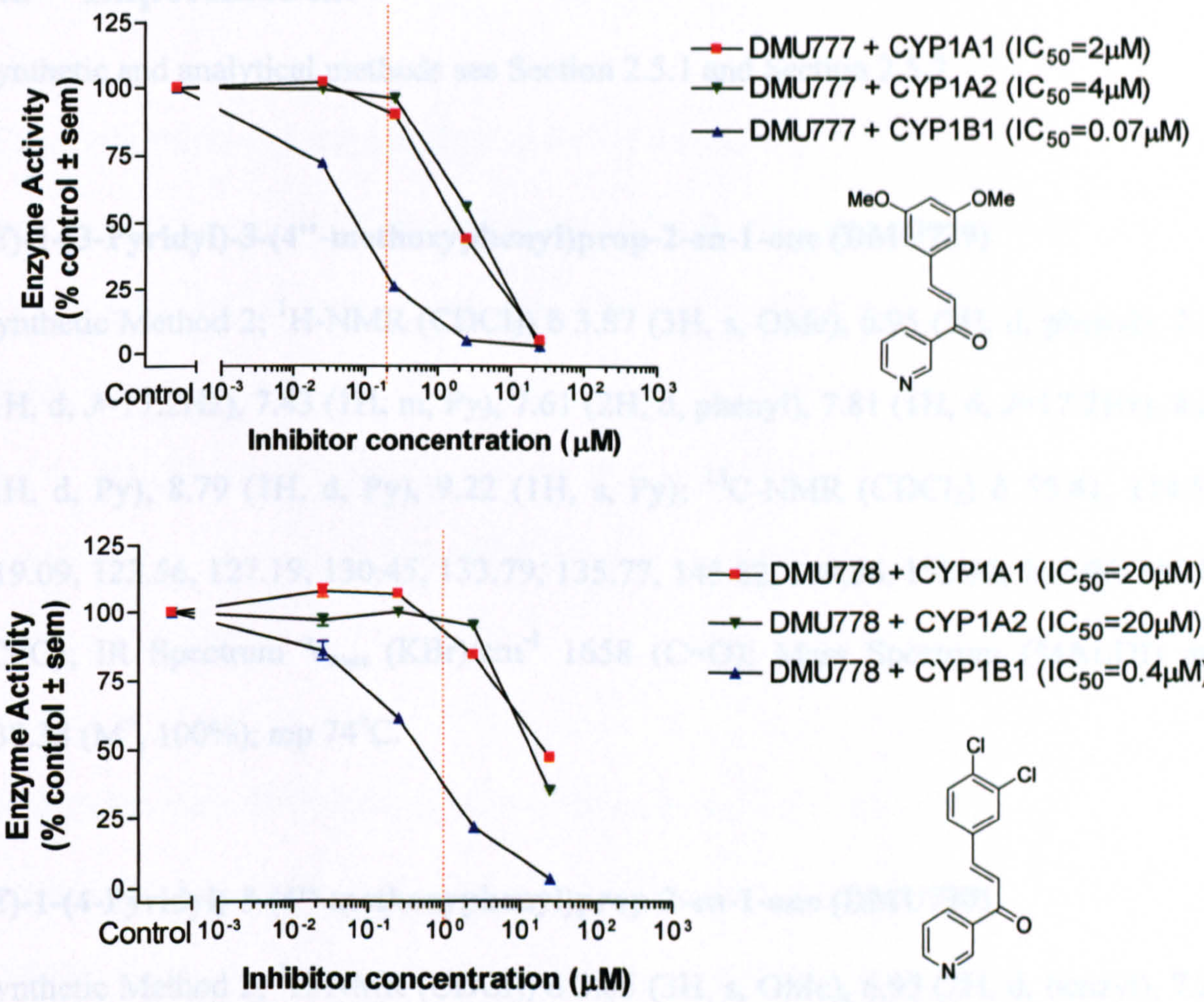

Figure 64: Selective inhibitors of CYP1A1 and CYP1B1

Dotted red lines indicate the recommended concentration for the inhibitors to be used in order to achieve maximum inhibitory effect.

4.5 Experimental

Synthetic and analytical methods see Section 2.5.1 and Section 2.5.2

(*E*)-1-(3-Pyridyl)-3-(4''-methoxyphenyl)prop-2-en-1-one (DMU729)

Synthetic Method 2; ^{1}H-NMR ($CDCl_3$) δ 3.87 (3H, s, OMe), 6.95 (2H, d, phenyl), 7.36 (1H, d, *J*=17.2Hz), 7.43 (1H, m, Py), 7.61 (2H, d, phenyl), 7.81 (1H, d, *J*=17.2Hz), 8.27 (1H, d, Py), 8.79 (1H, d, Py), 9.22 (1H, s, Py); ^{13}C-NMR ($CDCl_3$) δ 55.41, 114.53, 119.09, 123.56, 127.19, 130.45, 133.79, 135.77, 145.82, 149.66, 152.92, 162.06, 189.07 (C=O); IR Spectrum V_{max} (KBr)/cm^{-1} 1658 (C=O); Mass Spectrum (MALDI) m/z 238.38 (M^+, 100%); mp 74°C.

(*E*)-1-(4-Pyridyl)-3-(4''-methoxyphenyl)prop-2-en-1-one (DMU730)

Synthetic Method 2; ^{1}H-NMR ($CDCl_3$) δ 3.85 (3H, s, OMe), 6.95 (2H, d, benzyl), 7.29 (1H, d, *J*=16.2Hz), 7.61 (2H, d, benzyl), 7.75 (2H, d, Py), 7.79 (1H, d, *J*=16.2Hz), 8.82 (2H, d, Py); ^{13}C-NMR ($CDCl_3$) δ 55.43, 114.56, 118.91, 121.45, 127.06, 130.55, 144.77, 146.65, 150.71, 162.23, 189.78 (C=O); IR Spectrum V_{max} (KBr)/cm^{-1} 1659 (C=O); Mass Spectrum (MALDI) m/z 239.49 (M^+, 100%); mp 92-93°C.

(*E*)-1-(4-Pyridyl)-3-(1-naphthyl)prop-2-en-1-one (DMU755)

Synthetic Method 1; ^{1}H-NMR ($CDCl_3$) δ 6.67 (1H, d, *J*=16.3Hz), 7.28-7.38 (4H,m), 7.48-7.55 (2H, m), 8.22 (2H, d, naphthyl), 8.70 (2H, d, Py), 8.87 (2H, d, Py); ^{13}C-NMR ($CDCl_3$) δ 120.52, 121.56, 123.26, 123.62, 125.94, 126.49, 127.27, 128.21, 131.53, 131.74, 133.82, 143.64, 144.39, 150.16, 150.91, 189.60 (C=O); IR Spectrum V_{max} (KBr)/cm^{-1} 1666 (C=O); Mass Spectrum (MALDI) m/z 259.31 (M^+, 100%); mp 101-

102°C.

(*E*)-1-(3-Pyridyl)-3-(1-naphthyl)prop-2-en-1-one (DMU756)

Synthetic Method 3; ^{1}H-NMR ($CDCl_3$) δ 7.32-7.70 (5H, m), 7.83-7.99 (3H, m), 8.22 (1H, d), 8.32 (1H, d), 8.71 (1H, d, Py), 8.80 (1H, d, Py), 9.30 (1H, s, Py); ^{13}C-NMR ($CDCl_3$) δ 123.31, 123.68, 123.85, 125.29, 125.42, 126.39, 127.14, 128.83, 131.27, 131.76, 131.87, 133.50, 133.76, 135.91, 142.84, 149.83, 153.23, 188.87 (C=O); IR Spectrum V_{max} (KBr)/cm^{-1} 1666 (C=O); Mass Spectrum (MALDI) m/z 259.23 (M^+, 100%); mp 127°C.

(*E*)-1-(3-Pyridyl)-3-(2''-hydroxyphenyl)prop-2-en-1-one (DMU766)

Synthetic Method 3; ^{1}H-NMR (DMSO) δ 6.88 (1H, t, phenyl), 6.95 (1H, d, phenyl), 7.29 (1H, t, phenyl), 7.58 (1H, t, Py), 7.81 (1H, d, *J*=16.3Hz), 7.86 (1H, d, phenyl), 8.08 (1H, d, *J*=16.3Hz), 8.39 (1H, d, Py), 8.79 (1H, d, Py), 9.23 (1H, s, Py), 10.30 (1H, s, OH); ^{13}C-NMR (DMSO) δ 116.31, 119.70, 120.83, 121.23, 124.09, 128.89, 132.58, 133.29, 136.00, 140.42, 149.48, 153.17, 157.36, 188.98 (C=O); IR Spectrum V_{max} (KBr)/cm^{-1} 1654 (C=O); Mass Spectrum (MALDI) m/z 225.48 (M^+, 100%); mp 148°C.

(*E*)-1-(3-Pyridyl)-3-(3''-hydroxyphenyl)prop-2-en-1-one (DMU767)

Synthetic Method 3; ^{1}H-NMR (DMSO) δ 6.89 (1H, d, phenyl), 7.18-7.32 (3H, m), 7.58 (1H, t, Py), 7.65 (1H, d, *J*=15.7Hz), 7.77 (1H, d, *J*=15.7Hz), 8.42 (1H, d, Py), 8.79 (1H, d, Py), 9.21 (1H, s, Py), 9.67 (1H, s, OH); ^{13}C-NMR (DMSO) δ 115.19, 118.32, 120.45, 121.78, 124.23, 130.24, 132.99, 135.70, 136.27, 145.34, 149.45, 153.28, 157.54, 188.98 (C=O); IR Spectrum V_{max} (KBr)/cm^{-1} 1662 (C=O); Mass Spectrum (MALDI) m/z

225.48 (M^+, 100%); mp 192-193°C.

(*E*)-1-(3-Pyridyl)-3-(4''-hydroxyphenyl)prop-2-en-1-one (DMU768)

Synthetic Method 3; ^{1}H-NMR (DMSO) δ 6.63 (2H, d, phenyl), 7.36 (1H, t, Py), 7.45-7.59 (4H, m), 8.21 (1H, d, Py), 8.59 (1H, d, Py), 9.08 (1H, s, Py), 9.91 (1H, s, OH); ^{13}C-NMR (DMSO) δ 115.94, 118.37, 123.91, 125.67, 131.36, 133.24, 135.83, 145.37, 149.55, 153.07, 160.50, 188.25 (C=O); IR Spectrum V_{max} (KBr)/cm^{-1} 1654 (C=O); Mass Spectrum (MALDI) m/z 225.48 (M^+, 100%); mp 188-189°C.

(*E*)-1-(3-Pyridyl)-3-(3,4-methylenedioxyphenyl) prop-2-en-1-one (DMU769)

Synthetic Method 2; ^{1}H-NMR ($CDCl_3$) δ 6.07 (2H, methylene), 7.87 (1H, d), 7.16 (2H, m), 7.29 (1H, d, *J*=16.8Hz), 7.41 (1H, m), 7.74 (1H, d, *J*=16.8Hz), 8.25 (1H, d, Py), 8.80 (1H, d, Py), 9.21 (1H, s, Py); ^{13}C-NMR ($CDCl_3$) δ 101.76, 106.76, 108.78, 119.47, 123.63, 125.65, 128.98, 133.74, 135.81, 145.84, 148.57, 149.70, 150.37, 153.05, 188.97 (C=O); IR Spectrum V_{max} (KBr)/cm^{-1} 1662 (C=O); Mass Spectrum (MALDI) m/z 253.33 (M^+, 100%); mp 144-145°C.

(*E*)-1-(3-Pyridyl)-3-(3'',4''-dimethoxyphenyl)prop-2-en-1-one (DMU774)

Synthetic Method 3; ^{1}H-NMR ($CDCl_3$) δ 3.90 (3H, s, OMe), 3.92 (3H, s, OMe), 6.90 (1H, d, phenyl), 7.15 (1H, s, phenyl), 7.21 (1H, d, phenyl), 7.31 (1H, d, *J*=16.8Hz), 7.43 (1H, m, Py), 7.79 (1H, d, *J*=16.8Hz), 8.25 (1H, d, Py), 8.77 (1H, d, Py), 9.22 (1H, s, Py); ^{13}C-NMR ($CDCl_3$) δ 56.04, 56.06, 110.26, 111.27, 119.46, 123.58, 127.50, 133.85, 135.85, 146.18, 149.43, 149.72, 151.94, 153.00, 189.15 (C=O); IR Spectrum V_{max} (KBr)/cm^{-1} 1658 (C=O); Mass Spectrum (MALDI) m/z 268.92 (M^+, 100%); mp 88-

89°C.

(*E*)-1-(3-Pyridyl)-3-(3'',4''-dichlorophenyl)prop-2-en-1-one (DMU778)

Synthetic Method 2; ^{1}H-NMR ($CDCl_3$) δ 7.45-7.55 (4H, m), 7.71-7.78 (2H, m), 8.30 (1H, d, Py), 8.83 (1H, d, Py), 9.24 (1H, s, Py); ^{13}C-NMR ($CDCl_3$) δ 122.78, 123.69, 127.53, 129.94, 131.04, 133.47, 134.47, 135.84, 142.95, 149.74, 153.44, 188.48 (C=O); IR Spectrum V_{max} (KBr)/cm^{-1} 1670 (C=O); Mass Spectrum (MALDI) m/z 278.13 (M^+, 100%); mp 168°C.

(*E*)-1-(1-Naphthyl)-3-(4-pyridyl)prop-2-en-1-one (DMU779)

Synthetic Method 3; ^{1}H-NMR ($CDCl_3$) δ 7.47-7.61 (7H, m), 7.81 (1H, d, naphthyl), 7.92 (1H, d, naphthyl), 8.03 (1H, d, naphthyl), 8.48 (1H, d, naphthyl), 8.67 (2H, d, Py); ^{13}C-NMR ($CDCl_3$) δ 122.02, 124.47, 125.54, 126.70, 127.75, 127.83, 128.59, 130.48, 130.71, 132.42, 133.94, 136.19, 141.91, 142.19, 150.68, 194.46 (C=O); IR Spectrum V_{max} (KBr)/cm^{-1} 1655 (C=O); Mass Spectrum (MALDI) m/z 259.31 (M^+, 100%); oil.

(*E*)-1-(2-Naphthyl)-3-(4-pyridyl)prop-2-en-1-one (DMU780)

Synthetic Method 3; ^{1}H-NMR ($CDCl_3$) δ 7.46 (2H, d, Py), 7.53-7.64 (2H, m), 7.72 (1H, d, *J*=15.4Hz), 7.80 (1H, d, *J*=15.4Hz), 7.88 (1H, d, naphthyl), 7.93 (1H, d, naphthyl), 7.98 (1H, d, naphthyl), 8.08 (1H, d, naphthyl), 8.52 (1H, s, naphthyl), 8.68 (2H, d, Py); ^{13}C-NMR ($CDCl_3$) δ 122.01, 124.24, 126.02, 126.95, 127.85, 128.70, 128.78, 129.55, 130.26, 132.48, 134.85, 135.65, 141.36, 142.10, 150.63, 189.42 (C=O); IR Spectrum V_{max} (KBr)/cm^{-1} 1663 (C=O); Mass Spectrum (MALDI) m/z 259.18 (M^+, 100%); mp 126°C.

(*E*)-1-(2',5'-Dimethoxyphenyl)-3-(4-pyridyl)prop-2-en-1-one (DMU781)

Synthetic Method 3; ^{1}H-NMR ($CDCl_3$) δ 3.83 (3H, s, OMe), 3.90 (3H, s, OMe), 6.98 (1H, d, benzyl), 7.09 (1H, m, benzyl), 7.26 (1H, d, benzyl), 7.43 (2H, d, Py), 7.56 (1H, d, *J*=15.9Hz), 7.63 (1H, d, *J*=15.9Hz), 8.68 (2H, d, Py); ^{13}C-NMR ($CDCl_3$) δ 55.83, 56.43, 113.44, 114.47, 120.13, 121.98, 128.79, 130.77, 139.19, 142.51, 150.49, 152.98, 153.74, 191.25 (C=O); IR Spectrum V_{max} (KBr)/cm^{-1} 1674 (C=O); Mass Spectrum (MALDI) m/z 269.59 (M^+, 100%); mp 79°C.

(*E*)-1-(3-Pyridyl)-3-(3''-methoxyphenyl)prop-2-en-1-one (DMU789)

Synthetic Method 2; ^{1}H-NMR ($CDCl_3$) δ 3.89 (3H, s, OMe), 6.98 (1H, d, phenyl), 7.15 (1H, s, phenyl), 7.23 (1H, d, phenyl), 7.33 (1H, t, phenyl), 7.43 (1H, t, Py), 7.45 (1H, d, *J*=14.8Hz), 7.79 (1H, d, *J*=14.8Hz), 8.27 (1H, d, Py), 8.79 (1H, d, Py), 9.23 (1H, s, Py); ^{13}C-NMR ($CDCl_3$) δ 53.68, 111.91, 115.11, 119.58, 120.05, 121.96, 128.36, 131.80, 134.18, 144.19, 148.10, 151.48, 158.35, 187.41 (C=O); IR Spectrum V_{max} (KBr)/cm^{-1} 1662 (C=O); Mass Spectrum (MALDI) m/z 239.68 (M^+, 100%); mp 78°C.

(*E*)-1-(3-Pyridyl)-3-(2''-methoxyphenyl)prop-2-en-1-one (DMU790)

Synthetic Method 2; ^{1}H-NMR ($CDCl_3$) δ 3.90 (3H, s, OMe), 6.91-7.01 (2H, m), 7.35-7.45 (2H, m), 7.58 (1H, d, *J*=14.3Hz), 7.61 (1H), 8.11 (1H, d, *J*=14.3Hz), 8.27 (1H), 8.78 (1H, d, Py), 9.22 (1H, s, Py); ^{13}C-NMR ($CDCl_3$) δ 55.49, 111.27, 120.77, 122.16, 123.53, 129.56, 130.62, 132.18, 135.51, 141.52, 149.73, 152.84, 158.95, 189.59 (C=O); IR Spectrum V_{max} (KBr)/cm^{-1} 1663 (C=O); Mass Spectrum (MALDI) m/z 239.38 (M^+, 100%); mp 95-96°C.

(*E*)-1-(3-Pyridyl)-3-(3'',4''-difluorophenyl) prop-2-en-1-one (DMU2101)

Synthetic Method 2; ^{1}H-NMR ($CDCl_3$) δ 7.24 (1H, m), 7.43 (1H, d, *J*=14.8Hz), 7.46-7.54 (3H, m), 7.77 (1H, d, *J*=14.8Hz), 8.30 (1H, d, Py), 8.83 (1H, d, Py), 9.24 (1H, s, Py); ^{13}C-NMR ($CDCl_3$) δ 116.56, 116.82, 117.87, 118.15, 122.20, 123.69, 125.48, 133.18, 135.82, 143.37, 149.70, 153.37, 188.53 (C=O); IR Spectrum V_{max} (KBr)/cm^{-1} 1670 (C=O); Mass Spectrum (MALDI) m/z 245.48 (M^+, 100%); mp 135-136°C.

(*E*)-1-(3-Pyridyl)-3-(3''-hydroxy-4''-methoxyphenyl)prop-2-en-1-one (DMU2103)

Synthetic Method 3; ^{1}H-NMR ($CDCl_3$) δ 3.98 (3H, s, OMe), 5.94 (1H, s, OH), 6.89 (1H, d, phenyl), 7.17 (1H, d, phenyl), 7.30 (1H, s, phenyl), 7.34 (1H, d, *J*=14.6Hz), 7.45 (1H, m, Py), 7.78 (1H, d, *J*=14.6Hz), 8.29 (1H, d, Py), 8.80 (1H, d, Py), 9.23 (1H, s, Py); ^{13}C-NMR ($CDCl_3$) δ 55.86, 112.09, 115.21, 119.39, 122.59, 124.02, 127.56, 133.27, 135.97, 145.47, 146.84, 149.64, 150.76, 153.20, 188.43 (C=O); IR Spectrum V_{max} (KBr)/cm^{-1} 1658 (C=O); Mass Spectrum (MALDI) m/z 255.55 (M^+, 100%); mp 157°C.

(*E*)-1-(3-Pyridyl)-3-(2-naphthyl)prop-2-en-1-one (DMU2105)

Synthetic Method 3; ^{1}H-NMR ($CDCl_3$) δ 7.46 (1H, m), 7.51-7.56 (2H, m), 7.58 (1H, d, *J*=15.7Hz), 7.78 (1H, d), 7.83-7.92 (3H, m), 8.01 (1H, d, *J*=15.7Hz), 8.04 (1H, s), 8.30 (1H, d, Py), 8.81 (1H, d, Py), 9.29 (1H, s, Py); ^{13}C-NMR ($CDCl_3$) δ 121.54, 123.60, 123.70, 126.92, 127.67, 127.87, 128.76, 128.92, 131.13, 132.00, 133.37, 133.65, 134.63, 135.91, 146.10, 149.82, 153.19, 189.10 (C=O); IR Spectrum V_{max} (KBr)/cm^{-1} 1654 (C=O); Mass Spectrum (MALDI) m/z 259.70 (M^+, 100%); mp 136°C.

(*E*)-1-(4-Pyridyl)-3-(2-naphthyl)prop-2-en-1-one (DMU2106)

Synthetic Method 3; ^{1}H-NMR ($CDCl_3$) δ 7.52-7.59 (2H, m), 7.85 (1H, d, *J*=15.5Hz), 7.87-8.02 (7H, m), 8.23 (1H, s, naphthyl), 8.83 (2H, d, Py); ^{13}C-NMR ($CDCl_3$) δ 119.44, 119.53, 122.01, 124.62, 125.44, 125.55, 126.46, 126.50, 129.02, 129.85, 130.91, 132.14, 141.76, 143.77, 148.50, 186.94 (C=O); IR Spectrum V_{max} (KBr)/cm^{-1} 1659 (C=O); Mass Spectrum (MALDI) m/z 259.09 (M^+, 100%); mp 152°C.

(*E*)-1-(3-Pyridyl)-3-(3'',4'',5''-trimethoxyphenyl)prop-2-en-1-one (DMU2114)

Synthetic Method 2; ^{1}H-NMR ($CDCl_3$) δ 3.92 (9H, s, OMe), 6.88 (2H, s, phenyl), 7.37 (1H, d, *J*=14.5Hz), 7.45 (1H, t, Py), 7.74 (1H, d, *J*=14.5Hz), 8.28 (1H, d, Py), 8.80 (1H, d, Py), 9.23 (1H, s, Py); ^{13}C-NMR ($CDCl_3$) δ 56.21, 60.93, 105.92, 120.75, 123.64, 129.82, 133.58, 135.83, 140.92, 146.09, 149.64, 153.01, 153.50, 189.03 (C=O); IR Spectrum V_{max} (KBr)/cm^{-1} 1662 (C=O); Mass Spectrum (MALDI) m/z 299.18 (M^+, 100%); mp 123-124°C.

(*E*)-1-(3-Pyridyl)-3-(2'',3'',4''-trimethoxyphenyl)prop-2-en-1-one (DMU2117)

Synthetic Method 2; ^{1}H-NMR ($CDCl_3$) δ 3.85 (3H, s, OMe), 3.93 (3H, s, OMe), 3.99 (3H, s, OMe), 6.73 (1H, d, phenyl), 7.39 (1H, d, phenyl), 7.43 (1H, t, Py), 7.52 (1H, d, *J*=15.2Hz), 8.03 (1H, d, *J*=15.2Hz), 8.27 (1H, d, Py), 8.79 (1H, d, Py), 9.22 (1H, s, Py); ^{13}C-NMR ($CDCl_3$) δ 55.85, 60.82, 61.34, 107.66, 120.52, 121.47, 123.53, 124.12, 133.83, 135.35, 141.30, 142.42, 149.63, 152.78, 153.93, 156.19, 189.34 (C=O); IR Spectrum V_{max} (KBr)/cm^{-1} 1658 (C=O); Mass Spectrum (MALDI) m/z 298.93 (M^+, 100%); mp 78-79°C.

(*E*)-1-(3-Pyridyl)-3-(phenyl)prop-2-en-1-one (DMU2118)

Synthetic Method 2; ^{1}H-NMR ($CDCl_3$) δ 7.35-7.45 (4H, m), 7.48 (1H, d, *J*=14.1Hz), 7.62 (2H, t, phenyl), 7.82 (1H, d, *J*=14.1Hz), 8.27 (1H), 8.79 (1H, d, Py), 9.24 (1H, s, Py); ^{13}C-NMR ($CDCl_3$) δ 121.37, 123.59, 128.57, 128.99, 130.92, 133.43, 134.41, 135.78, 145.84, 149.71, 153.09, 188.98 (C=O); IR Spectrum V_{max} (KBr)/cm^{-1} 1666 (C=O); Mass Spectrum (MALDI) m/z 209.76 (M^+, 100%); mp 79°C.

(*E*)-1,3-di(3-Pyridyl)prop-2-en-1-one (DMU2141)

Synthetic Method 2; ^{1}H-NMR (DMSO) δ 7.52 (1H, t), 7.63 (1H, t), 7.83 (1H, d, *J*=15.5Hz), 8.10 (1H, d, *J*=15.5Hz), 8.39 (1H, d), 8.49 (1H, d), 8.65 (1H, d), 8.86 (1H, d), 9.06 (1H, s), 9.37 (1H, s); ^{13}C-NMR (DMSO) δ 123.83, 124.42, 127.48, 131.51, 132.63, 133.73, 136.79, 145.25, 149.64, 150.00, 153.43, 155.11 189.78 (C=O); IR Spectrum V_{max} (KBr)/cm^{-1} 1666 (C=O); Mass Spectrum (MALDI) m/z 210.48 (M^+, 100%); mp 123-124°C.

(*E*)-1-(3,4-Methylenedioxyphenyl)-3-(4-pyridyl)prop-2-en-1-one (DMU2143)

Synthetic Method 2; ^{1}H-NMR ($CDCl_3$) δ 6.08 (2H, s, methylenedioxy), 6.90 (1H, d, benzyl), 7.45 (2H, d, Py), 7.51 (1H, s, benzyl), 7.57-7.70 (3H, m), 8.68 (2H, d, Py); ^{13}C-NMR ($CDCl_3$) δ 101.98, 107.97, 108.35, 121.92, 124.99, 125.81, 132.31, 140.87, 142.18, 148.47, 150.57, 152.16, 187.45 (C=O); IR Spectrum V_{max} (KBr)/cm^{-1} 1655 (C=O); Mass Spectrum (MALDI) m/z 253.27 (M^+, 100%); mp 114°C.

(*E*)-1-(4-Pyridyl)-3-(3,4-methylenedioxyphenyl)prop-2-en-1-one (DMU2144)

Synthetic Method 2; ^{1}H-NMR ($CDCl_3$) δ 6.03 (2H, s, methylenedioxy), 6.85 (1H, d,

benzyl), 7.09-7.18 (2H, m), 7.23 (1H, d, *J*=16.2Hz), 7.68-7.79 (3H, m), 8.80 (2H, d, Py); ^{13}C-NMR ($CDCl_3$) δ 101.76, 106.67, 108.73, 119.16, 121.42, 125.83, 128.78, 144.60, 146.57, 148.53, 150.48, 150.70, 189.55 (C=O); IR Spectrum V_{max} (KBr)/cm^{-1} 1655 (C=O); Mass Spectrum (MALDI) m/z 253.02 (M^+, 100%); mp 123°C.

(*E*)-1-(4-Pyridyl)-3-(3'',4'',5''-trimethoxyphenyl)prop-2-en-1-one (DMU2157)

Synthetic Method 2; ^{1}H-NMR ($CDCl_3$) δ 3.85 (6H, s, OMe), 3.90 (3H, s, OMe), 6.88 (2H, s, benzyl), 7.29 (1H, d, *J*=17.5Hz), 7.68-7.71 (3H, m), 8.83 (2H, d, Py); ^{13}C-NMR ($CDCl_3$) δ 51.21, 55.93, 100.99, 115.55, 116.43, 124.63, 136.11, 139.49, 141.92, 145.71, 148.51, 184.80 (C=O); IR Spectrum V_{max} (KBr)/cm^{-1} 1666 (C=O); Mass Spectrum (MALDI) m/z 299.46 (M^+, 100%); mp 110-111°C.

Summary of Structures

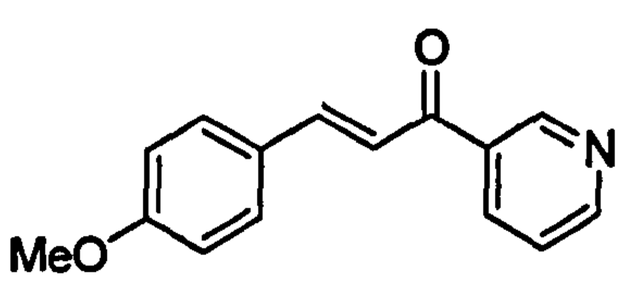

DMU729

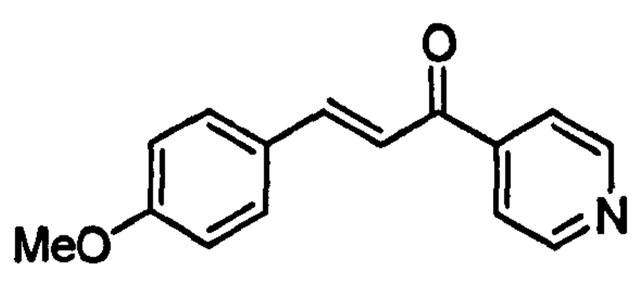

DMU730

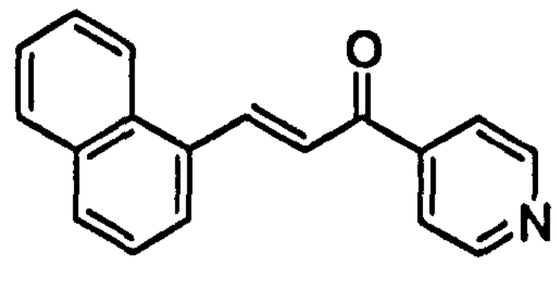

DMU755

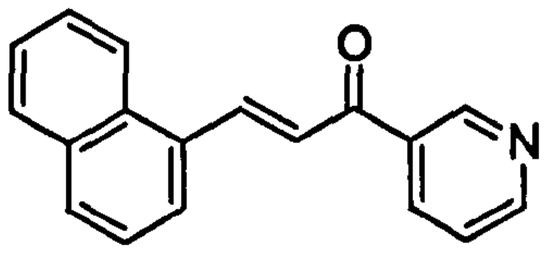

DMU756

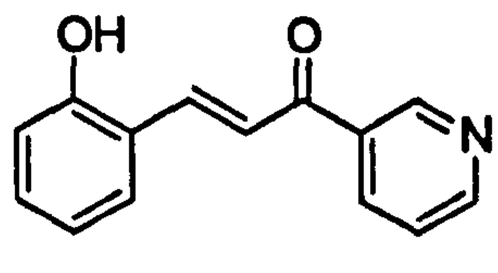

DMU766

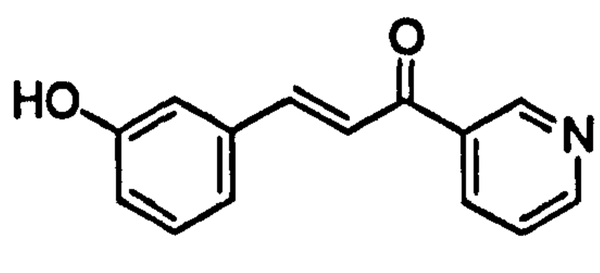

DMU767

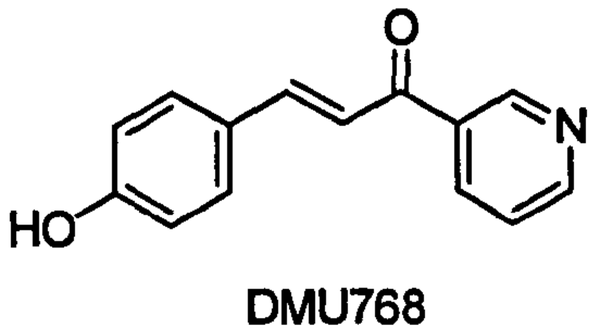

DMU768

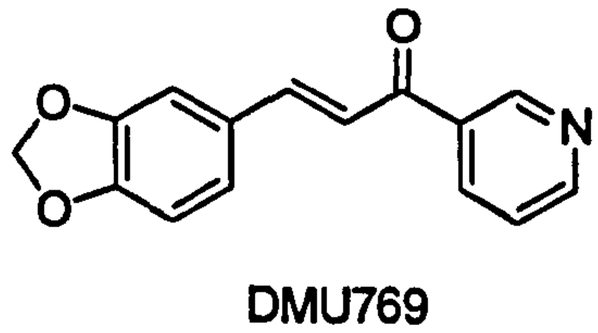

DMU769

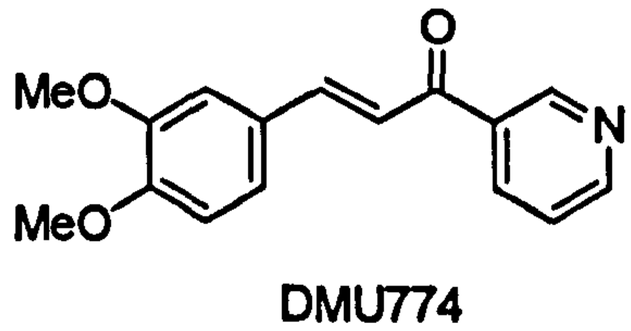

DMU774

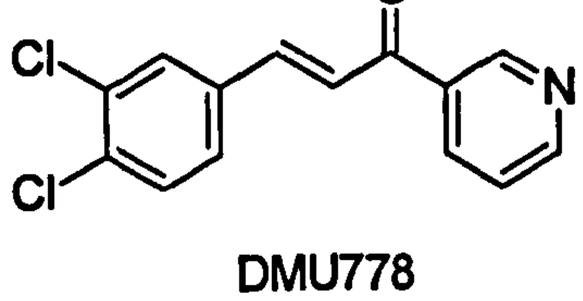

DMU778

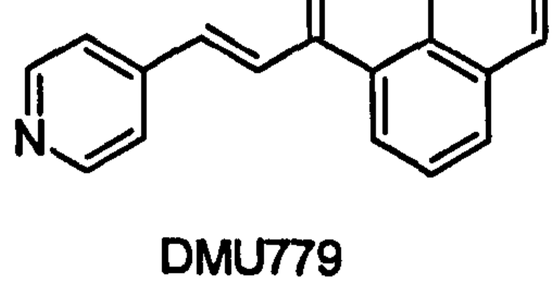

DMU779

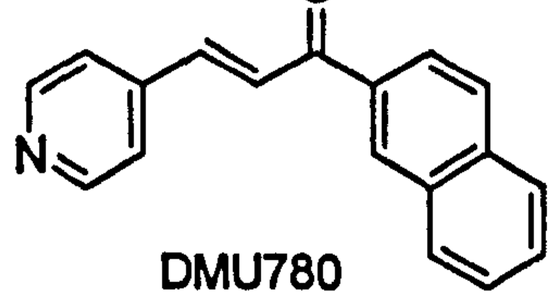

DMU780

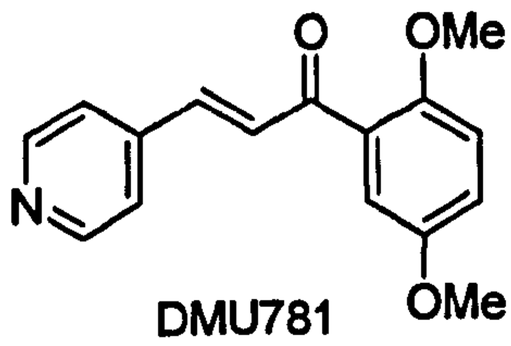

DMU781

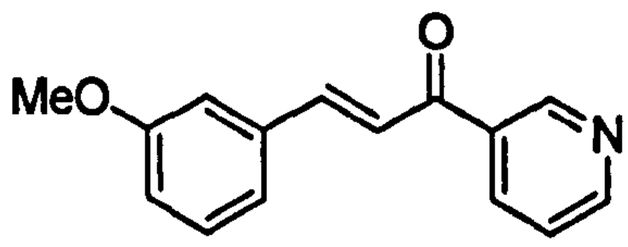

DMU789

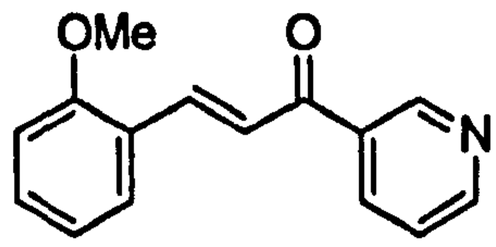

DMU790

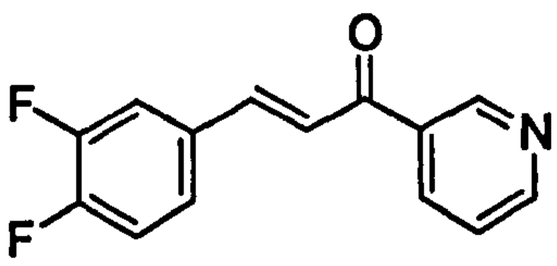

DMU2101

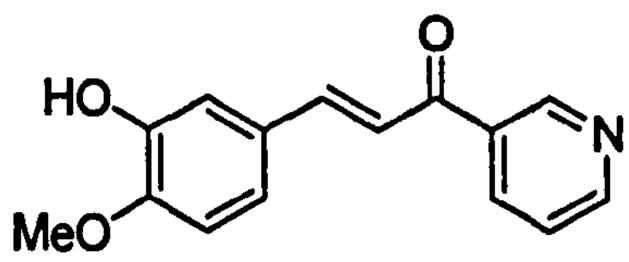

DMU2103

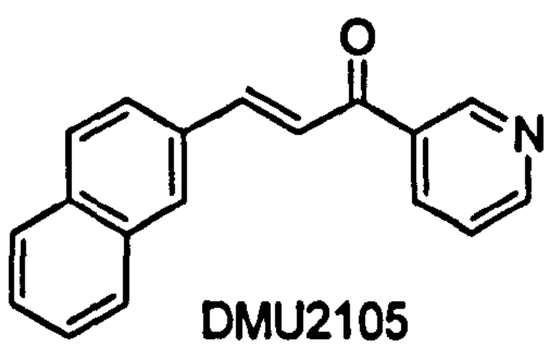

DMU2105

CYP1 enzyme inhibition by "reverse" 3- & 4-pyridyl chalcones

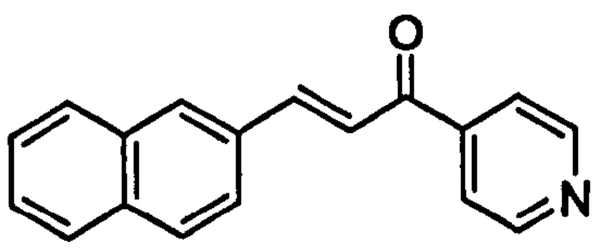

DMU2106

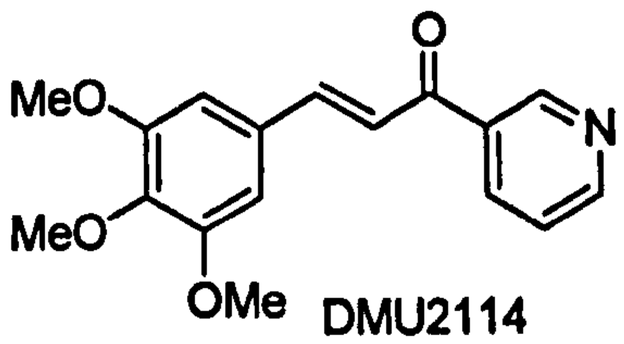

DMU2114

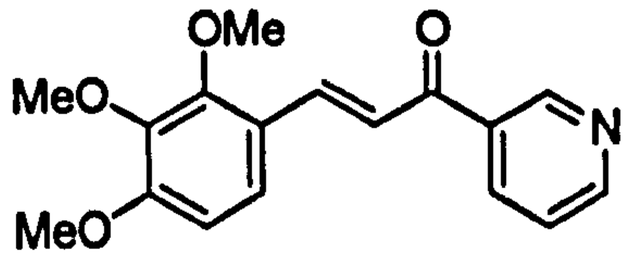

DMU2117

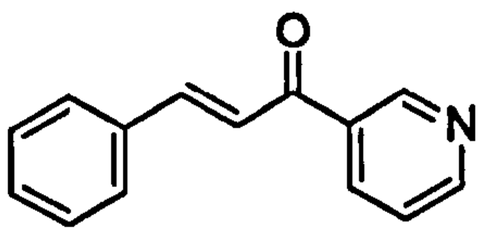

DMU2118

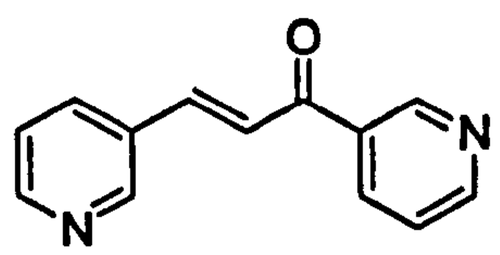

DMU2141

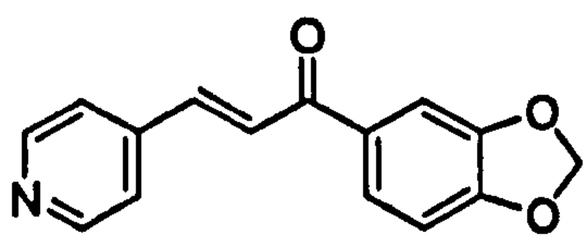

DMU2143

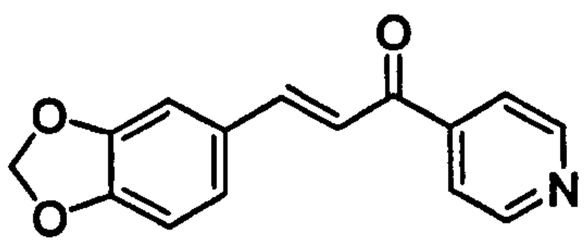

DMU2144

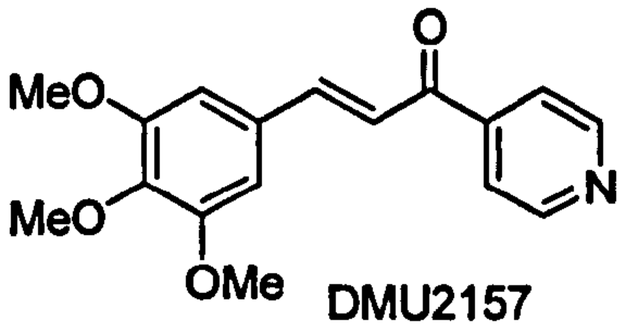

DMU2157

Chapter 5

The Intrinsic Toxicity of Heterocyclic Chalcones: Discovery of CYP1A1 Selective Anticancer Prodrugs

5.1 Introduction

Several inhibitors for each individual CYP1 enzymes have been described in previous chapters. The intrinsic toxicity of these inhibitors has to be determined, because any identified inhibitors would potentially apply to *in vitro* and *in vivo* testing of CYP1B1 and CYP1A1 activated anticancer prodrugs in order to validate the prodrugs efficacy. It is desirable to have a non-toxic inhibitor in the assay so that any cytotoxicity observed can only be caused by the prodrug but not by the inhibitor.

The intrinsic toxicity of the inhibitors was assayed using the *in vitro* MTT-cytotoxicity test described by Park *et. al.*[165] (MTT = 3-(4,5-dimethylthiazol-2-yl)-2,5-diphenyl tetrazolium bromide). The human breast cell line MCF10A was used in the MTT-assay for the measurement of inhibitors intrinsic toxicity. MCF10A was used because this cell line contains very small amount of P450 enzymes. MCF10A has been shown to express *CYP2C*, *CYP3A4* and *CYP2D6* mRNA[166,167] however, analysis of CYP protein only consistently showed the presence of the CYP2C family[168,169]. There was no DMU212 3'-hydroxylase activity in the MCF10A breast cell line, indicating the absence of CYP1 enzymes[139]. The use of cell line with minimal P450 level is crucial for assessing the intrinsic toxicity of inhibitors. This is because the non-heterocyclic part of the inhibitors can be potentially metabolised by CYP enzymes. This may drastically change the intrinsic toxicity of the inhibitors and lead to erroneous conclusions.

In addition to the intrinsic toxicity measurement, it was also of interest to assess if the compounds could undergo metabolic bioactivation by CYPs and hence act as potential prodrugs. Although inhibitors are unlikely to be activated by the enzyme they inhibit, it was deemed worthwhile to evaluate if any of these compounds could function as substrates. The reason for this is that the bioactivation of these compounds, if any

detected, could provide leads into developing novel CYP1A1/CYP1B1 bioactivated prodrugs. In other words, these inhibitors were screened in case they may possibly be activated by the target enzymes they inhibit.

Two human breast cancer cell lines were used for the bioactivation screening. The MCF7 induced with 10nM 2,3,7,8-tetrachlorodibenzo-*p*-dioxin (TCDD) 24 hours prior to experiment was used to demonstrate CYP1A1 bioactivation whilst the multi-drug resistant MDA-MB-468 (MDA468) cell line was used to illustrate CYP1A1/CYP1B1 activation. The CYP1A1 and CYP1B1 content in both cell lines have been elucidated by Wilsher in the study of the cis-stilbene prodrug DMU213[139]. In this study Whilser demonstrated that conversion of DMU213 to DMU215 and CM3 was exclusively catalysed by CYP1A1 and CYP1B1, respectively, in individual CYP metabolism assay. The author has shown that the level of DMU215 detected after incubation of DMU213 with TCDD pre-treated MCF7 was 20-fold higher than that of MDA468, which in turn 20-fold higher than naïve MCF7 cells. The CYP1B1 specific metabolite CM3 was only detected in MDA468 cells. These data indicated that there is only basal level of CYP1A1 in the MCF7 cell. Pre-treatment of MCF7 with 10nM TCDD induced the expression of CYP1A1 but not CYP1B1, given that the CYP1B1 specific metabolite of DMU213 was not detected. The induction of CYP1A1 in MCF7 treated cell is corroborated by studies reported elsewhere[170,171]. The induction of CYP1B1 in TCDD pre-treated MCF7 has been reported[172]. However, CYP1B1 activity was not detected in Wilsher's study. Since CM3 was only detectable in MDA468, this provides evidence that CYP1B1 is constitutively expressed by this cell line.

The MTT-assay with MCF10A provides the intrinsic toxicity of the inhibitor whilst TCDD induced MCF7 only indicates bioactivation by CYP1A1. The MDA468 MTT-

screening provides an assay to indicate bioactivation by CYP1A1/CYP1B1. The comparison of the recorded IC_{50} values of induced and naïve MCF7 cells provides the activation factor (AF; calculated as $IC_{50\ (naive\ MCF7)}$/ $IC_{50\ (Induced\ MCF7)}$) caused by CYP1A1. The data from MCF10A and MDA468 provide the tumour selective factor (TS) calculated as $IC_{50\ (MCF10A)}$/ $IC_{50\ (MDA468)}$. The selective CYP1B1 bioactivation of inhibitors can be elucidated by comparing data from induced MCF7 and MDA468 MTT-assay.

5.2 Experimental

5.2.1 Materials and method for the MTT-cytotoxic assay

All human breast cell lines were obtained from the American Type Culture Collection.

MCF7 cells were grown in RPMI 1640 with phenol red whereas MDA468 was grown in the same medium without phenol red. MCF10A was grown in DMEM:HAM's F-12 with 10 μg/mL insulin, 500 ng/mL water soluble hydrocortisone and 20 ng/mL epidermal growth factor. All media were supplemented with 10% v/v heat inactivated foetal calf serum (heated to 56°C for 45 minutes to inactivate complement). Cells were maintained at 37°C, 5% CO_2 in air with 100% humidity and passaged at sub-confluence using trypsin-EDTA (0.5% and 0.2% w/v, respectively). No antibiotics were used in any assay.

To harvest adhered cells for experiments, the medium was aspirated and 1mL of a 1% trypsin-EDTA solution was added to the cells and gently agitated for 30 seconds. Following removal of the trypsin-EDTA solution, a further 0.5-1.0mL of the solution

was added and the cells incubated at 37°C for 5 (MCF7 and MDA468) or 15 minutes (MCF10A). The resultant cell suspension was placed in a sterile container with 10mL of fresh medium. To determine the density of the cell suspension, an aliquot (100μL) was added to 100μL of a trypan blue solution (0.4% w/v) and the number of cells determined using a haemocytometer.

The cell suspension was diluted with medium to give 2 X 10^3 cells per 100μL medium per well of 96-well flat-bottomed plates (Nunc 96-well microtitre plate, Fisher Scientific). After 4 hours to allow adherence, 100μL of medium containing TCDD (2,3,7,8-tetrachlorodibenzo-*p*-dioxin, from 100μM stock in DMSO; custom prepared) or medium with 0.2% v/v DMSO as control was added to each well to give a final concentration of 10nM TCDD (0.1% v/v DMSO), for 24 hours to allow CYP1A1/CYP1B1 expression in MCF7 cells. The medium was then carefully aspirated and 100μL fresh medium added. Within 30 minutes compound was added in quadruplicate in 100μL medium at double the final concentration from 100mM stock in DMSO to give a final concentration of not more than 0.1% v/v DMSO, or DMSO solvent alone at 0.1% v/v as control. The cells were then allowed to grow on for 96 hours to give 80-90% confluence in the control wells after which 50μL MTT (3-(4,5-dimethylthiazol-2-yl)-2,5-diphenyl tetrazolium bromide) at 2mg/mL in RPMI 1640 without phenol red was added to each well for 1.5 hours. All medium was aspirated and the formazan product generated by viable cells was solubilized with 150μL DMSO. Plates were vortexed and the absorbance at 540nm determined using a plate reader. Maintenance of cell cultures and preparation of microtitre plates for cytotoxic studies was performed by Paul Butler, Cancer Drug Discovery Group.

5.2.2 Materials and methods for the microsomal incubation and HPLC analysis of DMU2123 and DMU2127

Materials

Cytochrome P450 CYP1A1, CYP1A2, CYP1B1, CYP2D6, CYP3A4, CYP3A5 were prepared from insect cells transformed using a baculovirus vector expressing human Cytochrome P450 with co-expression of human NADPH-cytochrome P450 reductase (Supersomes^{TM}) were obtained from Gentest Corporation, USA via Cambridge Biosciences, UK. Control microsomes prepared from insect cells treated with the only vector plasmid were also obtained from Gentest Corporation, USA. β-Nicotinamide adenine dinucleotide phosphate reduced form (NADPH), was obtained from Sigma Chemical Co. HPLC grade acetonitrile, methanol, water, dimethylsulfoxide (DMSO), general reagent grade sodium hydroxide (NaOH), hydrochloric acid (HCl) microcentrifuge tube, and propylene microtitre plates were obtained from Fisher Scientific. Magnesium chloride ($MgCl_2 \cdot 6H_20$), potassium chloride (KCl), anhydrous disodium hydrogen orthophosphate (Na_2HPO_4) and anhydrous potassium dihydrogen orthophosphate (KH_2PO_4) were obtained from BDH. HPLC analytical columns were supplied by Phenomenex.

HPLC analytical method for DMU2123 and DMU2127

Separation of DMU2123 was achieved by using the following analytical conditions: Phenomenex Luna 5µm Phenyl-Hexyl (250×4.60mm) analytical column at 30°C, UV detector using wavelengths of 304nm. The mobile phase consisted of 60% solvent A (10mM ammonium acetate in water) and 40% solvent B (5% propanol in acetonitrile). A linear gradient was initiated immediately on the start of analysis with solvent B rising

to 70% over 10 minutes and held at 90% for 1 minute before returning to the initial conditions (using a flow rate of 1mL/min). A re-equilibrium time of 8 minutes was allowed between each sample analysis. The retention time of DMU2123 is 10.59 minutes. For DMU2127, the analytical conditions is almost the same as for DMU2123, except for the wavelengths used to detect the DMU2127 is 303nm. The retention time of DMU2127 is 11.08 minutes.

Quantitation of DMU2123 and DMU2127

To quantify DMU2123, as well as DMU2127, the denatured, pooled microsomes were spiked with authentic standard DMU2123 solution in DMSO (100μM) to give a final calibration concentration of 1, 2, 3, 4, 5, 6, 7, 8, 9, 10μM, then the calibration standards were treated exactly the same with incubated samples before analysed by HPLC. Calibration curves were linear in the concentration ranges used with correlation coefficients of >0.995.

Microsomal Incubations

The compound was incubated with Supersomes™ and control insect microsomes under the following conditions: compound (10μM), CYP (20pmol.mL^{-1}), NADPH (0.5mM), and $MgCl_2$ (0.5mM) in Pi-buffer (10mM) at 37°C in a humidified incubator. Samples (100μL) were taken at 0, 5, 10, 15, 20, 25min.

Sample preparation

The enzymatic reaction in the sample terminated immediately by addition of an equal volume of ice-cold solvent B (5% v/v propanol in acetonitrile). Following

centrifugation (13000rpm, 4min, 4°C), the supernatants were removed, placed in glass HPLC vials and analysed by HPLC. All samples have been done in duplicate.

The microsomal incubation and HPLC analysis of the disappearance of DMU2123 and DMU2127 was performed by Somchaiya Surichan, Cancer Drug Discovery Group.

5.2.3 Data analysis

Analytical data were collected and the chromatograms of the analysis were plotted using Borwin HPLC software. Data collected from MTT-assay was processed by Prism, version 4.02 (GraphPad Software Inc.). A dose-response curve was constructed and the IC_{50} value was obtained manually from the curve. This was necessary because the calculated IC_{50} value from Prism, using non-linear regression curve fit, was often inaccurate.

5.3 Results

All inhibitors synthesised have been screened for their intrinsic toxicity and potential bioactivation using the MTT-cytotoxic assay employing three human breast cell lines, namely MCF10A, MCF7 and MDA468. Table 27 shows the MTT-assay results for the initial six inhibitors designed to probe CYP1 enzymes active site (discussed in Chapter 2). DMU721 and DMU722 have shown a very low intrinsic toxicity with IC_{50} values for MCF10A of 20μM and 50μM, respectively. The more CYP1A1 selective inhibitors DMU709 and DMU710 were relatively toxic to MCF10A breast cell line. This may

impair the potential of these inhibitors for cell based *in vitro* and *in vivo* assay. DMU724 was bioactivated in the MDA468 cell line (IC_{50} 0.1μM) with a tumour selective factor (TS) of 50.

Table 28: Cytotoxicity of heterocyclic chalcone inhibitors

	IC_{50} (μM)					
Inhibitors	MCF7	$MCF7^+$	MCF10A	MDA468	AF	TS
DMU709	1.8	2	1.7	0.8	0.9	2.1
DMU710	1.4	1.4	1.5	1.4	1.0	1.1
DMU720	6	6	7	2	1.0	3.5
DMU721	20	26	20	25	0.8	0.8
DMU722	50	50	50	15	1.0	3.3
DMU724	3	2	5	0.1	1.5	50.0

Note: $MCF7^+$ = MCF7 pre-treated with TCDD; AF = activation factor (**IC_{50} MCF7 / IC_{50} $MCF7^+$**); TS = tumour selective factor (**IC_{50} MCF10A / IC_{50} MDA468**).

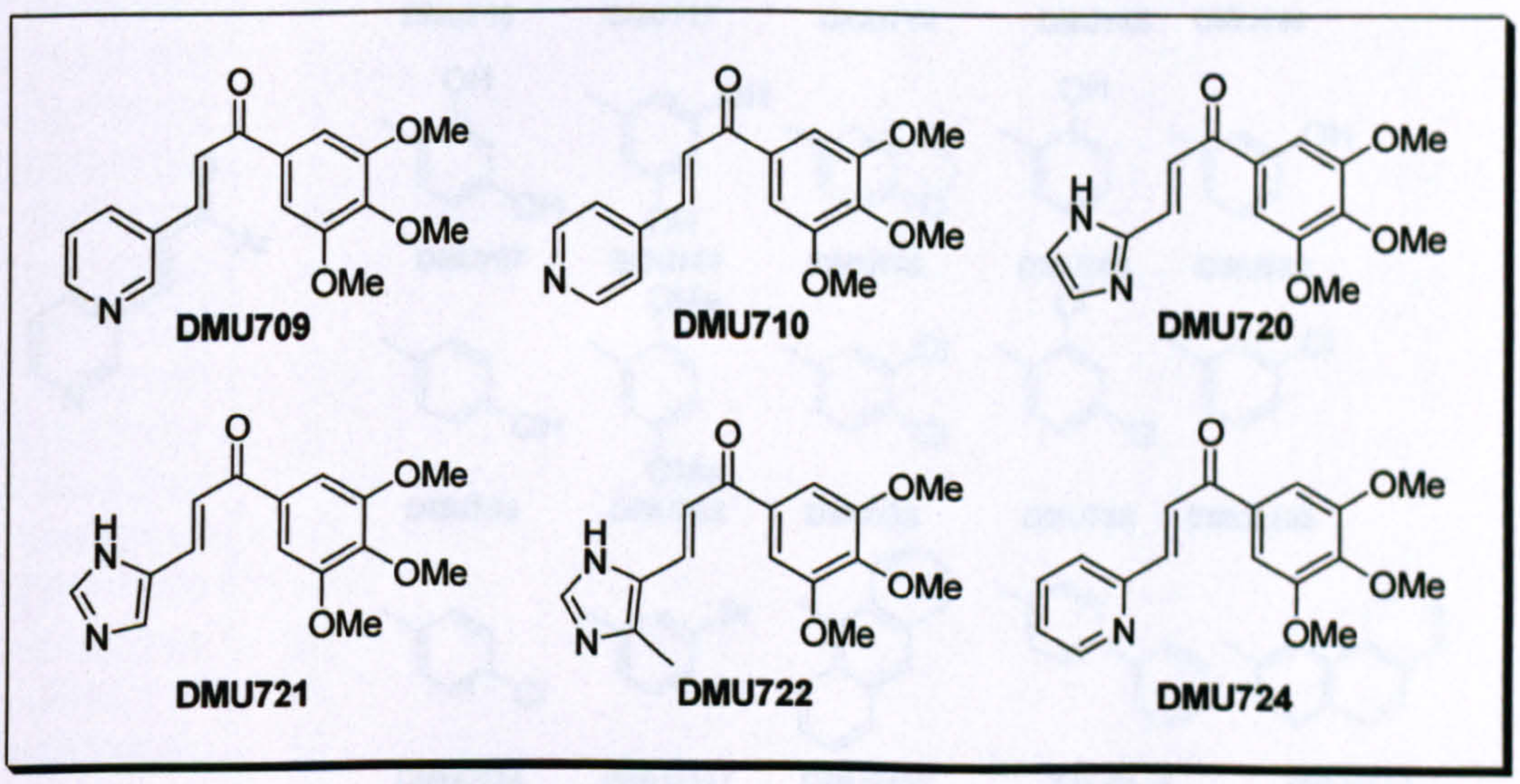

Figure 65: Chemical structure of heterocyclic chalcones listed in Table 28

There are some interesting data collected from MTT-screening on the 3-pyridyl chalcones discussed in Chapter 3. DMU711 and DMU717 have been shown to be

activated by CYP1A1 but CYP1B1 deactivated these two compounds. Several compounds, such as DMU712, DMU713, DMU714, DMU718 and DMU2140 have shown deactivation by CYP1B1. There is clear evidence to indicate bioactivation of the triaryl compounds DMU2154 and DMU2156 by CYP1A1. DMU2123 and DMU2127 are potential CYP1A1 activated anticancer prodrugs with 125- and 300-fold tumour selective factor, respectively. An initial DMPK studies have been performed on these two compounds and will be discussed later in this chapter.

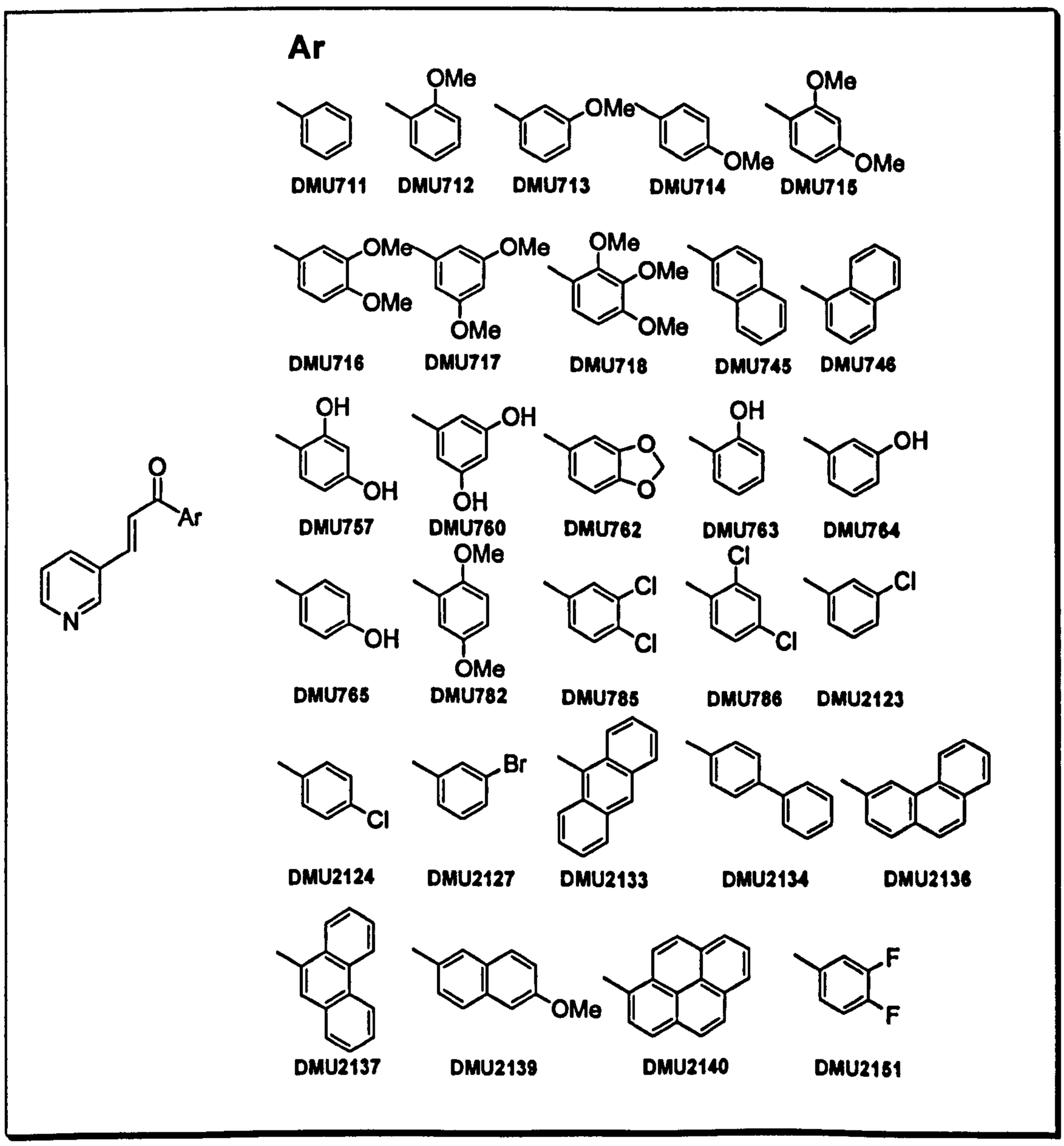

Figure 66: ***Chemical structure of 3-pyridyl chalcones listed in Table 29***

Table 29: Cytotoxicity of 3-pyridyl chalcones and other heterocyclic compounds discussed in Chapter 3

	IC_{50} (µM)					
Inhibitors	MCF7	$MCF7^+$	MCF10A	MDA468	AF	TS
DMU711	5	0.6	6	11	8.3	0.5
DMU712	2.5	1.5	4	7	1.7	0.6
DMU713	3	2	4	10	1.5	0.4
DMU714	4	3	5	11	1.3	0.5
DMU715	4	3	5	5	1.3	1.0
DMU716	4	3	4	8	1.3	0.5
DMU717	0.9	0.4	3	8	2.3	0.4
DMU718	5	3	5	9	1.7	0.6
DMU744	>100	30	60	20	>3.0	3.0
DMU745	5	5	2	1	1.0	2.0
DMU746	4	4	2	0.5	1.0	4.0
DMU757	5	4	3	1	1.3	3.0
DMU760	NT	NT	NT	NT	nd	nd
DMU762	2	1.5	7	1	1.3	7.0
DMU763	20	10	16	8	2.0	2.0
DMU764	1.5	0.8	5	2	1.9	2.5
DMU765	90	>100	NT	40	deactivating	activating
DMU782	2	0.7	2	0.3	2.9	6.7
DMU785	6	4	2	0.6	1.5	3.3
DMU786	3	2	4	2	1.5	2.0
DMU2120	9	9	15	6	1.0	2.5
DMU2123	6	0.4	5	0.04	15.0	125.0
DMU2124	4	2	45	5	2.0	9.0
DMU2127	2	0.03	6	0.02	66.7	300.0
DMU2133	5	3	4	0.4	1.7	10.0
DMU2134	7	7	6	4	1.0	1.5
DMU2136	7	7	3	2	1.0	1.5
DMU2137	5	5	3	1	1.0	3.0
DMU2139	7	6	5	3	1.2	1.7
DMU2140	1	1	1	4	1.0	0.3
DMU2151	4	3	6	4	1.3	1.5
DMU2154	30	4	NT	7	7.5	nd
DMU2155	NT	NT	NT	NT	nd	nd
DMU2156	15	0.6	NT	3	25.0	nd

Note: NT = non toxic; nd = not determined; $MCF7^+$ = induced MCF7.

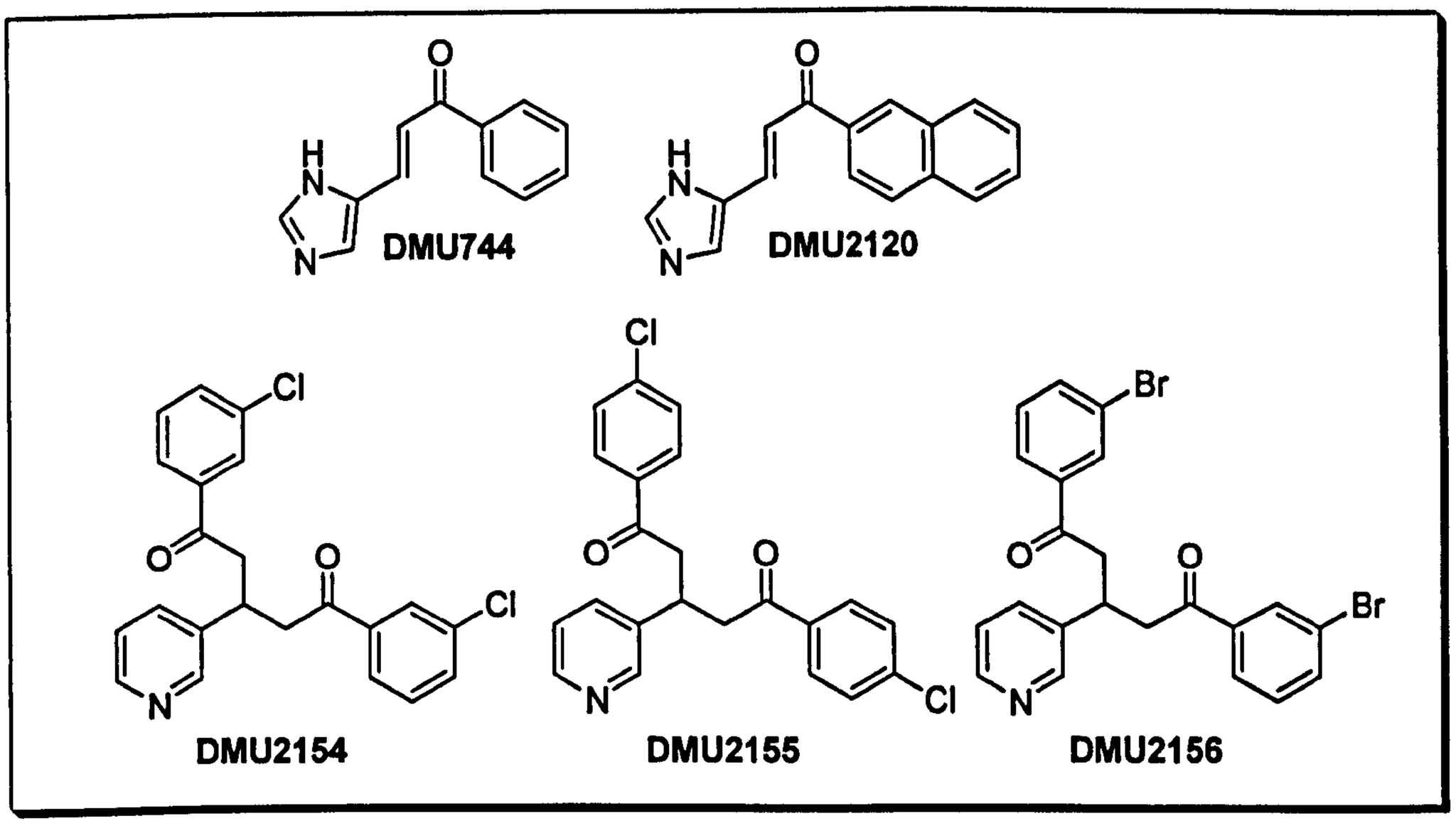

Figure 67: Chemical structure of other heterocyclic compounds listed in Table 29

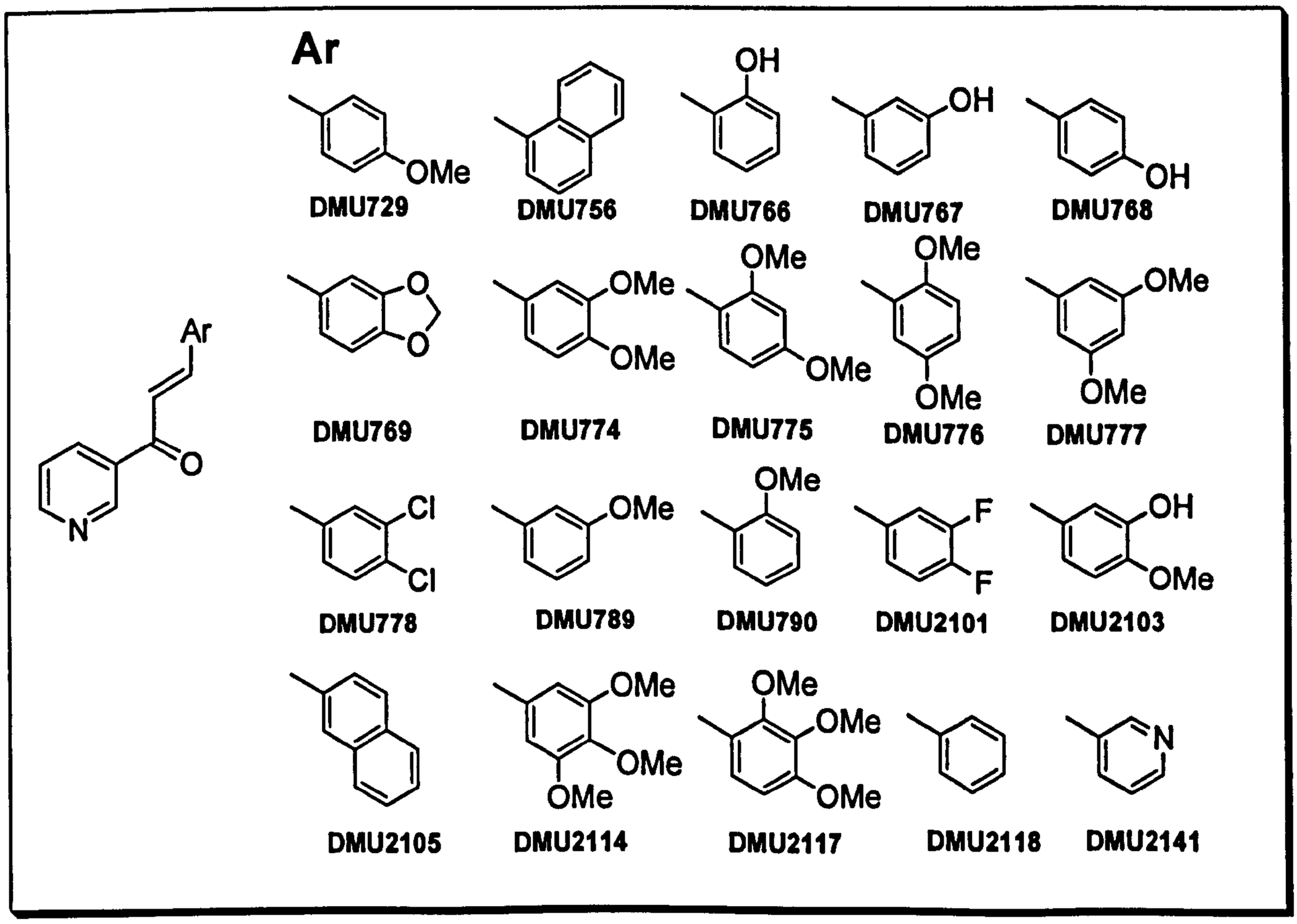

Figure 68: Chemical structure of reverse 3-pyridyl chalcones and the di-3-pyridyl chalcone DMU2141

In the reverse 3-pyridyl series (see Figure 68), CYP1B1 bioactivated DMU729, DMU778 and DMU2103 with recorded IC_{50} values of 5μM, 4μM and 4μM, respectively (MTT-assay with MDA468). DMU769 is a more selective substrate for CYP1A1 (Table 30)

Table 30: Intrinsic cytotoxicity of reverse 3-pyridyl chalcones and DMU2141

	IC_{50} (μM)					
Inhibitors	MCF7	MCF7$^+$	MCF10A	MDA468	AF	TS
DMU729	21	20	20	5	1.1	4.0
DMU756	10	8	7	4	1.3	1.8
DMU766	2.5	0.9	7	2	2.8	3.5
DMU767	7	6	10	2	1.2	5.0
DMU768	27	25	15	6	1.1	2.5
DMU769	10	6	25	5	1.7	5.0
DMU774	11	11	20	8	1.0	2.5
DMU775	9	8	25	5	1.1	5.0
DMU776	6	6	12	3.5	1.0	3.4
DMU777	2	0.5	4	2.5	4.0	1.6
DMU778	23	23	20	4	1.0	5.0
DMU789	6	4	7	20	1.5	0.4
DMU790	6	4	10	3	1.5	3.3
DMU2101	10	6	4	4	1.7	1.0
DMU2103	25	15	25	4	1.7	6.3
DMU2105	6	5	4	3	1.2	1.3
DMU2114	5	3	7	4	1.7	1.8
DMU2117	10	7	15	18	1.4	0.8
DMU2118	6	1.5	12	6	4.0	2.0
DMU2141	6	4	14	4.5	1.5	3.1

The intrinsic toxicity and bioactivation data for the 4-pyridyl and reverse 4 pyridyl chalcones is tabulated in Table 31. The CYP1A1 inhibitor DMU2157 undergoes metabolic activation by the same P450 the compound tries to inhibit. DMU779, DMU2106 and DMU2144 are all deactivated by CYP1A1.

Table 31: Intrinsic toxicity of 4-pyridyl and reverse 4-pyridyl analogues

	IC_{50} (μM)					
Inhibitors	MCF7	MCF7$^+$	MCF10A	MDA468	AF	TS
DMU730	29	16	20	5.5	1.8	3.6
DMU755	8	5	4	3	1.6	1.3
DMU779	3	2.5	0.8	0.6	1.2	1.3
DMU780	3	3.5	2	1.5	0.9	1.3
DMU781	1.2	0.6	0.8	0.3	2.0	2.7
DMU2106	12	12	6	4	1.0	1.5
DMU2143	6	4	5	2	1.5	2.5
DMU2144	19	19	9	5	1.0	1.8
DMU2157	7	4	15	5	1.8	3.0

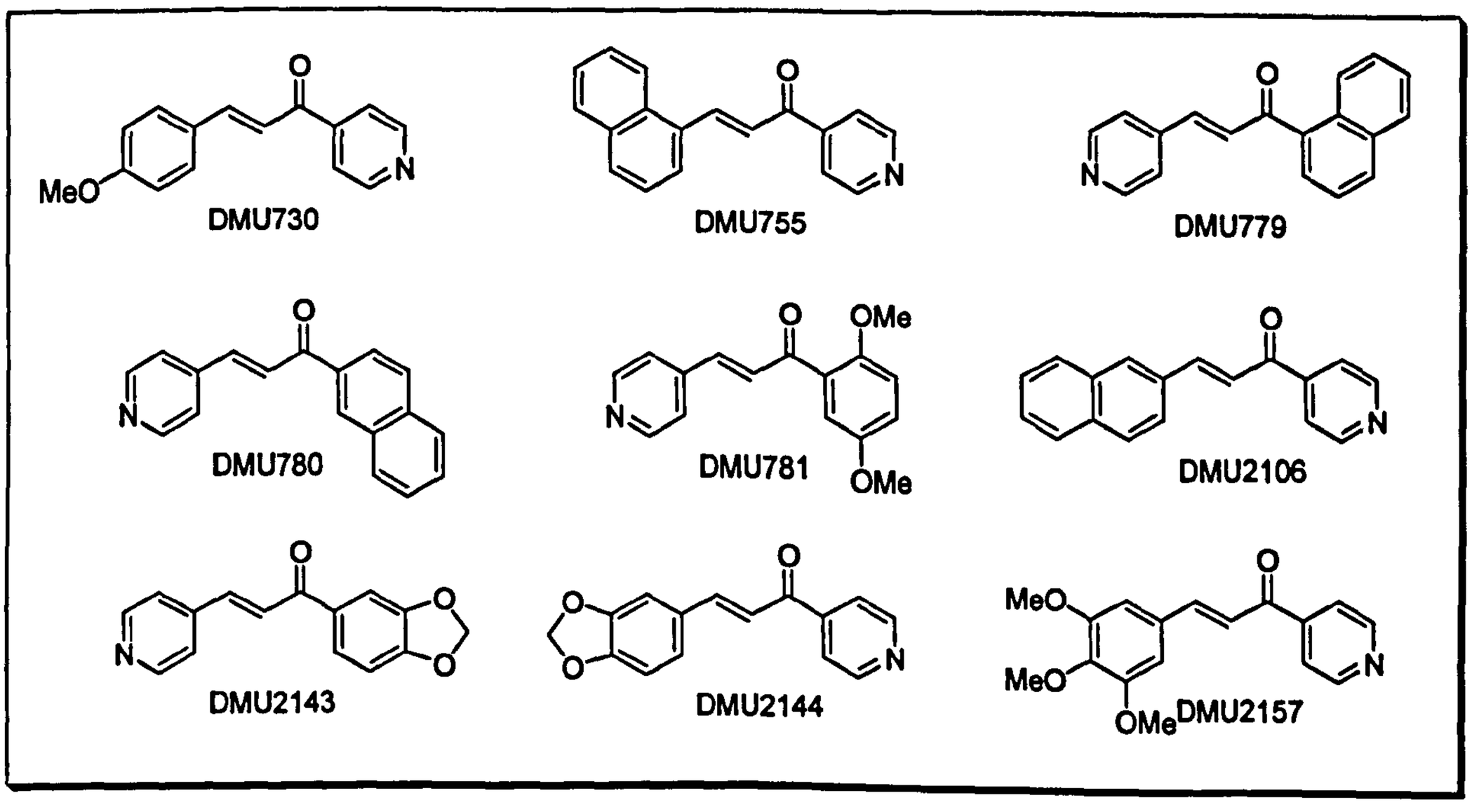

Figure 69: Chemical structures of 4-pyridyl and reverse 4-pyridyl chaolcones listed in Table 31

5.4 Discussion

Amongst the inhibitors listed in Table 28, DMU724 showed a 50-fold selectivity towards the MDA468 human breast cancer model in the MTT-cytotoxic assay. There was no apparent difference observed in cytotoxic IC_{50} values between the MCF10A and MCF7 cell lines (IC_{50} 5μM and 3μM). The IC_{50} for induced MCF7 was 2μM. No differences in toxicity were observed in MCF10A and MCF7 but the induced MCF7 cell IC_{50} value was higher than the MDA468, indicated that bioactivation of DMU724 in MDA468 was probably mediated by CYP1B1. However, the EROD results contradict this suggestion, since DMU724 is very weak inhibitor of CYP1B1. The exact mechanism of bioactivation is unknown but probably due to 3'-demethylation of the B-ring of DMU724. The hydroxyl group of demethylated product may inhibit tyrosine kinases by mimicking the tyrosine residue. Further work is required to elucidate the mechanism of bioactivation of this compound but it is outside the scope of this project.

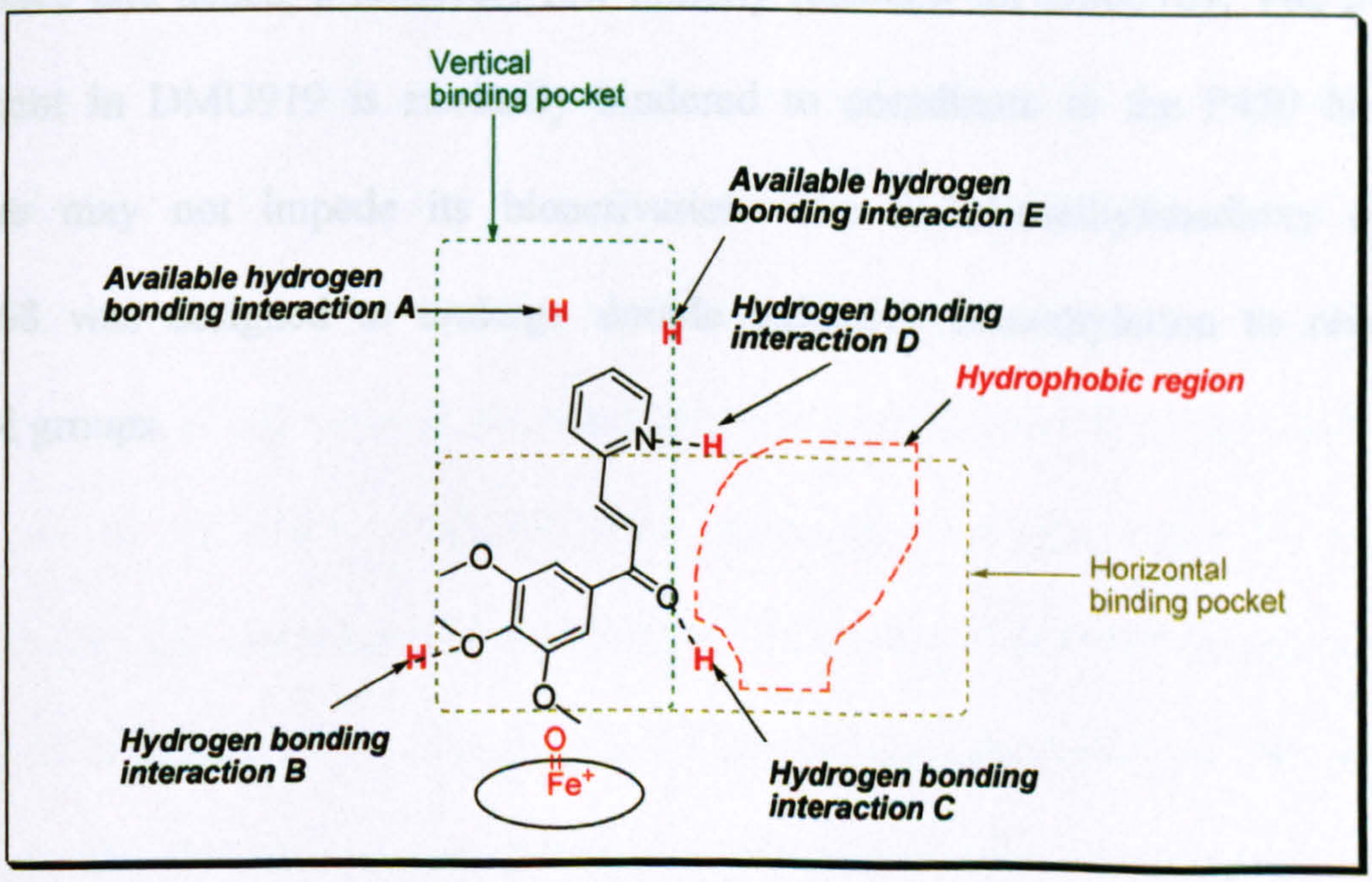

Figure 70: ***Mapping of DMU724 into CYP1B1 pharmacophore ready for 3'-demethylation***

Based on the observations that the 3,4-methylenedioxy 3-pyridyl chalcone and its reverse 3-pyridyl analogue (DMU762 and DMU769, respectively) have tumour selective factor of 5 and above, three 3,4-methylenedioxy compounds were made as potential CYP1 activated prodrugs (see Figure 71). DMU918 is an analogue of DMU724. It is hope that by oxidative demethylation of the methylenedioxyphenyl group, the catechol metabolite of DMU918 would be much more toxic than the proposed metabolite of DMU724. The catechol group is widely known to possess anti tyrosine kinase activities and it may undergo redox cycling to generate reactive oxygen species and quinone. The reactive oxygen species and quinone can cause DNA damage and lead to cell death.

DMU919 is the 2-pyridyl analogue of the 3-pyridyl DMU769. DMU769 is probably bioactivated by CYP1A1 since there is no difference in IC_{50} values between the induced MCF7 and MDA468 cell lines. The 3-pyridyl moiety in DMU769 can inhibit the enzyme that bioactivate the compound and therefore only some degree of activation takes place and hence, a relatively low toxicity recorded for DMU769. The 2-pyridyl substituent in DMU919 is sterically hindered to coordinate to the P450 haem and therefore may not impede its bioactivation. The di-3,4-methylenedioxy chalcone DMU968 was designed to undergo double oxidative demethylation to reveal two catechol groups.

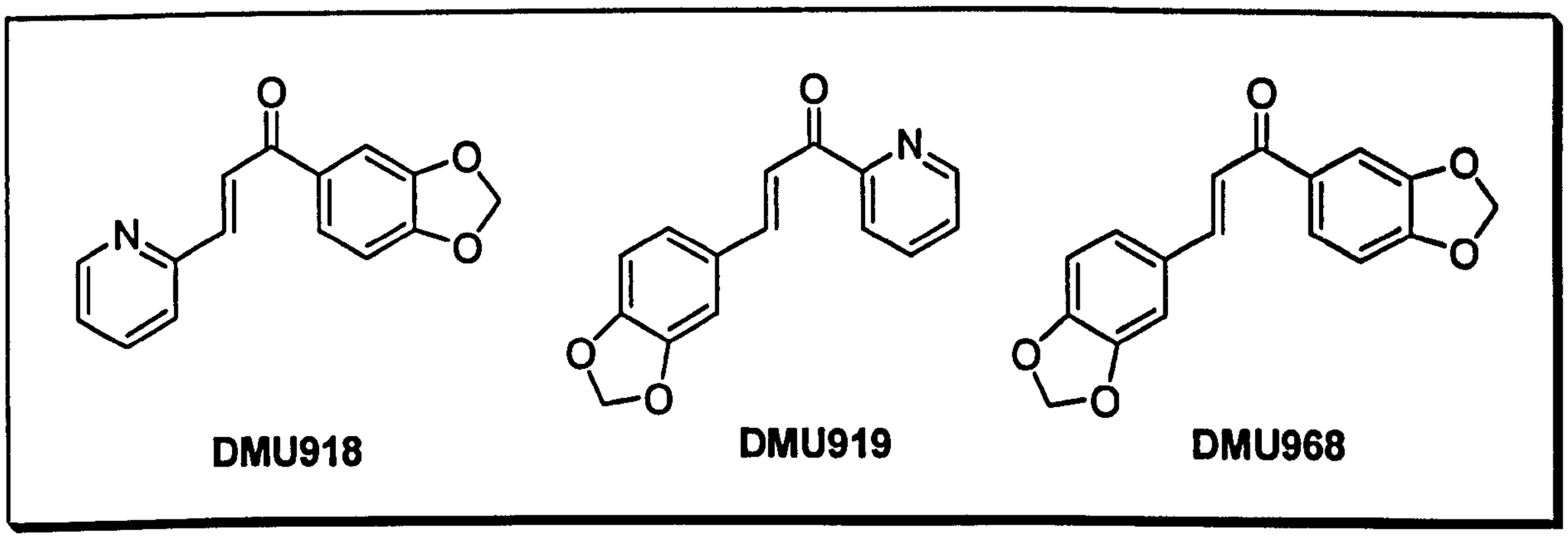

Figure 71: Chemical structure of DMU918, DMU919 and DMU968

Table 32: CYP1 enzymes inhibition and cytotoxicity of DMU918, DMU919 and DMU968

	IC_{50} (μM)						
Inhibitor	CYP1A1	CYP1A2	CYP1B1	MCF7	MCF7^{+}	MCF10A	MDA468
DMU918	5	50	7	5	2	5	0.8
DMU919	1	100	9	25	15	20	60
DMU968	2.5	NI	NI	30	30	25	17

Note: NI = no inhibition; MCF7^{+} = induced MCF7.

The reduction in IC_{50} value comparing naïve and induced MCF7 as well as MCF10A and MDA468 revealed that DMU918 was bioactivated by CYP1A1 however, DMU918 metabolite may not have the structural requirements to mediate cytotoxicity. There was no apparent difference between the recorded toxicity of DMU919 in naïve and induced MCF7 so as MCF10A. DMU919 was deactivated in the MDA468 cell line. Unfortunately, the mechanism of deactivation is unknown. DMU968 are relatively non-toxic in all cell lines tested. DMU968 is a CYP1A1 selective inhibitor with an IC_{50} of 2.5μM. In the EROD assay DMU968 did not inhibit either CYP1A2 or CYP1B1. Combining its low toxicity in normal and tumour cells and its selectivity for CYP1A1,

DMU968 may be a potential specific CYP1A1 inhibitor for *in vitro* and *in vivo* assay.

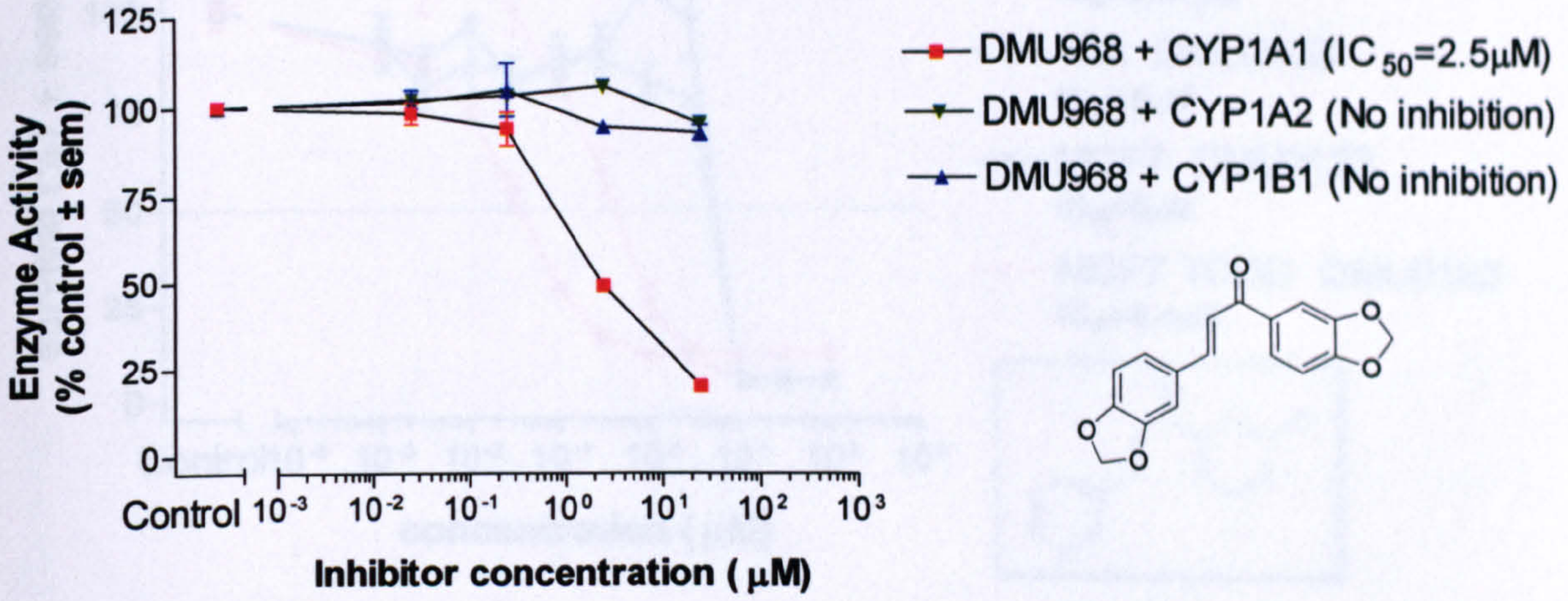

Figure 72: DMU968: A highly selective inhibitor of CYP1A1

DMU2123 and DMU2127 are activated by both the induced MCF7 and MDA468 cell lines to highly cytotoxic species (Figure 73). The MTT-assay results provide the evidence that both DMU2123 and DMU2127 can be bioactivated by CYP1A1 and/or CYP1B1. In order to confirm bioactivation of these potential anticancer agents is CYP1 mediated, the MTT-cytotoxicity assays have been repeated with co-incubation of CYP1 enzyme inhibitors acacetin or α-naphthaflavone[173,174] at 1μM.

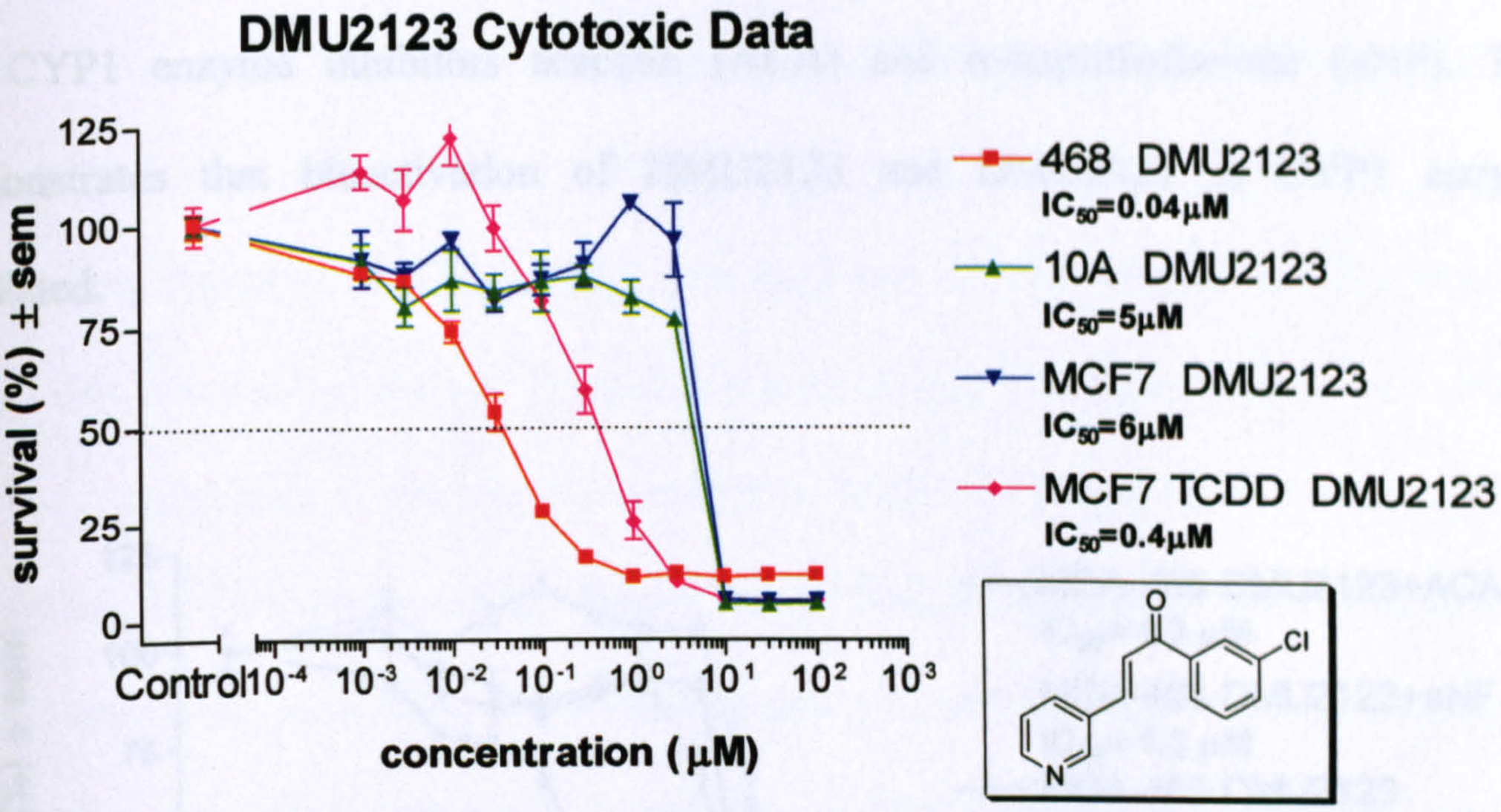

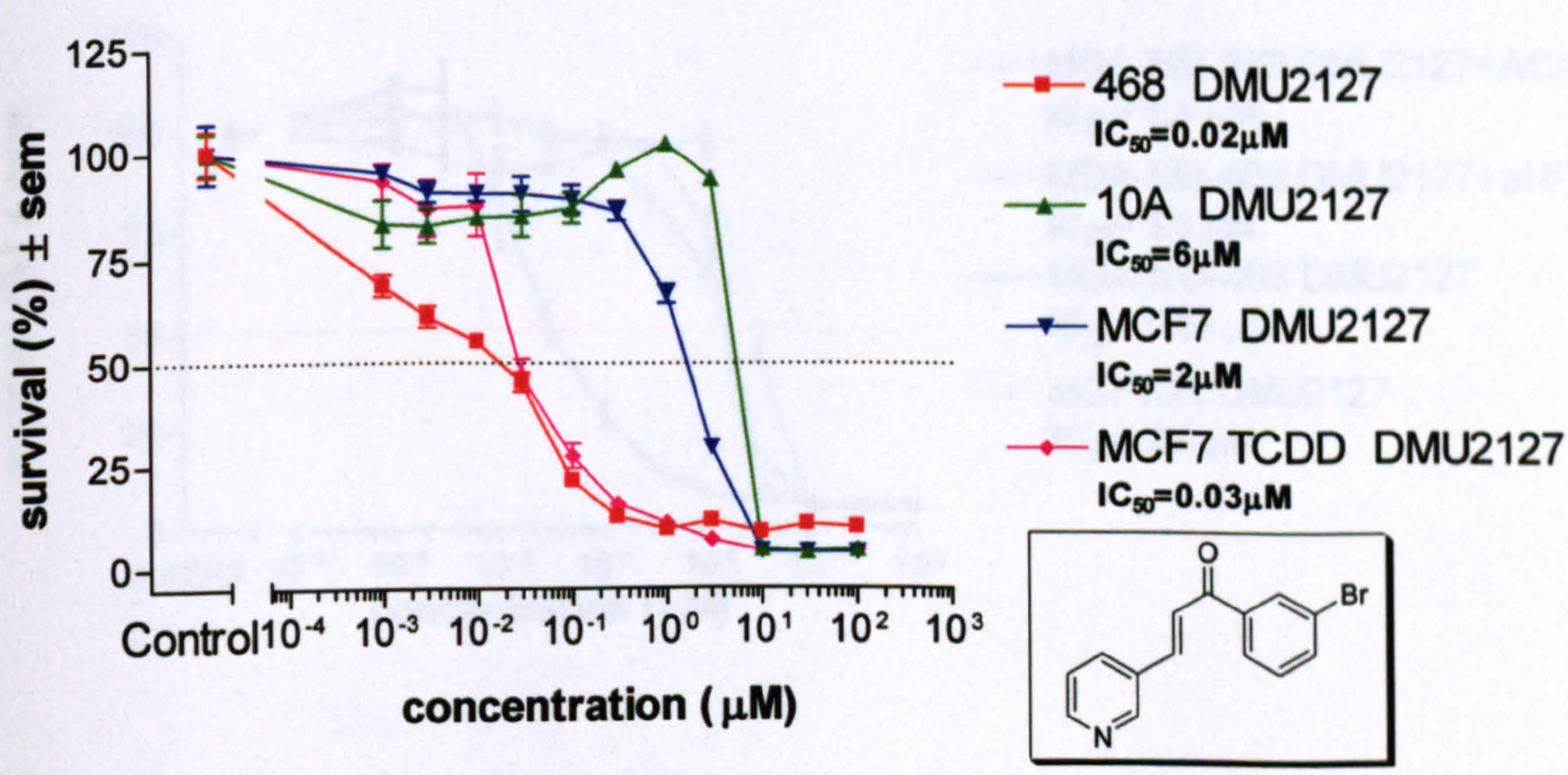

Figure 73: Bioactivation of DMU2123 and DMU2127 by CYP1A1/CYP1B1

Note: 468 = MDA468; 10A = MCF10A; MCF7 TCDD = MCF7 induced with 10nM TCDD.

Figure 74 show that the bioactivation of DMU2123 and DMU2127 could be reversed by the CYP1 enzyme inhibitors acacetin (ACA) and α-naphthaflavone (aNF). This demonstrates that bioactivation of DMU2123 and DMU2127 is CYP1 enzyme mediated.

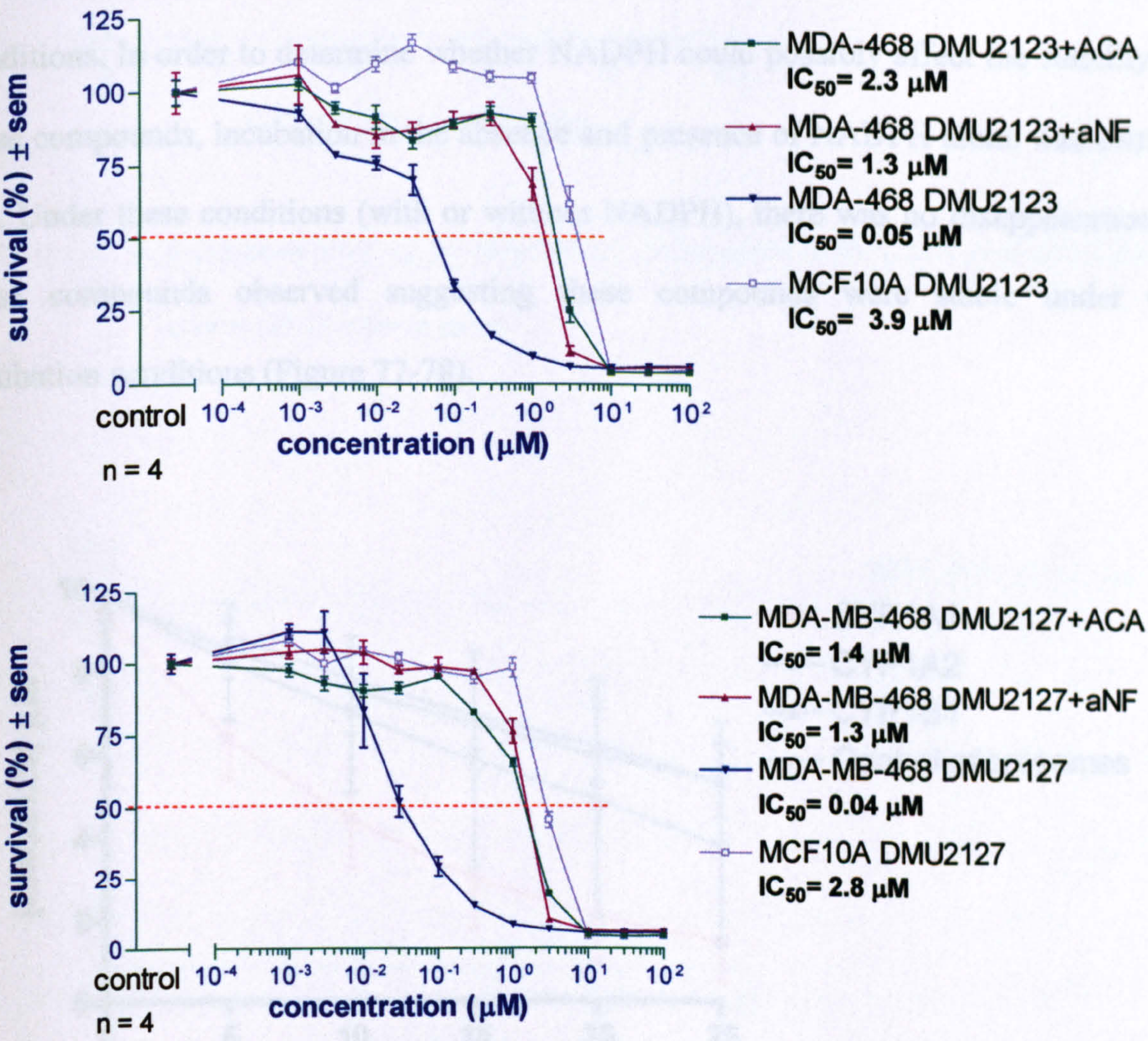

Figure 74: Cytotoxicity of DMU2123 and DMU2127 in the absence and presence of CYP1 enzyme inhibitors

To further assess the selectivity of CYP1 enzyme in bioactivating DMU2123 and DMU2127, analysis of the disappearance of DMU2123 and DMU2127 after incubation

with CYP1 Supersomes™ was carried out. Incubation of DMU2123 and DMU2127 with control microsomes showed an unexpected disappearance of these molecules (Figure 75-76).

It was first thought that these compounds may not be stable under the experimental conditions. Incubation of these compounds without any P450 and control microsomes has been undertaken to observe the stability of these compounds under the incubation conditions. In order to determine whether NADPH could possibly affect the stability of these compounds, incubation in the absence and presence of NADPH alone was carried out. Under these conditions (with or without NADPH), there was no disappearance of these compounds observed suggesting these compounds were stable under the incubation conditions (Figure 77-78).

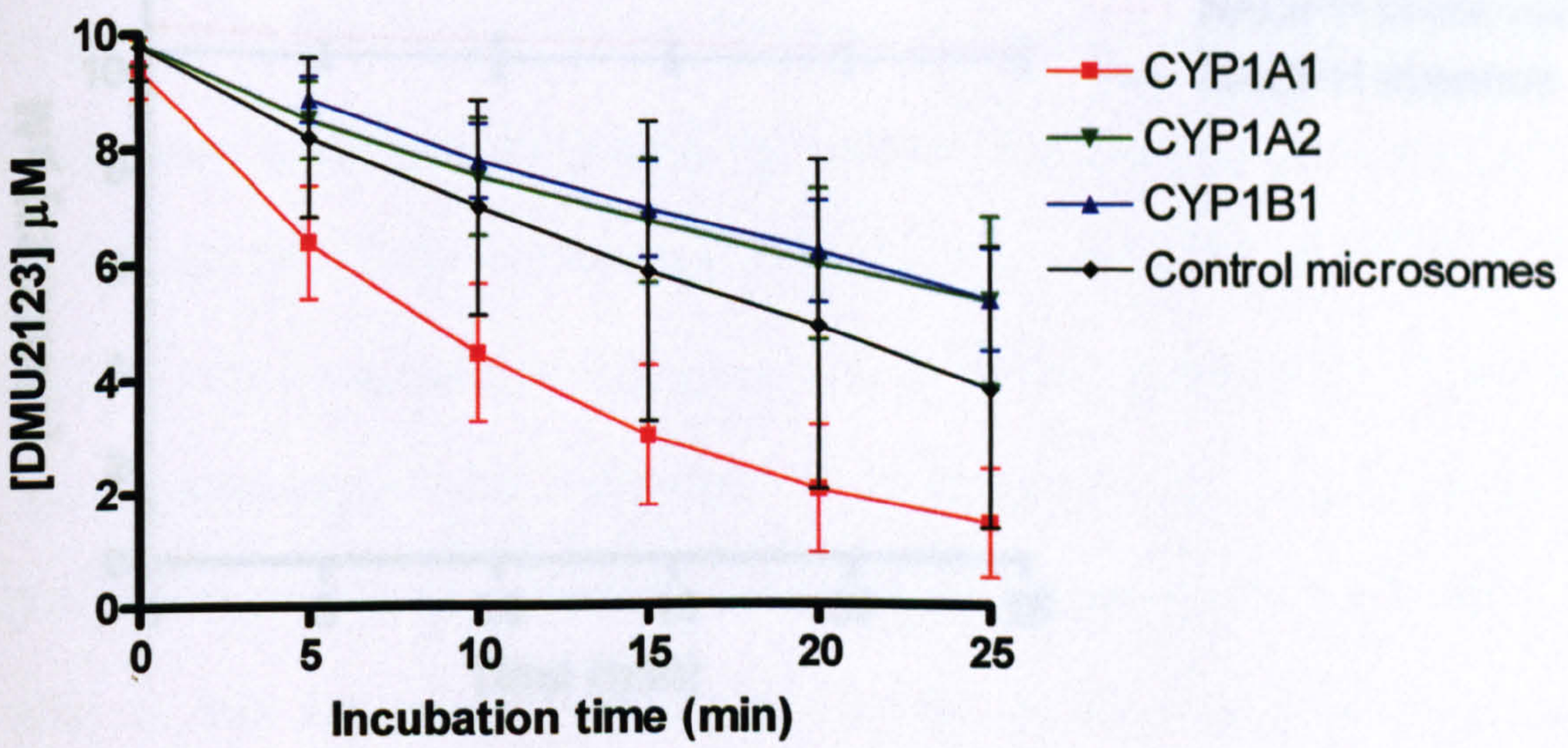

Figure 75: Disappearance of DMU2123 on incubation with CYP1 family enzymes and control microsomes

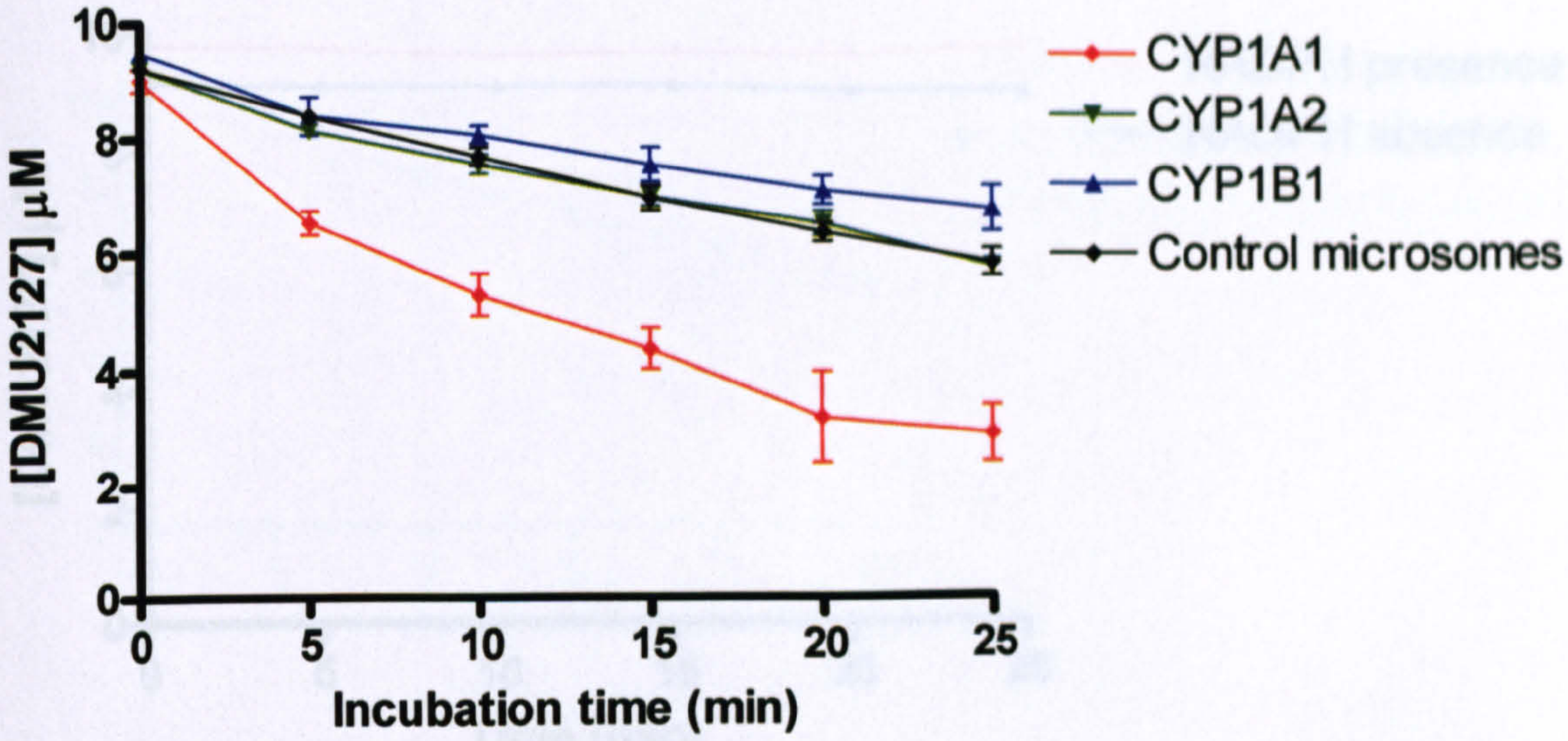

Figure 76: Disappearance of DMU2127 on incubation with CYP1 family enzymes and control microsomes

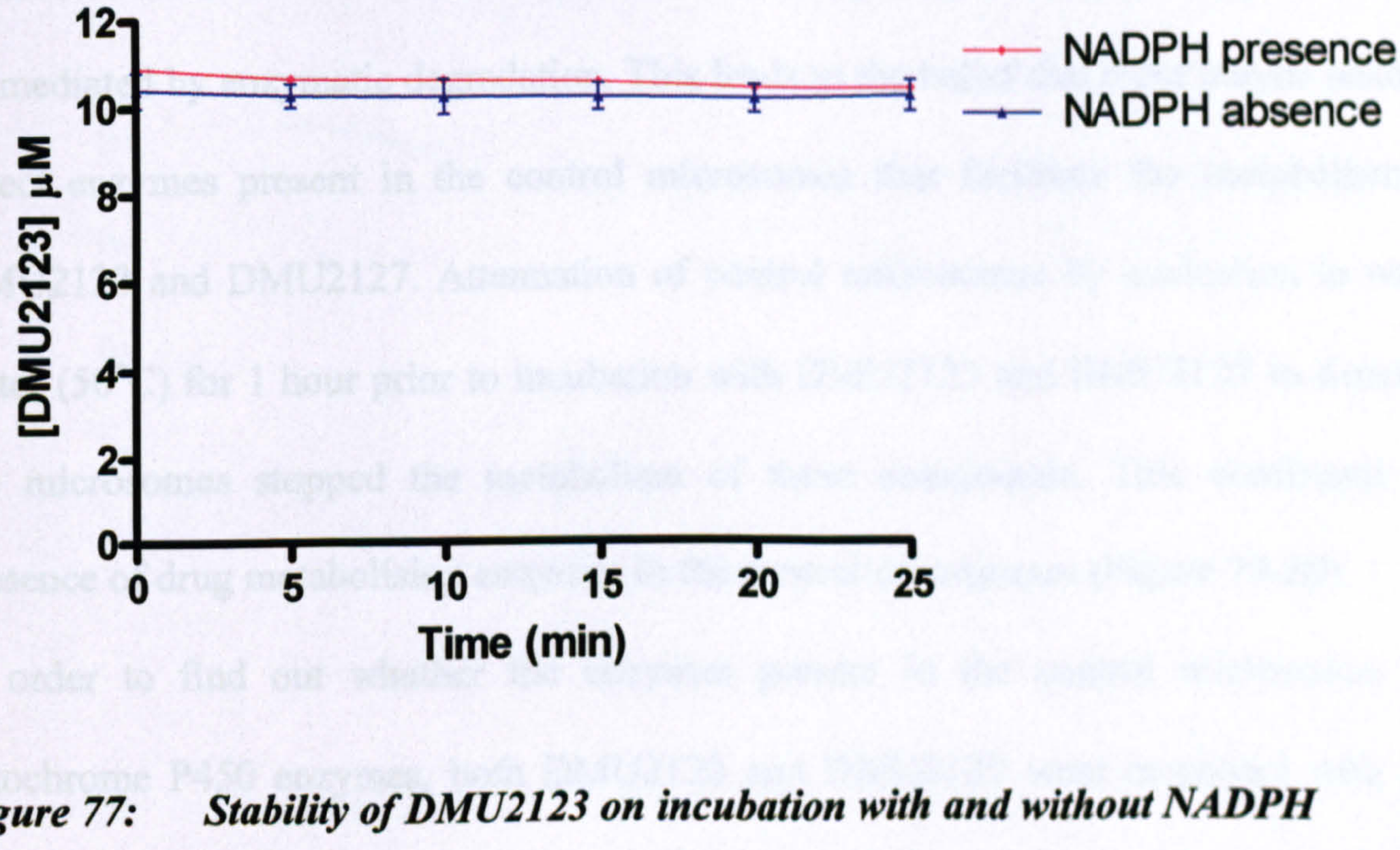

Figure 77: Stability of DMU2123 on incubation with and without NADPH

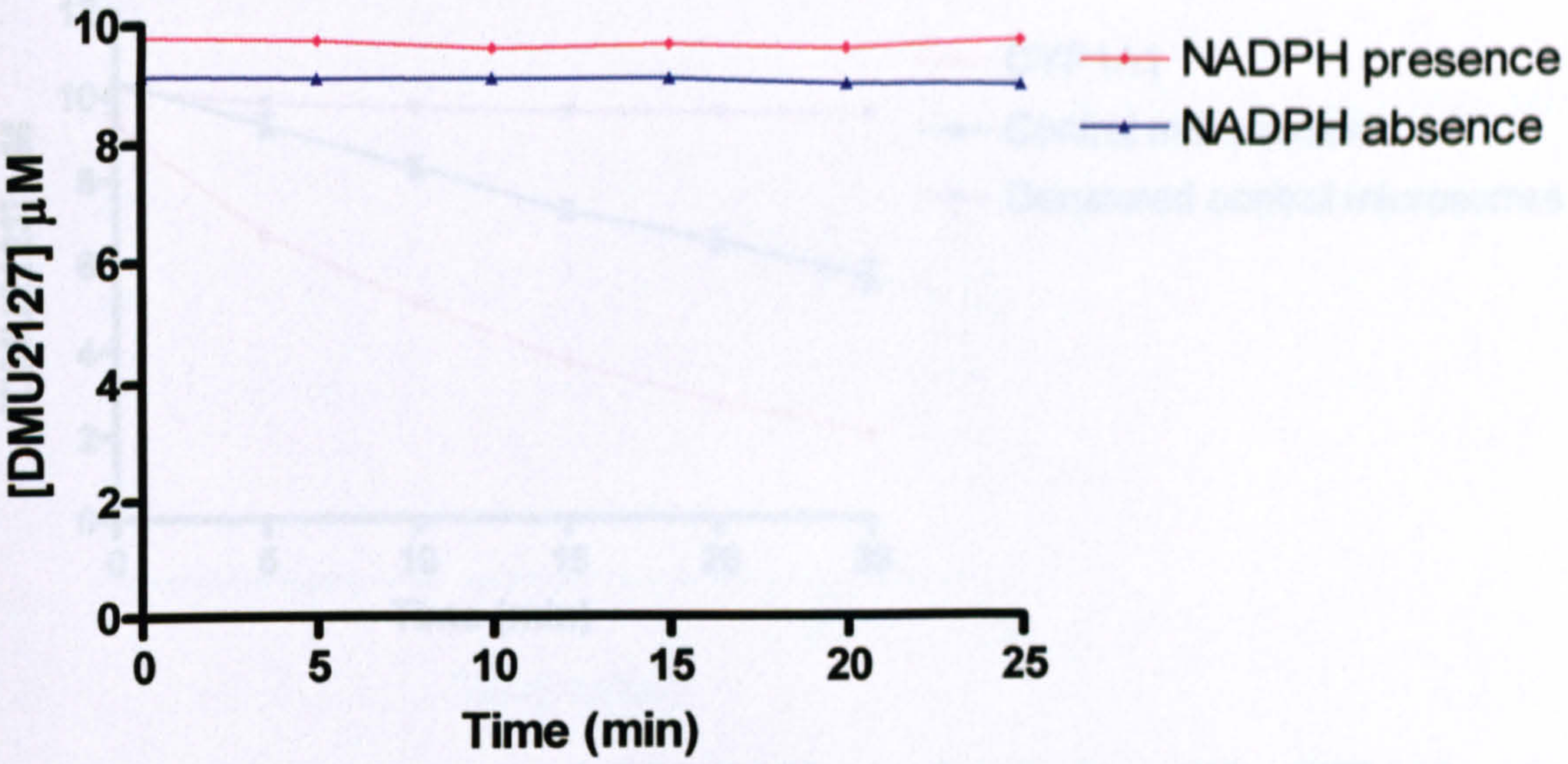

Figure 78: Stability of DMU2127 on incubation with and without NADPH

Since the disappearance of DMU2123 and DMU2127 is not due to instability of these molecules under the incubation conditions, the disappearance of these compounds must be mediated by enzymatic degradation. This leads to the belief that there maybe residual insect enzymes present in the control microsomes that facilitate the metabolism of DMU2123 and DMU2127. Attenuation of control microsomes by sonication in warm water (50°C) for 1 hour prior to incubation with DMU2123 and DMU2127 to denature the microsomes stopped the metabolism of these compounds. This confirmed the presence of drug metabolising enzymes in the control microsomes (Figure 79-80).

In order to find out whether the enzymes present in the control microsomes are cytochrome P450 enzymes, both DMU2123 and DMU2127 were incubated with and without NADPH. This showed that NADPH was indeed required for the metabolism of these compounds. The requirement of NADPH for the control microsomes to metabolise DMU2123 and DMU2127 indicates that the enzymes present in the control microsomes are insect cytochrome P450 enzymes (Figure 81-84).

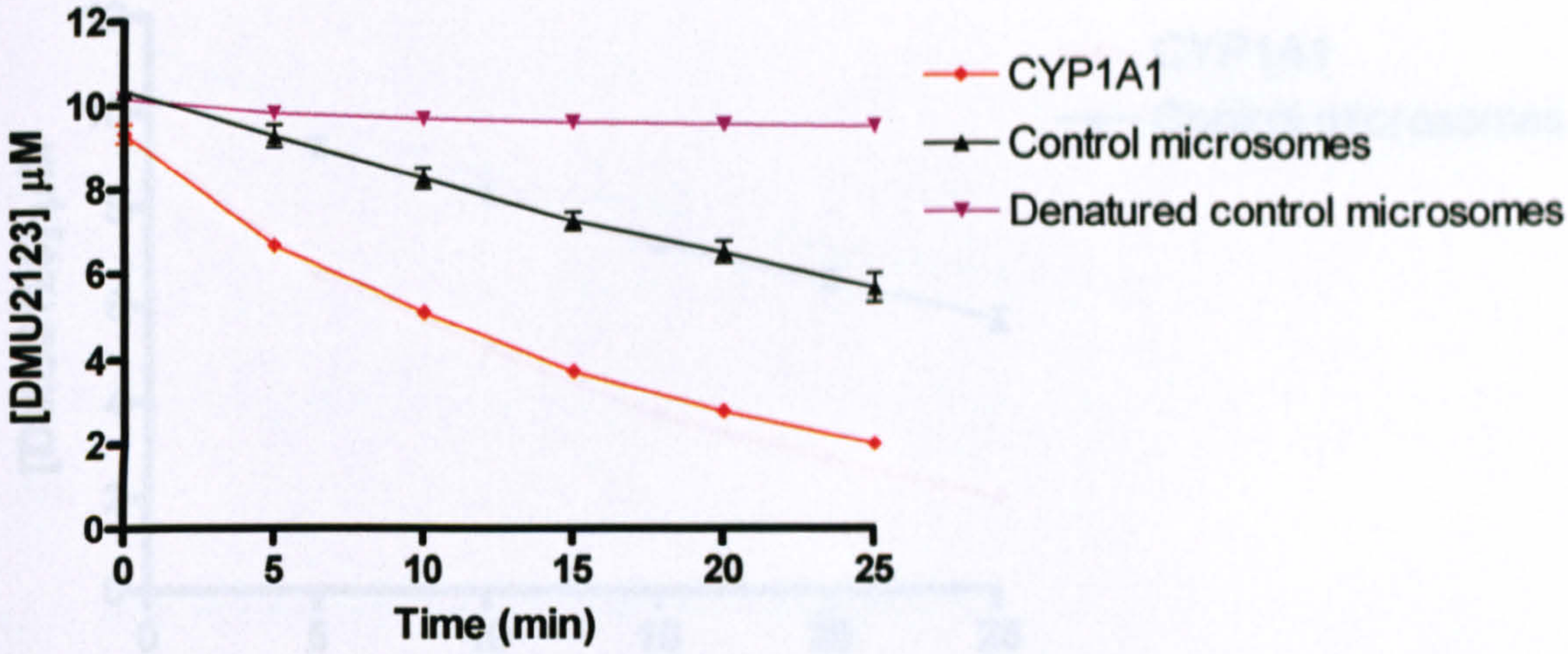

Figure 79: ***Disappearance of DMU2123 on incubation with CYP1A1, control microsomes and denatured control microsomes***

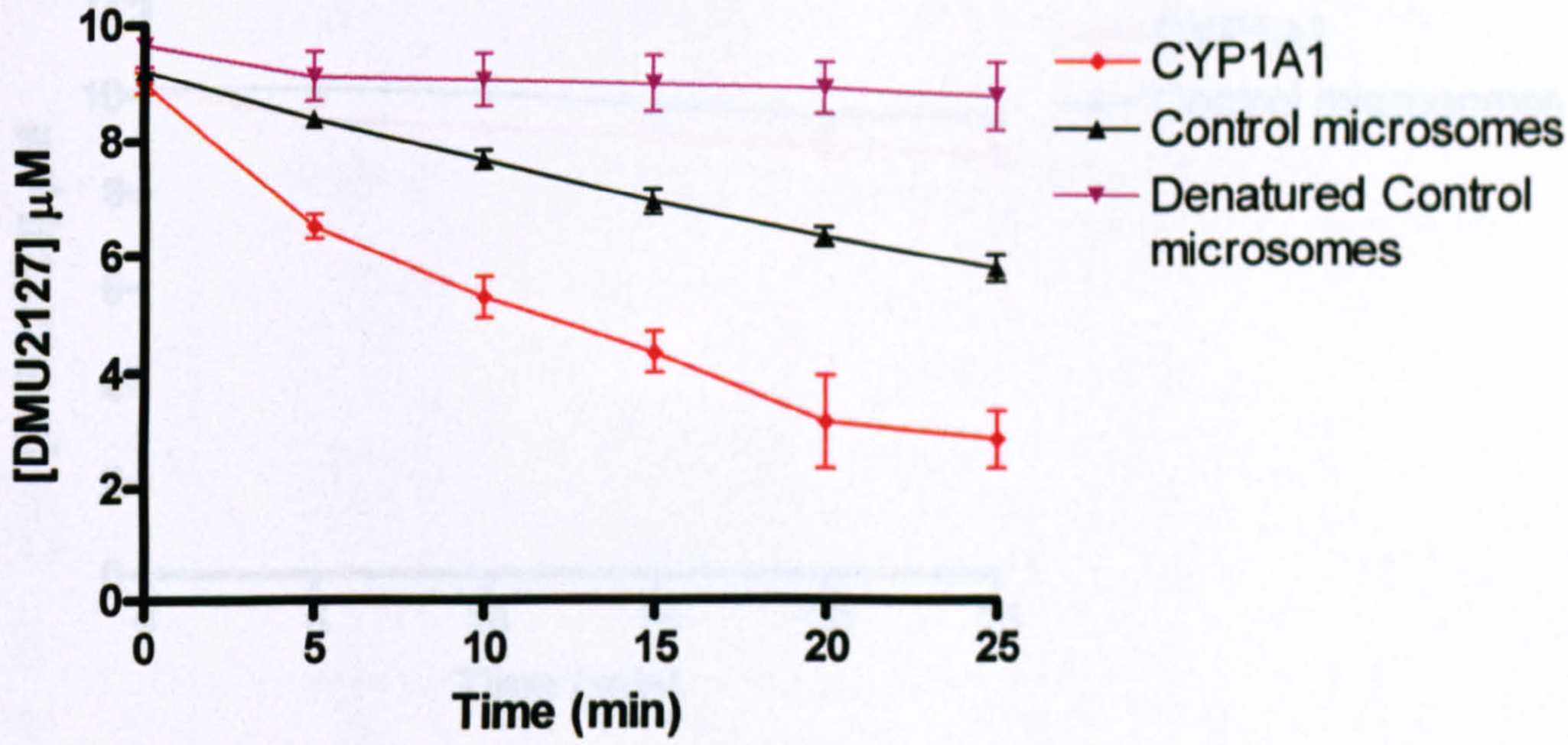

Figure 80: ***Disappearance of DMU2127 on incubation with CYP1A1, control microsomes and denatured control microsomes***

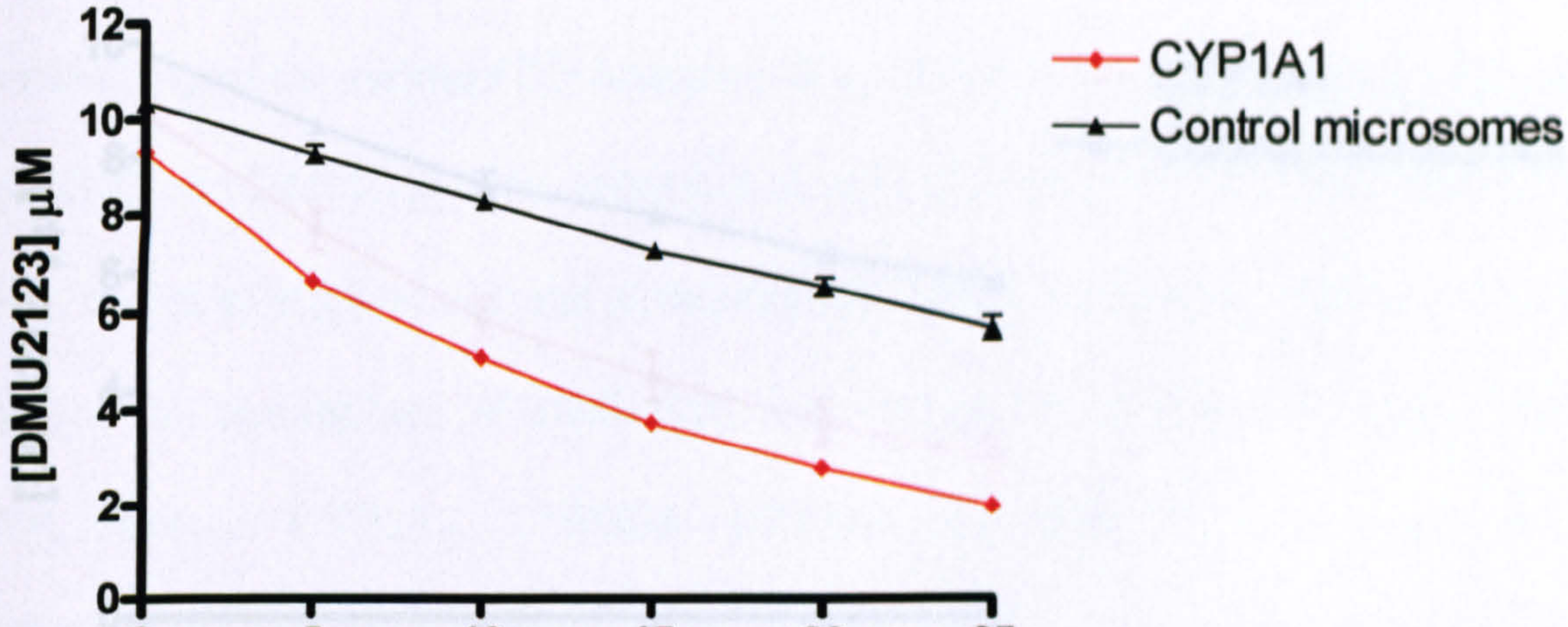

Figure 81: ***Disappearance of DMU2123 on incubation with CYP1A1 and control microsomes in the presence of NADPH***

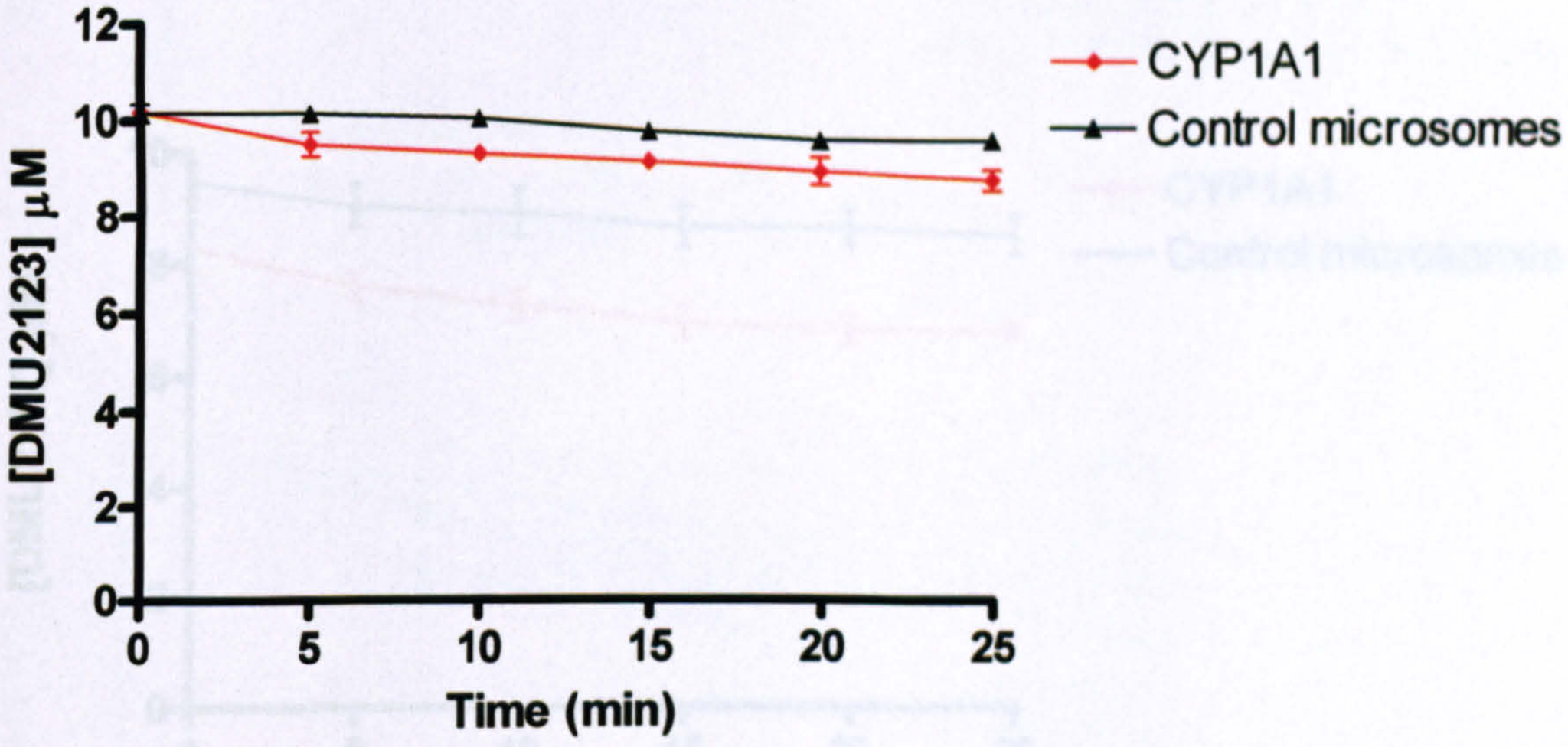

Figure 82: ***Disappearance of DMU2123 on incubation with CYP1A1 and control microsomes in the absence of NADPH***

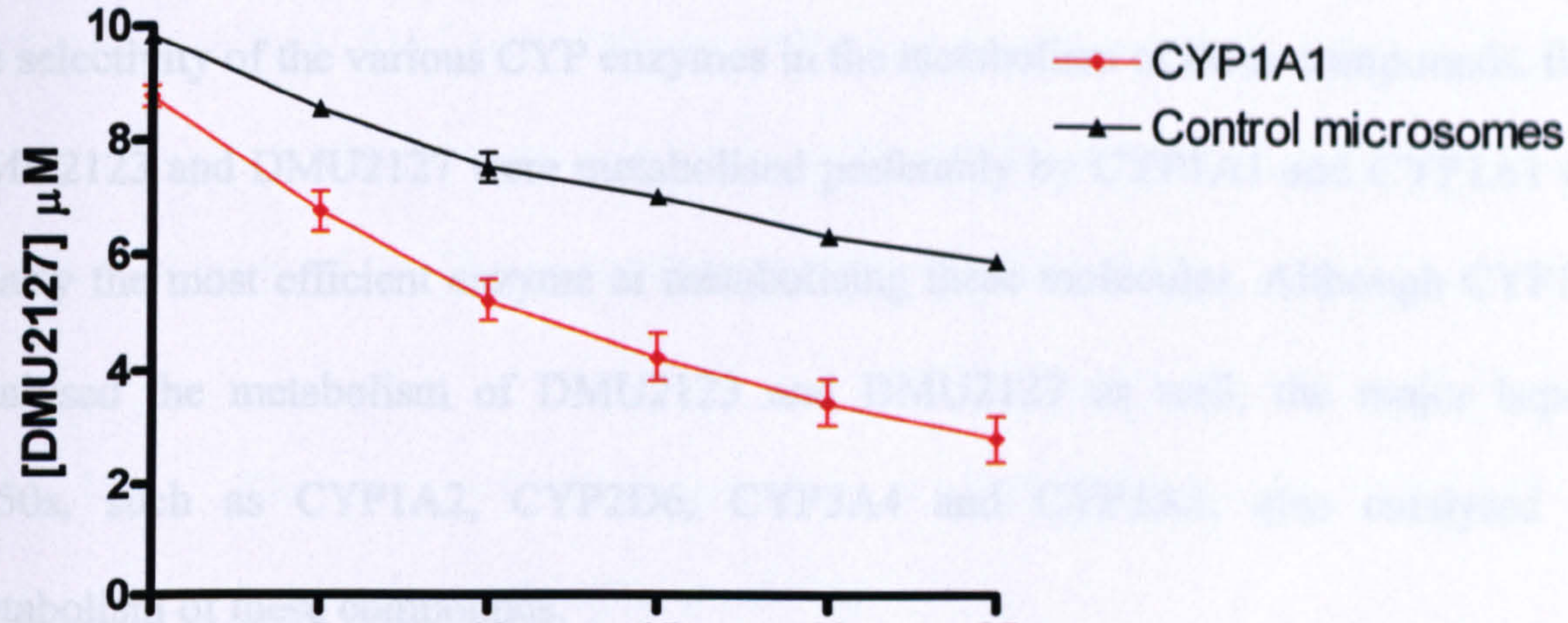

Figure 83: ***Disappearance of DMU2127 on incubation with CYP1A1 and control microsomes in the presence of NADPH***

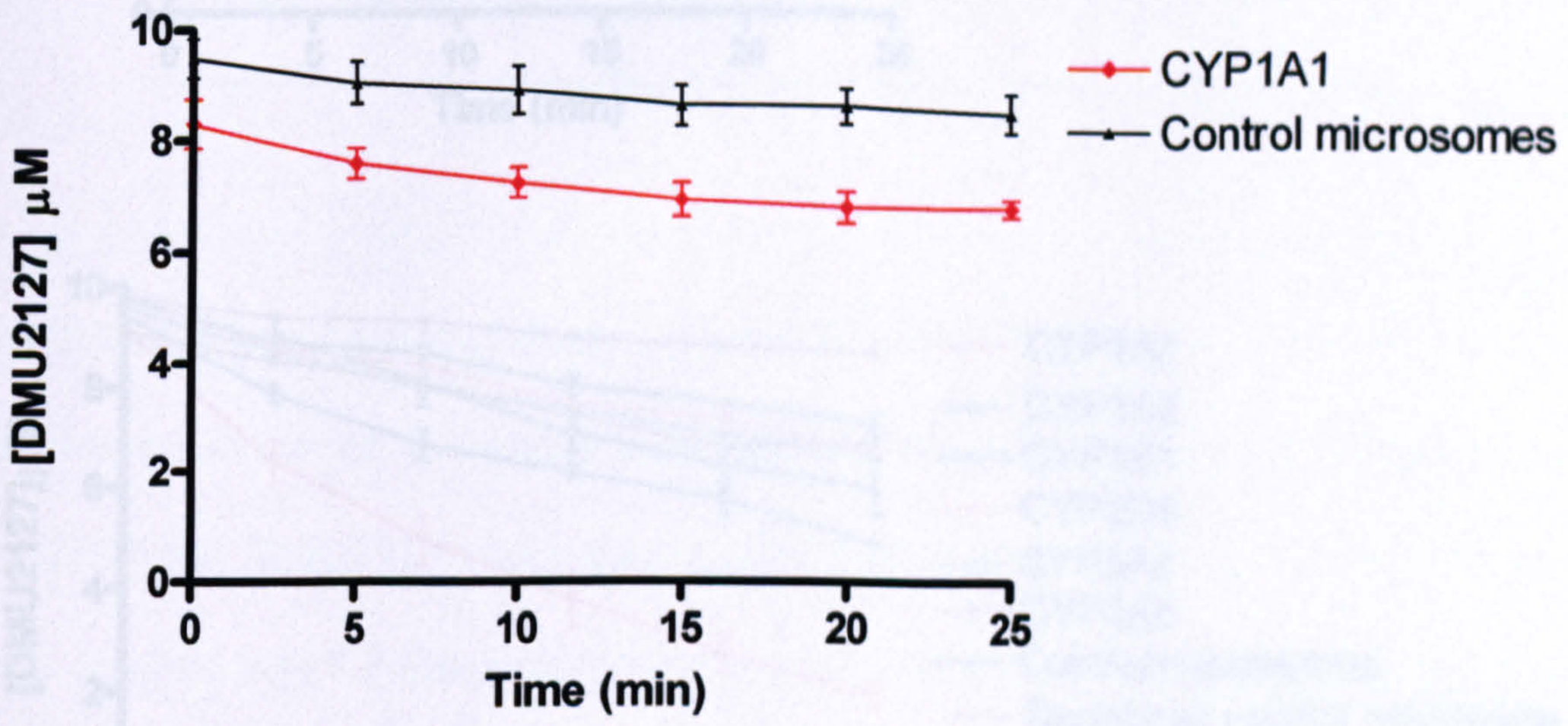

Figure 84: ***Disappearance of DMU2127 on incubation with CYP1A1 and control microsomes in the absence of NADPH***

DMU2123 and DMU2127 were incubated with a panel of six different P450s to assess the selectivity of the various CYP enzymes in the metabolism of these compounds. Both DMU2123 and DMU2127 were metabolised preferably by CYP1A1 and CYP1A1 was clearly the most efficient enzyme at metabolising these molecules. Although CYP1B1 catalysed the metabolism of DMU2123 and DMU2127 as well, the major hepatic P450s, such as CYP1A2, CYP2D6, CYP3A4 and CYP3A5, also catalysed the metabolism of these compounds.

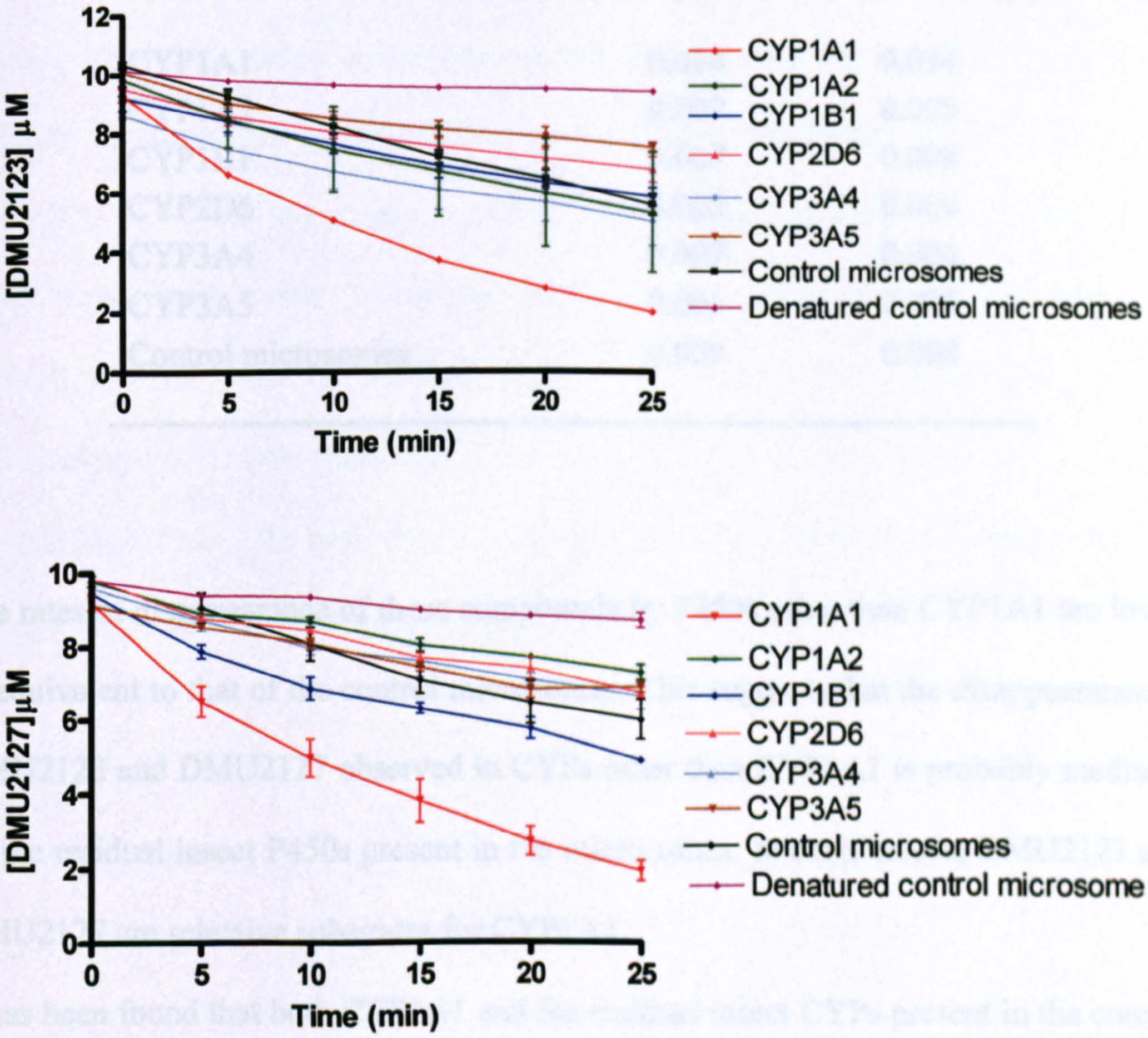

Figure 85: Metabolism of DMU2123 and DMU2127 by a panel of six different Supersomes™

To further assess the selectivity of the substrates, the relative rates of disappearance of DMU2123 and DMY2127 with different CYPs was determined. This was calculated by dividing the rate of disappearance (ie. slope in Figure 85) with the concentration of CYP used (i.e. 20 pmol.mL^{-1}). These results are tabulated in table below.

Table 33: The rate of disappearance of DMU2123 and DMU2127 on incubation with different P450s

Microsomes	Rate of disappearance (nmol.min^{-1}pmol^{-1} CYP) DMU2123	DMU2127
CYP1A1	0.014	0.014
CYP1A2	0.009	0.005
CYP1B1	0.007	0.008
CYP2D6	0.005	0.006
CYP3A4	0.007	0.006
CYP3A5	0.005	0.005
Control microsomes	0.009	0.008

The rates of disappearance of these compounds by P450s other than CYP1A1 are lower or equivalent to that of the control microsomes. This suggests that the disappearance of DMU2123 and DMU2127 observed in CYPs other than CYP1A1 is probably mediated by the residual insect P450s present in the microsomes. In other words, DMU2123 and DMU2127 are selective substrates for CYP1A1.

It has been found that both CYP1A1 and the residual insect CYPs present in the control microsomes and Supersome™ can metabolise DMU2123 and DMU2127. However, no metabolite peak could be detected. The size of the solvent front peak was quite large.

There is a possibility that the polar metabolite co-eluted with the solvent front. After careful inspection of chromatograms from the stability experiment, even if no metabolite was formed (due to the absence of the enzyme), the big solvent front peak was detected in samples incubated with NADPH but only a very small peak detected in sample with no NADPH. These observations indicate that the big solvent front peak is a result of the presence of the NADPH itself rather that the metabolite of DMU2123 and DMU2127.

The inability to detect metabolite peak for DMU2123 and DMU2127 in HPLC analysis suggests a highly reactive species has been generated by oxidative metabolism. The reactive metabolites could bind to microsomal proteins, and this would account for the inability to detect the metabolites. These elusive metabolites of DMU2123 and DMU2127 have been designated as DMU2123M and DMU2127M, respectively. These metabolites have been tentatively assigned as (*E*)-1-(3'-chlorosylphenyl)-3-(3-pyridyl)prop-2-en-1-one (DMU2123M) and (*E*)-1-(3'-bromosylphenyl)-3-(3-pyridyl)prop-2-en-1-one (DMU2127M). The formation of the perchlorate metabolite from DMU2123 and the perbromate metabolite DMU2127 are mechanistically feasible, and this mechanism is illustrated below.

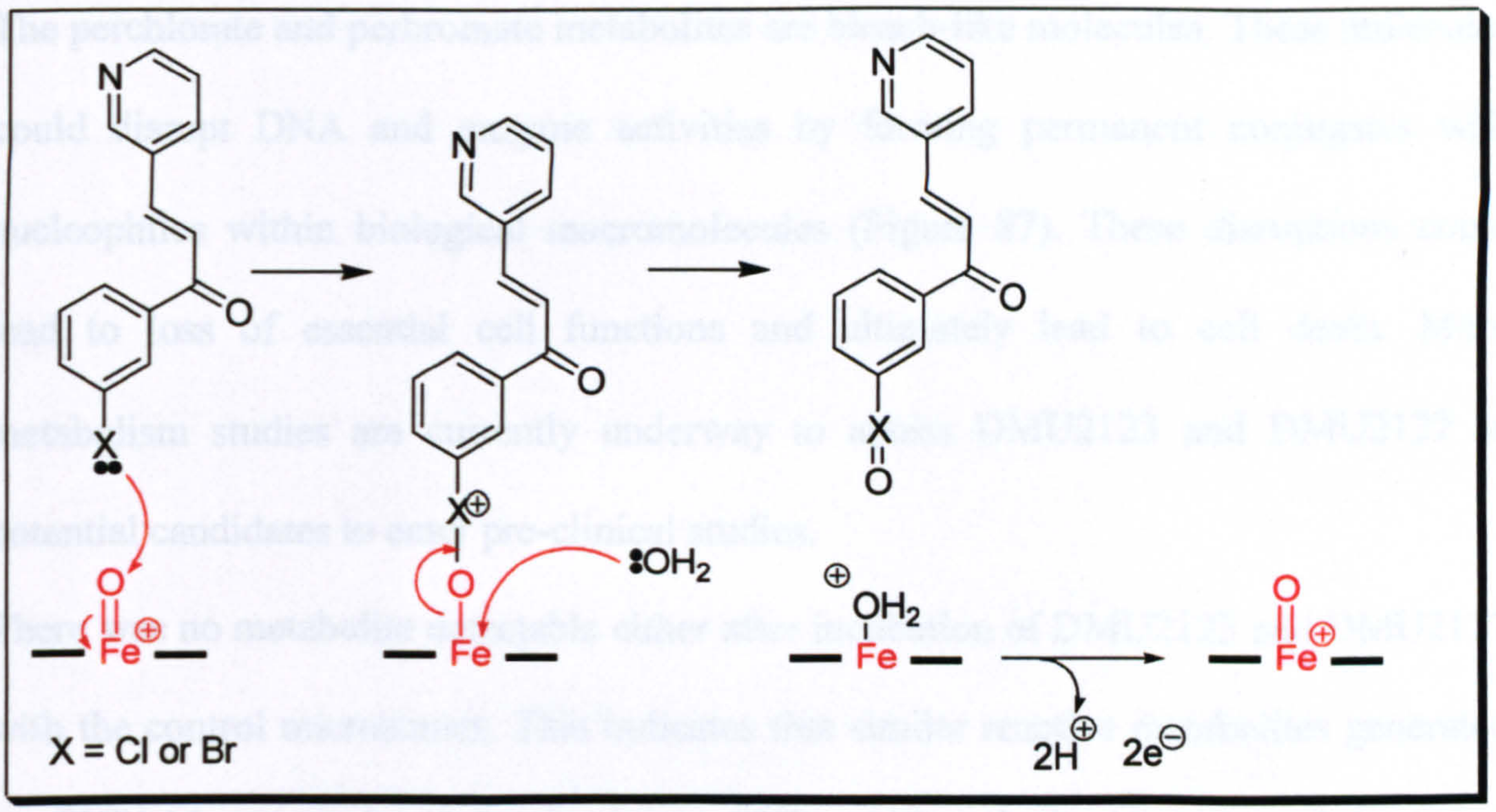

Figure 86: Proposed mechanism for CYP1A1 catalysed formation of DMU2123M (X = Cl) and DMU2127M (X = Br)

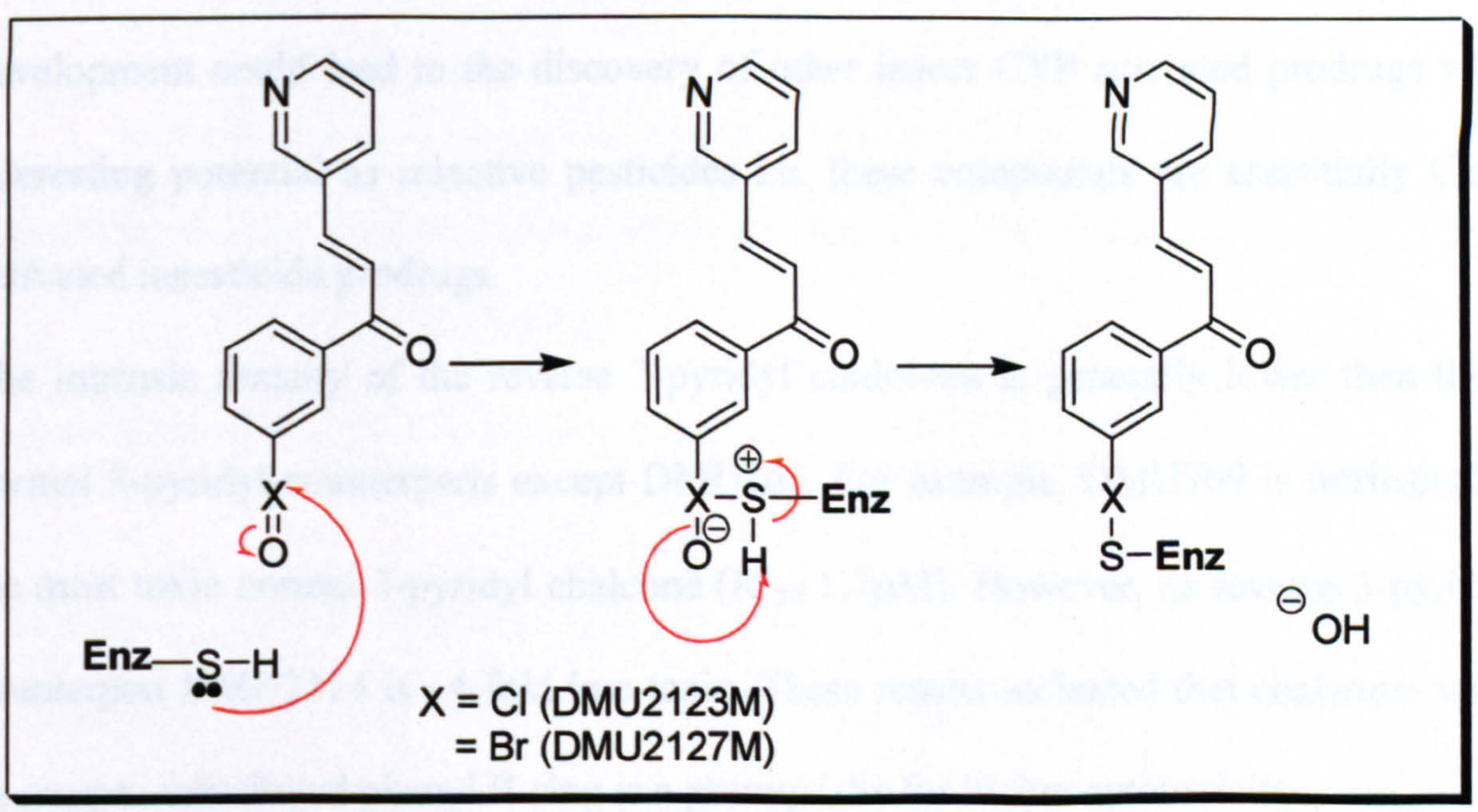

Figure 87: Proposed mechanism of cytotoxicity by DMU2123M and DMU2127M

The metabolites of DMU2123 and DMU2127 could form covalent conjugates with nucleophiles from functional proteins and DNA. This is illustrated by the formation of a conjugate linkage between the thiol residue in the enzyme. Notes: Enz-SH = thiol residue from an enzyme.

The perchlorate and perbromate metabolites are bleach-like molecules. These molecules could disrupt DNA and enzyme activities by forming permanent conjugates with nucleophiles within biological macromolecules (Figure 87). These disruptions could lead to loss of essential cell functions and ultimately lead to cell death. More metabolism studies are currently underway to assess DMU2123 and DMU2127 as potential candidates to enter pre-clinical studies.

There was no metabolite detectable either after incubation of DMU2123 and DMU2127 with the control microsomes. This indicates that similar reactive metabolites generated by CYP1A1 are produced by the insect CYPs. Although the identities of the insect CYPs are still unknown, nevertheless DMU2123 and DMU2127 may represent a novel class of insecticide that requires bioactivation by a cytochrome P450 enzyme. These would be highly selective for insect expressing a particular CYP and further development could lead to the discovery of other insect CYP activated prodrugs with interesting potential as selective pesticides i.e. these compounds are essentially CYP activated insecticide prodrugs.

The intrinsic toxicity of the reverse 3-pyridyl chalcones is generally lower than their normal 3-pyridyl counterparts except DMU768. For example, DMU709 is intrinsically the most toxic normal 3-pyridyl chalcone (IC_{50} 1.7μM). However, its reverse 3-pyridyl counterpart DMU2114 is ~4-fold less toxic. These results indicated that chalcones with an oxygen substituted phenyl B-ring is a prerequisite for higher cytotoxicity.

The toxicity measured in MCF10A breast cell line for the reverse 3-pyridyl chalcone DMU768 is 15μM but its normal 3-pyridyl analogue (DMU765) is non-toxic (>100μM) to the same cell line. Although it is thought that substituted phenyl B-ring in chalcones is important to mediate cytotoxicity, the nitrogen lone pair of electrons in DMU768 can

afford hydrogen bonding interactions and therefore contribute to its cytotoxicity. The comparison of DMU765 and DMU768 intrinsic toxicity reveals that hydrogen bonding at 3'-position of the chalcones B-ring is important in mediating cytotoxicity.

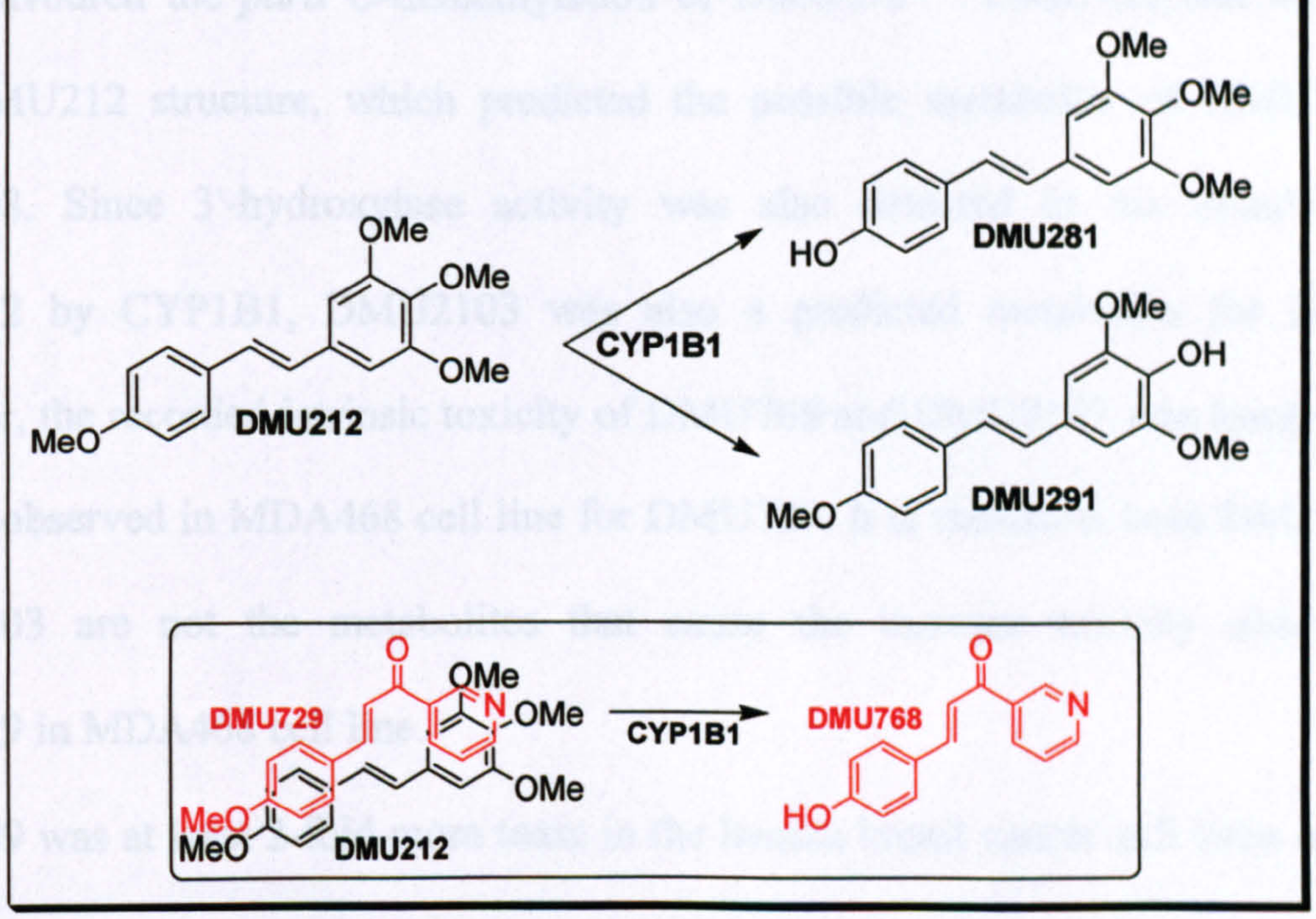

Figure 88: The predicted metabolism of DMU729 based on the metabolism of DMU212 by CYP1B1

Inlet shows mapping of DMU729 onto DMU212 and the predicted metabolism of DMU729.

Although the reverse 3-pyridyl chalcones were designed to be inhibitors of the CYP1 enzymes, the results from the MTT-assay has shown that a few inhibitors were actually substrate for the CYP1 mono-oxygenases (Table 30). DMU729 and DMU768 are deduced to be CYP1B1 selective substrates since they are only bioactivated in the MDA468 cell line. DMU769 is a CYP1A1 selective substrate since bioactivation was observed in the MCF7 as well as the MDA468 cell line.

The difference in cytotoxic IC_{50} values between induced MCF7 (IC_{50} 15μM) and

MDA468 (IC_{50} 4μM) for DMU2103 indicates the major CYP that causes bioactivation of DMU2103 is probably CYP1B1.

The CYP1B1 bioactivation of DMU729 is in accordance with the metabolism of the trans-stilbene anticancer prodrug DMU212[138,140] (Figure 88). CYP1B1 was found to be highly favoured the *para O*-demethylation of DMU212[139]. DMU729 can be mapped onto DMU212 structure, which predicted the possible metabolite of DMU729 was DMU768. Since 3'-hydroxylase activity was also detected in the metabolism of DMU212 by CYP1B1, DMU2103 was also a predicted metabolite for DMU729. However, the recorded intrinsic toxicity of DMU768 and DMU2103 was lower than the toxicity observed in MDA468 cell line for DMU729. It is therefore, both DMU768 and DMU2103 are not the metabolites that cause the increase toxicity observed for DMU729 in MDA468 cell line.

DMU769 was at least 2-fold more toxic in the human breast cancer cell lines indicative that this compound was bioactivated by CYP1 enzymes. The predicted metabolite of DMU769 is (*E*)-1-(3-pyridyl)-3-(3",4"-dihydroxyphenyl)prop-2-en-1-one (or 3,4-dihydroxy reverse 3-pyridyl chalcone). As the recorded cytotoxic IC_{50} values for MDA468 cell line have shown no apparent difference for DMU729, DMU768, DMU769 and DMU2103 (4-6μM), the metabolite that causes toxicity in MDA468 for DMU729, DMU768, DMU769 and DMU2103 has been tentatively assigned as the 3,4-dihydroxy reverse 3-pyridyl chalcone.

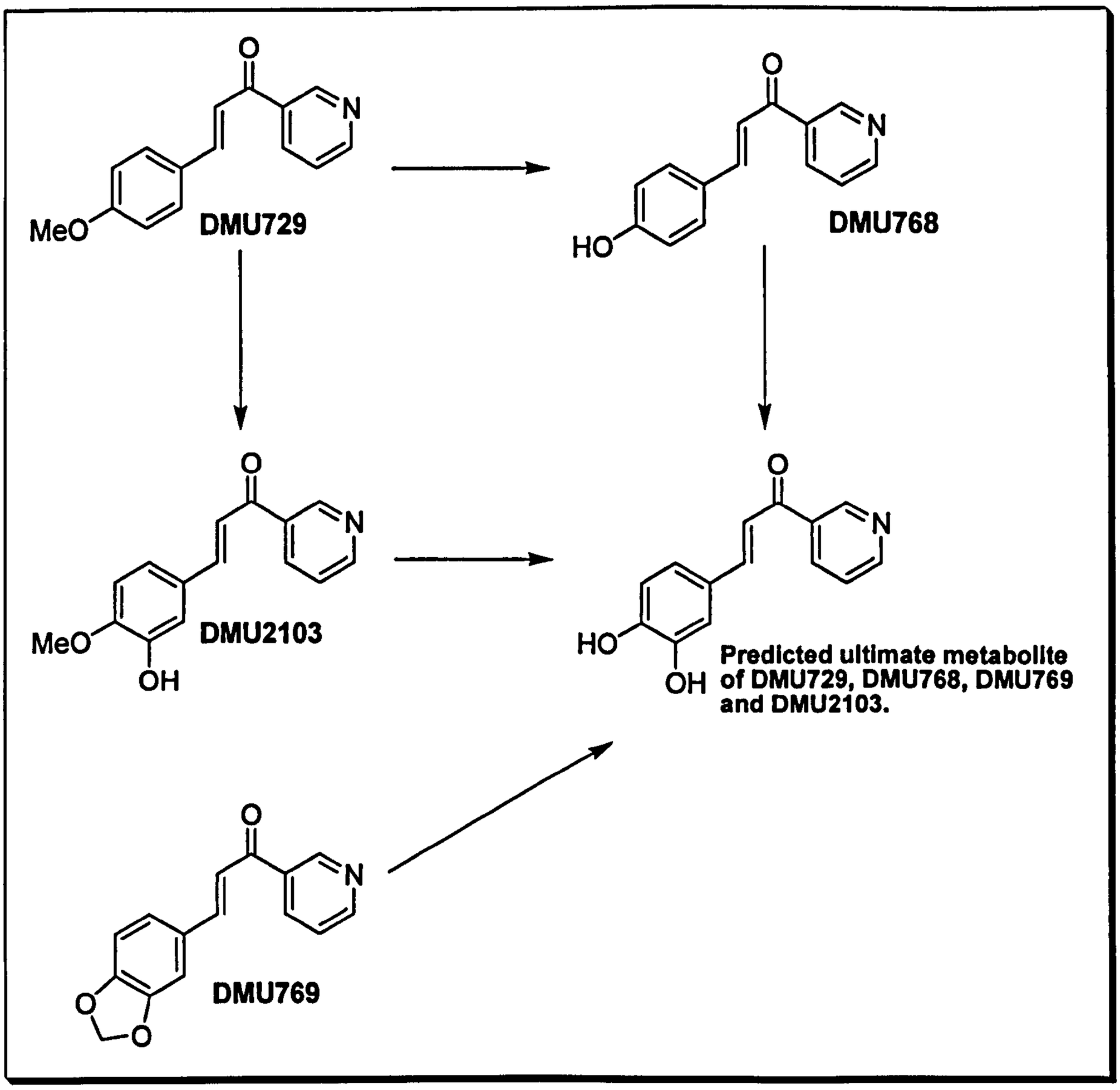

Figure 89: Proposed bioactivation pathway of DMU729, DMU768, DMU769 and DMU2103

DMU2123 and DMU2127 are selectively bioactivated by CYP1A1. Since elevated expression of CYP1A1 has been shown in the cancer of prostate[129], stomach[130,131] and bladder[132], these compounds have the potential to be CYP1A1 selective anti-tumour prodrugs.

The investigation of DMU2123 and DMU2127 analogues is outside the scope of this project. The synthesis of these potential anticancer agents is currently undertaken by Ketan Ruparelia, Cancer Drug Discovery Group.

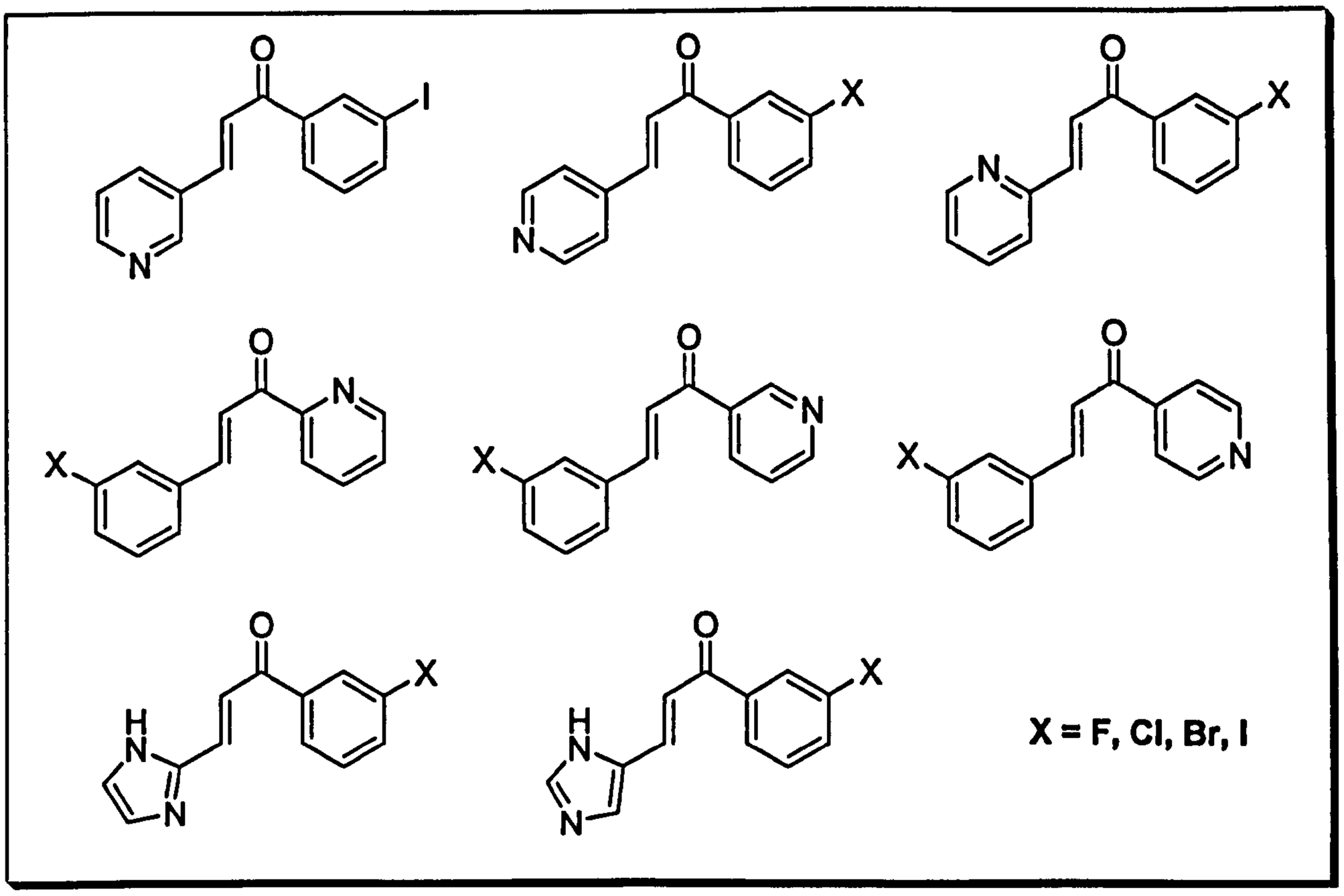

Figure 90: ***Potential tumour selective anticancer prodrugs***

5.5 Experimental

Synthesis and analytical methods see Section 2.5.1 to Section 2.5.2

(*E*)-1-(3,4-methylenedioxyphenyl)-3-(2-pyridyl)prop-2-en-1-one (DMU918)

Synthetic Method 2; ^{1}H-NMR ($CDCl_3$) δ 6.05 (2H, s, methylenedioxy), 6.88 (1H, d, benzyl), 7.28 (1H, t, Py), 7.45 (1H, d, benzyl), 7.57 (1H, s, benzyl), 7.69-7.78 (3H, m), 8.06 (1H, d, *J*=14.9Hz), 8.68 (1H, d, Py); ^{13}C-NMR ($CDCl_3$) δ 101.86, 107.88, 108.43, 124.25, 125.16, 125.27, 125.37, 132.71, 136.81, 142.14, 148.33, 150.10, 151.92, 153.29, 188.18 (C=O); IR Spectrum V_{max} (KBr)/cm^{-1} 1662 (C=O); Mass Spectrum (MALDI) m/z 252.96 (M^+, 100%); mp 112-113°C.

(*E*)-1-(2-pyridyl)-3-(3,4-methylenedioxyphenyl)prop-2-en-1-one (DMU919)

Synthetic Method 2; ^{1}H-NMR ($CDCl_3$) δ 6.03 (2H, s, methylenedioxy), 6.85 (1H, d, benzyl), 7.20 (1H, d, benzyl), 7.28 (1H, s, benzyl), 7.48 (1H, d, Py), 7.82-7.90 (2H, m), 8.13 (1H, d, *J*=15.4Hz), 8.18 (1H, d, Py), 8.73 (1H, d, Py); ^{13}C-NMR ($CDCl_3$) δ 101.56, 107.08, 108.54, 118.98, 122.81, 125.55, 126.71, 129.75, 136.93, 144.59, 148.35, 148.77, 149.94, 154.39, 189.28 (C=O); IR Spectrum V_{max} (KBr)/cm^{-1} 1666 (C=O); Mass Spectrum (MALDI) m/z 253.32 (M^+, 100%); mp 132°C.

(*E*)-1,3-di(3,4-methylenedioxyphenyl)prop-2-en-1-one (DMU968)

Synthetic Method 2; ^{1}H-NMR (DMSO) δ 6.08 (2H, s, methylenedioxy), 6.13 (2H, s, methylenedioxy), 6.93 (1H, d, benzyl), 7.01 (1H, d, benzyl), 7.25 (1H, d, benzyl), 7.55-7.65 (2H, m), 7.72 (1H, d, *J*=16.5Hz), 7.83 (1H, d, benzyl), 8.23 (1H, s, benzyl); ^{13}C-NMR (DMSO) δ 101.64, 102.02, 106.97, 108.03, 108.05, 108.46, 119.95, 124.90, 125.72, 129.44, 132.62, 143.47, 148.06, 148.21, 149.54, 151.47, 186.88 (C=O); IR Spectrum V_{max} (KBr)/cm^{-1} 1647 (C=O); Mass Spectrum (MALDI) m/z 296.45 (M^+, 100%); mp 163°C.

Chapter 6

Validate The Efficacy of Selective CYP1 Enzyme Inhibitors and The CYP1B1 Pharmacophore Model

6.1 Selective CYP1 enzyme inhibitors in the MTT-bioactivation assay

Apart from delineating the structure-activity relationship of the cytochrome P450 CYP1 mono-oxygenases, one of the objectives for this project is to identify suitable CYP1 selective inhibitors for future *in vitro* and *in vivo* biological assay. A selective CYP1 inhibitor is a valuable tool to examine the efficacy of CYP1A1 or CYP1B1 activated anticancer prodrugs. The suitability of an inhibitor for cell based and animal experiments depends on the toxicity of the compound. Ideally, the inhibitor must have low intrinsic toxicity so that it will not interfere with the final results. This is particularly important if the inhibitor is to be used for *in vivo* assay. Secondly, metabolite(s) of the inhibitor should also be non-toxic. In other words, inhibitor with high intrinsic toxicity or toxicity after metabolic activation will give erroneous conclusions in the evaluation process of potential CYP1 activated anticancer agents.

In this project, the intrinsic toxicity and toxicity of the inhibitor metabolites have been examined. The intrinsic toxicity of the inhibitors synthesised was measured using MTT-cytotoxic assay with the human breast cell line MCF10A. This cell line was used because of its low CYPs content. So far, only protein from the CYP2C family has been discovered[168,169] and the presences of CYP1 enzymes were not detected[139] in MCF10A. Although the synthesised inhibitors in this project were designed to inhibit CYP1 mono-oxygenases, bioactivation and deactivation of these inhibitors by the very enzymes that they try to inhibit have been demonstrated (see Chapter 5). Since the efficacy of CYP1A1/CYP1B1 activated prodrugs are evaluated in MTT-assay with naïve and induced MCF7, as well as MDA468 cell lines, the inhibitor metabolites should ideally non-toxic or otherwise will interfere the final outcomes.

Table 34: Enzyme selectivity and cytotoxicity of CYP1A1 inhibitors

	EROD IC_{50} (μM)			Cytotoxic IC_{50} (μM)			
Inhibitor	CYP1A1	CYP1A2	CYP1B1	MCF7	MCF7^{+}	MCF10A	MDA468
DMU709	0.3	25	7	1.8	2	1.7	0.8
DMU710	0.5	4	19	1.4	1.4	1.5	1.4
DMU968	2.5	NI	NI	30	30	25	17
DMU2114	0.6	8	3	5	3	7	4
DMU2157	0.3	5	9	7	4	15	5

Note: NI = no inhibition.

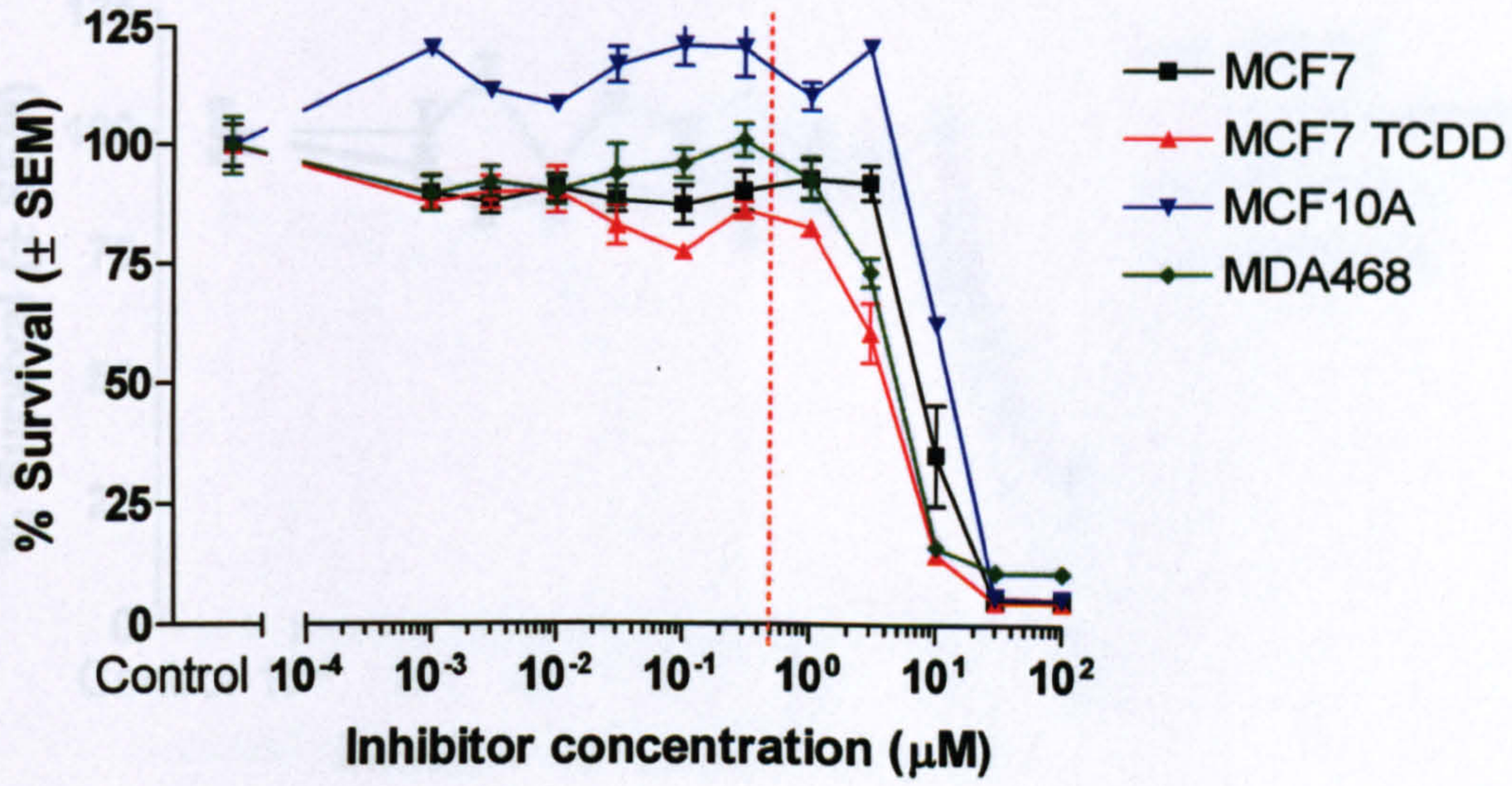

Figure 91: Cytotoxicity and enzyme selectivity of DMU2157

Five more selective CYP1A1 inhibitors have been discovered and their enzyme selectivity and toxicity are tabulated in Table 34. DMU2157 has the best profile due to its potency for CYP1A1 inhibition and relatively low toxicity. Co-incubation of DMU2157 at 0.5-1.0μM in prodrug activation studies will not cause any toxicity to all human breast cell lines but can afford at least 60% inhibition of CYP1A1 activity. DMU968 is relatively non-toxic, it can be use at up to 3μM without causing any toxicity to the cell lines.

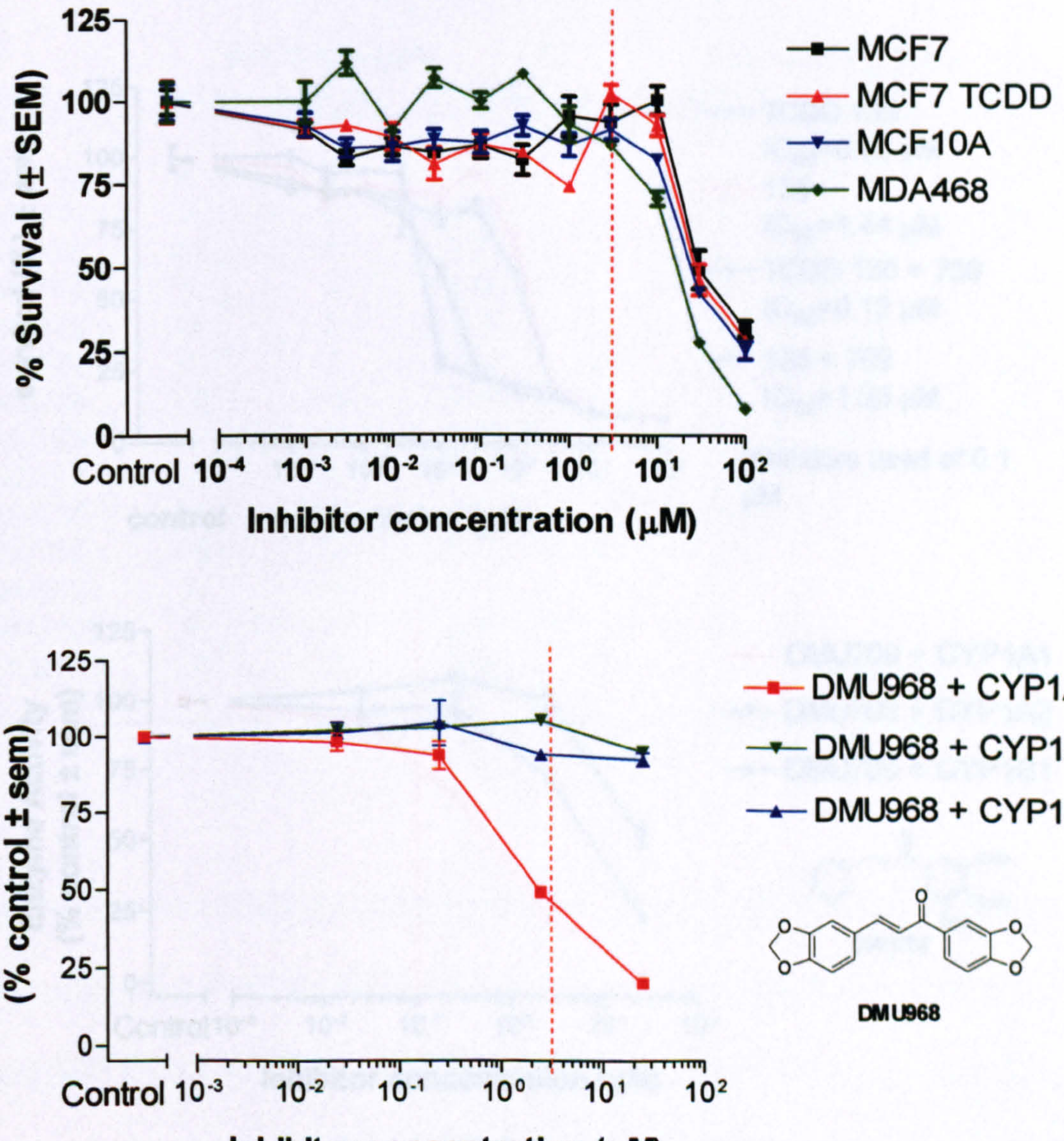

Figure 92: Cytotoxicity and enzyme selectivity of DMU968

One of the CYP1A1 inhibitors, namely DMU709, has been used to evaluate the efficacy of the CYP1A1 activated anticancer agent DMU135[145]. As a result of the toxicity of this inhibitor, only 0.1μM was co-incubated with the prodrug in MCF7 and MCF7 pre-treated with 10nM TCDD (Figure 93). The presence of inhibitor caused a 2-fold increase in IC_{50} value compared to incubation of the prodrug alone in the induced MCF7 cells. Only small inhibition observed in this case because at 0.1μM, DMU709 only inhibits ~25% of CYP1A1 activity.

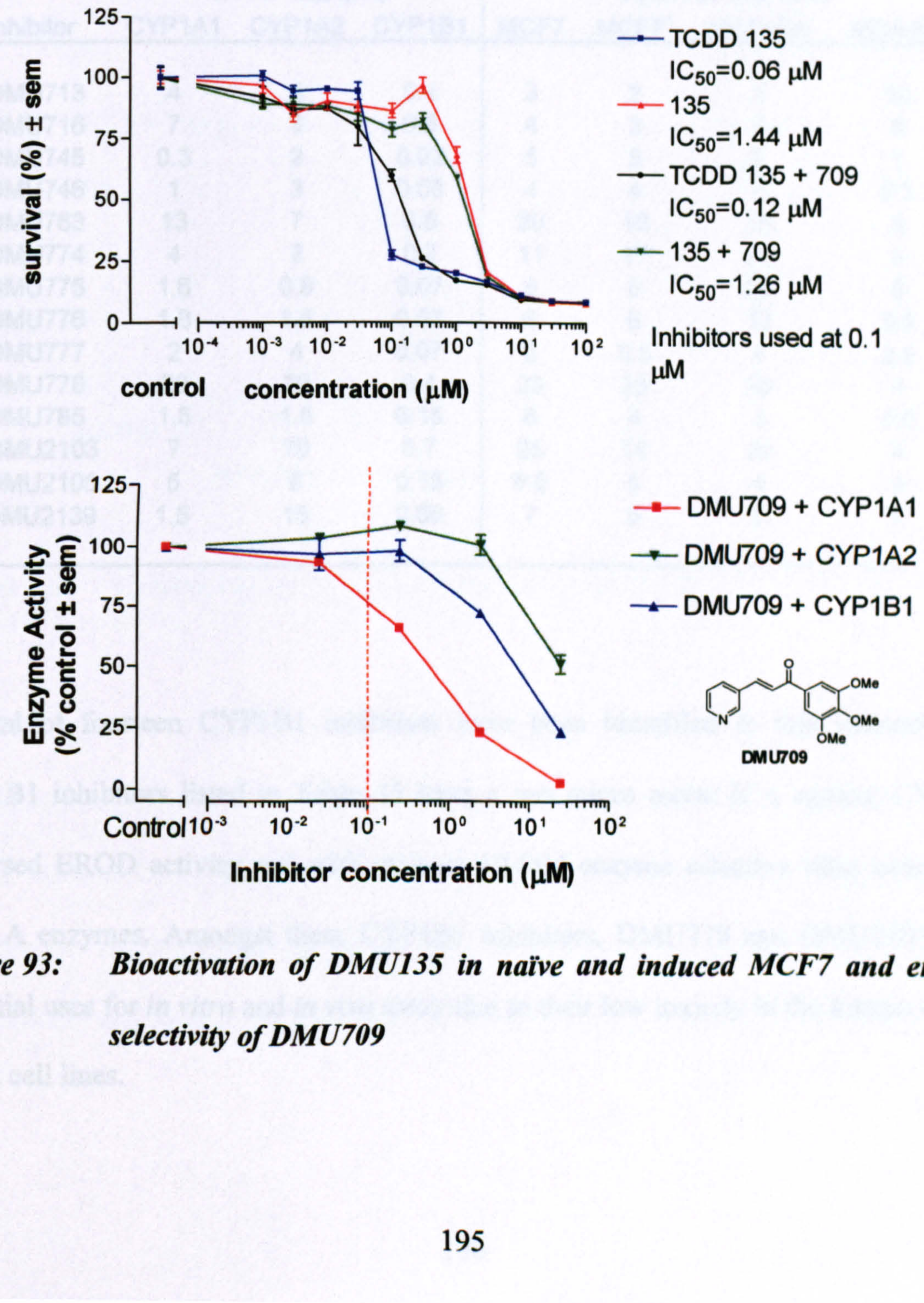

Figure 93: ***Bioactivation of DMU135 in naïve and induced MCF7 and enzyme selectivity of DMU709***

9-Acetylphenanthrene was identified as CYP1A2 inhibitor. The cytotoxicity of 9-acetylphenanthrene was not determined in this project. 9-Acetylphenanthrene is a general chemical for organic synthesis. There is no specific hazard label associated with this compound and therefore, it is thought that this compound is relatively non-toxic. More work is pending to determine the suitability of this inhibitor in any biological assay.

Table 35: Enzyme selectivity and toxicity of CYP1B1 inhibitors

	EROD IC_{50} (μM)			Cytotoxic IC_{50} (μM)			
Inhibitor	CYP1A1	CYP1A2	CYP1B1	MCF7	$MCF7^+$	MCF10A	MDA468
DMU713	4	5	0.4	3	2	4	10
DMU716	7	8	0.6	4	3	4	8
DMU745	0.3	2	0.02	5	5	2	1
DMU746	1	3	0.09	4	4	2	0.5
DMU763	13	7	0.8	20	10	16	8
DMU774	4	2	0.2	11	11	20	8
DMU775	1.6	0.9	0.07	9	8	25	5
DMU776	1.8	1.5	0.07	6	6	12	3.5
DMU777	2	4	0.07	2	0.5	4	2.5
DMU778	20	20	0.4	23	23	20	4
DMU785	1.5	1.5	0.15	6	4	2	0.6
DMU2103	7	70	0.7	25	15	20	4
DMU2105	5	8	0.15	6.5	5	4	3
DMU2139	1.5	15	0.08	7	6	5	3

A total of fourteen CYP1B1 inhibitors have been identified in this research. All CYP1B1 inhibitors listed in Table 35 have a sub micro molar IC_{50} against CYP1B1 catalysed EROD activity and with at least 10-fold enzyme selective ratio over other CYP1A enzymes. Amongst these CYP1B1 inhibitors, DMU778 and DMU2103 have potential uses for *in vitro* and *in vivo* assay due to their low toxicity in the human cancer breast cell lines.

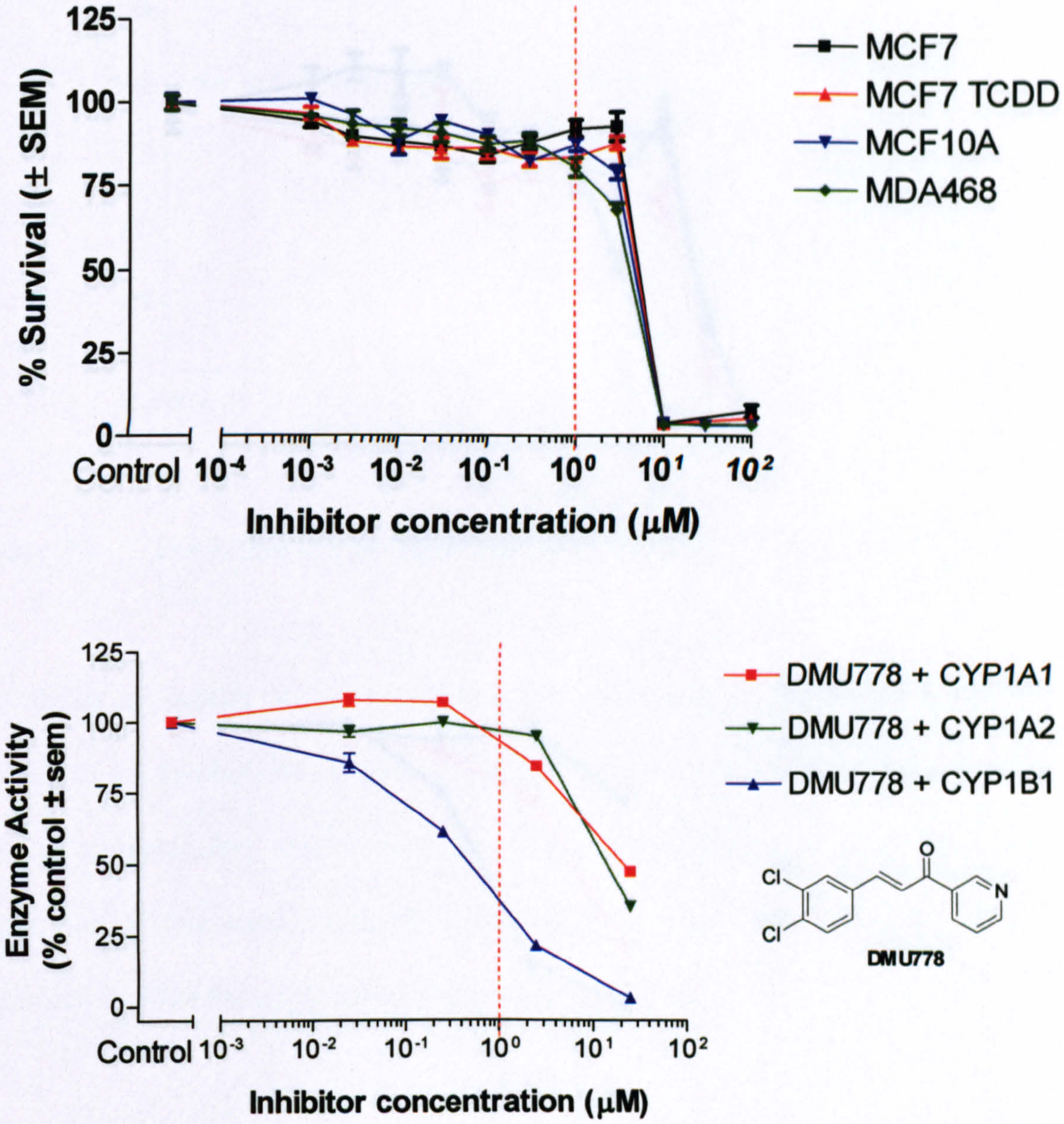

Figure 94: Cytotoxicity and enzyme selectivity of DMU778

DMU778 can be co-incubated in prodrug bioactivation assay at 1μM. At this concentration, DMU778 does not cause toxicity to any human breast cell lines and can inhibit ~60% of CYP1B1 activity. Same as DMU778, DMU2103 can be used at 1μM as an inhibitor. At this concentration DMU2103 only cause some slight toxicity to the breast cancer cell lines and it can inhibit ~60% of CYP1B1 mediated bioactivation.

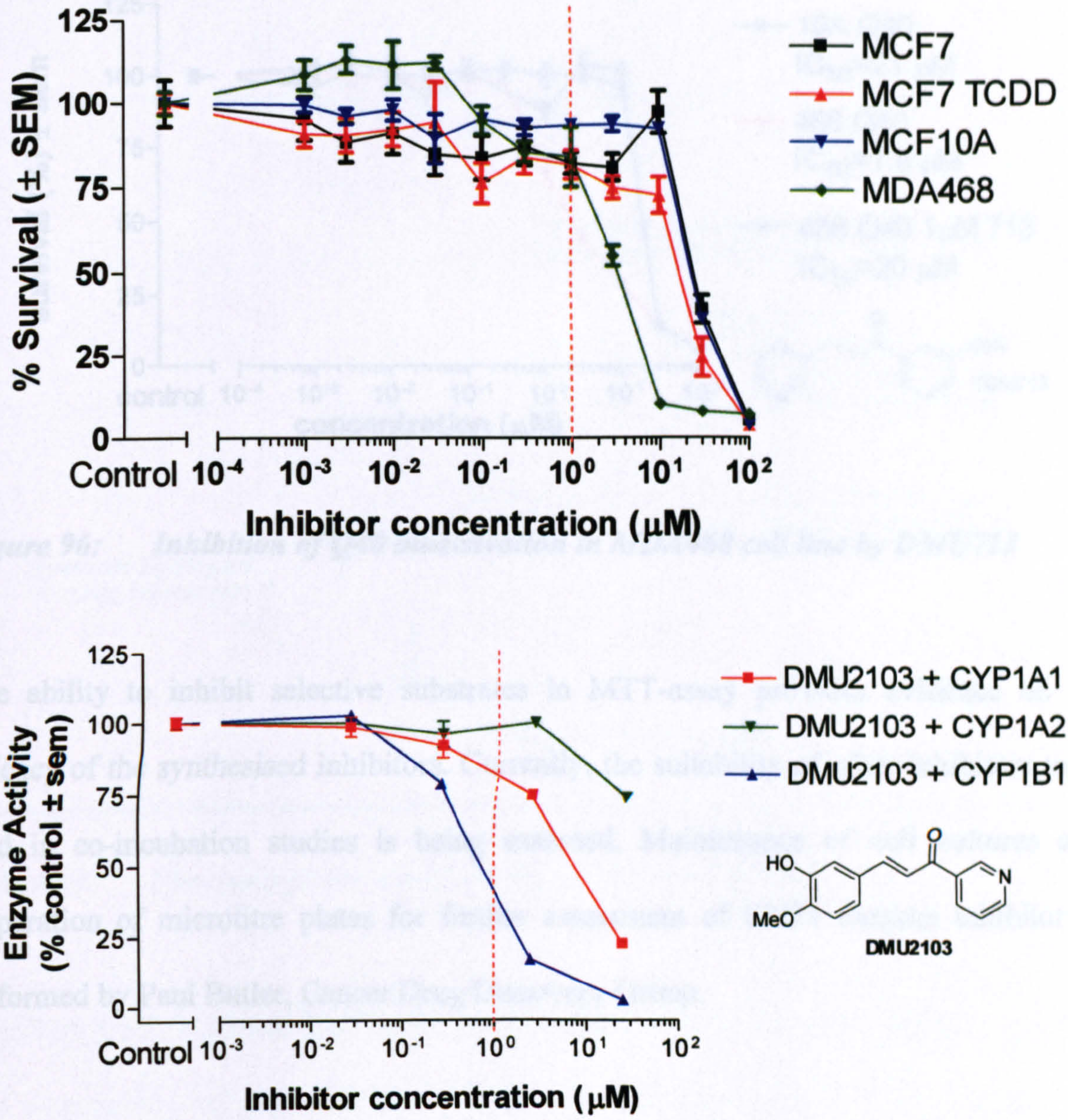

Figure 95: Cytotoxicity and enzyme selectivity of DMU2103

A CYP1B1 inhibitor DMU713 has been used to evaluate the selective bioactivation of a natural compound Q40. Q40 was identified in house as a selective substrate for CYP1B1. Using DMU713 at 1μM, the bioactivation of Q40 by CYP1B1 was inhibited (Figure 96).

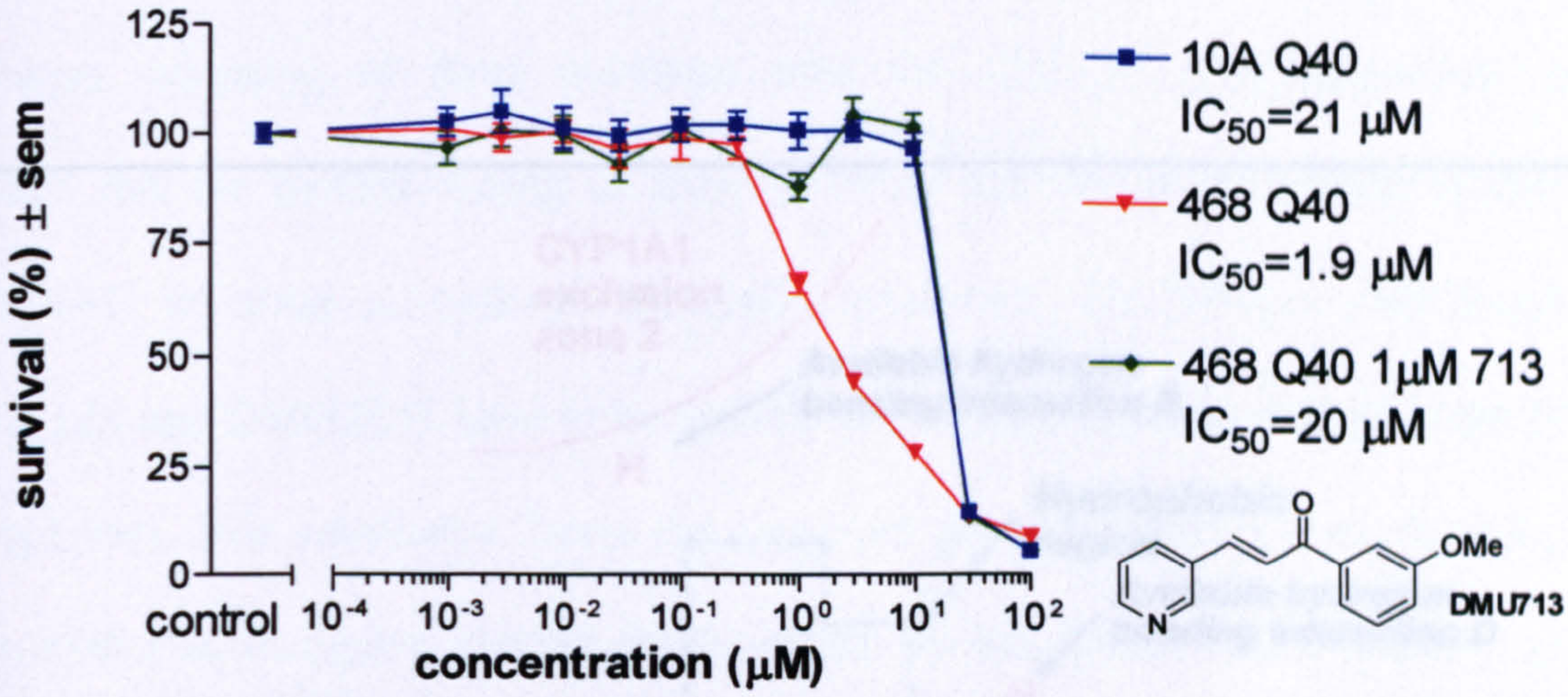

Figure 96: Inhibition of Q40 bioactivation in MDA468 cell line by DMU713

The ability to inhibit selective substrates in MTT-assay provides evidence on the efficacy of the synthesised inhibitors. Currently, the suitability of other inhibitors to be used in co-incubation studies is being assessed. Maintenance of cell cultures and preparation of microtitre plates for further assessment of CYP1 enzyme inhibitor is performed by Paul Butler, Cancer Drug Discovery Group.

6.2 Validation of CYP1 enzyme pharmacophore models

Using the differential inhibition of cytochrome P450 CYP1 mono-oxygenases by a range of structurally diverse heterocyclic chalcones and drug metabolism data from elsewhere, the pharmacophore models of each CYP1 enzymes were constructed. The CYP1A1 pharmacophore model consists of a diagonal binding pocket. The two exclusion zones limit the binding of larger substrates/inhibitors. Finally, the selectivity of the substrate and the inhibitor of CYP1A1 is afforded by four hydrogen bonding

interactions and the hydrophobic region.

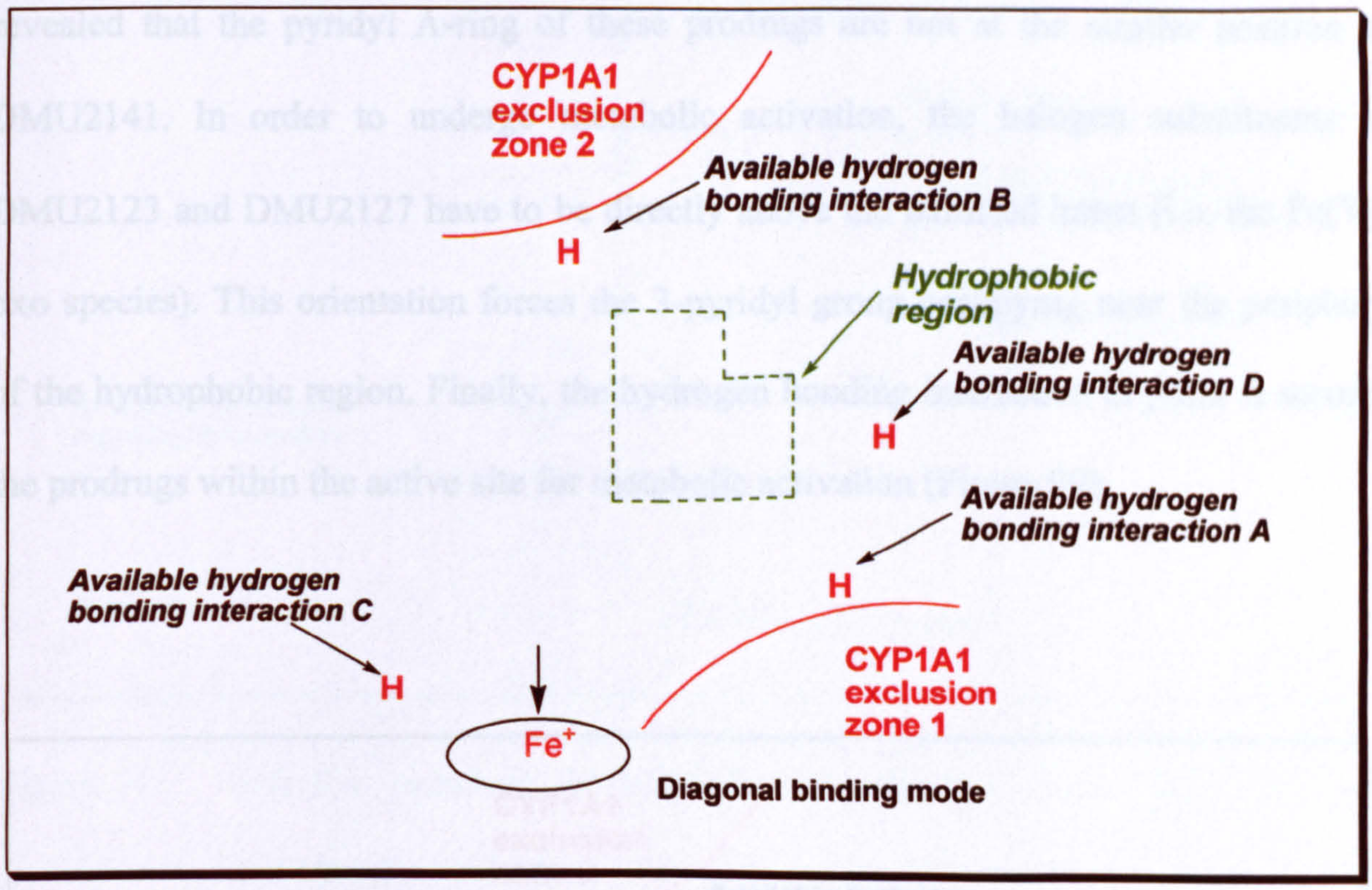

Figure 97: Pharmacophore model for the cytochrome P450 CYP1A1

DMU135, DMU2123 and DMU2127 are potential CYP1A1 activated anticancer agents. The cytotoxicity of DMU135 is mediated by CYP1A1 demethylation of the 3,4-methylenedioxy moiety. Mapping of DMU135 into CYP1A1 pharmacophore model corroborates with the metabolic profile of this prodrug. Within the enzyme active site, the hydrophobic trimethoxyphenyl group of the prodrug mapped onto the hydrophobic region. Hydrogen bonding interactions at point A and point D also help to anchor DMU135 ready for oxidative demethylation (Figure 98).

The di-3-pyridyl chalcone DMU2141 does not inhibit CYP1A1. One may have concluded that selective bioactivation of DMU2123 and DMU2127 by CYP1A1 would be impossible, since the 3-pyridyl moiety of the prodrugs have to be mapped within the

hydrophobic region of the enzyme in order for the prodrugs to undergo metabolic activation. Mapping of these prodrugs onto the CYP1A1 pharmacophore model revealed that the pyridyl A-ring of these prodrugs are not at the similar position as DMU2141. In order to undergo metabolic activation, the halogen substituents of DMU2123 and DMU2127 have to be directly above the oxidised haem (i.e. the Fe(V)-oxo species). This orientation forces the 3-pyridyl group occupying near the periphery of the hydrophobic region. Finally, the hydrogen bonding interaction at point B secures the prodrugs within the active site for metabolic activation (Figure 99).

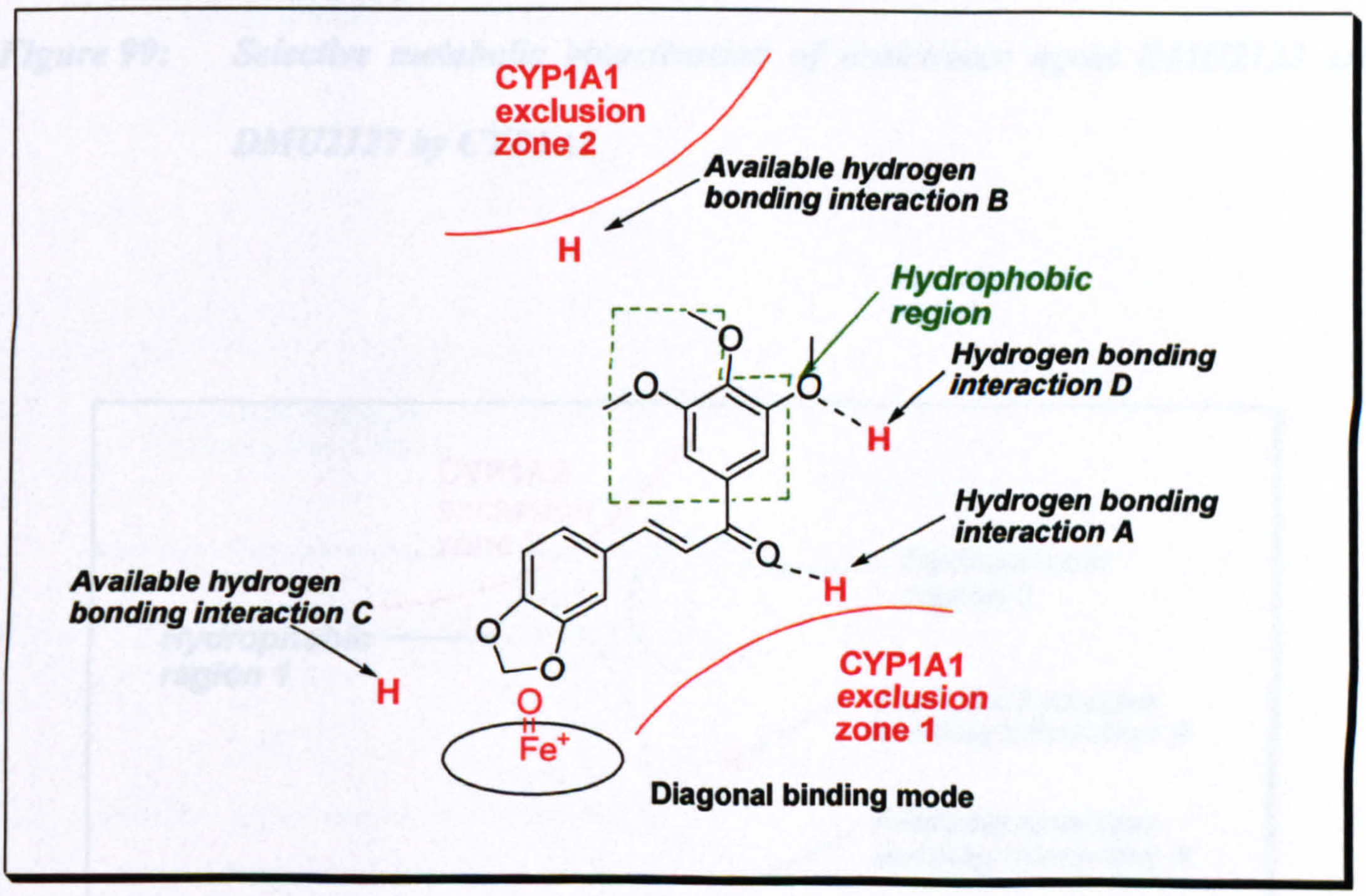

Figure 98: Selective metabolic bioactivation of anticancer agent DMU135 by CYP1A1

Validate the efficacy of selective CYP1 enzyme inhibitors and the CYP1B1 pharmacophore model

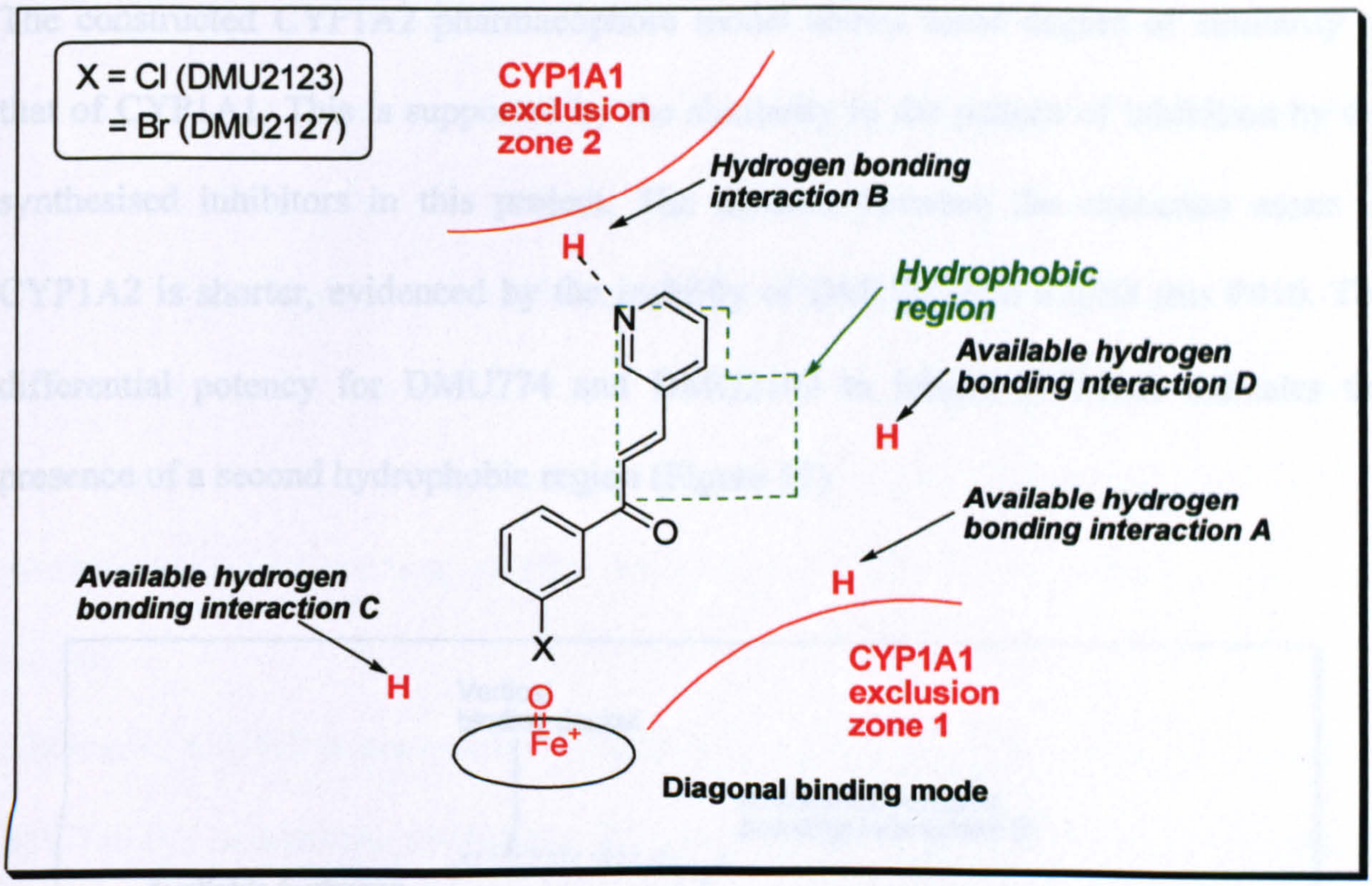

Figure 99: Selective metabolic bioactivation of anticancer agent DMU2123 and DMU2127 by CYP1A1

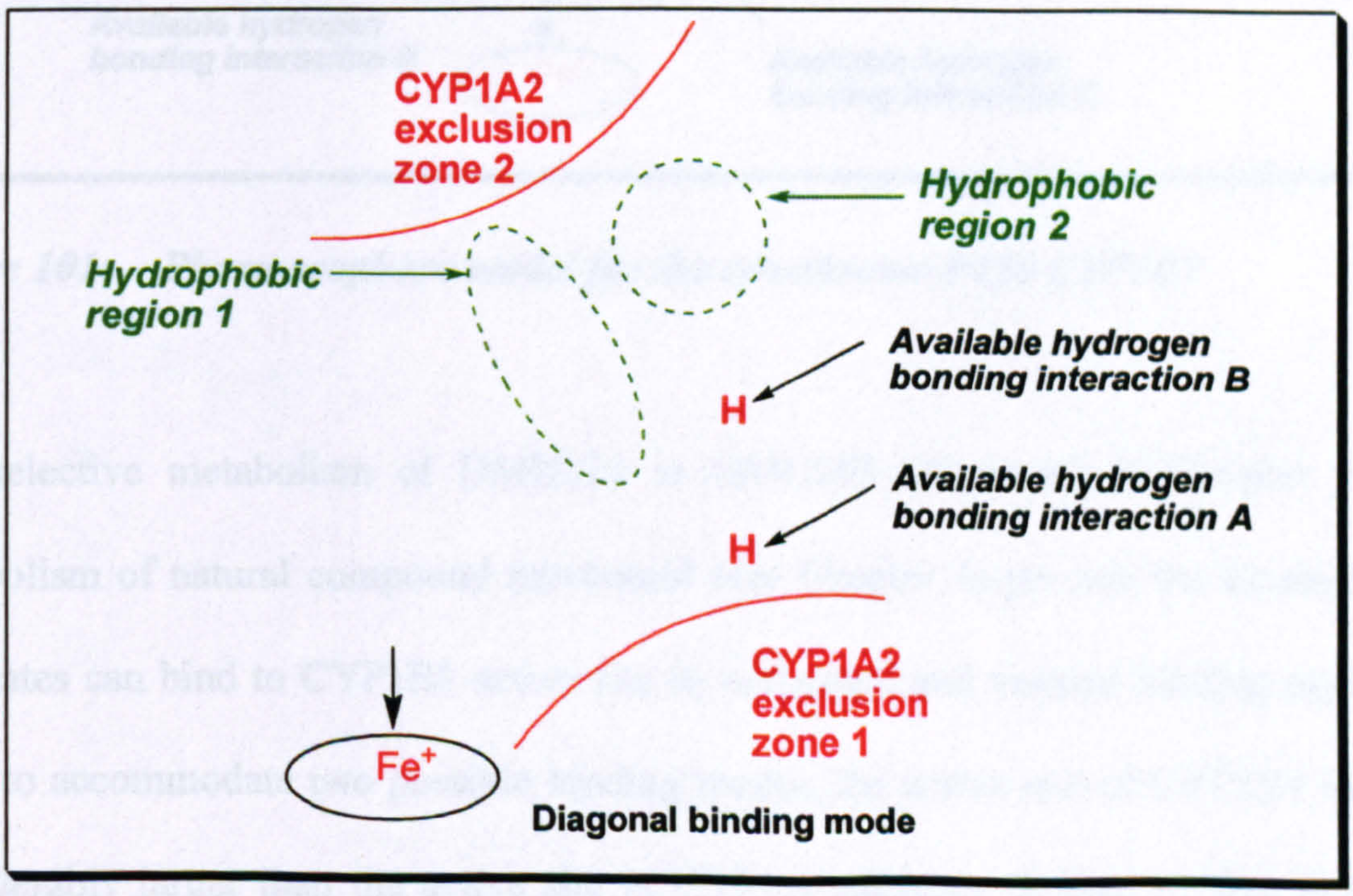

Figure 100: Pharmacophore model for the cytochrome P450 CYP1A2

The constructed CYP1A2 pharmacophore model shows some degree of similarity to that of CYP1A1. This is supported by the similarity in the pattern of inhibition by the synthesised inhibitors in this project. The distance between the exclusion zones in CYP1A2 is shorter, evidenced by the inability of DMU2134 to inhibit this P450. The differential potency for DMU774 and DMU2103 to inhibit CYP1A2 indicates the presence of a second hydrophobic region *(Figure 57)*.

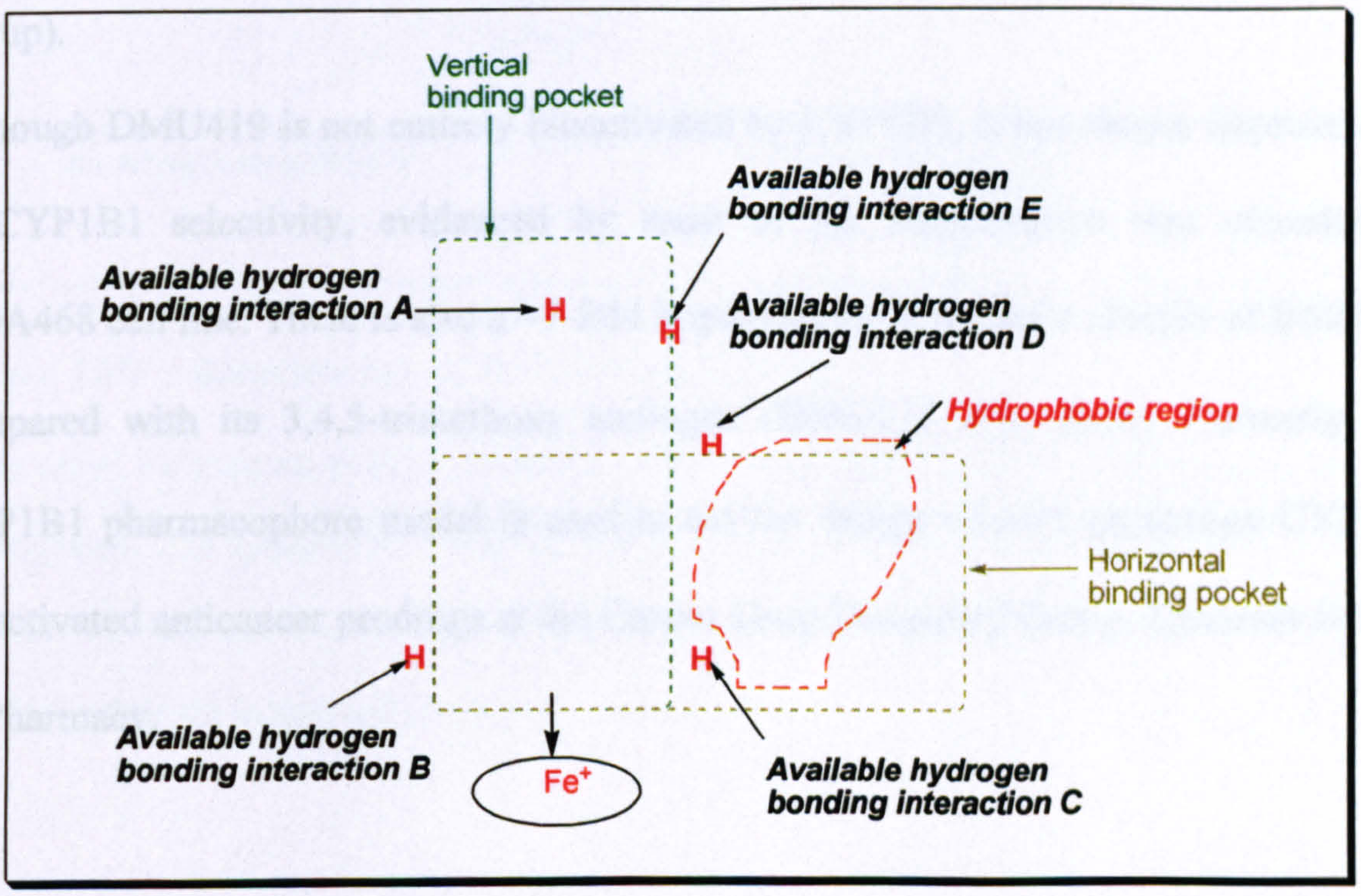

Figure 101: Pharmacophore model for the cytochrome P450 CYP1B1

The selective metabolism of DMU214 to DMU293 (discussed in Chapter 4) and metabolism of natural compound resveratrol (see Chapter 3) provide the evidence that substrates can bind to CYP1B1 active site in horizontal and vertical binding modes. In order to accommodate two possible binding modes, the active site of CYP1B1 must be considerably larger than the active site in CYP1A enzymes. A total of five hydrogen bonding interactions has been identified. The ability of some 3-pyridyl chalcones with

polycyclic aromatic B-ring substituents to inhibit CYP1B1 with high potency demonstrates the presence of a hydrophobic region within the horizontal binding pocket. It is thought that part of the hydrophobic region in CYP1B1 is formed by two groups of bulky hydrophobic amino acids residue arranged in layers parallel to each other. This restrict amount of space available for non-planar bulky substituents. Knowing the structural requirements of CYP1B1, DMU419 was designed and synthesised (patent pending; synthesised by Ketan Ruparelia, Cancer Drug Discovery Group).

Although DMU419 is not entirely bioactivated by CYP1B1, it has shown improvement in CYP1B1 selectivity, evidenced by most of the bioactivation was recorded in MDA468 cell line. There is also a ~7-fold improvement in intrinsic toxicity of DMU419 compared with its 3,4,5-trimethoxy analogue (DMU135 IC_{50} 2μM). Currently, the CYP1B1 pharmacophore model is used to aid the design of next generation CYP1B1 bioactivated anticancer prodrugs at the Cancer Drug Discovery Group, Leicester School of Pharmacy.

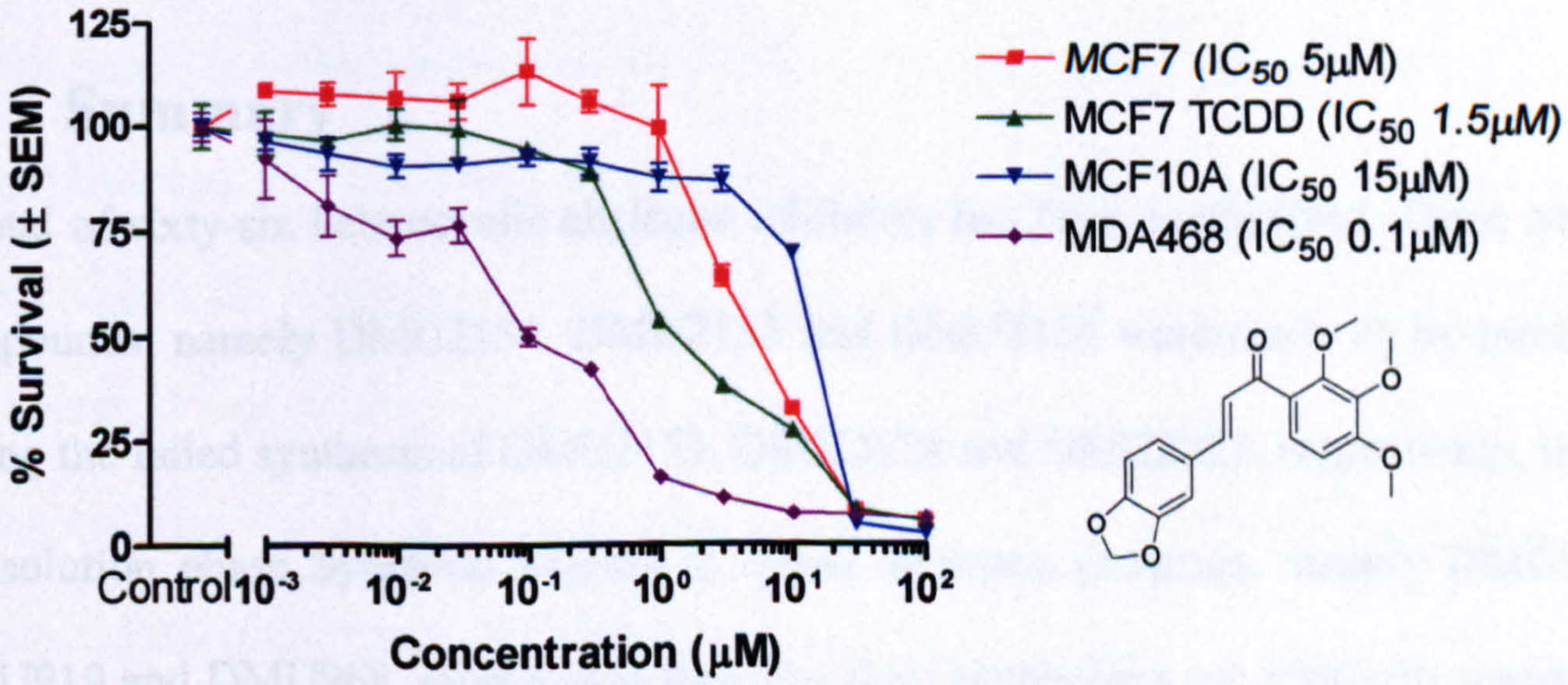

Figure 102: DMU419 cytotoxicity on human breast cell lines

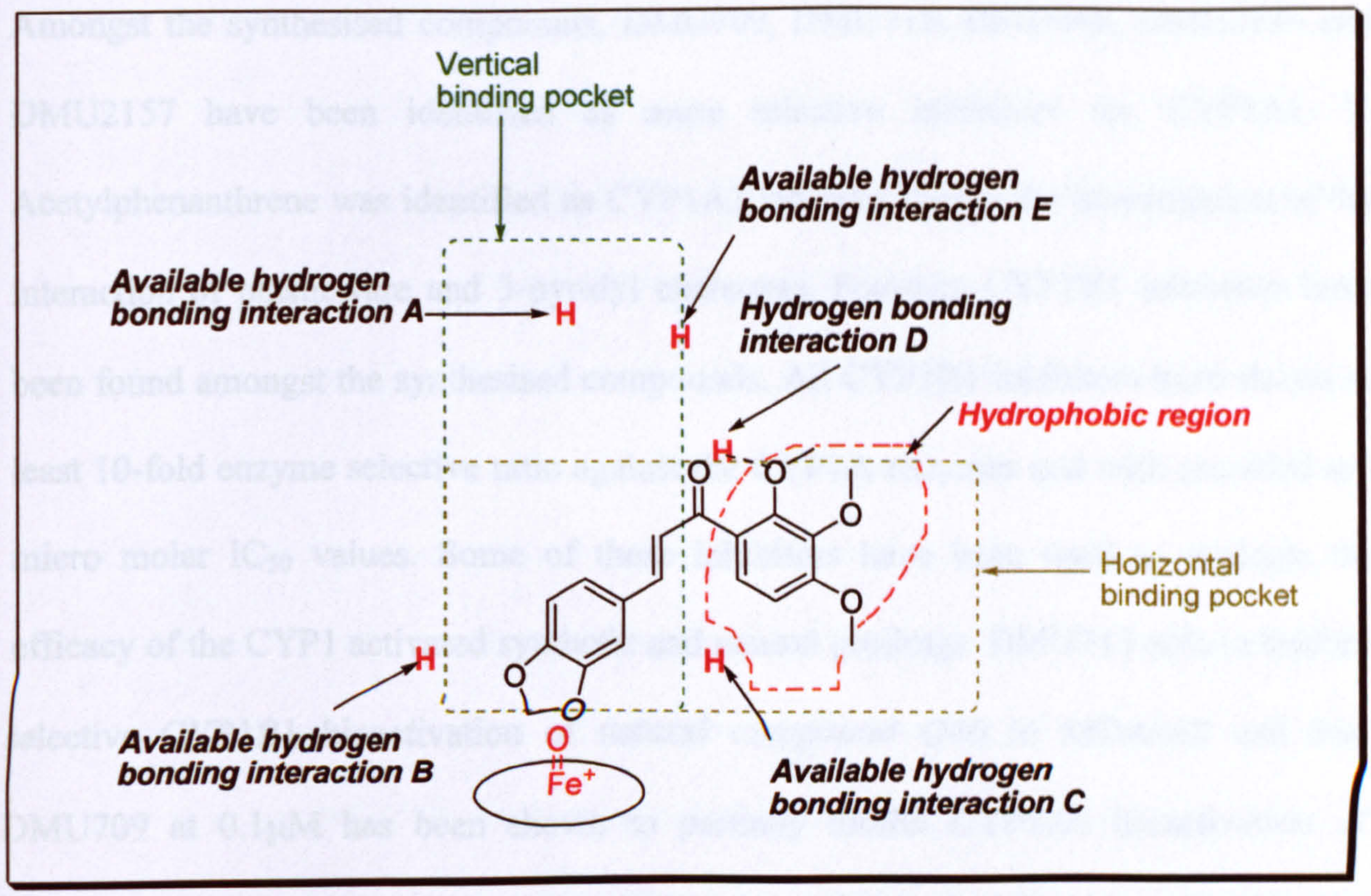

Figure 103: Bioactivation of DMU419 by CYP1B1

Figure shows the mapping of DMU419 onto CYP1B1 pharmacophore model ready to undergo oxidative demethylation. The hydrophobic trimethoxyphenyl B-ring is mapped into the hydrophobic region. The hydrogen bonding interaction at point D and the oxygen in the 2-methoxy substituent help to anchor DMU419 within the enzyme active site.

6.3 Summary

A total of sixty-six heterocyclic chalcone inhibitors has been synthesised. Three triaryl compounds, namely DMU2154, DMU2155 and DMU2156 were made as by-products during the failed synthesis of DMU2123, DMU2124 and DMU2127, respectively, using the solution phase Synthetic Method 2. Three chalcone prodrugs, namely DMU918, DMU919 and DMU968, were synthesised but their metabolites are relatively non-toxic due to lack of functionalities to mediate toxicity in the human cancer breast cell lines.

Amongst the synthesised compounds, DMU709, DMU710, DMU968, DMU2114 and DMU2157 have been identified as more selective inhibitors for CYP1A1. 9-Acetylphenanthrene was identified as CYP1A2 inhibitor during the investigation of the interaction of plasticware and 3-pyridyl chalcones. Fourteen CYP1B1 inhibitors have been found amongst the synthesised compounds. All CYP1B1 inhibitors have shown at least 10-fold enzyme selective ratio against the CYP1A enzymes and with recorded sub micro molar IC_{50} values. Some of these inhibitors have been used to evaluate the efficacy of the CYP1 activated synthetic and natural prodrugs. DMU713 able to inhibits selective CYP1B1 bioactivation of natural compound Q40 in MDA468 cell line. DMU709 at 0.1μM has been shown to partially inhibit CYP1A1 bioactivation of DMU135. Higher concentration of DMU709 in co-incubation studies is not feasible due to the intrinsic toxicity of the compound. Ideally, all identified inhibitors should be assayed to determine their suitability as inhibitor in the MTT-cytotoxic experiment. This is because apart from enzyme selectivity, other factors such as non-specific protein binding and metabolic degradation by other enzymes presence in the cell lines can affect the efficacy of these compounds as inhibitors.

Although DMU2123 and DMU2127 were designed to be CYP1 family inhibitors, these two compounds were bioactivated by CYP1A1. It was also found that residual insect P450s presence in the control microsomes and other Supersome™ also metabolised these compounds. Since no metabolite was detected in HPLC analysis after microsomal incubation, it was postulated that the metabolite of DMU2123 and DMU2127 must be highly reactive. The metabolites of these compounds have been tentatively assigned as the DMU2123 perchlorate and DMU2127 perbromate. The perchlorate and perbromate metabolites are bleach-like compounds and can disrupt biological macromolecules such

as DNA and enzymes by forming permanent covalent conjugates. There was no metabolite peak detected in other incubation studies suggesting the insect P450s also generated the same metabolites as by CYP1A1. DMU2123 and DMU2127 have shown 125- and 300-fold tumour selective ratio, respectively. They are potential anticancer agents for further preclinical studies. DU2123 and DMU2127 may also represent a novel class of insecticides that require P450 bioactivation.

The structure-activity relationship for CYP1 inhibitors has been investigated. CYP1 pharmacophore models, based on inhibitor data and drug metabolism results, were constructed. The pharmacophore models have been used to design next generation prodrugs, such as DMU419, with improved CYP1B1 selectivity. The validity of the pharmacophore models constructed have been proven by other newly designed CYP1B1 selective prodrugs synthesised within the Cancer Drug Discovery Group at Leicester School of Pharmacy.

References

(1) Porter, T. D.; Coon, M. J. Cytochrome-P-450 - Multiplicity of Isoforms, Substrates, and Catalytic and Regulatory Mechanisms. *Journal of Biological Chemistry* **1991**, *266*, 13469-13472.

(2) Lewis, D. F. V. *Guide to Cytochrome P450- Structure and Function*; Taylor & Francis: London and New York, 2001.

(3) Axelrod, J. The enzymatic demethylation of ephedrine. *Journal of Pharmacology* **1955**, *114*, 430-438.

(4) Garfinkel, D. Studies on pig liver microsomes. I. Enzymic and pigment composition of different microsomal fractions. *Achives of Biochemistry and Biophysics* **1958**, *77*, 493-509.

(5) Klingenberg, M. Pigments of rat liver microsomes. *Achives of Biochemistry and Biophysics* **1958**, *75*, 376-386.

(6) Verkade, P. E. Studies on the metabolism of fats. *Proceedings of The Koninklijke Nederlandse Akademie van Wetenschappen* **1932**, *35*, 251-266.

(7) Carter, H. E. The oxidation of branched-chain fatty acids. *Biological Symposia*; Jacques Cattell Press: Lancaster, PA, 1941; pp 47-63.

(8) Bergstrom, S.; Borgstrom, B.; Tryding, N.; Westoo, G. Intestinal absorption and metabolism of 2:2-dimethylstearic acid in the rat. *Biochemical Journal* **1954**, *58*, 604-608.

(9) Omura, T., and Sato, R. A new cytochrome in liver microsomes. *Journal of Biological Chemistry* **1962**, *237*, 1375-1376.

(10) Omura, T.; Sato, R. The carbon monoxide binding pigment of liver microsomes. I. Evidence for its haemoprotein nature. *Journal of Biological Chemistry* **1964**, *239*, 2370-2378.

(11) Omura, T.; Sato, R.; Cooper, D. Y.; Rosenthal, O.; Estabrook, R. W. Function of cytochrome P-450 of microsomes. *Federation Proceedings* **1965**, *24*, 1181-1189.

(12) Nebert, D. W.; Nelson, D. R.; Adesnik, M.; Coon, M. J.; Estabrook, R. W.; Gonzalez, F. J.; Guengerich, F. P.; Gunsalus, I. C.; Johnson, E. F.; Kemper, B.; Levin, W.; Phillips, I. R.; Sato, R.; Waterman, M. R. The P450 Superfamily - Updated Listing of All Genes and Recommended Nomenclature for the Chromosomal Loci. *DNA* **1989**, *8*, 1-13.

(13) Nebert, D. W.; Nelson, D. R.; Feyereisen, R. Evolution of the cytochrome P450 genes. *Xenobiotica* **1989**, *19*, 1149-1160.

(14) Nelson, D. R.; Kamataki, T.; Waxman, D. J.; Guengerich, F. P.; Estabrook, R. W.; Feyereisen, R.; Gonzalez, F. J.; Coon, M. J.; Gunsalus, I. C.; Gotoh, O.; Okuda, K.; Nebert, D. W. The P450 Superfamily - Update on New Sequences, Gene-Mapping, Accession Numbers, Early Trivial Names of Enzymes, and Nomenclature. *DNA and Cell Biology* **1993**, *12*, 1-51.

(15) Nelson, D. R.; Koymans, L.; Kamataki, T.; Stegeman, J. J.; Feyereisen, R.; Waxman, D. J.; Waterman, M. R.; Gotoh, O.; Coon, M. J.; Estabrook, R. W.; Gunsalus, I. C.; Nebert, D. W. P450 superfamily: update on new sequences, gene mapping, accession numbers and nomenclature. *Pharmacogenetics* **1996**, *6*, 1-42.

(16) Ortiz de Montellano, P. R. *Cytochrome P450- Structure, Mechanism, and Biochemistry*; Plenum Press: New York and London, 1995.

(17) Nebert, D. W.; Adesnik, M.; Coon, M. J.; Estabrook, R. W.; Gonzalez, F. J.; Guengerich, F. P.; Gunsalus, I. C.; Johnson, E. F.; Kemper, B.; Levin, W.; Phillips, I. R.; Sato, R.; Waterman, M. R. The P450 Gene Superfamily - Recommended Nomenclature. *DNA* **1987**, *6*, 1-11.

(18) http://drnelson.utmem.edu/CytochromeP450.html Cytochrome P450 Homepage; Nelson, D. R., 2004.

(19) Lu, A. Y.; Coon, M. J. Role of hemoprotein P-450 in fatty acid omega-hydroxylation in a soluble enzyme system from liver microsomes. *Journal of Biological Chemistry* **1968**, *243*, 1331-1332.

(20) Lu, A. Y.; Junk, K. W.; Coon, M. J. Resolution of the cytochrome P-450-containing omega-hydroxylation system of liver microsomes into three components. *Journal of Biological Chemistry* **1969**, *244*, 3714-3721.

(21) Strobel, H. W.; Lu, A. Y.; Heidema, J.; Coon, M. J. Phosphatidylcholine requirement in the enzymatic reduction of hemoprotein P-450 and in fatty acid, hydrocarbon, and drug hydroxylation. *Journal of Biological Chemistry* **1970**, *245*, 4851-4854.

(22) Gotoh, O.; Fujii-Kuriyama, Y. Evolution, structure and gene regulation of cytochrome P450. *Frontiers in Biotransformation* **1989**, *1*, 195-243.

(23) Creighton, T. E. *Proteins: Structure and Molecular Properties*; Freeman: New York, 1993.

(24) Tajima, F.; Nei, M. Estimation of Evolutionary Distance between Nucleotide-Sequences. *Molecular Biology and Evolution* **1984**, *1*, 269-285.

(25) Nelson, D. R.; Strobel, H. W. Evolution of Cytochrome-P-450 Proteins. *Molecular Biology and Evolution* **1987**, *4*, 572-593.

(26) Nebert, D. W.; Nelson, D. R.; Coon, M. J.; Estabrook, R. W.; Feyereisen, R.;

Fujiikuriyama, Y.; Gonzalez, F. J.; Guengerich, F. P.; Gunsalus, I. C.; Johnson, E. F.; Loper, J. C.; Sato, R.; Waterman, M. R.; Waxman, D. J. The P450 Superfamily - Update on New Sequences, Gene-Mapping, and Recommended Nomenclature. *DNA and Cell Biology* **1991**, *10*, 1-14.

(27) Nelson, D. R. Metazoan cytochrome P450 evolution. *Comparative Biochemistry and Physiology Part C: Pharmacology, Toxicology and Endocrinology* **1998**, *121*, 15-22.

(28) Cleaves, H. J.; Miller, S. L. Oceanic protection of prebiotic organic compounds from UV radiation. *Proceedings of the National Academy of Sciences of the United States of America* **1998**, *95*, 7260-7263.

(29) Wickramashighe, R. H.; Villee, C. A. Early role during chemical evolution for cytochrome P450 in oxygen detoxification. *Nature* **1975**, *256*, 509-510.

(30) Knoll, A. H. The Early Evolution of Eukaryotes - a Geological Perspective. *Science* **1992**, *256*, 622-627.

(31) Nelson, D. R. Cytochrome P450 and the Individuality of Species. *Archives of Biochemistry and Biophysics* **1999**, *369*, 1-10.

(32) Gonzalez, F. J.; Nebert, D. W. Evolution of the P450-Gene Superfamily - Animal Plant Warfare, Molecular Drive and Human Genetic-Differences in Drug Oxidation. *Trends in Genetics* **1990**, *6*, 182-186.

(33) Le Bail, J. C.; Varnat, F.; Nicolas, J. C.; Habrioux, G. Estrogenic and antiproliferative activities on MCF7 human breast cancer cells by flavonoids. *Cancer Letters* **1998**, *130*, 209-216.

(34) Le Bail, J. C.; Laroche, T.; Marre-Fournier, F.; Habrioux, G. Aromatase and 17β-hydroxysteroid dehydrogenase inhibition by flavonoids. *Cancer Letters* **1998**, *133*, 101-106.

(35) Le Bail, J. C.; Champavier, Y.; Chulia, A. J.; Habrioux, G. Effects of phytoestrogens on aromatase, 3β- and 17β-hydroxysteroid dehydrogenase activities and human breast cancer cells. *Life Sciences* **2000**, *66*, 1281-1291.

(36) Youdim, K. A.; Dobbie, M. S.; Kuhnle, G.; Proteggente, A. R.; Abbott, N. J.; Rice-Evans, C. Interaction between flavonoids and the blood-brain barrier: in vitro studies. *Journal of Neurochemistry* **2003**, *85*, 180-192.

(37) Waxman, D. J. P450 Gene Induction by Structurally Diverse Xenochemicals: Central Role of Nuclear Receptors CAR, PXR, and PPAR. *Archives of Biochemistry and Biophysics* **1999**, *369*, 11-23.

(38) Whitlock, J. P. Mechanistic Aspects of Dioxin Action. *Chemical Research in Toxicology* **1993**, *6*, 754-763.

(39) Nebert, D. W.; Jones, J. E. Regulation of the Mammalian Cytochrome P450 (CYP1A1) Gene. *International Journal of Biochemistry* **1989**, *21*, 243-252.

(40) Wilhelmsson, A.; Cuthill, S.; Denis, M.; Wikstrom, A. C.; Gustafsson, J. A.; Poellinger, L. The Specific DNA-Binding Activity of the Dioxin Receptor Is Modulated by the 90 Kd Heat-Shock Protein. *Embo Journal* **1990**, *9*, 69-76.

(41) Kazlauskas, A.; Poellinger, L.; Pongratz, I. Evidence that the Co-chaperone p23 regulates ligand responsiveness of the dioxin (aryl hydrocarbon) receptor. *Journal of Biological Chemistry* **1999**, *274*, 13519-13524.

(42) Ma, Q.; Whitlock, J. P. A novel cytoplasmic protein that interacts with the Ah receptor, contains tetratricopeptide repeat motifs, and augments the transcriptional response to 2,3,7,8- tetrachlorodibenzo-p-dioxin. *Journal of Biological Chemistry* **1997**, *272*, 8878-8884.

(43) LaPres, J. J.; Glover, E.; Dunham, E. E.; Bunger, M. K.; Bradfield, C. A. ARA9 modifies agonist signaling through an increase in cytosolic aryl hydrocarbon receptor. *Journal of Biological Chemistry* **2000**, *275*, 6153-6159.

(44) Petrulis, J. R.; Hord, N. G.; Perdew, G. H. Subcellular localization of the aryl hydrocarbon receptor is modulated by the immunophilin homolog hepatitis B virus X- associated protein 2. *Journal of Biological Chemistry* **2000**, *275*, 37448-37453.

(45) Pongratz, I.; Mason, G. G. F.; Poellinger, L. Dual Roles of the 90-Kda Heat-Shock Protein Hsp90 in Modulating Functional Activities of the Dioxin Receptor - Evidence That the Dioxin Receptor Functionally Belongs to a Subclass of Nuclear Receptors Which Require Hsp90 Both for Ligand-Binding Activity and Repression of Intrinsic DNA-Binding Activity. *Journal of Biological Chemistry* **1992**, *267*, 13728-13734.

(46) Carver, L. A.; LaPres, J. J.; Jain, S.; Dunham, E. E.; Bradfield, C. A. Characterization of the Ah receptor-associated protein, ARA9. *Journal of Biological Chemistry* **1998**, *273*, 33580-33587.

(47) Matsushita, N.; Sogawa, K.; Ema, M.; Yoshida, A.; Fujiikuriyama, Y. A Factor-Binding to the Xenobiotic Responsive Element (XRE) of P-4501A1 Gene Consists of at least 2 Helix-Loop-Helix Proteins, Ah Receptor and Arnt. *Journal of Biological Chemistry* **1993**, *268*, 21002-21006.

(48) Whitlock, J. P.; Chichester, C. H.; Bedgood, R. M.; Okino, S. T.; Ko, H. P.; Ma, Q.; Dong, L. Q.; Li, H.; ClarkeKatzenberg, R. Induction of drug-metabolizing enzymes by dioxin. *Drug Metabolism Reviews* **1997**, *29*, 1107-1127.

(49) Whitlock, J. P., Jr. Induction of cytochrome P4501A1. *Annu Rev Pharmacol Toxicol* **1999**, *39*, 103-125.

(50) Lees, M. J.; Whitelaw, M. L. Multiple roles of ligand in transforming the dioxin

receptor to an active basic helix-loop-helix/PAS transcription factor complex with the nuclear protein Arnt. *Molecular and Cellular Biology* **1999**, *19*, 5811-5822.

(51) Tan, Z. Q.; Chang, X. Q.; Puga, A.; Xia, Y. Activation of mitogen-activated protein kinases (MAPKs) by aromatic hydrocarbons: Role in the regulation of aryl hydrocarbon receptor (AhR) function. *Biochemical Pharmacology* **2002**, *64*, 771-780.

(52) Mimura, J.; Ema, M.; Sogawa, K.; Fujii-Kuriyama, Y. Identification of a novel mechanism of regulation of Ah (dioxin) receptor function. *Genes & Development* **1999**, *13*, 20-25.

(53) Kim, D. W.; Gazourian, L.; Quadri, S. A.; Romieu-Mourez, R.; Sherr, D. H.; Sonenshein, G. E. The RelA NF-kappa B subunit and the aryl hydrocarbon receptor (AhR) cooperate to transactivate the c-myc promoter in mammary cells. *Oncogene* **2000**, *19*, 5498-5506.

(54) Silverman, N.; Maniatis, T. NF-kappa B signaling pathways in mammalian and insect innate immunity. *Genes & Development* **2001**, *15*, 2321-2342.

(55) Ghosh, S.; May, M. J.; Kopp, E. B. NF-kappa B and rel proteins: Evolutionarily conserved mediators of immune responses. *Annual Review of Immunology* **1998**, *16*, 225-260.

(56) Reiners, J. J.; Clift, R. E. Aryl hydrocarbon receptor regulation of ceramide-induced apoptosis in murine hepatoma 1c1c7 cells - A function independent of aryl hydrocarbon receptor nuclear translocator. *Journal of Biological Chemistry* **1999**, *274*, 2502-2510.

(57) Chan, W. K.; Yao, G.; Gu, Y. Z.; Bradfield, C. A. Cross-talk between the aryl hydrocarbon receptor and hypoxia inducible factor signaling pathways: Demonstration of competition and compensation. *Journal of Biological Chemistry* **1999**, *274*, 12115-12123.

(58) Remmer, H.; Schenkman, J.; Estabrook, R. W.; Sasame, H.; Gillette, J.; Narasimhulu, S.; Cooper, D. Y.; Rosenthal, O. Drug interaction with hepatic microsomal cytochrome. *Molecular Pharmacology* **1966**, *2*, 187-190.

(59) Schenkman, J. B.; Remmer, H.; Estabrook, R. W. Spectral studies of drug interaction with hepatic microsomal cytochrome. *Molecular Pharmacology* **1967**, *3*, 113-123.

(60) Haniu, M.; Armes, L. G.; Yasunobu, K. T.; Shastry, B. A.; Gunsalus, I. C. Amino acid sequence of the Pseudomonas putida cytochrome P450. II. Cyanogen-bromide peptides, acid cleavage peptides, and the complete sequence. *Journal of Biological Chemistry* **1982**, *257*, 12664-12671.

(61) Poulos, T. L.; Finzel, B. C.; Gunsalus, I. C.; Wagner, G. C.; Kraut, J. The 2.6A

Crystal-Structure of Pseudomonas putida Cytochrome P450. *Journal of Biological Chemistry* **1985**, *260*, 6122-6130.

(62) Atkins, W. M.; Sligar, S. G. The Roles of Active-Site Hydrogen-Bonding in Cytochrome P450cam as Revealed by Site-Directed Mutagenesis. *Journal of Biological Chemistry* **1988**, *263*, 18842-18849.

(63) Schenkman, J. B.; Greim, H.; Zange, M.; Remmer, H. On the problem of possible other forms of cytochrome P450 in liver microsomes. *Biochimica Et Biophysica Acta* **1969**, *171*, 23-31.

(64) Schenkman, J. B.; Cinti, D. L.; Moldeus, P. W.; Orrenius, S. Newer aspects of substrate binding to cytochrome P-450. *Drug Metababolism and Disposition* **1973**, *1*, 111-120.

(65) Yasukochi, Y.; Masters, B. S. Some properties of a detergent-solubilized NADPH-cytochrome c (cytochrome P450) reductase purified by biospecific affinity chromatography. *Journal of Biological Chemistry* **1976**, *251*, 5337-5344.

(66) Dignam, J. D.; Strobel, H. W. NADPH-cytochrome P450 reductase from rat liver: purification by affinity chromatography and characterization. *Biochemistry* **1977**, *16*, 1116-1123.

(67) Vermilion, J. L.; Coon, M. J. Purified liver microsomal NADPH-cytochrome P450 reductase. Spectral characterization of oxidation-reduction states. *Journal of Biological Chemistry* **1978**, *253*, 2694-2704.

(68) Vermilion, J. L.; Coon, M. J. Identification of the high and low potential flavins of liver microsomal NADPH-cytochrome P450 reductase. *Journal of Biological Chemistry* **1978**, *253*, 8812-8819.

(69) Vermilion, J. L.; Ballou, D. P.; Massey, V.; Coon, M. J. Separate roles for FMN and FAD in catalysis by liver microsomal NADPH-cytochrome P450 reductase. *Journal of Biological Chemistry* **1981**, *256*, 266-277.

(70) Groves, J. T.; McClusky, G. A. Aliphatic hydroxylation by highly purified liver microsomal cytochrome P450. Evidence for a carbon radical intermediate. *Biochemical and Biophysical Research Communications* **1978**, *81*, 154-160.

(71) Lewis, D. F. V.; Lake, B. G.; George, S. G.; Dickins, M.; Eddershaw, P. J.; Tarbit, M. H.; Beresford, A. P.; Goldfarb, P. S.; Guengerich, F. P. Molecular modelling of CYP1 family enzymes CYP1A1, CYP1A2, CYP1A6 and CYP1B1 based on sequence homology with CYP102. *Toxicology* **1999**, *139*, 53-79.

(72) Williams, P. A.; Cosme, J.; Sridhar, V.; Johnson, E. F.; McRee, D. E. Mammalian Microsomal Cytochrome P450 Monooxygenase: Structural Adaptations for Membrane Binding and Functional Diversity. *Molecular Cell* **2000**, *5*, 121-131.

(73) Lewis, D. F. V. Modelling human cytochromes P450 involved in drug metabolism from the CYP2C5 crystallographic template. *Journal of Inorganic Biochemistry* **2002**, *91*, 502-514.

(74) Lewis, D. F. V.; Gillam, E. M. J.; Everett, S. A.; Shimada, T. Molecular modelling of human CYP1B1 substrate interactions and investigation of allelic variant effects on metabolism. *Chemico-Biological Interactions* **2003**, *145*, 281-295.

(75) Lewis, D. F. V.; Lake, B. G.; Bird, M. G.; Loizou, G. D.; *Dickins, M.; Goldfarb,* P. S. Homology modelling of human CYP2E1 based on the CYP2C5 crystal structure: investigation of enzyme-substrate and enzyme-inhibitor interactions. *Toxicology in Vitro* **2003**, *17*, 93-105.

(76) Williams, P. A.; Cosme, J.; Ward, A.; Angova, H. C.; Vinkovic, D. M.; Jhoti, H. Crystal structure of human cytochrome P4502C9 with bound warfarin. *Nature* **2003**, *424*, 464-468.

(77) Williams, P. A.; Cosme, J.; Vinkovic, D. M.; Ward, A.; Angove, H. C.; Day, P. J.; Vonrhein, C.; Tickle, I. J.; Jhoti, H. Crystal structures of human cytochrome P450 3A4 bound to metyrapone and progesterone. *Science* **2004**, *305*, 683-686.

(78) Hasemann, C. A.; Kurumbail, R. G.; Boddupalli, S. S.; Peterson, J. A.; Deisenhofer, J. Structure and Function of Cytochromes P450 - a Comparative Analysis of 3 Crystal-Structures. *Structure* **1995**, *3*, 41-62.

(79) High, S.; Dobberstein, B. Mechanisms that determine the transmembrane disposition of proteins. *Current Opinions in Cell Biolology* **1992**, *4*, 581-586.

(80) Hsu, L. C.; Hu, M. C.; Cheng, H. C.; Lu, J. C.; Chung, B. C. The N-Terminal Hydrophobic Domain of P450c21 Is Required for Membrane Insertion and Enzyme Stability. *Journal of Biological Chemistry* **1993**, *268*, 14682-14686.

(81) http://info.cancerresearchuk.org/cancerstats/incidence/commoncancers/ UK Cancer Incidence 2002; Cancer Research UK, 2002.

(82) www.cancerresearchuk.org/aboutus/publications/scientific_yearbook/ The size of the challenge – the latest cancer statistics; Cancer Research UK, 2003.

(83) Renan, M. J. How Many Mutations Are Required for Tumorigenesis - Implications from Human Cancer Data. *Molecular Carcinogenesis* **1993**, *7*, 139-146.

(84) Hahn, W. C.; Weinberg, R. A. Modelling the molecular circuitry of cancer. *Nature Reviews Cancer* **2002**, *2*, 331-341.

(85) Hahn, W. C.; Weinberg, R. A. Mechanisms of disease: Rules for making human tumor cells. *New England Journal of Medicine* **2002**, *347*, 1593-1603.

(86) Shimada, T.; Yamazaki, H.; Mimura, M.; Inui, Y.; Guengerich, F. P. Interindividual variations in human liver cytochrome P450 enzymes involved in the oxidation of drugs, carcinogens and toxic chemicals: Studies with liver microsomes of 30 Japanese and 30 Caucasians. *Journal of Pharmacology and Experimental Therapeutics* **1994**, *270*, 414-423.

(87) Hayes, C. L.; Spink, D. C.; Spink, B. C.; Cao, J. Q.; Walker, N. J.; Sutter, T. R. 17β-Estradiol hydroxylation catalyzed by human cytochrome P450 1B1. *Proceedings of the National Academy of Sciences of the USA* **1996**, *93*, 9776-9781.

(88) Badawi, A. F.; Cavalieri, E. L.; Rogan, E. G. Role of human cytochrome P450 1A1, 1A2, 1B1, and 3A4 in the 2-, 4-, and 16α-hydroxylation of 17β-estradiol. *Metabolism-Clinical and Experimental* **2001**, *50*, 1001-1003.

(89) Cavalieri, E. L.; Stack, D. E.; Devanesan, P. D.; Todorovic, R.; Dwivedy, I.; Higginbotham, S.; Johansson, S. L.; Patil, K. D.; Gross, M. L.; Gooden, J. K.; Ramanathan, R.; Cerny, R. L.; Rogan, E. G. Molecular origin of cancer: Catechol estrogen-3,4-quinones as endogenous tumor initiators. *Proceedings of the National Academy of Sciences of the United States of America* **1997**, *94*, 10937-10942.

(90) Cavalieri, E. L.; Devanesan, P.; Bosland, M. C.; Badawi, A. F.; Rogan, E. G. Catechol estrogen metabolites and conjugates in different regions of the prostate of Noble rats treated with 4-hydroxyestradiol: implications for estrogen-induced initiation of prostate cancer. *Carcinogenesis* **2002**, *23*, 329-333.

(91) Liehr, J.; Ulubelen, A.; Strobel, H. Cytochrome P450-mediated redox cycling of estrogens. *Journal of Biological Chemistry* **1986**, *261*, 16865-16870.

(92) Liehr, J. G. Genotoxic Effects of Estrogens. *Mutation Research* **1990**, *238*, 269-276.

(93) Liehr, J. G.; Roy, D. Free-Radical Generation by Redox Cycling of Estrogens. *Free Radical Biology and Medicine* **1990**, *8*, 415-423.

(94) Guengerich, F. P.; Shimada, T. Oxidation of Toxic and Carcinogenic Chemicals by Human Cytochrome P450 Enzymes. *Chemical Research in Toxicology* **1991**, *4*, 391-407.

(95) Kim, J. H.; Stansbury, K. H.; Walker, N. J.; Trush, M. A.; Strickland, P. T.; Sutter, T. R. Metabolism of benzo[a]pyrene and benzo[a]pyrene-7,8-diol by human cytochrome P450 1B1. *Carcinogenesis* **1998**, *19*, 1847-1853.

(96) Turesky, R. J.; Guengerich, F. P.; Guillouzo, A.; Langouet, S. Metabolism of heterocyclic aromatic amines by human hepatocytes and cytochrome P4501A2. *Mutation Research-Fundamental and Molecular Mechanisms of Mutagenesis* **2002**, *506*, 187-195.

(97) Crofts, F. G.; Sutter, T. R.; Strickland, P. T. Metabolism of 2-amino-1-methyl-6-phenylimidazo[4,5-b]pyridine by human cytochrome P4501A1, P4501A2 and P4501B1. *Carcinogenesis* **1998**, *19*, 1969-1973.

(98) Shimada, T.; Hayes, C. L.; Yamazaki, H.; Amin, S.; Hecht, S. S.; Guengerich, F. P.; Sutter, T. R. Activation of chemically diverse procarcinogens by human cytochrome P450 1B1. *Cancer Research* **1996**, *56*, 2979-2984.

(99) Pottenger, L. H.; Jefcoate, C. R. Characterization of a Novel Cytochrome P450 from the Transformable Cell-Line, C3h-10t1/2. *Carcinogenesis* **1990**, *11*, 321-327.

(100) Sutter, T. R.; Guzman, K.; Dold, K. M.; Greenlee, W. F. Targets for Dioxin - Genes for Plasminogen-Activator Inhibitor- 2 and Interleukin-1-Beta. *Science* **1991**, *254*, 415-418.

(101) Sutter, T. R.; Tang, Y. M.; Hayes, C. L.; Wo, Y. Y.; Jabs, E. W.; Li, X.; Yin, H.; Cody, C. W.; Greenlee, W. F. Complete cDNA sequence of a human dioxin-inducible mRNA identifies a new gene subfamily of cytochrome P450 that maps to chromosome 2. *Journal of Biological Chemistry* **1994**, *269*, 13092-13099.

(102) Vadlamuri, S. V.; Glover, D. D.; Turner, T.; Sarkar, M. A. Regiospecific expression of cytochrome P4501A1 and 1B1 in human uterine tissue. *Cancer Letters* **1998**, *122*, 143-150.

(103) Hakkola, J.; Pasanen, M.; Pelkonen, O.; Hukkanen, J.; Evisalmi, S.; Anttila, S.; Rane, A.; Mantyla, M.; Purkunen, R.; Saarikoski, S.; Tooming, M.; Raunio, H. Expression of CYP1B1 in human adult and fetal tissues and differential inducibility of CYP1B1 and CYP1A1 by Ah receptor ligands in human placenta and cultured cells. *Carcinogenesis* **1997**, *18*, 391-397.

(104) Zhang, Q. Y.; Dunbar, D.; Ostrowska, A.; Zeisloft, S.; Yang, J.; Kaminsky, L. S. Characterization of human small intestinal cytochromes P450. *Drug Metabolism and Disposition* **1999**, *27*, 804-809.

(105) Rodriguez-Antona, C.; Donato, M. T.; Pareja, E.; Gomez-Lechon, M. J.; Castell, J. V. Cytochrome P450 mRNA expression in human liver and its relationship with enzyme activity. *Archives of Biochemistry and Biophysics* **2001**, *393*, 308-315.

(106) Chang, T. K. H.; Chen, J.; Pillay, V.; Ho, J. Y.; Bandiera, S. M. Real-time polymerase chain reaction analysis of CYP1B1 gene expression in human liver. *Toxicological Sciences* **2003**, *71*, 11-19.

(107) Murray, G. I.; Taylor, M. C.; McFadyen, M. C. E.; McKay, J. A.; Greenlee, W. F.; Burke, M. D.; Melvin, W. T. Tumor-specific expression of cytochrome P450 CYP1B1. *Cancer Research* **1997**, *57*, 3026-3031.

(108) Shehin, S. E.; Stephenson, R. O.; Greenlee, W. F. Transcriptional regulation of

the human CYP1B1 gene: Evidence for involvement of an aryl hydrocarbon receptor response element in constitutive expression. *Journal of Biological Chemistry* **2000**, *275*, 6770-6776.

(109) McFadyen, M. C.; Breeman, S.; Payne, S.; Stirk, C.; Miller, I. D.; Melvin, W. T.; Murray, G. I. Immunohistochemical localization of cytochrome P450 CYP1B1 in breast cancer with monoclonal antibodies specific for CYP1B1. *Journal of Histochemistry & Cytochemistry* **1999**, *47*, 1457-1464.

(110) Gibson, P.; Gill, J. H.; Khan, P. A.; Seargent, J. M.; Martin, S. W.; Batman, P. A.; Griffith, J.; Bradley, C.; Double, J. A.; Bibby, M. C.; Loadman, P. M. Cytochrome P450 1B1 (CYP1B1) is overexpressed in human colon adenocarcinomas relative to normal colon: Implications for drug development. *Molecular Cancer Therapeutics* **2003**, *2*, 527-534.

(111) Carnell, D. M.; Smith, R. E.; Daley, F. M.; Barber, P. R.; Hoskin, P. J.; Wilson, G. D.; Murray, G. I.; Everett, S. A. Target validation of cytochrome P450CYP1B1 in prostate carcinoma with protein expression in associated hyperplastic and premalignant tissue. *International Journal of Radiation Oncology Biology Physics* **2004**, *58*, 500-509.

(112) McFadyen, M. C. E.; Melvin, W. T.; Murray, G. I. Cytochrome P450 CYP1B1 activity in renal cell carcinoma. *British Journal of Cancer* **2004**, *91*, 966-971.

(113) Kumarakulasingham, M.; Rooney, P. H.; Dundas, S. R.; Telfer, C.; Melvin, W. T.; Curran, S.; Murray, G. I. Cytochrorne P450 profile of colorectal cancer: Identification of markers of prognosis. *Clinical Cancer Research* **2005**, *11*, 3758-3765.

(114) Maecker, B.; von Bergwelt-Baildon, M. S.; Anderson, K. S.; Vonderheide, R. H.; Anderson, K. C.; Nadler, L. M.; Schultze, J. L. Rare naturally occurring immune responses to three epitopes from the widely expressed tumour antigens hTERT and CYP1B1 in multiple myeloma patients. *Clinical and Experimental Immunology* **2005**, *141*, 558-562.

(115) Tokizane, T.; Shiina, H.; Igawa, M.; Enokida, H.; Urakami, S.; Kawakami, T.; Ogishima, T.; Okino, S. T.; Li, L. C.; Tanaka, Y.; Nonomura, N.; Okuyama, A.; Dahiya, R. Cytochrome P450 1B1 is overexpressed and regulated by hypomethylation in prostate cancer. *Clinical Cancer Research* **2005**, *11*, 5793-5801.

(116) Oyama, T.; Morita, M.; Isse, T.; Kagawa, N.; Nakata, S.; So, T.; Mizukami, M.; Ichiki, Y.; Ono, K.; Sugaya, M.; Uramoto, H.; Yoshimatsu, T.; Hanagiri, T.; Sugio, K.; Kawamoto, T.; Yasumoto, K. Immunohistochemical evaluation of cytochrome P450 (CYP) and p53 in breast cancer. *Frontiers in Bioscience* **2005**, *10*, 1156-1161.

(117) Downie, D.; McFadyen, M. C. E.; Rooney, P. H.; Cruickshank, M. E.; Parkin, D. E.; Miller, I. D.; Telfer, C.; Melvin, W. T.; Murray, G. I. Profiling

cytochrome P450 expression in ovarian cancer: Identification of prognostic markers. *Clinical Cancer Research* **2005**, *11*, 7369-7375.

(118) Sheibani, N.; Wang, S.; Wu, Z.; Sorenson, C. M.; Jefcoate, C. R. CYP1B1 Deficient Mice Exhibit Reduced Retinal Vascular Density and Fail to Respond to Hypoxia-Induced Neovascularization. *ARVO Meeting Abstracts* **2003**, *44*, 2893-.

(119) Fernandez-Salguero, P.; Pineau, T.; Hilbert, D. M.; McPhail, T.; Lee, S. S. T.; Kimura, S.; Nebert, D. W.; Rudikoff, S.; Ward, J. M.; Gonzalez, F. J. Immune-System Impairment and Hepatic-Fibrosis in Mice Lacking the Dioxin-Binding Ah Receptor. *Science* **1995**, *268*, 722-726.

(120) Schmidt, J. V.; Su, G. H. T.; Reddy, J. K.; Simon, M. C.; Bradfield, C. A. Characterization of a murine Ahr null allele: Involvement of the Ah receptor in hepatic growth and development. *Proceedings of the National Academy of Sciences of the United States of America* **1996**, *93*, 6731-6736.

(121) Fernandez-Salguero, P. M.; Ward, J. M.; Sundberg, J. P.; Gonzalez, F. J. Lesions of aryl-hydrocarbon receptor-deficient mice. *Veterinary Pathology* **1997**, *34*, 605-614.

(122) Potter, G. A. The role of CYP1B1 as a tumour suppressor enzyme. *British Journal of Cancer* **2002**, *86*, S12-S12.

(123) Potter, G. A.; Patterson, L. H.; Wanogho, E.; Perry, P. J.; Butler, P. C.; Ijaz, T.; Ruparelia, K. C.; Lamb, J. H.; Farmer, P. B.; Stanley, L. A.; Burke, M. D. The cancer preventative agent resveratrol is converted to the anticancer agent piceatannol by the cytochrome P450 enzyme CYP1B1. *British Journal of Cancer* **2002**, *86*, 774-778.

(124) Ferrigni, N. R.; McLaughlin, J. L.; Powell, R. G.; Smith, C. R. Use of potato disk and brine shrimp bioassays to detect activity and isolate piceatannol as the antileukemic principle from the seeds of Euphorbia lagascae. *Journal of Natural Products* **1984**, *47*, 347-352.

(125) Peters, J. D.; Furlong, M. T.; Asai, D. J.; Harrison, M. L.; Geahlen, R. L. Syk, Activated by Cross-linking the B-cell Antigen Receptor, Localizes to the Cytosol Where It Interacts with and Phosphorylates alpha-Tubulin on Tyrosine. *Journal of Biological Chemistry* **1996**, *271*, 4755-4762.

(126) Su, L.; David, M. Distinct mechanisms of STAT phosphorylation *via* the interferon-α/β receptor: Selective inhibition of STAT3 and STAT5 by piceatannol. *Journal of Biological Chemistry* **2000**, *275*, 12661-12666.

(127) Lu, J. B.; Ho, C. T.; Ghai, G.; Chen, K. Y. Resveratrol analog, 3,4,5,4 '-tetrahydroxystilbene, differentially induces pro-apoptotic p53/Bax gene expression and inhibits the growth of transformed cells but not their normal counterparts. *Carcinogenesis* **2001**, *22*, 321-328.

(128) Dark, G. G.; Hill, S. A.; Prise, V. E.; Tozer, G. M.; Pettit, G. R.; Chaplin, D. J. Combretastatin A-4, an agent that displays potent and selective toxicity toward tumor vasculature. *Cancer Research* **1997**, *57*, 1829-1834.

(129) Sterling, K. M.; Cutroneo, K. R. Constitutive and inducible expression of cytochromes P4501A (CYP1A1 and CYP1A2) in normal prostate and prostate cancer cells. *Journal of Cellular Biochemistry* **2004**, *91*, 423-429.

(130) Murray, G. I.; Taylor, M. C.; Burke, M. D.; Melvin, W. T. Enhanced expression of cytochrome P450 in stomach cancer. *British Journal of Cancer* **1998**, *77*, 1040-1044.

(131) Zhang, K. L.; Ma, J. X.; Chen, X. Y.; Sun, Y.; Kong, Q. Y.; Liu, J.; Li, H. Frequent CYP1A1 expression in gastric cancers and their related lesions. *Oncology Reports* **2004**, *12*, 1335-1340.

(132) Murray, G. I.; Taylor, V. E.; McKay, J. A.; Weaver, R. J.; Ewen, S. W. B.; Melvin, W. T.; Burke, M. D. Expression of Xenobiotic-Metabolizing Enzymes in Tumors of the Urinary-Bladder. *International Journal of Experimental Pathology* **1995**, *76*, 271-276.

(133) Klotz, U.; Hoensch, H.; Schutz, T.; Beaune, P.; Zanger, U.; Bode, J. C.; Fritz, P. Expression of intestinal drug-metabolizing enzymes in patients with chronic inflammatory bowel disease. *Current Therapeutic Research-Clinical and Experimental* **1998**, *59*, 556-563.

(134) Rochat, B.; Morsman, J. M.; Murray, G. I.; Figg, W. D.; McLeod, H. L. Human CYP1B1 and anticancer agent metabolism: Mechanism for tumor-specific drug inactivation? *Journal of Pharmacology and Experimental Therapeutics* **2001**, *296*, 537-541.

(135) McFadyen, M. C. E.; Melvin, W. T.; Murray, G. I. Anti-cancer drug interaction with cytochrome P450CYP1B1. *British Journal of Cancer* **2003**, *88*, S16-S16.

(136) McFadyen, M. C. E.; McLeod, H. L.; Jackson, F. C.; Melvin, W. T.; Doehmer, J.; Murray, G. I. Cytochrome P450CYP1B1 protein expression: a novel mechanism of anticancer drug resistance. *Biochemical Pharmacology* **2001**, *62*, 207-212.

(137) Potter, G. A.; Patterson, L. H.; Burke, M. D.; Butler, P. C. Hydroxylation activated prodrugs for cancer chemotherapy. *PCT International Applications* **1999**, *WO99/40056*.

(138) Potter, G.; Patterson, L. H.; Burke, M. D.; Butler, P. Aromatic hydroxylation activated prodrugs. *US Patent Application* **2000**, *09/633,699*.

(139) Wilsher, N. E. PhD Thesis: CYP1B1 Bioactivation of Novel Anticancer Prodrugs and Related Natural Products. In *Leicester School of Pharmacy*; De Montfort University, Leicester, 2003.

(140) Potter, G. A.; Butler, P. C.; Ruparelia, K. C.; Ijaz, T.; Wilsher, N. E.; Wanogho, E.; Tan, H. L.; Hoang, T. T. V.; Stanley, L. A.; Burke, M. D. DMU212: A novel CYP1B1 activated anticancer prodrug. *British Journal of Cancer* **2002**, *86*, S117.

(141) Sale, S.; Verschoyle, R. D.; Boocock, D.; Jones, D. J. L.; Wilsher, N.; Ruparelia, K. C.; Potter, G. A.; Farmer, P. B.; Steward, W. P.; Gescher, A. J. Pharmacokinetics in mice and growth-inhibitory properties of the putative cancer chemopreventive agent resveratrol and the synthetic analogue trans 3,4,5,4 '-tetramethoxystilbene. *British Journal of Cancer* **2004**, *90*, 736-744.

(142) Potter, G. A.; Barrie, S. E.; Jarman, M.; Rowlands, M. G. Novel Steroidal Inhibitors of Human Cytochrome P450(17-Alpha) (17-Alpha-Hydroxylase-C-17,C-20-Lyase) - Potential Agents for the Treatment of Prostatic-Cancer. *Journal of Medicinal Chemistry* **1995**, *38*, 2463-2471.

(143) Ling, Y. Z.; Li, J. S.; Liu, Y.; Kato, K.; Klus, G. T.; Brodie, A. 17-imidazolyl, pyrazolyl, and isoxazolyl androstene derivatives. Novel steroidal inhibitors of human cytochrome C- 17,C-20-lyase (P450(17 alpha)). *Journal of Medicinal Chemistry* **1997**, *40*, 3297-3304.

(144) Njar, V. C. O.; Kato, K.; Nnane, I. P.; Grigoryev, D. N.; Long, B. J.; Brodie, A. M. H. Novel 17-azolyl steroids, potent inhibitors of human cytochrome 17 alpha-hydroxylase-C-17,C-20-lyase (P450(17 alpha)): Potential agents for the treatment of prostate cancer. *Journal of Medicinal Chemistry* **1998**, *41*, 902-912.

(145) Potter, G. A.; Butler, P. C.; Wanogho, E. Chalcone Therapeutic Agents. In *British Patent PCT: GB01/01341*, 2001.

(146) Dhar, D. N. The Chemistry of Chalcones and Related Compounds; John Wiley & Sons: New York, 1981; pp 3.

(147) Dimmock, J. R.; Kandepu, N. M.; Hetherington, M.; Quail, J. W.; Pugazhenthi, U.; Sudom, A. M.; Chamankhah, M.; Rose, P.; Pass, E.; Allen, T. M.; Halleran, S.; Szydlowski, J.; Mutus, B.; Tannous, M.; Manavathu, E. K.; Myers, T. G.; De Clercq, E.; Balzarini, J. Cytotoxic activities of Mannich bases of chalcones and related compounds. *Journal of Medicinal Chemistry* **1998**, *41*, 1014-1026.

(148) Dimmock, J. R.; Elias, D. W.; Beazely, M. A.; Kandepu, N. M. Bioactivities of chalcones. *Current Medicinal Chemistry* **1999**, *6*, 1125-1149.

(149) Lin, C. N.; Lee, T. H.; Hsu, M. F.; Wang, J. P.; Ko, F. N.; Teng, C. M. 2',5'-dihydroxychalcone as a potent chemical mediator and cyclooxygenase inhibitor. *Journal of Pharmacy and Pharmacology* **1997**, *49*, 530-536.

(150) Middleton, E.; Kandaswami, C.; Theoharides, T. C. The effects of plant flavonoids on mammalian cells: Implications for inflammation, heart disease, and cancer. *Pharmacological Reviews* **2000**, *52*, 673-751.

(151) Sogawa, S.; Nihro, Y.; Ueda, H.; Izumi, A.; Miki, T.; Matsumoto, H.; Satoh, T. 3,4-Dihydroxychalcones as Potent 5-Lipoxygenase and Cyclooxygenase Inhibitors. *Journal of Medicinal Chemistry* **1993**, *36*, 3904-3909.

(152) Dhar, D. N. The Chemistry of Chalcones and Related Compounds; John Wiley & Sons: New York, 1981; pp 8-19.

(153) Dhar, D. N. The Chemistry of Chalcones and Related Compounds; John Wiley & Sons: New York, 1981; pp 4.

(154) Burke, M. D.; Mayer, R. T. Ethoxyresorufin: direct fluorimetric assay of a microsomal O-dealkylation which is preferentially inducible by 3-methylcholanthrene. *Drug Metabolism and Disposition* **1974**, *2*, 583-588.

(155) http://www.gentest.com/; Gentest Corporation, 2000.

(156) Chan, F. C. Y. PhD Thesis: Synthesis of Chiral Anti-Cancer Drugs. In *Drug Development Section, Institute of Cancer Research, Sutton, Surrey*; University of London, 1994.

(157) Mogilaiah, K.; Rao, R. B. Claisen-Schmidt condensation in the solid state. *Indian Journal of Chemistry Section B-Organic Chemistry Including Medicinal Chemistry* **1999**, *38*, 869-871.

(158) Shimada, T.; Yamazaki, H.; Foroozesh, M.; Hopkins, N. E.; Alworth, W. L.; Guengerich, F. P. Selectivity of polycyclic inhibitors for human cytochrome P450s 1A1, 1A2, and 1B1. *Chemical Research in Toxicology* **1998**, *11*, 1048-1056.

(159) Ghose, A. K.; Crippen, G. M. Atomic Physicochemical Parameters for 3-Dimensional-Structure-Directed Quantitative Structure-Activity-Relationships .2. Modeling Dispersive and Hydrophobic Interactions. *Journal of Chemical Information and Computer Sciences* **1987**, *27*, 21-35.

(160) Segura, J.; Garcia, I.; Tarrus, E. Some Pharmacokinetic Characteristics of Furafylline, a New 1,3,8-Trisubstituted Xanthine. *Journal of Pharmacy and Pharmacology* **1986**, *38*, 615-618.

(161) Sesardic, D.; Boobis, A. R.; Murray, B. P.; Murray, S.; Segura, J.; Delatorre, R.; Davies, D. S. Furafylline Is a Potent and Selective Inhibitor of Cytochrome-P450ia2 in Man. *British Journal of Clinical Pharmacology* **1990**, *29*, 651-663.

(162) Potter, G. A.; McCague, R. Coupling of low-order organocopper complexes with organoiron cations: Synthesis of Tamandron, a novel potentially antiandrogenic analog of Tamoxifen. *Journal of the Chemical Society-Chemical Communications* **1992**, 635-637.

(163) Coombes, R. C.; Haynes, B. P.; Dowsett, M.; Quigley, M.; English, J.; Judson, I. R.; Griggs, L. J.; Potter, G. A.; McCague, R.; Jarman, M. Idoxifene: Report of a

Phase I study in patients with metastatic breast cancer. *Cancer Research* **1995**, *55*, 1070-1074.

(164) Potter, G. A.; Barrie, S. E.; Jarman, M.; Rowlands, M. G. Novel steroidal inhibitors of human cytochrome P450 (17α-Hydroxylase-C17,C20-Lyase): Potential agents for the treatment of prostatic cancer. *Journal of Medicinal Chemistry* **1995**, *38*, 2463-2471.

(165) Park, J. G.; Kramer, B. S.; Steinberg, S. M.; Carmichael, J.; Gazdar, A. F.; Minna, J. D. Use of a Tetrazolium-Based Colorimetric Assay (Mtt) for Chemosensitivity Testing of Human Colorectal-Carcinoma Cell- Lines. *Proceedings of the American Association for Cancer Research* **1987**, *28*, 422-422.

(166) Huang, Z.; Fasco, M. J.; Figge, H. L.; Keyomarsi, K.; Kaminsky, L. S. Expression of cytochromes P450 in human breast tissue and tumors. *Drug Metabolism and Disposition* **1996**, *24*, 899-905.

(167) Iscan, M.; Klaavuniemi, T.; Coban, T.; Kapucuoglu, N.; Pelkonen, O.; Raunio, H. The expression of cytochrome P450 enzymes in human breast tumours and normal breast tissue. *Breast Cancer Research and Treatment* **2001**, *70*, 47-54.

(168) Forrester, L. M.; Hayes, J. D.; Millis, R.; Barnes, D.; Harris, A. L.; Schlager, J. J.; Powis, G.; Wolf, C. R. Expression of glutathione S-transferases and Cytochrome P450 in normal and tumor breast tissue. *Carcinogenesis* **1990**, *11*, 2163-2170.

(169) Hellmold, H.; Rylander, T.; Magnusson, M.; Reihner, E.; Warner, M.; Gustafsson, J. A. Characterization of cytochrome P450 enzymes in human breast tissue from reduction mammaplasties. *Journal of Clinical Endocrinology and Metabolism* **1998**, *83*, 886-895.

(170) Spink, D. C.; Spink, B. C.; Cao, J. Q.; DePasquale, J. A.; Pentecost, B. T.; Fasco, M. J.; Li, Y.; Sutter, T. R. Differential expression of CYP1A1 and CYP1B1 in human breast epithelial cells and breast tumor cells. *Carcinogenesis* **1998**, *19*, 291-298.

(171) Angus, W. G. R.; Larsen, M. C.; Jefcoate, C. R. Expression of CYP1A1 and CYP1B1 depends on cell-specific factors in human breast cancer cell lines: Role of estrogen receptor status. *Carcinogenesis* **1999**, *20*, 947-955.

(172) Spink, D. C.; Hayes, C. L.; Young, N. R.; Christou, M.; Sutter, T. R.; Jefcoate, C. R.; Gierthy, J. F. The effects of 2,3,7,8-tetrachlorodibenzo-*p*-dioxin on estrogen metabolism in MCF7 breast cancer cells: Evidence for induction of a novel 17β-estradiol 4-hydroxylase. *Journal of Steroid Biochemistry and Molecular Biology* **1994**, *51*, 251-258.

(173) Chang, T.; Gonzalez, F.; Waxman, D. Evaluation of triacetyloleandomycin, α–naphthoflavone and diethyldithiocarbamate as selective chemical probes for

inhibition of human cytochromes P450. *Archives of Biochemistry and Biophysics* **1994**, *311*, 437-442.

(174) Doostdar, H.; Burke, M. D.; Mayer, R. T. Bioflavonoids: Selective substrates and inhibitors for cytochrome P450 CYP1A and CYP1B1. *Toxicology* **2000**, *144*, 31-38.